The Role of ACE2 and Apelin in Cardiac and Vascular Diseases

by

Wang Wang

A thesis submitted in partial fulfillment of the requirements for the degree of

Doctor of Philosophy

Department of Physiology
University of Alberta

ABSTRACT

Both ACE2 and apelin have been reported playing important roles in regulating cardiovascular structure and function. In this study, we used ACE2 or apelin gene knockout or knockdown mice to explore the roles of ACE2 or apelin in cardiovascular diseases. In particular, we created animal disease models of various cardiovascular remodeling or heart failure by exogenous Angiotensin II infusion or increasing the cardiac afterload or myocardial ischemia/infarction by surgeries. We also used *ex vivo*. disease models in isolated heart or vascular perfusion. Thereafter we performed cardiovascular morphological studies together with functional assays and signaling pathways studies. The results show that ACE2 is a protective factor against Ang II or transverse aortic constriction induced pathological remodeling by decreasing fibrosis, reactive oxygen species and direct degrading of Ang II. Apelin also shows beneficial effects in ischemic heart disease by promoting angiogenesis; apelin also counteracts Ang II by up-regulate ACE2 and mediates Ang II induced ACE2 up-regulation. In a separate group of studies, we confirmed that ACE2 degrades Apelin *in vivo* with significant functional changes. All these results added to the understanding of how ACE2 and apelin maintain the homeostasis of the cardiovascular system and the involvement in diseases conditions. Finally, we designed and tested apelin analogues; the results showing the potential of apelin, especially apelin analogues with C-terminal active and protected from ACE2 hydrolysis, as a new target for treating cardiovascular disease.

Preface

Cardiac tissue from patients with end stage heart failure due to idiopathic dilated cardiomyopathy was studied as part of the Human Explanted Heart Program (HELP) at the Mazankowski Alberta Heart Institute. All patients underwent cardiac transplantation. Non-failing human hearts were collected as part of the Human Organ Procurement and Exchange (HOPE) program for research. All experiments were performed in accordance with the institutional guidelines and were approved by Institutional Ethics Committee. Informed consent was obtained from all study subjects.

The research projects in the current thesis are mainly performed in Dr. Gavin Oudit lab. Parts of the work were done in collaboration with Dr. Zam Kassiri, Dr. John Vederas and Dr. Allan Murray laboratories. More specific contributions of each particular experimental operation, data analysis and experimental design are elaborated in the beginning of each chapters.

ACKNOWLEDGEMENTS

I would like to express my gratitude to Dr. Gavin Y. Oudit. As my supervisor, Dr. Oudit continuously supported my Ph.D. study and research. His guidance helped me in all the time of research, oral presenting skills and writing of scientific literature including this thesis. Besides my supervisor, I would like to thank the rest of my thesis committee: Prof. Zamaneh Kassiri, Prof. John Seubert, Prof. Gary Lopaschuk, Prof. Gregory D. Funk and Prof. Edward R.M. O'Brien for their insightful comments and advice. My sincere thanks also goes to Dr. John Vederas, Dr. Alan Murray and Dr. Zamaneh Kassiri, who provided me opportunities to collaborate with their labs, and who gave insights into research projects and access to the experimental resources. Without their support, studies presented in this thesis would be of much less weight. I thank all my fellow lab mates, for the help in experimental operations. I would also thank my wife Yushan Feng, my mother Zuohui Zhou, my father Pinquan Wang and my daughter Runxi Wang for the support they provided me through my entire life.

This research would not have been possible without the financial assistance of Mazankowski Graduate Studentship, Motyl Graduate Studentship, 75th Anniversary Graduate Student Award from Faculty of Medicine & Dentistry as well as CIHR operating grant under Dr. Oudit.

TABLE OF CONTENTS

LIST OF FIGURES

LIST OF TABLES

LIST OF ABBREVIATION

A	atrial transmitral filling wave
A.U.	arbitrary unit
$[\alpha_D]^{26}$	specific rotation at 26 °C
AAA	abdominal aorta aneurysm
Abz	2-aminobenzoic acid, anthranilic acid
AC	adenylate cyclase
Ac	acetyl
ACE	angiotensin-converting enzyme
ACE2	angiotensin-converting enzyme 2
ACEi	angiotensin-converting enzyme inhibitor
Acpc	1-aminocyclopropane carboxylic acid
AEBSF	4-(2-aminoethyl) benzenesulfonyl fluoride
Aib	2-aminoisobutyric acid
Akt	protein kinase B
Ala, A	alanine
All	allyl
Alloc	allyloxycarbonyl
AMC	7-amino-4-methylcoumarin
AMP	adenosine monophosphate
ANF	atrial natriuretic factor
Ang	angiotensin
Ang II	Angiotensin II
Ang-1	angiopoeitin-1
Ang-2	angiopoetin-2
APJ	apelin receptor
APLN	Apelin

Ar	aryl
ARB	Ang II type 1 receptor blocker
Arg, R	arginine
Asn, N	asparagine
ASP	ammonium sulfate pellet
Asp, D	aspartic acid
AT_1	angiotensin II receptor, type 1
AT1R	angiotensin type 1 (AT1) receptor
ATP	adenosine triphosphate
BHT	butylated hydroxytoluene
Bn	benzyl
BNP	brain natriuretic peptide
Boc	*tert*-butyloxycarbonyl
BPB	2-[N-(N'benzylprolyl)amino]benzophenone
br	broad
Bu	butyl
c	concentration
cAMP	cyclic adenosine monophosphate
Cbz	carboxybenzyl
CD	circular dichroism
CDI	1,1'-carbonyldiimidazole
Cha	cyclohexylalanine
CHES	N-cyclohexyl-2-aminoethanesulfonic acid
CK	creatine kinase
C-terminus	carboxy terminus
Cys, C	cysteine
δ	chemical shift

DAP	diaminopimelic acid
DBU	1,8-diazabicyclo[5.4.0]undec-7-ene
DCC	N,N'-dicyclohexylcarbodiimide
DCE	1,2-dichloroethane
DCM	dilated cardiomyopathy
Dha	dehydroalanine
Dhb	dehydrobutyrine
DHE	Dihydroethidium
DIC	N,N'-diisopropylcarbodiimide
DIPEA	N,N-diisopropylethylamine
DM I	Diabetes Mellitus Type I
DM II	Diabetes Mellitus Type II
DMAP	4-dimethylaminopyridine
DMF	dimethylformamide
DMSO	dimethylsulfoxide
dP/dt	change in pressure over change in time
DSS	2,2-dimethyl-2-silapentane-5-sulfonic acid
DTT	dithiothreitol
E	early transmitral filling wave;
E'	early tissue Doppler velocity.
EDTA	ethylenediaminetetraacetic acid
EF	ejection fraction and
EI	electron ionization
EIC	extracted ion chromatogram
eNOS	endothelial nitric oxide synthase
ER	endoplasmic reticulum
ERK	extracellular-signal-regulated kinases

ESI, ES	electrospray ionization
Et	ethyl
ET-1	endothelin-1
FFPE	formalin fixed paraffin embedded
Fmoc	9*H*-fluorenylmethyloxycarbonyl
Fmoc-Osu	9*H*-fluorenylmethylsuccinimidyl carbonate
FRET	Förstner resonance energy transfer
FS	fractional shortening;
FTICR	Fourier-transform ion cyclotron resonance
Gln, E	glutamic acid
Gln, Q	glutamine
Gly, G	glycine
GPCR	G-protein coupled receptor
GPCR	G protein-coupled receptor
GTP	guanosine triphosphate
HATU	O-(7-Aza-1H-benzotriazol-1-yl)-N,N,N'N'-tetramethyluronium hexafluorophosphate
HBSS	Hank's balanced salt solution
HBTU	O-(1H-benzotriazol-1-yl)-N,N,N'N'-tetramethyluronium hexafluorophosphate
HCCA	α–χψανο–4–ηψδροξψχιννναμιχ αχιδ
HCF	human cardiac fibroblasts
hEPCs	endothelial progenitor cells
HF	Heart Failure
HIF-1α	hypoxia inducible factor-1 alpha
His, H	histidine
HIV	human immunodeficiency virus
HMWK	high molecular weight kininogen

HOAt	1-hydroxy-7-azabenzotriazole
HOBt	1-hydroxybenzotriazole
HPLC	high performance liquid chromatography
HPLC	high performance liquid chromatography
HRMS	high resolution mass spectrometry
HUVECs	Human umbilical vein endothelial cells
HW	Heart weight
I/R	ischemia-reperfusion
IA	iodoacetamide
IB	immunoblotting
IC_{50}	half maximal inhibitory concentration
IGF	Insulin-like Growth Factor
Ile, I	isoleucine
Inf	Infarct Region
Inp	isonipecotic acid, 4-piperidine carboxylic acid
IR	infrared
J	coupling constant
KAHA	α−κετοαχιδ ηψδροξψλαμινε
k_{cat}	turnover number
kDa	kilodalton
KLK1	kallikrein 1, tissue kallikrein, kidney/pancreas/salivary gland kallikrein
KLKB1	plasma kallikrein
K_m	Michaelis constant
KO	knockout
LAD	left anterior descending
LC-MS/MS	liquid chromatography-tandem mass spectrometry
Leu, L	leucine

LV	left ventricular
LVEDD	LV end-diastolic dimension
LVW	left ventricular weight
Lys, K	lysine
MABP	mean arterial blood pressure
MALDI-TOF	matrix-assisted laser desorption ionization time of flight
MAPK	mitogen activated protein kinase
Mas R	Ang-(1-7) receptor
Me	methyl
MES	2-(N-morpholino)ethanesulfonic acid
Met, M	methionine
MI	myocardial infarction
mmHg	millimeters of mercury
MMPs	matrix metalloproteinases
mol	mole
MQ	Milli-Q water filtration system
mRNA	messenger ribonucleic acid
MRS	de Man Rogosa and Sharpe
MRSA	methicillin-resistant *Staphylococcus aureus*
Ms	methanesulfonyl
MS	mass spectrometry
mTOR	mechanistic target of rapamycin
MWCO	molecular weight cut off
NA	noradrenaline
NADPH	Nicotinamide adenine dinucleotide phosphate
Nal	naphthyl
NCL	native chemical ligation

NEP	neutral-endopeptidase
NFAT	nuclear factor of activated T cells
NFC	non-failing control
NFC	non-failing control
Nle	norleucine
NMM	N-methylmorpholine
NMR	nuclear magnetic resonance
NO	nitric oxide
NO	nitric oxide
NO_2Y	3-nitrotyrosine
NOE	nuclear Overhauser effect
NOESY	nuclear Overhauser effect spectroscopy
Non	Non-Infarct Region
NRPS	non-ribosomal peptide synthetase
N-terminus	amino terminus
Orn	ornithine
PAH	Pulmonary arterial hypertension
PaMH	Pathological Myocardial Hypertrophy
Pbf	2,2,4,6,7-pentamethyldihydrobenzofuran-5-sulfonyl
p-BrPhe	*para*-bromophenylalanine
PCSK3	proprotein convertase subtilisin/kexin 3, furin
PE	phenylephrine
PEG	polyethylene glycol
PEP	prolyl-endopeptidase
Peri	Peri-Infarct Region
pGlu, pE	pyroglutamic acid
Phe	phenylalanine

Phe, F	phenylalanine
PhMH	Physiological Myocardial Hypertrophy
PI	Propidium iodide
pI	isoelectric point
PI3K	phosphoinositide 3-kinase
PKA	protein kinase A
PKC	protein kinase C
PLCb	1-phosphatidylinositol-4,5-bisphosphate phosphodiesterase b
Pmc	2,2,5,7,8-pentamethylchroman-6-sulfonyl
PMSF	phenylmethylsulfonyl fluoride
*p*NB	*para*-nitrobenzyl
*p*NZ	*para*-nitrobenzyloxycarbonyl
PP_{II}	polyproline II helix
ppm	parts per million
Pr	propyl
Pro, P	proline
PSR	picrosirius red
p-Ts	*para*-toluenesulfonyl
PyBOP	benzotriazole-1-yl-oxytrispyrrolidinophosphonium hexafluorophosphate
Q-sepharose	quaternary ammonium strong anion exchange resin
R.E.	relative expression
RAS	renin-angiotensin system
RCM	ring-closing metathesis
R_f	retention factor
rh	recombinant human
ROESY	rotating frame nuclear Overhauser effect spectroscopy
ROS	reactive oxygen species

RP	reversed phase
RTK	receptor tyrosine kinase
RV	right ventricle
RVLM	rostral ventrolateral medulla
SAR	structure activity relationship
Ser, S	serine
SERCA	sarco/endoplasmic reticulum Ca^{2+}-ATPase
SHR	spontaneous hypertensive rat
S_N2	bimolecular nucleophilic substitution
SPPS	solid phase peptide synthesis
SP-sepharose	sulfopropyl strong cation exchange resin
TAC	transverse aortic constriction
tBu	*tertiary*-butyl
TCEP	tris(2-carboxyethyl)phosphine
TEMPO	2,2,6,6-tetramethyl-1-piperidine 1-oxyl
Tf	trifluoromethanesulfonyl
TFA	trifluoroacetic acid
TGFβ1	transforming growth factor beta1
THF	tetrahydrofuran
Thr, T	threonine
TIPS	triisopropylsilane
TL	tibial length
TLC	thin layer chromatography
TOCSY	total correlation spectroscopy
Tris	tris(hydroxylmethyl)aminomethane
Trp, W	tryptophan
Trt	trityl

TTC	Tetrazolium Chloride
TUNEL	Transferase dUTP nick end labeling
Tyr, Y	tyrosine
UV	ultraviolet
v/v	volume per volume
Val, V	valine
VCFC	velocity of circumferential shortening corrected for heart rate
VEGF	vascular endothelial growth factor
V_{max}	enzyme maximum rate
VRE	vancomycin-resistant *Enterococci*
VSMCs	vascular smooth muscle cells
WMSI	wall motion score index
WT	Wildtype
α-SkA	alpha-skeletal actin
α-SMA	alpha-smooth muscle actin

CHAPTER ONE

LITERATURE REVIEW: ROLES OF ACE2 AND APELIN IN THE CARDIOVASCULAR SYSTEM

1.1 Cardiovascular Hypertrophy

Tissues and organs of the human body are subject to the remodeling influences upon functional demands. Hypertrophy and hyperplasia are two basic types of remodeling. Hyperplasia is different from hypertrophy in that the change in hypertrophy is an increase in the size of cells, whereas hyperplasia involves an increase in the number of cells.[1]

1.1.1 Pathological and physiological myocardial hypertrophy. Pathological Myocardial Hypertrophy (PaMH) refers to an increase in the heart weight and size with associated cardiac diastolic or systolic dysfunction driven at a cellular level by a combination of cardiomyocyte hypertrophy, cardiomyocyte apoptosis, cardiomyofibroblast proliferation, and adverse interstitial and peri-vascular fibrosis;[2-4] PaMH is a poor prognostic sign and is associated with nearly all forms of heart failure.[5] The etiology of PaMH is complex and not fully defined, but involves aberrances in hemodynamic,[2, 3, 6-9] neurohumoral physiology[10] and can also be caused by genetic defects.[11-13] In the Framingham Heart Study, echocardiographic left ventricular hypertrophy was found to be present in 15% of

the population and was independently associated with several cardiovascular endpoints, including coronary heart disease and stroke.[14]

Myocardial hypertrophy secondary to exercise is a striking exception to the association between hypertrophy and incidence of heart failure.[15, 16] Because of the favorable outcomes of exercised induced hypertrophy (it also exists during pregnancy and cardiovascular development), it is termed Physiological Myocardial Hypertrophy (PhMH). The benefits of exercise are multifactorial, including reduction of adipocyte mass and body mass index as well as positively affecting insulin sensitivity, glucose uptake by skeletal muscle, and cholesterol profiles.[17] Exercise has also been associated with beneficial changes in both the systemic and coronary vasculature, including enhanced endothelial-mediated vasodilation, improved arterial compliance, and reductions in systolic and coronary blood pressure.[18, 19] Moreover, the cardiac associated changes in physiological hypertrophy include: (a) improved cardiomyocyte Ca^{2+} sensitivity and contractility[20] with increased sarco/endoplasmic reticulum Ca^{2+}-ATPase (SERCA) activity[21] and preserved t-tubule density and structure;[22] (b) increased coronary blood flow and oxygen extraction, as well as improved endothelial function;[23] (c) preserved energy consumption and homeostasis in physiological cardiac remodeling;[24, 25] (d) endurance exercise of mice induces cardiomyocyte proliferation.[26]

1.1.2 Molecular signaling pathways in physiological and pathological hypertrophy

Although PaMH and PhMH share a common feature – increased heart size, they have a significantly different physio-pathological status, which can be related to the activation of distinct cellular signaling pathways. To date, the best characterized pathway responsible for pathological hypertrophy is through G-protein coupled receptor GPCR-Gαq mediated pathway[27-29]. In this pathway, pathological stimulus *e.g.* chronic pressure overload or volume overload lead to the secretion of Angiotensin II (Ang II), endothelin-1 (ET-1) or noradrenaline (NA), which activate their GPCR receptor which binds to Gαq and subsequently active mitogen activated protein kinase (MAPK) or nuclear factor of activated T cells (NFAT) leading to pathological hypertrophy. However, for physiological hypertrophy, growth factors *e.g.* Insulin-like Growth Factor (IGF) mediated by receptor tyrosine kinase (RTK) and subsequent post receptor signal transduction (PI3K-Akt) lead to physiological hypertrophy. Also, exercise has been shown to improve endothelial function by eNOS mediated production of NO[30] as well as up-regulation in Sirt1, Sirt3, AMPK, PGC-1α and HIF-1α,[31] which lead to physiological hypertrophy with coordinated myocardial angiogenesis.

1.1.3 Angiogenesis in myocardial hypertrophy

In the development of myocardial hypertrophy with increased heart mass and size as well as work load, promotion of angiogenesis is critical for sufficient supply of

blood to the myocardium.[32, 33] Vascular rarefaction in the setting of pathological hypertrophy may cause tissue hypoxia and lead to contractile dysfunction. One prominent molecular mechanism responsible for coronary angiogenesis is the PI3K-Akt pathway, which may act locally through cardiomyocyte-PI3K-Akt-VEGF centred signaling,[34, 35] or by recruiting endothelial progenitor cells;[34] the Apelin-APLNR (Apelin receptor or called APJ) axis has been associated with both of these processes.[36] These pathways are down-regulated in pathological myocardial hypertrophy while up-regulated in physiological hypertrophy. Exercise can also increase angiogenesis by a PGC-1α-VEGF pathway independent of HIF-1α[37].

There is evidence that coronary angiogenesis is enhanced during the acute phase of adaptive cardiac growth but reduced as hearts undergo pathological remodeling. Both heart size and cardiac function are angiogenesis dependent, and disruption of angiogenesis in coordination with tissue growth in the heart may contribute to the progression from adaptive cardiac hypertrophy to heart failure.[32] Also, enhancement of angiogenesis in patients with PaMH may help preserve cardiac function and improve prognosis.

1.1.4 Manipulating angiogenesis in myocardial hypertrophy by targeting apelin-APJ axis.

Apelin is the endogenous ligand for the APJ (putative receptor protein related to AT1)[38] receptor and is synthesized as a 77-amio acid prepropeptide which is processed into C-terminal fragments denoted by their lengths as Apelin-36, Apelin-19, Apelin-17 and Apelin-13.[39, 40]

Apelin is predominantly expressed in the endocardial and vascular endothelial cells while the APJ receptor is localized to endothelial and smooth muscle cells as well as cardiomyocytes, allowing for autocrine and paracrine effects of apelin in the heart.[40-42] Apelin mediates a positive inotropic effect on isolated cardiomyocytes,[43] isolated perfused[44] and *in vivo*[45] rat hearts, and mediates endothelium-dependent vasodilation.[46] Genetic variation in the APJ receptor modifies the progression of heart failure in patients with dilated cardiomyopathy[47] and the apelin/APJ system is compromised in human heart failure.[41, 48] In patients with chronic heart failure, apelin administration increased cardiac index and lowered peripheral vascular resistance in the absence of hypotension, providing a promising new drug target for heart failure.[49]

Apelin-APJ also has shown effects in angiogenesis as demonstrated by promoting endothelial cell proliferating and regulating caliber size and permeability of neovessels.[50] Germ line knock out apelin in mice showed

decreased angiogenesis in embryos;[51] particularly the study showed loss of apelin caused narrow blood vessels in intersomitic vessels during embryogenesis and apelin treatment enhanced endothelial cell proliferation in the presence of vascular endothelial growth factor (VEGF) and promoted cell-to-cell aggregation. A recent study reported apelin's role as a chemoattractant for circulating APJ^+ stem cells during early myocardial repair, providing myocardial protection against ischemic damage by improving neovascularization via paracine action.[36]

1.2 Biochemical aspects of ACE2, apelin and APJ

1.2.1 Biochemical aspects of ACE2

ACE2 (Angiotensin Converting Enzyme 2) is homologous to ACE (Angiotensin Converting Enzyme) and both works as carboxypeptidase.[52] ACE2 contains 805 amino acids, which include an N-terminal signal sequence, a single active-site catalytic region, a hydrophobic membrane-anchor region and a C-terminal cytoplasmic domain.[53] ACE2 removes a single amino acid from the C-terminus of its substrates, since it possesses only one site in the C-terminus portion of the enzyme and functions as a monocarboxypeptidase. In comparison, the somatic ACE has two active-site domains containing the prototypical zinc-binding HEXXH motif. The catalytic domains of the two enzymes share a single anion binding site mediating the anion-dependent activation observed in both ACE and ACE2; however, ACE2 is insensitive to classical ACE inhibitors.[53, 54] Although

ACE2 is a plasma membrane-bound ectoenzyme, a soluble form of this enzyme is also found in plasma and urine;[55] Tumor necrosis factor alpha converting enzyme (TACE/ADAM17) is the sheddase responsible for the ectodomain cleavage and shedding of membrane ACE2.[56, 57] Although the soluble ACE2 remains active, this shedding process may change the local ACE2 expression and RAS balance, and shedding may be considered as degrading pathway of ACE2. As a carboxymonopeptidase ACE2 functions predominantly with a substrate preference for hydrolysis between proline and a hydrophobic or basic C-terminal residue.[58]

1.2.2 Biochemical aspects of apelin and APJ

Apelin was identified for the first time as a 36-amino acid peptide in 1998 by Tatemoto and colleagues and termed after **APJ** **e**ndogenous **li**ga**n**d.[39] The human, rat and mouse gene encoding apelin, termed *APLN* or *Apln* is located on chromosome Xq25–26.1, Xq35 or XA3.2 respectively.[59] Apelin is widely expressed in various organs as a 77 amino acid pre-proapelin. Pre-proapelin precursors of Bovine, human, rat and mouse have 76-95% homology[60] and exist as a dimeric protein, as a consequence of disulphide bridges formed between cysteine residues.[61] While the 23 C-terminal amino acids have 100% homology between species.[61] Several active fragments of apelin have been known (apelin-36, apelin-19, apelin-17, apelin-16, apelin-13 and apelin-12).

Angiotensin Converting Enzyme 2 (ACE2), which catalyses the C-terminal peptide cleavage of Ang II to Ang 1–7, also hydrolyzes apelins at C-terminal phenylalanine (Phe) at high catalytic efficiency.[58] The C-terminal Phe cleavage of apelins is a deactivating process based on our data that shows decreased hypotensive as well as NO generating effects. Meanwhile, apelins that lack the C-terminal have been shown to be ineffective at inducing receptor internalisation or regulating blood pressure but retain the capability to bind to APJ and inhibit forskolin-stimulated cAMP production.[62, 63]

APJ was identified in 1993 by O'Dowd and colleagues[38] as an orphan GPCR without an endogenous ligand. As a typical GPCR, it contains seven hydrophobic transmembrane domains, with consensus sites for phosphorylation by protein kinase A (PKA), palmitoylation and glycosylation.[38] Different fragments of apelin regulate the same effectors, via the preferential coupling of the apelin receptor to G_{i1} or G_{i2}, but they promote a differential desensitization pattern that may be central to their respective physiological roles.[64] The internalized APJ molecules were recycled to the cell surface within 60 min after removal of Apelin-13, but most of the internalized APJ still remained in the cytoplasm, even 2 hours after washout of Apelin-36[65], suggesting diversiform responses to ligand apelins binding. APJ also could be activated by stretching, which in heart increases cardiomyocytes cell size and induces molecular markers of hypertrophy.[66] Although

apelin stimulates APJ to activate Gαi, stretch signals in an APJ-dependent, G-protein-independent fashion.[66] APJ distribution in cardiovascular tissues indicates APJ to be present in ventricular cardiomyocytes, vascular smooth muscle cells (VSMCs) and intramyocardial endothelial cells[67].

1.3 Inter-regulation of AngII, ACE2 and Apelin

ACE2 regulates Ang II and Apelin: ACE2 hydrolyzes Angiotensin II (Ang II) with high catalytic efficiency: Ang II (k_{cat}/K_m = 1.9 x 10^6 M^{-1} s^{-1}) and hydrolyzes apelin-13 (k_{cat}/K_m = 2.1 x 10^6 M^{-1} s^{-1})[58], indicating both Ang II and apelin are efficient substrate of ACE2 *in vitro*[68]. In Chapter 4, *in vivo* study in wild-type versus ACE-2 knock-out mice or mice with ACE2 pharmaceutical knock down, results showed apelin is likely a physiological substrate of ACE2 *in vivo* with significant pathophysiological implications.

Ang II regulates ACE2: It has been reported that Ang II regulates the expression of ACE2 by increasing or decreasing in different cell type and experimental systems. In cultured neonatal rat cerebellar or medullary astrocytes, Ang II caused reduced ACE2 mRNA and protein by 60% and 50% respectively[69]. This regulation was blocked by the angiotensin type 1 (AT1) receptor antagonist losartan or valsartan, but not the angiotensin type 2 (AT2) antagonist

PD123319.[69] Similarly, in cultured human kidney tubular cells, Ang II was able to down-regulate ACE2 mRNA and protein, which is blocked by angiotensin II (AT1) receptor antagonist (losartan), but not by an AT2 receptor blocker (PD123319).[70] Furthermore, aortic ACE2 protein was reportedly reduced in WT mice in response to Ang II[71], where aortic smooth muscle cells as the main cell type. Meanwhile, a different study using similar experimental settings reported that AngII dramatically increased ACE2 mRNA and protein expression as well as ACE2 activity in the aorta.[72] In primary neonatal rat cardiomyocytes, Angiotensin II was reported had no effect on ACE2 mRNA level.[73] Another study showed Ang II infusion in wild-type mice resulted in substantial decrease in myocardial ACE2 protein levels and activity with corresponding increase in plasma ACE2 activity, by promoting TNF-α converting enzyme (TACE) activity.[57] On the contrary, in cultured human cardiac fibroblasts (HCF), Ang II upregulates ACE2 expression. This action is modulated through activation of Ang II type 1 receptor (AT1R).[74]

AngII regulates Apelin expression: Preliminary data from our group showed that Angiotensin II upregulated apelin protein expression by a large scale (3 times increase) in Ang II treated mouse aortas. The mechanism behind this regulation is not clear and needs to be studied in the future.

Apelin regulates ACE2 expression: Apelin, via activation of its receptor, APJ, increased ACE2 promoter activity *in vitro* and upregulated ACE2 expression in failing hearts *in vivo*. [75] We also observed about 60% decreased ACE2 in *Apln* KO mouse aortas and a limited increase of ACE2 upon Ang II treatment in *Apln* KO mouse aorta, suggesting Ang II induced ACE2 up-regulation may be partly Apelin dependent.

These regulatory relationships are summarized in **Table 1.1**. ACE2 couples the RAS to the apelin system; and besides their own physiological roles, Ang II, ACE2 and Apelin heavily inter-regulate each other and pose important roles in cardiovascular system homeostasis.

Table 1.1 Inter-regulation among Ang II, Apelin and ACE2.

Regulation	Experimental brief/References
Ang II up regulates ACE2	• Ang II treatment in cultured neonatal rat cerebellar or medullary astrocytes[69]; • Ang II treatment WT mice *in vivo*, aortic ACE2 protein assessment[72]; • Ang II treatment in cultured HCF[74].
Ang II down regulates ACE2	• Ang II treatment in cultured human kidney tubular cells[70]; • Ang II treatment WT mice in vivo, aortic ACE2 protein assessment[71]; • Ang II infusion in WT mice myocardial ACE2 protein assessment[57].
ACE2 down regulates Ang II	• Enzymatic kinetics *in vitro*[58]; • Ang II treatment in WT or ACE2 KO mice, myocardial Ang II assessment[68].
ACE2 down regulates Apelin	• ACE2 hydrolyzed Apelin *in vitro* and *in vivo* (Data submitted).
Apelin up regulates ACE2	• Apelin increased ACE2 promoter activity *in vitro*; upregulated ACE2 expression in failing hearts *in vivo*[75]; • Decreased ACE2 in *Apln* KO mouse aorta (Data shown in Chapter 6).
Ang II up regulates Apelin	• Ang II upregulated apelin protein expression *in vivo* (Data shown in Chapter 6).

1.4 ACE2 in heart failure and vascular disease

ACE2 can cleave Ang II to generate Ang 1-7. The ACE2/Ang 1-7/Mas axis is an endogenous counter-regulatory pathway within the RAS and its genetic and pharmacological manipulation offers the chance to use endogenous mechanisms to prevent and treat heart failure **(Figure 1.1)**. ACE2 mRNA is present in virtually

all organs, and ACE2, as an endothelium-bound carboxypeptidase, is widely expressed in cardiovascular and non-cardiovascular tissues,[76-78] including the heart, kidney, brain, and vasculature. Specifically in the heart, ACE2 is expressed in the various cellular compartments including the coronary microcirculation[54], cardiofibroblasts and cardiomyocytes.[68, 79] ACE2 is also expressed in vascular smooth muscle cells of the intrarenal arteries and coronary blood vessels.[54]

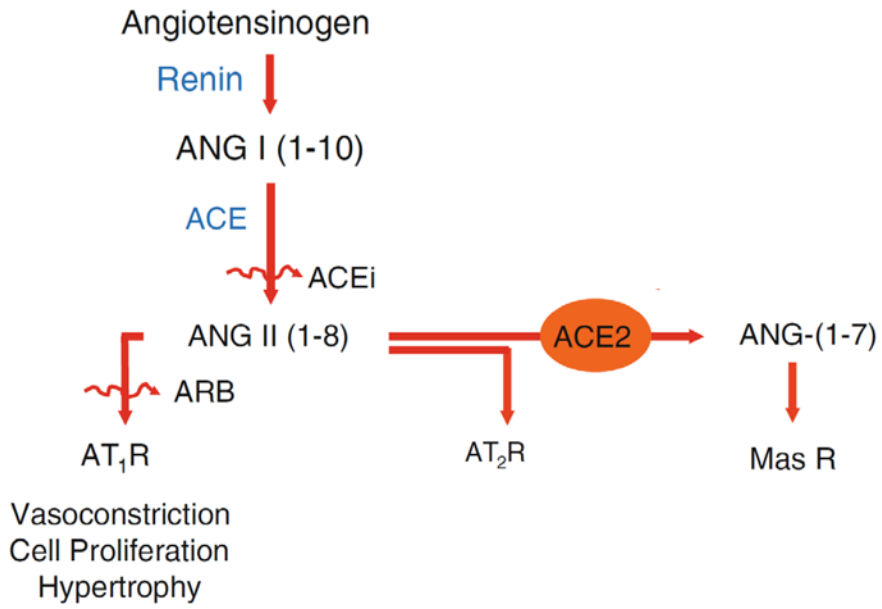

Figure 1.1 Schematic view of the renin-angiotensin system cascade and the role of ACE2. The ACE2-Ang-(1-7)-Mas axis finely balances the actions of the ACE-Ang II-AT1 receptor arm of the RAS. ACE, angiotensin-converting enzyme; PEP, prolyl-endopeptidase; NEP, neutral-endopeptidase 24.11; ACEi, angiotensin-converting enzyme inhibitor; Ang, angiotensin; ARB, Ang II type 1 receptor blocker; AT1R, Ang II type 1 receptor; AT2R, Ang II type 2 receptor; Mas R, Ang-(1-7) receptor. (Figure 1.1 is adapted from Fig 4. Of *Role of ACE2 in diastolic and systolic heart failure*[80]).

ACE2 expression is highly regulated by many pathological stimuli as documented in experimental animal disease models as well as in human disease samples. For example, in failing human heart ventricles, ACE2 protein and activity are significantly increased, resulting in increased Ang (1-7) production resulting from Ang II cleavage.[81, 82] These regulations and their relevance in the establishment and development of cardiovascular diseases showed that ACE2 is highly involved in the pathophysiological processes of the cardiovascular system.

ACE2 functions as a key enzyme catalyzing Ang II to produce Ang 1-7 by cleavage of the C-terminal amino acid. In the classic pathway of the renin angiotensin system (RAS), Ang II is the central effector in RAS as a potent regulator of fluid volumes, blood pressure and cardiovascular remodeling by binding to its receptor (AT_1R).

The RAS is a major regulator of blood pressure homeostasis and atherosclerosis, two major risk factors for cardiovascular disease and heart failure.[83] Ang II plays a key role in the progression of atherosclerosis and ACE2 is an important negative regulator of atherosclerosis. The etiology of essential hypertension is multi-factorial, consisting of both environmental and genetic modulators acting in concert.[84] The in vitro biochemical activity of ACE2 supports its role as a potential regulator of blood pressure homeostasis, via its modulation of the RAS as well as other regulatory peptide pathways.[53, 54, 58, 84]

The potential role of ACE2 in essential hypertension is supported by earlier studies showing that ACE2 maps to QTL loci on the X-chromosome, which contributes to hypertension in a salt-induced model of hypertension (Sabra rats), spontaneous hypertensive rat (SHR), and SHR-stroke-prone (SHRSP) rats.[85] In these models of hypertension, ACE2 mRNA and protein levels were greatly reduced in association with increased blood pressure.[85] Importantly, ACE2 suppresses the acute and chronic Ang II-induced hypertensive response in murine models.[68, 86] Based on in vitro biochemical data and in vivo findings, a reduction in ACE2 levels can lead to elevated Ang II levels, thus promoting increased blood pressure.[68, 86] Therefore, these genetic data argue for a pathophysiological role of ACE2 in hypertension in diet-induced and spontaneous hypertensive rat models. ACE2 immuno-reactivity was diffusely distributed in many cardiovascular regulatory neurons, including the rostral ventrolateral medulla (RVLM). Western blot analysis revealed a 40% decrease in ACE2 in the RVLM of spontaneously hypertensive rat compared with Wistar–Kyoto rats, while overexpression of ACE2 overcomes its intrinsic decrease in the RVLM and decreases high blood pressure in the spontaneously hypertensive rat.[87] Overexpression of ACE2 in the central nervous system modulates local Ang II/Ang-(1-7) levels, modulates autonomic function and attenuates neurogenic hypertension.[88] Overexpression of ACE2 in the vasculature reduces blood pressure and improves endothelial

function in hypertensive rats.[89] Indeed, loss of ACE2 accelerates endothelial dysfunction[90] and vascular inflammation and atherosclerosis in the ApoE knockout mouse model.[91] Overexpression of ACE2 inhibited the development of early atherosclerotic lesions by suppressing the growth of vascular smooth muscle cells and improving endothelial function,[89] suggesting that modulation of ACE2 could offer a therapeutic option for treating atherosclerosis.[92]

1.5 Apelin in heart failure and vascular disease

Apelin has direct biological effects including vasodilatory and inotropic effects.[93] Several previous studies have shown the cardioprotective effect of apelin in prevention of heart failure. Reduced circulating levels of apelin have been demonstrated in patients with essential hypertension.[94, 95] Genetic variation in apelin likely contributes to essential hypertension and to the onset of aged hypertension[96]. Taemoto *et al*. (2001) showed that arterial pressure after the administration of apelin-12, apelin-13 and apelin-36 at a dose of 10 nmol/kg resulted in a reduction in arterial blood pressure[97]. Cheng *et al*. (2003) examined dose response curves of apelin (10, 20 and 40 nmol/kg) in rats and concluded that apelin is an arterial and venous dilator in vivo[98]. Jepp *et al*. (2008) showed nitric oxide (NO)-dependent vasodilatory effect of apelin in 24 healthy volunteers in vivo.[99] However, the long-term effects of manipulating the apelin pathway and its effect on blood pressure are

unknown. Apelin/APJ is highly expressed in pulmonary vasculature.[67] Chandra *et al.* (2011) reported significantly lower serum apelin levels in patients with Pulmonary arterial hypertension (PAH) compared to control subjects.[100] Apelin expression also decreased in the pulmonary endothelial cells of patients with PAH[101]. It was shown that PAH in mice may originate from the disruption of apelin signaling which is mediated by decreased activation of adenosine monophosphate-activated protein kinase and endothelial synthase (eNOS).[100] Pyr-Apelin-13 treatment has been reported to down-regulate Ang II and endothelin-1 and could therefore attenuate right ventricle (RV) hypertrophy and diastolic dysfunction in rats with PAH[102]. Alastalo *et al*. (2011) have shown that apelin could have both autocrine and paracrine effects against PAH in pulmonary vasculature[101]. Bone morphogenetic protein-mediated apelin autocrine production results in enhanced pulmonary arterial endothelial survival, proliferation, and migration, which can protect the vasculature against PAH. Importantly, apelin autocrine function against PAH is based on attenuation of the pulmonary arterial smooth muscle cells response to growth factors and by promoting apoptosis[101].

Several studies have shown an association between apelin levels and overt diabetes [103]. Erdem *et al.* (2008) demonstrated that plasma apelin was lower in newly diagnosed and untreated patients with Diabetes Mellitus Type II (DM II) compared to healthy controls[104]. Soriguer *et al*. (2009) showed the association

between apelin levels and glucose concentrations and insulin sensitivity in diabetic patients suggesting the role of apelin in diabetes pathogenesis[105]. Furthermore, diabetic mice exhibited down regulation of apelin receptors and depressed aortic vascular tone[106]. However, Rittig *et al*. (2011) examined the association between apelin and atherosclerosis indicators (intima media thickness) in 344 subjects with an increased risk for DM II and did not show any association to diabetes risk pattern[107].

The effect of apelin in DM control has been shown in some animal studies. Intracerebroventricular injection of apelin in mice leads to improved glucose homeostasis via a NO dependent pathway [108]. Injection of apelin-13 (400 pmol/kg) for 10 weeks considerably reduced the pancreas endoplasmic reticulum (ER) stress in Akita mice, a model of Diabetes Mellitus Type I (DM I), which leads to modification of pancreatic islet mass reduction and preservation of insulin content[109]. This important effect of apelin-13 in type 1 diabetes mediated by inhibition of inositol requiring enzyme 1-α and JNK pathways indicate that these effects of apelin are mediated through the two important pathways of endoplasmic reticulum stress and cell death, respectively[109]. In mice with metabolic syndrome, apelin restores glucose tolerance and increases glucose utilization[110]. Apelin treatment has a favorable effect on vascular function in diabetic mice. Apelin treatment remarkably adjusts the abnormal aortic vascular reactivity in response to

Ang II and acetylcholine in DM II mice by increasing the phosphorylation of Akt and eNOS[106]. Apelin may improve the glycemic status and insulin sensitivity of the patients and also can ameliorate vascular functions of diabetic patients.

Plasma levels of apelin are inversely correlated to inflammatory markers (C-reactive protein and IL-6) in hemodialysis patients[111]. Apelin exerts acute anti-inflammatory effects on the vascular system; the results are promising and if these results can be extrapolated in chronic models, it can be a proper therapeutic modality for prevention of inflammation in the process of atherosclerosis. Apelin treatment in mice models of abdominal aorta aneurysm (AAA) clearly demonstrated its anti-inflammatory effects that could attenuate AAA formation[112]. Injected apelin can reduce the mRNA levels of pro-inflammatory markers (MCP-1, macrophage inflammatory protein-1α, IL6 and tumor necrosis factor-α)[112]. Apelin attenuates ultraviolet B-induced edema and inflammation in mice and plays an important role in stabilization of the tissue[113]. Pitkin *et al.* (2010) have shown an increase in apelin expression in atherosclerotic coronary arteries, with the additional peptide localizing to the atherosclerotic plaque[46]. The Apelin receptor was also found to be present within the atherosclerotic plaque and to have a similar distribution to its ligand[46]. Increased content of apelin and its receptor might be an indicator of increased anti-inflammatory activation of macrophages, thereby limiting plaque

instability. Due to lack of data and contradictory findings the exact role of apelin on atherosclerosis plaque remains inconclusive.

Apelin angiogenenic effects have been shown in a few animal studies. Tiani *et al.* (2009) showed the remarkable effect of apelin on portosystemic collateralization and splanchinc neovascularization in portal hypertensive rats[114]. Treatment of human umbilical vein endothelial cells with apelin dose-dependently augments angiogenic responses[115]. Kidoya *et al.* (2010) indicated that apelin together with Vascular Endothelial Growth Factor (VEGF) efficiently induced functional vessels larger than with VEGF alone, in the hind limb ischemia model of mice[50]. Apelin is a required factor for hypoxia-induced retinal angiogenesis in mice[116]. Available data imply that apelin is an effective factor in angiogenesis; however, none of the studies has been targeted coronary vessels to test the effect of apelin on their angiogenesis. If the effect of apelin on cardiac collateralization is proved in future studies, it can be considered as a valuable factor for the patients with Heart Failure (HF), in particular ischemic HF.

Decreased levels of apelin-36 at 5 days following ST-elevation MI have been reported.[117, 118]. Weir *et al.* (2009) also confirmed depressed level of apelin early after MI. They showed significant increase of apelin from base line to 24 weeks after MI[119]. None of these studies found any relation between apelin levels and left ventricular function.[117-119] Kadoglou *et al*. (2010) showed that both

groups of patients with unstable angina and acute MI had significantly lower level of apelin, however the patients with asymptomatic coronary artery disease[120]. The therapeutic effect of apelin in the management of patients with ACS has not been examined. Evaluation of apelin's role before and after acute events and its role in plaque stabilization is complicated in animals, as there is no model of unstable atherosclerotic plaque-induced ACS.

In the murine Langendorff model of I/R injury, apelin-13 increased Akt and ERK1/2 phosphorylation as well as increased Akt activity at 5 and 10 min reperfusion.[121] Activation of Akt and ERK1/2, two important members of the RISK pathway, can potentially protect the heart against I/R injury.[121] Administration of apelin can partly block the ER stress-dependent apoptosis activation in rat models of I/R injury at 2h of reperfusion, which resulted in protection against I/R injury[121]. This protection against I/R injury remained significant during time-related changes at 24 hours of reperfusion[121]. Administration of apelin (30 pM) in the Langendorff model of perfused isolated rat hearts favorably preserves the impaired cardiac function[122]. In rat cultured cardiomyocytes the antioxidant activity of apelin is thought largely due to inhibition of ROS production, malonaldehyde activity and lactate dehydrogenase leakage and also activation of superoxide dismutase.[122] Despite these positive results in animal models, apelin effects against I/R injury have not been tested in

humans. Application of apelin during the percutaneous coronary intervention and coronary artery bypass graft immediately and in early days after the procedure may have therapeutic benefits and reduce the incidence and severity of HF after I/R injury. Serum apelin levels are lower in the patients with Atrial fibrillation compared to controls.[123, 124] Low plasma apelin is an independent prognostic factor for arrhythmia recurrence in the patients with Atrial fibrillation under anti-arrhythmia medication[125]. Apelin, due to its effect on the propagation of action potential and contractility in cardiomyocytes, is thought to modulate the pathophysiology of Atrial fibrillation [126]. Apelin increases sarcomere shortening in normal as well as failing cardiomyocytes[126]. Moreover, apelin augments conduction velocity in monolayers of cultured neonatal rat cardiac myocytes[126]. According to our knowledge, the level of apelin has been investigated only in the patients with Atrial fibrillation and other forms of arrhythmia have not been investigated.

There is growing interest regarding the protective role of apelin in HF development. Apelin levels are considerably reduced in the patients with HF.[48, 127, 128] Several studies showed high expression of apelin/APJ in the heart and in vascular systems of rodents and humans.[44, 67, 128] The mechanisms by which apelin reduction causes HF are becoming clearer. Gao *et al* (2009) reported a significant increase of apelin as an indicator of improved cardiac function 3 to 21 days after

bone marrow mononuclear cell transplantation in the patients with HF through autocrine and paracrine mechanisms[127]. Apelin reduces left ventricular preload and afterload in rodents[129] and is known to be a strong positive inotropic agent [44-46] that could be therapeutic in the treatment of HF. Apelin knockout mice develop HF associated with aging and pressure overload[130]. Infusion of apelin-13[131] and apelin-12[132] enhances myocardial function of the left anterior descending artery ligation model of HF in rats. Perfusion of isolated rat hearts with apelin-16 caused an inotropic effect with a similar time course to endothelin-1.[44] Interestingly, apelin can present a gradually developing but sustained inotropic effect,[44] which is a significant difference compared to classical β-adrenergic effects. Apelin administration to the rats in ischemic HF significantly attenuates diastolic dysfunction.[45] The involvement of PLC, PKC, Na^+/H^+ and Na^+/Ca^{2+} pumps has been proved in positive inotropic effects of apelin.[43, 44, 133] The interaction between apelin and two important regulatory pumps has been proposed to be contributed to increased inotropic effects of apelin by restoration of calcium in the cardiomyocyte cytosol.

Japp *et al*. (2010) investigated the acute cardiovascular effect of intrabrachial infusion of Pyr-1-apelin-13 in the patients with chronic HF and healthy volunteers, and found that Pyr-1-apelin-13 caused vasodilatation in patients and control subjects[49]. Systemic infusions of Pyr-1-apelin-13 (30 to 300

nmol/min) results in elevated cardiac index, lowered mean arterial pressure and peripheral vascular resistance in HF patients and healthy control subjects.[49] An intracoronary bolus of apelin-36 leads to increased coronary blood flow and reduced peak and end-diastolic left ventricular pressures[49]. This remarkable peripheral and coronary vasodilatation effect of apelin, as well as its effect on cardiac output, shows the potential of apelin as a novel medication forpatients with HF. Decreased density of apelin receptors in the heart tissues with cardiomyopathy may block the inotropic effect of apelin on the heart[46]. However, showed increased APJ protein levels in myocardium of rats with HF[131].The APJ gene also has been suggested as a modifier gene for idiopathic dilated cardiomyopathy[47]. Further investigations should focus on combination of apelin therapy, possibly in combination with apelin receptor agonists. Synergistic effects of apelin with APJ agonists may increase the efficacy of apelin therapy for the patients with HF. Pitkin *et al*. (2010) suggested [Glp65,Nle75,Tyr77][125I]-apelin-13 as a potent agent with high affinity and reversible affect which might reflect its therapeutic efficacy in future [46].

The difference between APJ in myocardium and arterial system of the HF patients is not completely defined. Due to the dual ionotropic and hypotensive effects of apelin on the patients with HF we need to be cautious about the application of this agent in the clinical setting. Experimental evidence has

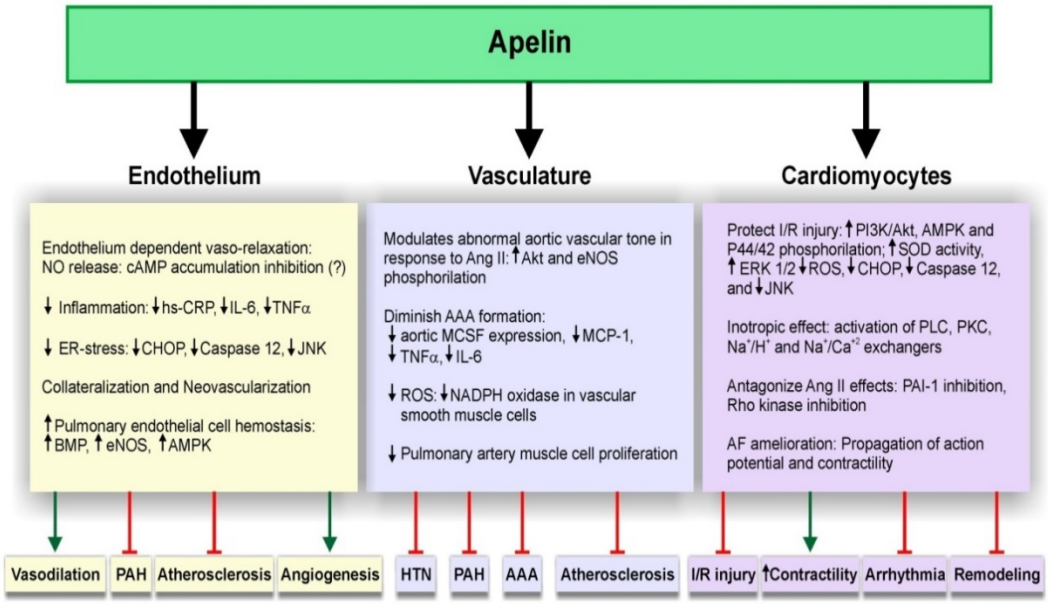

Figure 1.2 The diverse effects of apelin on the cardiovascular system. pGln=pyro-glutamyl residue; AAA: abdominal aorta aneurysm; AF: atrial fibrillation; Akt: protein kinase B; AMPK: adenosine monophosphate-activated protein kinase; BMP: bone morphogenetic protein; CHOP:CCAAT/enhancer binding protein homologous protein; eNOS: endothelial synthase; hs-CRP: high sensitivity C-reactive protein; ERK: extracellular signal-regulated kinase; I/R: ischemia reperfusion. (Figure 1.2 is adapted from Figure 2. of *Targeting the ACE2 and Apelin Pathways Are Novel Therapies for Heart Failure: Opportunities and Challenges*[138].)

established an association between Ang II and development of HF.[81, 134] Chun *et al.* (2008) proved that apelin signaling can antagonize Ang II actions in vascular disease by NO production and inhibiting Ang II cellular signaling[135]. Generally, apelin modulates Ang II-induced cardiovascular fibrosis[136] which may be linked to apelin's ability to inhibit the plasminogen activator inhibitor type-1 production resulting in secondary changes in the expression of matrix proteins and degrading

enzymes[136]. Apelin-13 inhibits Ang II-induced vascular contraction mainly through NO-dependent pathways[137]. The overall effects of the Apelin-APJ axis in cardiovascular system is summarized in (**Figure 1.2**).

1.6 Conclusions

Pharmacological therapies based on RAS blockade are used extensively for the treatment of hypertension and cardiovascular diseases including heart failure. However, in spite of their success in pharmacological blockade of the RAS, the prevalence of heart failure has risen steadily in the last several decades. These observations indicate that novel and innovative approaches are still needed for the treatment of heart failure. In this environment, ACE2 is an important target, since it is a multifunctional enzyme that is critical in tipping the balance of vasoconstrictive/proliferative to vasodilatory/antiproliferative axis of the RAS. Conceptually, the ACE2/Ang 1-7/Mas axis balances the adverse effects of the ACE-Ang II-AT1 receptor axis. On the other hand, aplein also showed its potential in treating cardiovascular diseases by maintaining physiological angiogenesis and counteracting hypertension, pathological hypertrophy, fibrosis and inflammation despite its relatively short plasma half-life *in vivo*.

1.7 Hypothesis and Objectives

We hypothesized that ACE2 and apelin would have cardioprotective effects against the development of heart failure resulting from several etiological origins including pressure overload, myocardial ischemia and elevated Ang II level.

The objectives of the current research project are 1) to study the impact of half decrease ACE2 level on the development of cardio hypertrophy and heart failure due to pressure overload or angiotensin II (Ang II); 2) to study how loss of apelin would affect the adaptive protective mechanism again myocardial ischemia and development of heart failure; 3) to study how loss of apelin would affect the myocardial angiogenesis response; 4) to study how ACE2, Ang II and apelin regulate each other *in vivo*; 5) to create apelin analogues to treat cardiovascular diseases.

CHAPTER TWO

Overview of Research Protocols

2.1 Use of Female ACE2 Heterozygote Mice

Protocol 1

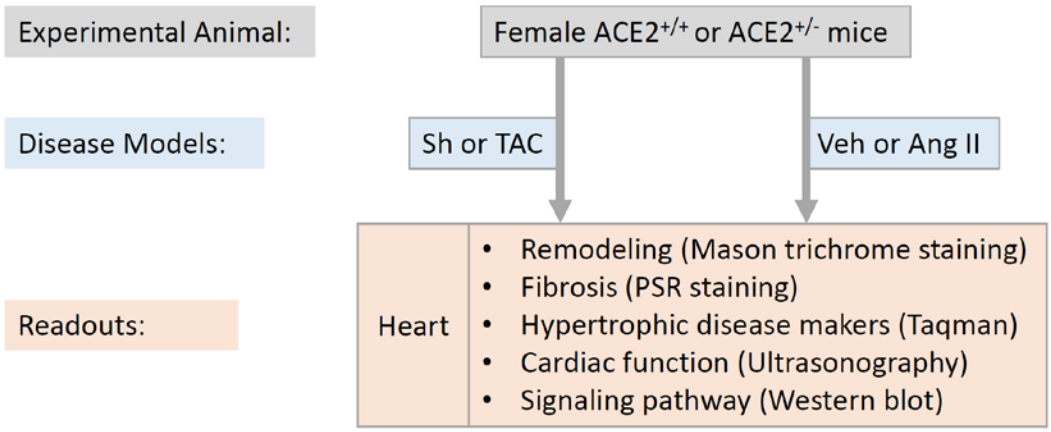

Sh: Sham; TAC: transverse aortic constriction; Veh: vehicle; Ang II: Angiotensin II; PSR: Picro Sirius Red.

Protocol 2

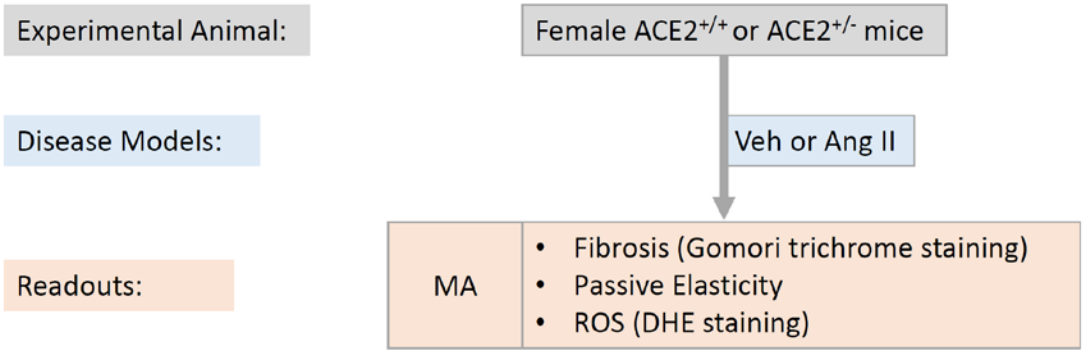

ROS: Reactive oxygen species; DHE: Dihydroethidium; MA: mesenteric artery.

2.2. ACE2 as a Proteolytic Enzyme for Apelin Peptides

Protocol 1

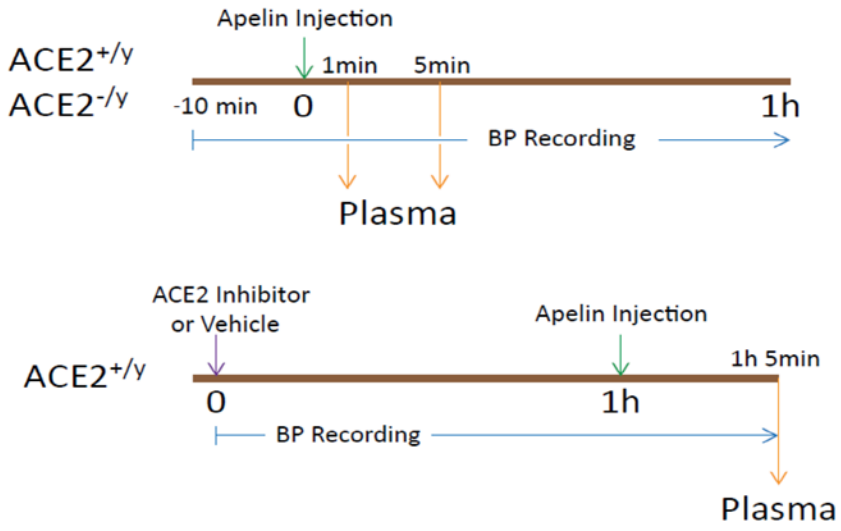

Protocol 2

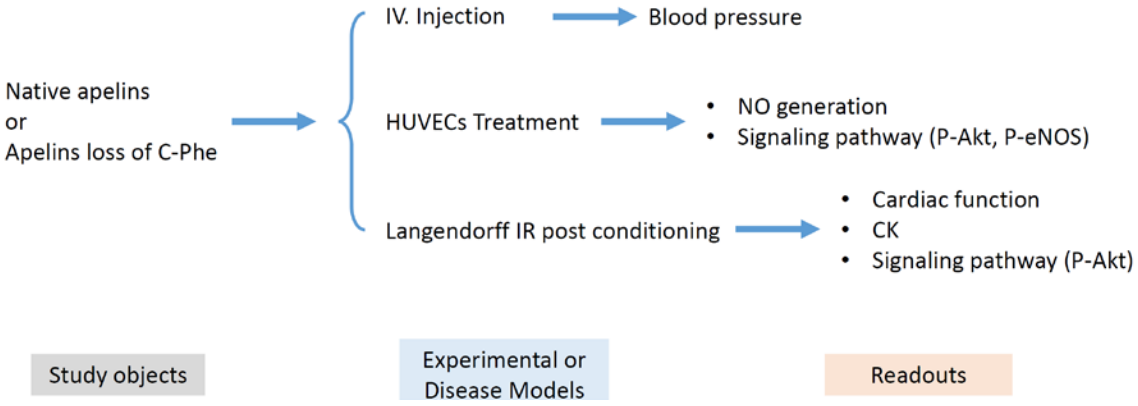

Protocol 3

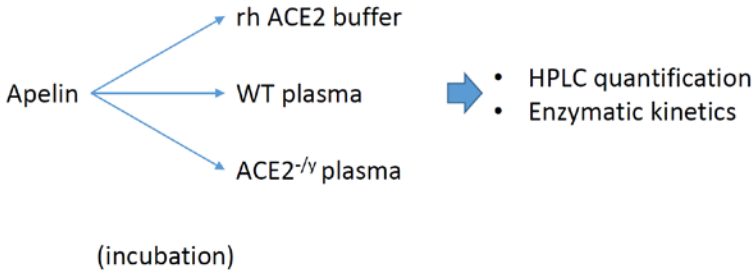

2.3 Use of Male Apelin Knockout Mice in Heart Disease

Protocol 1

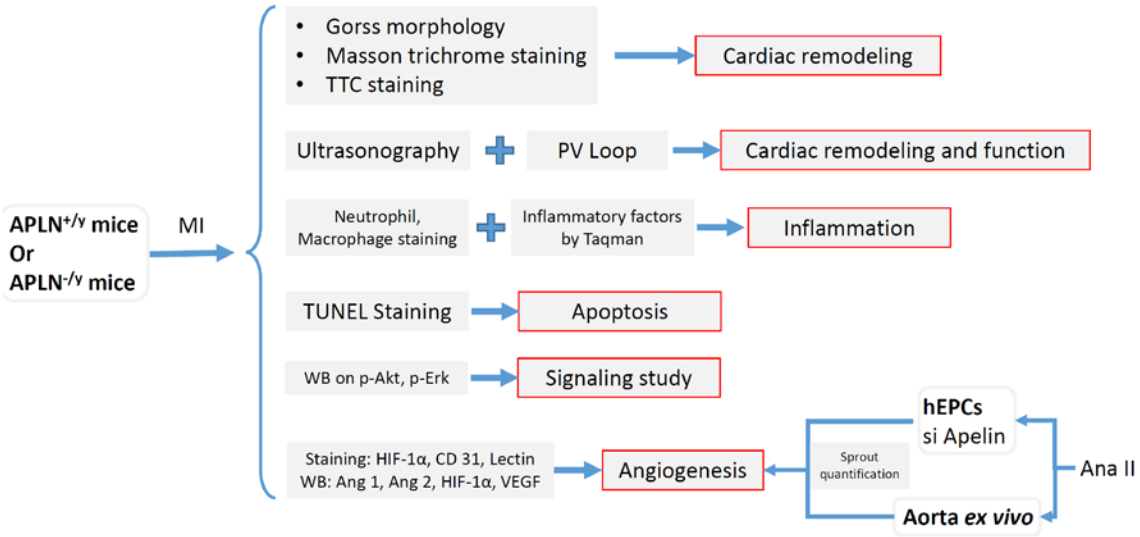

hEPCs: human endothelial progenitor cells; Ana II: apelin analogue II; Ang 1: angiopoietin 1; Ang 2: angiopoietin 2.

Protocol 2

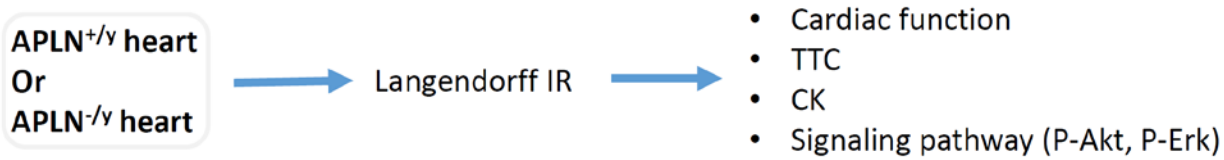

TTC: Tetrazolium chloride; CK: creatine kinase.

2.4 Use of Male Apelin Knockout Mice in Aortic Aneurysm

Protocol 1

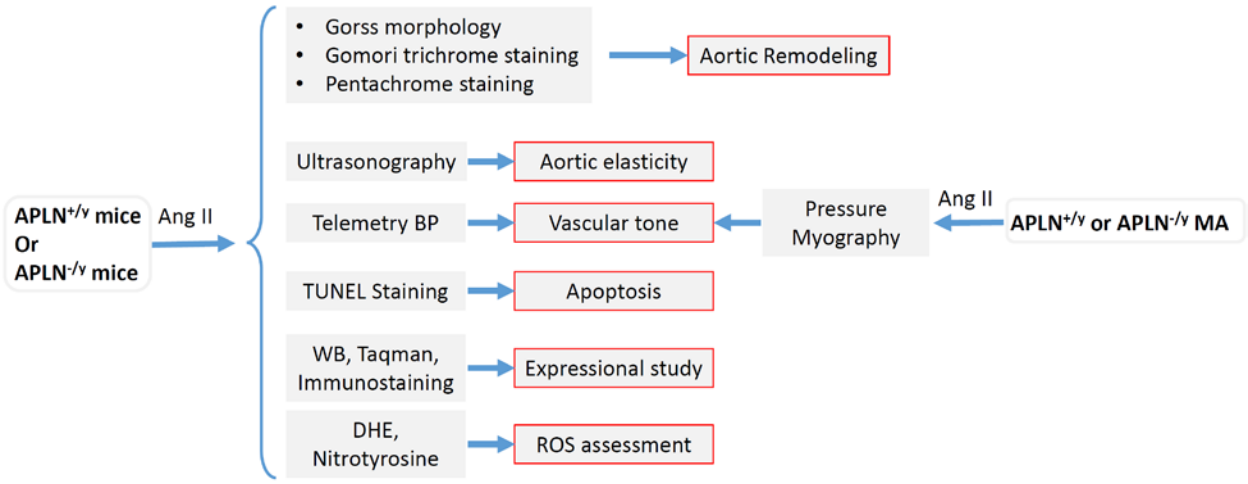

Protocol 2

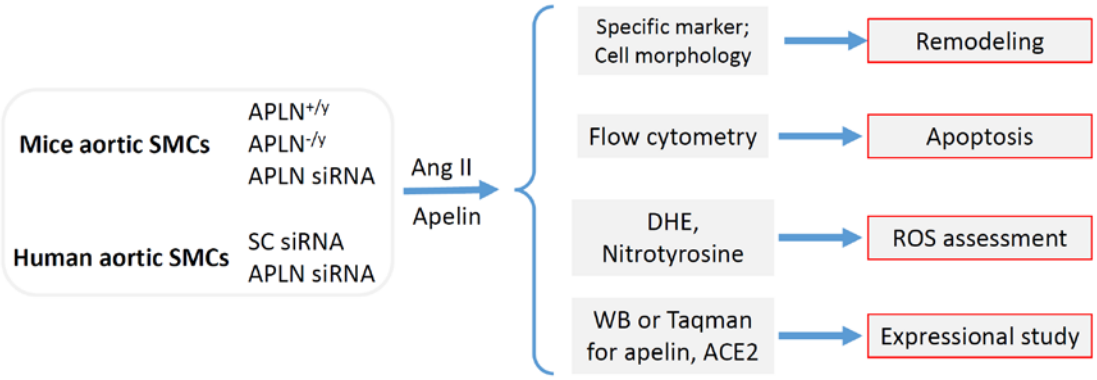

SC siRNA: scrambled siRNA

2.5 Design of Apelin Analogues as Potential Drugs

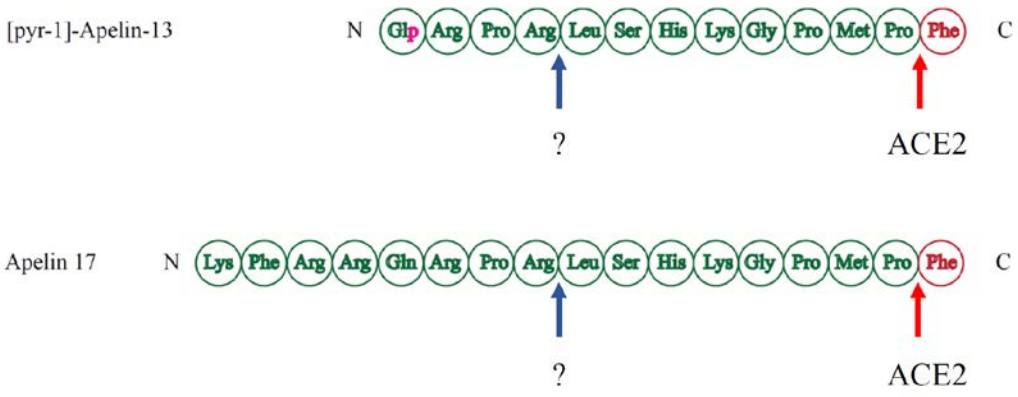

Hydrolysis sites of apelins

List of apelin analogues tested

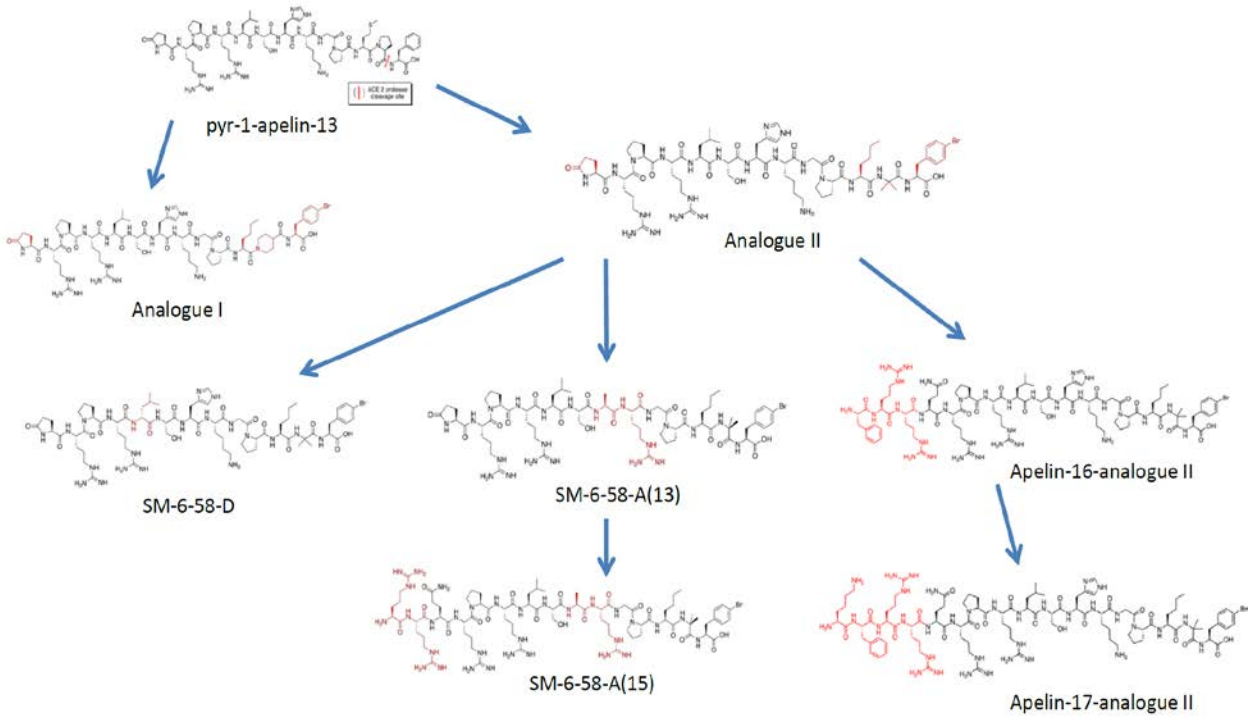

CHAPTER THREE

Heterozygote Loss of ACE2 is Sufficient to Increase the Susceptibility to Heart Disease

Wang Wang[1,2] MSc, Vaibhav B. Patel[1,2] PhD, Zuocheng Wang[1,2] PhD, Dong Fan[2,3] PhD, Ratnadeep Basu[2,3] MD, PhD, Zamaneh Kassiri[2,3] PhD,

Josef M. Penninger[4] MD and Gavin Y. Oudit[1,2,3] MD, PhD

[1]Division of Cardiology, Department of Medicine, [2]Mazankowski Alberta Heart Institute, University of Alberta, Edmonton, Canada, and [3]Department of Physiology, University of Alberta, Edmonton, Canada, [4]Institute of Molecular Biotechnology of the Austrian Academy of Sciences, Vienna, Austria

Author contribution: Wang Wang and Gavin Oudit designed the experiment and wrote the manuscript and figures; Wang Wang created the animal disease models, the basic histological studies, PSR staining, Taqman PCR and wire myography; Vaibhav Patel performed the immunostainings and imaging analysis; Zuocheng Wang performed the western blot assay; Dong Fan cultured and provided SMCs; Ratnadeep Basu performed the ultrasound analysis; Zam Kassiri and Josef Penninger reviewed manuscript.

A modified version of this chapter has been published in *Journal of Molecular Medicine (Berlin)*, 2014 Aug; 92(8): 847-58.

3.1 Abstract

Angiotensin converting enzyme 2 (ACE2) metabolizes Ang II into Ang 1-7 thereby negatively regulating the renin-angiotesnin system. However, heart disease in humans and in animal models is associated with only a partial loss of ACE2. ACE2 is an X-linked gene and as such we tested the clinical relevance of a partial loss of ACE2 by using female $ACE2^{+/+}$ (wildtype) and $ACE2^{+/-}$ (heterozygote) mice. Pressure-overload in $ACE2^{+/-}$ mice resulted in greater LV dilation and worsening systolic and diastolic dysfunction. These changes were associated with increased myocardial fibrosis, hypertrophy and upregulation of pathological gene expression. In response to Ang II infusion, while there was increased NADPH oxidase activity and myocardial fibrosis resulting in worsening of Ang II-induced diastolic dysfunction with preserved systolic function. Ang II-mediated cellular effects in cultured adult $ACE2^{+/-}$ cardiomyocytes and cardiofibroblasts were exacerbated. Ang II-mediated pathological signaling worsened in $ACE2^{+/-}$ hearts characterized by increase in phosphorylation of ERK1/2 and JNK1/2 and STAT-3 pathways. The $ACE2^{+/-}$ mice showed an exacerbated pressor response with increased vascular fibrosis and stiffness. Vascular superoxide and nitrotyrosine levels were increased in $ACE2^{+/-}$ vessels consistent with increased vascular oxidative stress. These changes occurred with increased renal fibrosis and superoxide production. Partial heterozygote loss of

ACE2 is sufficient to increase the susceptibility to heart disease secondary to pressure-overload and Ang II infusion.

Keywords: renin-angiotensin system, angiotensin converting enzyme 2, NADPH oxidase, heart failure, sex

3.2 Introduction

Several lines of experimental and clinical evidence implicate a key role for the renin-angiotensin system (RAS) in the pathophysiology of a number of cardiovascular diseases, such as myocardial infarction, hypertension and heart failure.[139, 140] Angiotensin II (Ang II), acting *via* AT1 and AT2 receptors, modulates production of reactive oxygen species (ROS), impairing myocardial contractility and extracellular matrix remodeling, thereby negatively impacting on heart function.[141] Angiotensin converting enzyme 2 (ACE2), a homologue of ACE, is a monocarboxypeptidase which metabolizes Ang II to yield Ang 1-7 and lowers Ang II/Ang 1-7 ratio.[53, 54, 68, 81, 85, 142] Angiotensin II (Ang II) receptor blockers (ARBs) that selectively antagonize the Ang II type 1 receptor (AT1R) became a valid alternative approach to interfere with the RAS axis also upregulates ACE2 resulting in generation of Ang 1-7.[76, 143-149]

Ang II-mediated oxidative stress, cardiac hypertrophy, contractile dysfunction and fibrosis are exacerbated in ACE2-deficient mice[81, 142], while recombinant human ACE2 attenuates these responses and improve cardiac function, with a marked reversal of Ang II-mediated signaling.[68] Many of the cardiac pathological effects of RAS activation and Ang II appear to be mediated through ROS, produced by a specific NADPH oxidase-dependent pathway in an AT1R-dependent manner.[150, 151] In this study, we showed that heart disease is

associated with a partial loss of ACE2 and we tested the relevance of a partial loss of ACE2 on the cardiac response to different pathological stimuli, pressure-overload and chronic Ang II exposure. We showed that the partial (heterozygote) loss of ACE2 is sufficient to increase the susceptibility to myocardial and vascular diseases in murine pre-clinical models.

3.3 Materials and Methods

Explanted Human Hearts. Cardiac tissue from patients with end stage heart failure due to idiopathic dilated cardiomyopathy was studied as part of the Human Explanted Heart Program (HELP) at the Mazankowski Alberta Heart Institute. All patients underwent cardiac transplantation. Non-failing human hearts were collected as part of the Human Organ Procurement and Exchange (HOPE) program for research. All experiments were performed in accordance with the institutional guidelines and were approved by Institutional Ethics Committee. Informed consent was obtained from all study subjects. Four non-failing control (NFC) donor hearts (3M/1F, age 44±4.5 yrs), which could not be transplanted for technical reasons were used. All NFC had no heart disease before death according to their medical records. The NFC and explanted hearts with dilated cardiomyopathy (4M, age 49.5±5.5 yrs) were cardiopleged prior to explantation, kept at 4^{o}C and tissue collected for molecular analysis within 15 mins.

Experimental Animals and Protocols. *Ace2*$^{-/y}$ and *Ace2*$^{-/-}$ mutant mice that were backcrossed into the C57BL/6 background for at least 8 generations were used in the present study.[81, 152, 153] All experiments were performed in accordance to institutional guidelines and the Guide for the Care and Use of Laboratory Animals published by the US National Institutes of Health (NIH Publication No. 85-23, revised 1996). The anesthesia used in our experimental protocols was delivered by inhalation, isoflurane/oxygen (2%).

Pressure-overload. Young (8-9 weeks old) female *Ace2*$^{+/+}$ (ACE2 wildtype; ACE2$^{+/+}$) and *Ace2*$^{-/+}$ (ACE2 Heterozygote; ACE2$^{-/+}$) mice were subjected to pressure-overload as previously described.[142, 154, 155] Mice were anesthetized with isoflurane. The skin was cleaned with Germex and Betadine. One dose of penicillin (10 mg/kg, 0.1 mL i.p.) was administered prior to start of surgery. Mice were placed supine and body temperature was maintained at 37°C with a heating pad. A horizontal skin incision of 1 cm in length was made at the level of second intercostal space, once the animal was in surgical plane of anesthesia. A 6-0 silk suture was passed under the aortic arch, a bent 27-gauge (27G) needle was then placed next to the aortic arch and the suture was snugly tied around the needle and aorta between the left carotid artery and the brachiocephalic trunk. The needle was quickly removed allowing the suture to constrict the aorta and the incision was closed in layers. Immediately after the surgery, mice received one dose of

buprenorphine. Sham animals underwent the same procedure without the aortic banding.

Ang II Infusion. An osmotic minipump (model 1002; Alza, Palo Alto, Calif., USA) was implanted subcutaneously at the dorsum of the neck to infuse a pressor dose of Ang II (1.5 $mg.kg^{-1}.d^{-1}$) or saline (vehicle) for 14 days in female WT and $ACE2^{-/+}$ mice.[68, 134]

Echocardiographic measurements. Mice were lightly anaesthetized and transthoracic echocardiography was performed as described previously.[68]

Isolation and Culture of Adult Cardiomyocytes and Cardiofibroblasts. Adult murine left ventricular (LV) cardiomyocytes and cardiofibroblasts from WT and $ACE2^{-/+}$ hearts were isolated and cultured as described previously.[68] Ang II (Sigma; 100nM) exposure over a duration of 30 mins and 24 hrs for cardiomyocytes and cardiofibroblasts, respectively.

Superoxide Assay and Dihydroethidium Fluorescence. The chemi-luminescence lucigenin assay was used to measure NADPH oxidase activity using a single-tube luminometer (Berthold FB12, Berthold Technologies, Germany).[68, 142, 153] Dihydroethidium (DHE) fluorescence studies were performed on 20 μM thick frozen myocardial and aorta sections, which were washed with Hank's

balanced salt solution (HBSS) and incubated at 37°C for 30 min with DHE (20 μM) in HBSS, and then imaged using confocal microscopy.[68, 153]

Myocardial Ang II Levels. Myocardial Ang II levels were measured by radioimmunoassay in the Hypertension and Vascular Disease Centre Core Laboratory at Wake Forest University School of Medicine as previously described.[68]

Taqman Real time PCR, Western Blot Analysis. Taqman real-time PCR and Western blot analysis of the LV free wall was carried out as previously described.[68, 142] Myocardial mRNA expression levels were quantified by Taqman RT-PCR as described previously.[68, 154] Western blotting was performed to detect total ACE2 and PKCα and PKCβ1, and total and phosphorylated ERK-1/2 (threonine-177), JNK1/2 (threonine-183/tyrosine-185), JAK2 (tyrosine-1007/1008), STAT3 (tyrosine-705), using specific antibodies (R&D Systems, Santa Cruz and Cell Signaling Inc.) as previously described.[68] Blots were scanned and quantified using ImageQuant™ LAS 4000 (GE Healthcare, Biosciences, Quebec, Canada).

Histological Analysis and Immunofluorescence. LV fibrosis, cardiomyocyte hypertrophy and renal cortical fibrosis was measured by Masson trichrome and picrosirius red (PSR) staining as described previously.[68, 153] Isolated cardiofibroblasts were double stained for α-SMA and vimentin, along with

nuclear-staining with DAPI (Invitrogen) and visualized and imaged using fluorescence microscopy. Mesenteric vessels were fixed in 10% formalin, paraffin-embedded, and used for Gomori trichrome. Nitrotyrosine immunofluorescence staining was performed in 5 μM thick aorta cryosections using rabbit anti-nitrotyrosine (Millipore, USA) primary antibody and TRITC conjugated goat anti-rabbit (Abcam, USA) secondary antibody. Five μm thick cryosections were used for immunofluorescence staining of ACE2. Briefly, the cryosections were fixed with 4% paraformaldehyde followed by rehydration in PBS. Sections were permeabilized with 0.1% triton X-100 for 5 minutes followed by blocking with 4% BSA for 1 hour. The sections were then incubated with primary antibodies against ACE2 (R&D Systems, Abcam) at 4°C for overnight. After washing with PBS the sections were incubated with alexa fluor 488 conjugated donkey anti-goat antibody (Invitrogen). The sections were stained with DAPI (Invitrogen) for nuclear counterstaining.

Wire Myography. To measure the resting wall tension of a resistance artery we used the wire myography method (DMT 620M system from Danish MyoTechnologies for vessel perfusion and Lab Chart 7. from AD instrument for data recording). Third-degree mesenteric artery was isolated under anaesthetizing by isoflurane/oxygen (1.5%/98.5%) and mounted to the wire myography system with blood vessels typically 90±15 μm in diameter and 2 mm in effective length.

The vessel was immerse in perfusion buffer with the following composition: NaCl, 130 mM; KCl, 4.7mM; KH_2PO_4, 1.18 mM; $MgSO_4$, 1.17 mM; $NaHCO_3$, 14.9 mM; glucose, 5.5 mM; $CaNa_2$ Versenate, 0.026 mM; $CaCl_2$, 0.16 mM, which was bubbled with 95% O_2 and 5% CO_2 and kept at 37°C. The vessels were then stabilized and the length between two wires was labeled as L_0. The artery was then gradually stretched by increasing the distance between the two wires by 50 μm, 100 μm, 150 μm and 200 μm; at each step the vessel was stabilized for 1 min. The resting wall tension was reported as force readout at each step per mm length of vessel.

Statistical Analysis. All data are shown as mean ± SEM. All statistical analyses were performed using SPSS software (Chicago, Illinois; Version 10.1). The effects of genotype were evaluated using ANOVA followed by the Student Neuman-Keuls test for multiple comparison testing and comparison between two groups were made using the Student's t test.

3.4 Results

Heterozygote loss of ACE2 promotes adverse myocardial remodeling in response to pressure-overload

Human HF has clearly been linked to activation of a local and systemic RAS leading to elevated Ang II levels.[156, 157] Western blot analysis showed a marked loss of ACE2 protein in the LV myocardium obtained from explanted failing hearts (n=5; age: 49.3±2.9 yrs; 3M/2F) in patients with dilated cardiomyopathy compared with non-failing controls (n=5; age: 42.6±2.5 yrs; 4M/1F) (**Figure 3.1A**). The decrease in ACE2 levels was associated with a concomitant loss of ACE2 activity (**Figure 3.1B**) while immunofluorescence staining confirmed a loss of ACE2 (**Figure 3.1C**) in LV of explanted failing human hearts. In a murine model of heart disease, pressure-overload resulted in a 50% reduction in myocardial ACE2 protein levels in WT and ACE2 heterozygote mice (**Figure 3.1D**). In order to critically examine whether a partial loss of ACE2 is sufficient to enhance the susceptibility to heart disease, we used the female ACE2 heterozygote mice. Western blot and mRNA expression confirmed a 50% loss of myocardial ACE2 protein and mRNA levels in female ACE2 heterozygote ($ACE2^{+/-}$) compared to female WT ($ACE2^{+/+}$) mice (**Figure 3.2**). Heterozygote female ACE2 mice showed a greater ventricular dilation and increased pathological hypertrophy, as assessed by morphometry and expression of pathological hypertrophic markers, ANF, BNP, βMHC and α-skeletal actin in $ACE2^{-/+}$ hearts (**Figure 3.1E-G**). Histological assessment using picrosirius red staining confirmed increased cardiomyocyte cross-sectional area (**Figure 3.1H**) and interstitial and perivascular fibrosis (**Figure 3.1I**) in the pressure-overloaded

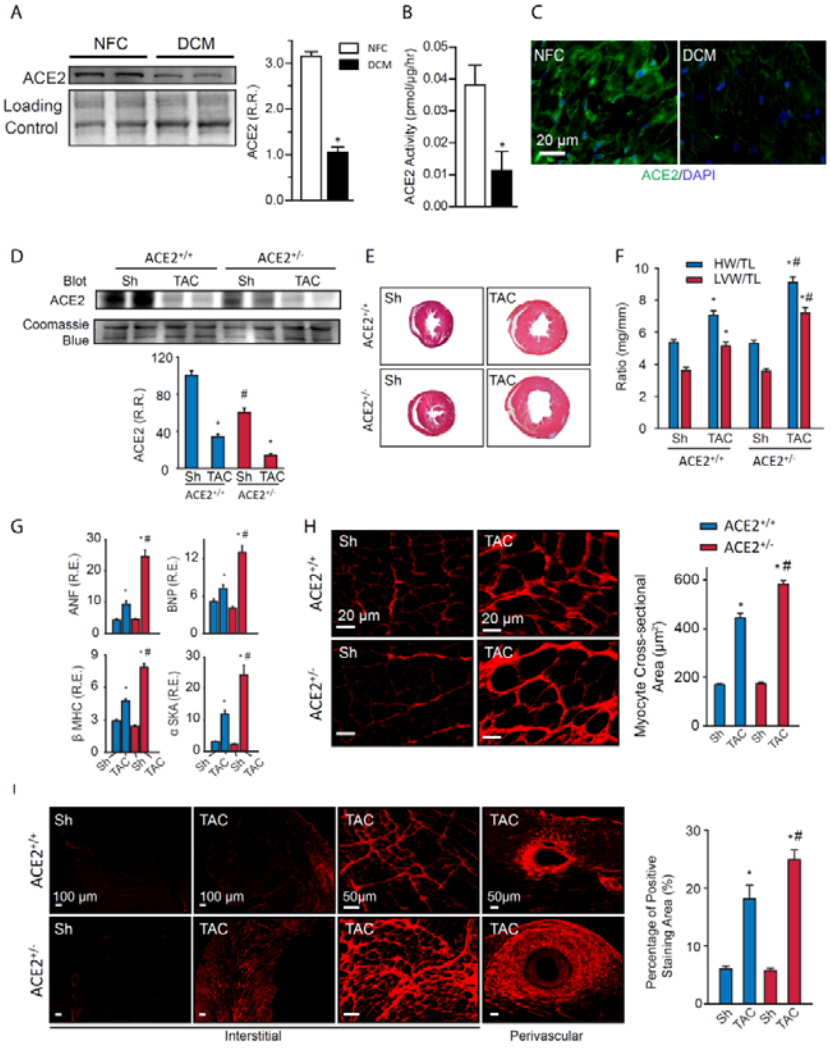

Figure 3.1 Pressure-overload induced greater increase in cardiac hypertrophy and myocardial fibrosis in female ACE2 heterozygote hearts. Human dilated cardiomyopathy is associated with reduced myocardial ACE2 levels shown by Western blot analysis (A), ACE2 activity (B) and immunofluorescence staining (C). Western blot Pressure-overload resulted in 50% reduction in ACE2 protein independent of genotype (D) and $ACE2^{+/-}$ hearts showed greater LV dilation based on trichrome staining (E) and increased hypertrophy based on morphometry (F) and mRNA expression analysis of ANF, BNP, βMHC and αSkA (G) at 9 weeks post-TAC. Histological analysis with picrosirius red staining showing increased cardiomyocyte cross-sectional area (H), and interstitial and perivascular myocardial fibrosis (I) in $ACE2^{+/-}$ hearts at 9 weeks post-TAC. R.R.=relative ratio; R.E.=relative expression; NFC=non-failing control; DCM=dilated cardiomyopathy; Sh=sham-operated; TAC=transverse aortic constriction; LVW=left ventricular weight; HW=Heart weight; TL=tibial length; ANF=atrial natriuretic factor; BNP=brain natriuretic peptide; βMHC=beta-myosin heavy chain; α-SkA=alpha-skeletal actin. n=8 for sham-operated; n=10 for TAC group. *$p<0.05$ compared with all other groups; $^{\#}p<0.05$ compared with corresponding $ACE2^{+/+}$ group.

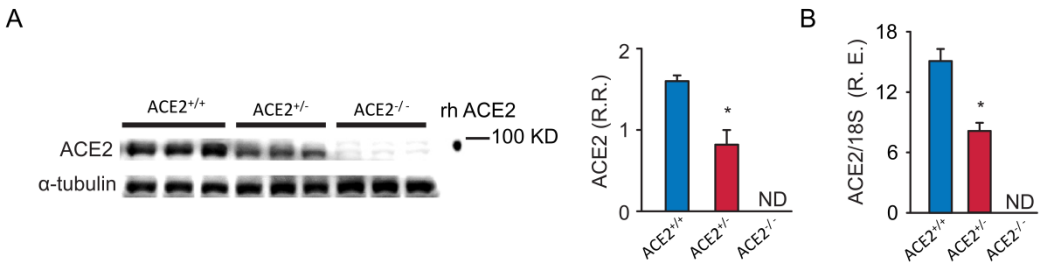

Figure 3.2 Expressional study of female ACE2 heterozygote ($ACE2^{+/-}$) compared to female WT ($ACE2^{+/+}$) mice. Western blot and mRNA expression confirmed a 50% loss of myocardial ACE2 protein (A) and mRNA levels (B) in female ACE2 heterozygote ($ACE2^{+/-}$) compared to female WT ($ACE2^{+/+}$) mice.

$ACE2^{+/-}$ hearts indicative of both cardiomyocyte and extracellular matrix dependent effects.Functional assessment using transthoracic echocardiography showed a hypertrophic response with moderate reduction in systolic function in pressure-overloaded $ACE2^{+/+}$ hearts while the $ACE2^{+/-}$ hearts showed greater LV dilation and reduction in systolic function (**Figure 3.3A-E**). Assessment of diastolic function was performed using transmitral flow pattern and tissue Doppler imaging revealed a greater increase in E/A and E/E' ratios, and lowered E' in pressure-overloaded $ACE2^{+/-}$ hearts (**Figure 3.3F-H**). These results clearly demonstrate that partial loss of ACE2 increases the susceptibility to biomechanical stress leading to increased myocardial fibrosis, hypertrophy with greater LV dilation and worsening systolic and diastolic dysfunction.

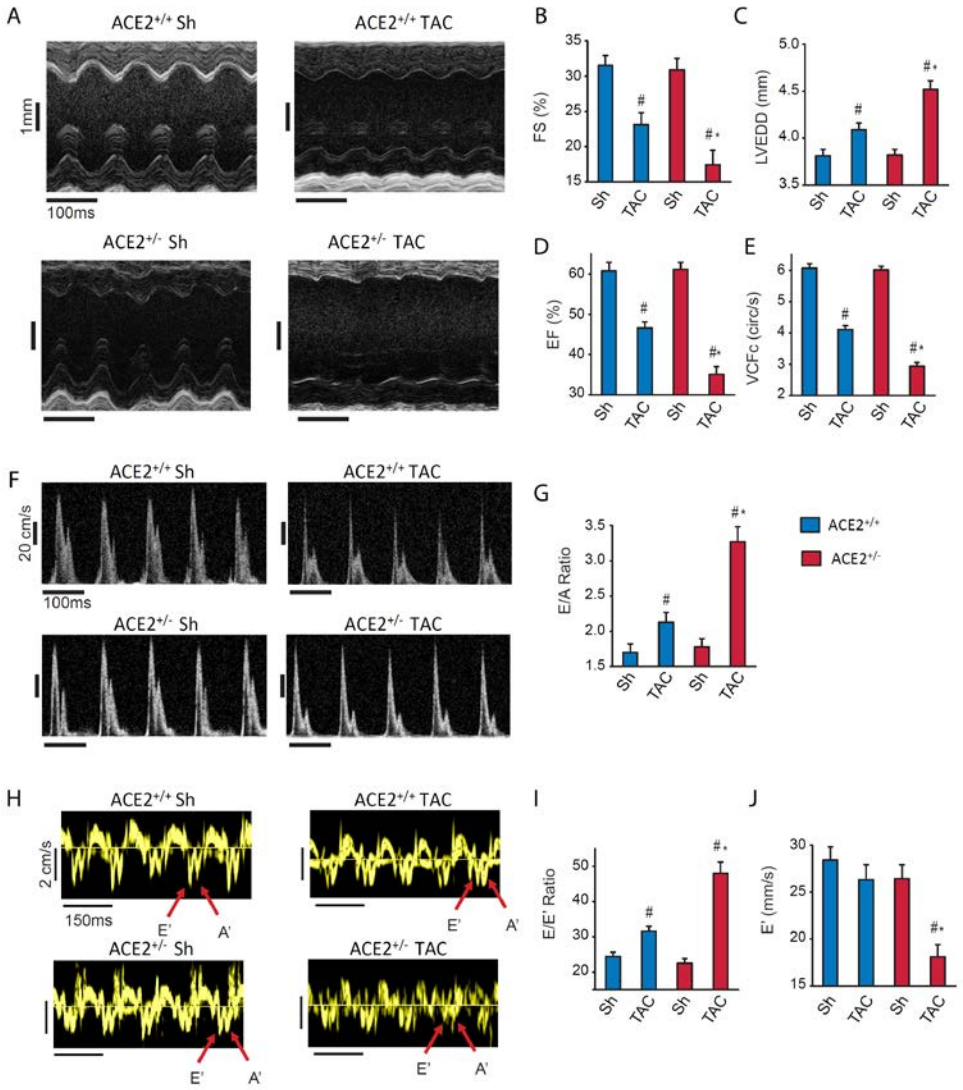

Figure 3.3 Echocardiographic assessment of systolic and diastolic function in response to pressure-overload in female ACE2 heterozygote mice. M-mode echocardiograms (A) and assessment of systolic function showing greater systolic dysfunction based on FS (B), LVEDD (C), EF (D) and VCFc (E)) in pressure-overloaded $ACE2^{+/-}$ hearts at 9 weeks post-TAC. Transmitral Doppler flow imaging (F) showing greater diastolic dysfunction characterized by a marked increase in E/A ratio (G) and tissue Doppler imaging (H) showing a marked increase in E/E' ratio (I) and lowering in E' (J) in pressure-overloaded $ACE2^{+/-}$ hearts at 9 weeks post-TAC. FS=fractional shortening; LVEDD=LV end-diastolic dimension; EF=ejection fraction and VCFC=velocity of circumferential shortening corrected for heart rate; E=early transmitral filling wave; A=atrial transmitral filling wave; E'=early tissue Doppler velocity. n=8 for sham-operated; n=10 for TAC group. *$p<0.05$ compared with all other groups; $^{\#}p<0.05$ compared with corresponding $ACE2^{+/+}$ group.

Heterozygote loss of ACE2 promotes adverse myocardial remodeling in response to Ang II

We next used the chronic Ang II infusion model as a well-described model of heart disease and vascular disease.[68, 134] Ang II resulted in greater hypertrophy based on morphometry (**Figure 3.4A**) and gene expression of pathological disease markers (**Figure 3.4B**). Histological analysis confirmed greater myocardial fibrosis based on picrosirius red and trichrome staining (**Figure 3.4C**). NADPH oxidase activation and enhanced oxidative stress is a common feature of the pathological effects of Ang II.[141, 158, 159] NADPH oxidase activation and ROS production measured by DHE fluorescence and quantification in association with increased NADPH oxidase activity (**Figure 3.4D-E**). To gain further insight into the cellular effects, we isolated, cultured and tested the cellular effects of Ang II on adult cardiomyocytes and cardiofibroblasts. Acute stimulation of cardiomyocytes with Ang II (100 nM) resulted in a marked increase in NADPH oxidase activity and superoxide formation (**Figure 3.4F-G**). In cardiofibroblasts, Ang II stimulation increased the expression of alpha-smooth muscle actin (α-SMA) resulting in increased accumulation of α-SMA, a well-accepted marker of activated fibroblasts (**Figure 3.4H-I**). The expression of transforming growth

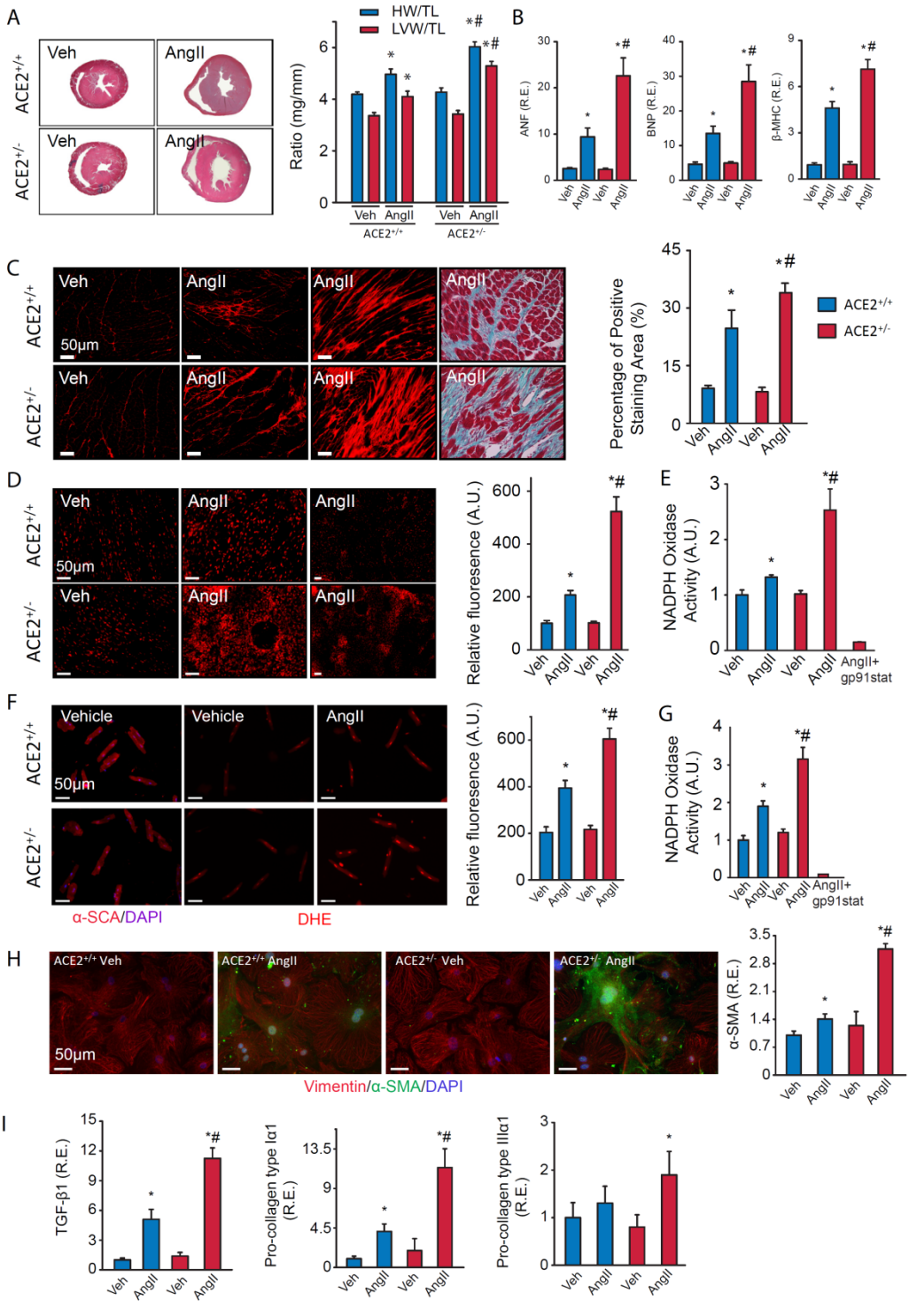
A
Veh
AngII
ACE2+/+
ACE2+/-
HW/TL
LVW/TL
Ratio (mg/mm)
B
ANF (R.E.)
BNP (R.E.)
β-MHC (R.E.)
C
50μm
Percentage of Positive Staining Area (%)
ACE2+/+
ACE2+/-
D
Relative fluoresence (A.U.)
E
NADPH Oxidase Activity (A.U.)
AngII+ gp91stat
F
Vehicle
α-SCA/DAPI
DHE
G
H
ACE2+/+ Veh
ACE2+/+ AngII
ACE2+/- Veh
ACE2+/- AngII
Vimentin/α-SMA/DAPI
α-SMA (R.E.)
I
TGF-β1 (R.E.)
Pro-collagen type Iα1 (R.E.)
Pro-collagen type IIIα1 (R.E.)

Figure 3.4 Heterozygote loss of ACE2 increases the susceptibility to Ang II-induced heart disease. $ACE2^{+/-}$ hearts showed greater hypertrophy based on trichrome staining and morphometry (A) and mRNA expression analysis of ANF, BNP, βMHC and αSkA (B), and histological analysis with picrosirius red staining and trichrome staining showing increased interstitial myocardial fibrosis (C) in response to Ang II. Ang II increases oxidative stress, as evident by increased dihydroethidium fluorescence (D) and NADPH oxidase activity (E) in $ACE2^{+/-}$ hearts. Acute stimulation of adult cardiomyocytes with Ang II (100 nM) resulted in a marked increase in superoxide formation based on dihydroethidium fluorescence (F) and NADPH oxidase activity (G) in $ACE2^{+/-}$ cardiomyocytes. In cardiofibroblasts, Ang II exposure stimulated increased immunostaining for α-SMA and mRNA expression of α-SMA (H) and mRNA expression of TGFβ1 and pro-collagen type Iα1 and IIIα1 (I). n=6 for each group. A.U.=arbitrary unit; R.E.=relative expression; α-SMA=alpha-smooth muscle actin; TGFβ1=transforming growth factor beta1. $^{*}p<0.05$ compared to all other groups; $^{\#}p<0.05$ compared with $ACE2^{+/+}$ group.

factor beta1 and pro-collagen type Iα and IIIα showed greater Ang II-dependent increase in $ACE2^{+/-}$ compared to $ACE2^{+/+}$ cardiofibroblasts. These results demonstrate that Ang II-mediated adverse myocardial and cellular remodeling is exacerbated by the heterozygote loss of ACE2.Heterozygote loss of ACE2 resulted in a greater increase in myocardial Ang II levels in response to systemic Ang II (**Figure 3.5A**). Ang II activates a series of pathological signaling pathways including mitogen-activated protein kinase (MAPK), JAK2/STAT3 and PKC signaling pathways.[68, 141, 142] Western blot analysis illustrated a greater increase in phosphorylation of ERK1/2 and JNK1/2 in $ACE2^{+/-}$ hearts in response to Ang II (**Figure 3.5B-C**). While the p38 pathway showed a basal difference with discordant response to Ang II, $ACE^{+/+}$ hearts showed a paradoxical decrease in phosphorylation of p38 while $ACE2^{+/-}$ hearts showed a marked increase in phosphorylation (**Figure 3.5D**). While JAK2 pathway did not vary in response to Ang II, basal STAT3 phosphorylation was lowered in $ACE2^{+/-}$ hearts but showed

a dramatic increase in response to Ang II (**Figure 3.5E-F**). Total levels of PKCα and PKCβ1 did not vary between genotypes or in response to Ang II (**Figure 3.5G**).

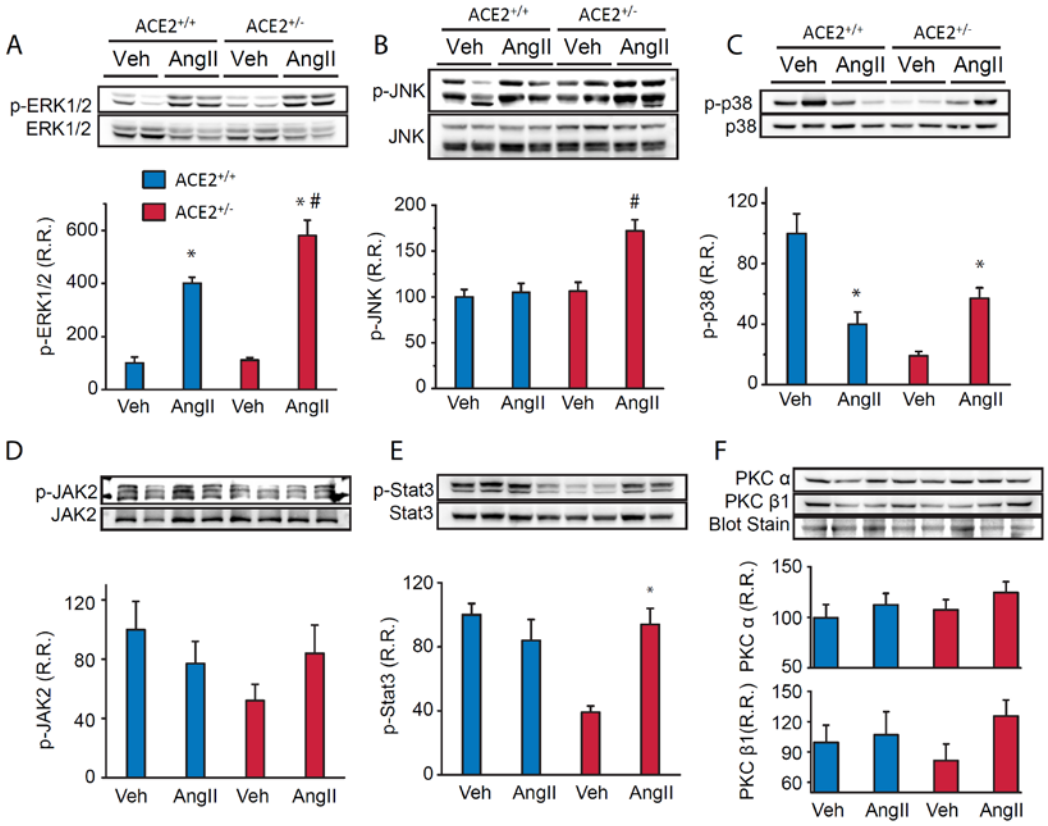

Figure 3.5 Increased activation of pathological signaling pathways in female ACE2 heterozygote mice in response to Ang II. Western blot analysis showing increased phosphorylation of ERK 1/2 (A), JNK1/2 (B), p38 (C), STAT3 (E), without changes in phosphorylation of JAK2 (D) and in levels of KPKC-α and PKC-β1 (F) in $ACE2^{+/-}$ hearts compared to $ACE2^{+/+}$ hearts in response to Ang II. R.E.=relative expression; ERK 1/2=extracellular signal-regulated kinase 1/2; JNK1/2= *c-jun-N-terminal kinase* 1/2; STAT3=signal transducer and activator of transcription 3; JAK2=Janus-activated kinase-2; PKC-α/β1= protein kinase c-α/beta1. n=5 for each group. A.U.=arbitary unit; R.E.=relative expression; $^{\#}p<0.05$ compared to all other groups; *$p<0.05$ compared to corresponding vehicle group.

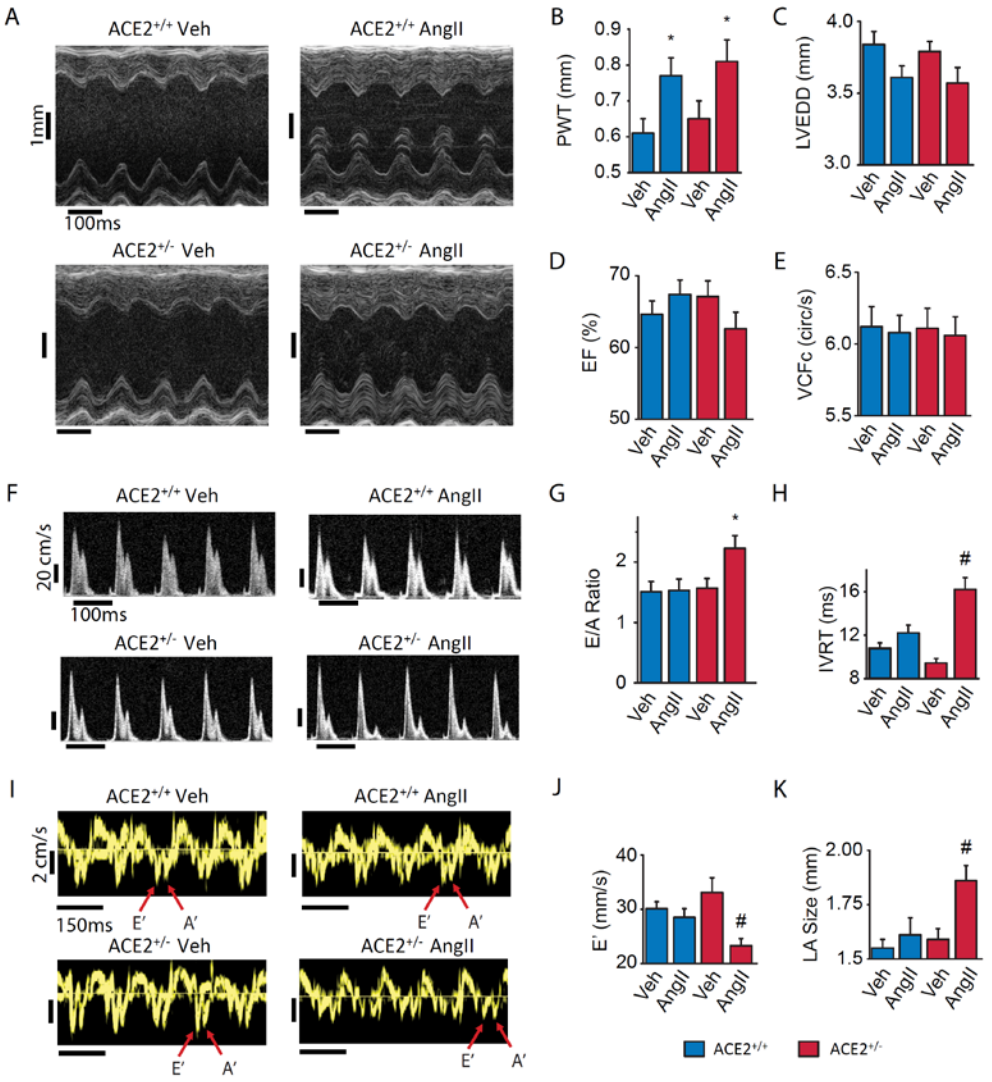

Figure 3.6 Echocardiographic assessment of systolic and diastolic function in response to Ang II in female ACE2 heterozygote mice. M-mode echocardiograms (A) and assessment of systolic function showing greater systolic dysfunction based on PWT (B), LVEDD (C), EF (D) and VCFc (E) in ACE2$^{+/-}$ hearts in response to Ang II. Transmitral Doppler flow imaging (F) showing greater diastolic dysfunction characterized by a marked increase in E/A ratio (G) and prolongation of IVRT (H) and tissue Doppler imaging (I) showing lowering in E' (J), and increased LA size (K) in ACE2$^{+/-}$ hearts in response to Ang II. FS=fractional PWT=LV posterior wall thickness; LVEDD=left ventricular end diastolic diameter; EF=ejection fraction; Vcfc=velocity of circumferential shortening, E wave=peak early transmitral inflow mitral E velocity; A wave=mitral Doppler A velocity; IVRT=isovolumetric relaxation time; E′=early diastolic tissue Doppler velocity; LA=left atrial. n=8 for vehicle group; n=10 for Ang II group. *p<0.05 compared with all other groups; $^{\#}$p<0.05 compared with corresponding ACE2$^{+/+}$ group.

Echocardiographic assessment confirmed an equivalent concentric hypertrophic response in $ACE2^{+/+}$ and $ACE2^{+/-}$ hearts with preserved systolic function (**Figure 3.6A-E**). In contrast, diastolic function was clearly worsened in $ACE2^{+/-}$ mice based on transmitral flow pattern and tissue Doppler imaging (**Figure 3.6F-K**).

These results demonstrate that heterozygote ACE2 mutant mice ($ACE2^{+/-}$) exhibited greater adverse pathological remodeling characterized by myocardial fibrosis and hypertrophy and altered signaling resulting in worsened diastolic dysfunction in response to chronic Ang II-mediated injury.

Vascular and Renal Effects of Ang II is exacerbated in ACE2 Heterozygote mice

The RAS and the ACE2 axis also have a profound effect on vascular and renal function. While baseline blood pressure was no different, Ang II resulted in a greater pressor response in $ACE2^{+/-}$ compared with $ACE2^{+/+}$ mice over a 2-week period (**Figure 3.7A**). Gomori trichrome Staining, which is a used used to stain and identify muscle fibers, collagen and nuclei, of the mesenteric arteries showed increased vascular wall and medial thickness with increased fibrosis (**Figure 3.7B**). These structural alterations resulted in functional changes characterized by increased vessel stiffness shown using an *ex vivo* wire myography system (**Figure 3.7C-D**). These functional and structural alterations were accompanied by increased vascular oxidative stress with increased vascular superoxide (**Figure**

3.7E) and nitrotyrosine (**Figure 3.7F**) levels in ACE2$^{+/-}$ compared to ACE2$^{+/+}$ aortas. The renal effects of Ang II were also exacerbated in the ACE2$^{+/-}$ mice leading to increased tubulointerstitial and glomerular renal fibrosis as shown by trichrome and picrosirius red staining and increased superoxide generation (**Figure 3.8**).

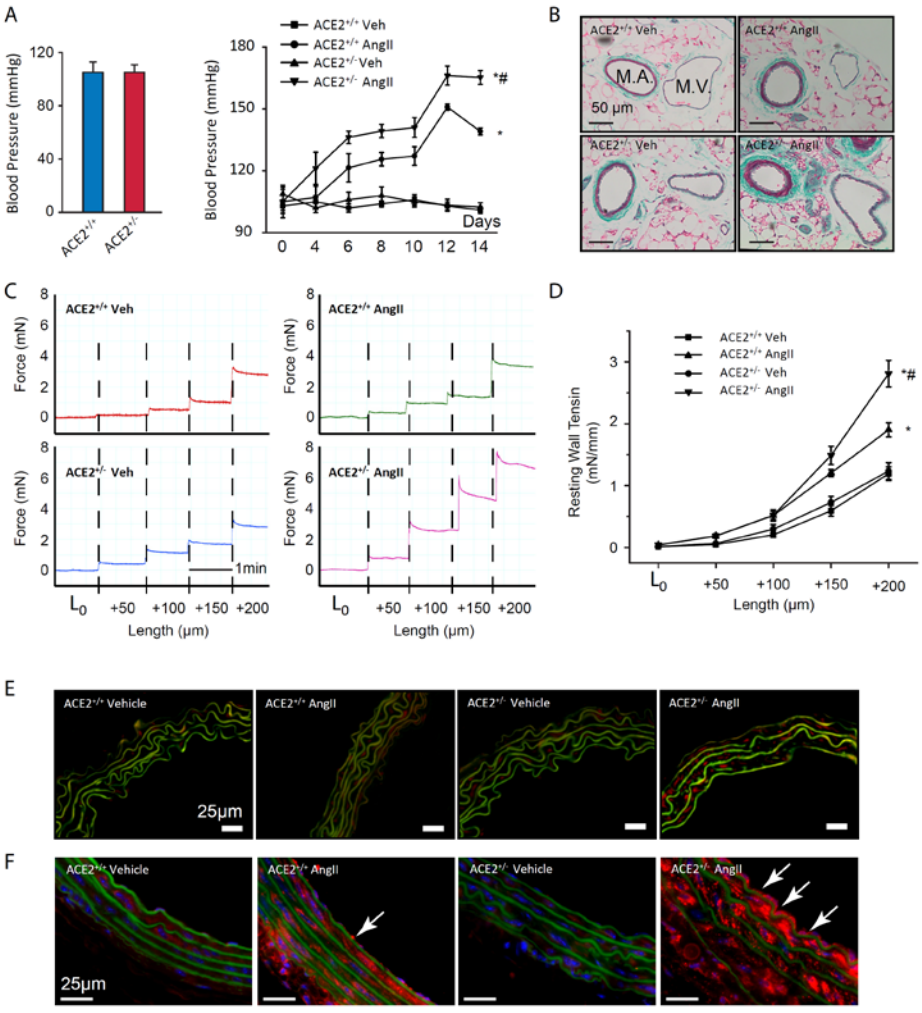

Figure 3.7 Vascular effects of angiotensin II in female ACE2 heterozygote mice. Tail-cuff blood pressures revealed no basal differences in systolic blood pressure (A) while in response to Ang II there was a greater pressor response over the 2-week course (B). Gomori trichrome shows increased medial thickness and perivascular fibrosis in $ACE2^{+/-}$ vessels resulting in increased passive stiffness in the mesenteric arteries based on wire myography measurements shown as representative traces (C) and the passive wall tension-length relationship (D). Vascular oxidative stress was as illustrated by dihydroethidium fluorescence (red) (with green elastin autofluorescence) showing increased superoxide levels in $ACE2^{+/-}$ aortas in response to Ang II (E). Representative images of nitrotyrosine, an adduct formed by the reaction of peroxynitrite with proteins, immunofluorescence showing increased nitrotyrosine levels in $ACE2^{+/+}$ aorta, which further increases in $ACE2^{+/-}$ aortas (F), with arrows indicating nitrotyrosine staining in endothelium in $ACE2^{+/-}$ aortas (nitrotyrosine [red], elastin autofluorescence [green], and DAPI-stained nuclei [blue]). Resting vessel length between the two wires was labeled as length 0 (L_0). n=6 for vehicle; n=8 for Ang II groups; *$p<0.05$ compared with the vehicle treated group; $^{\#}p<0.05$ compared with the $ACE2^{+/+}$ group.

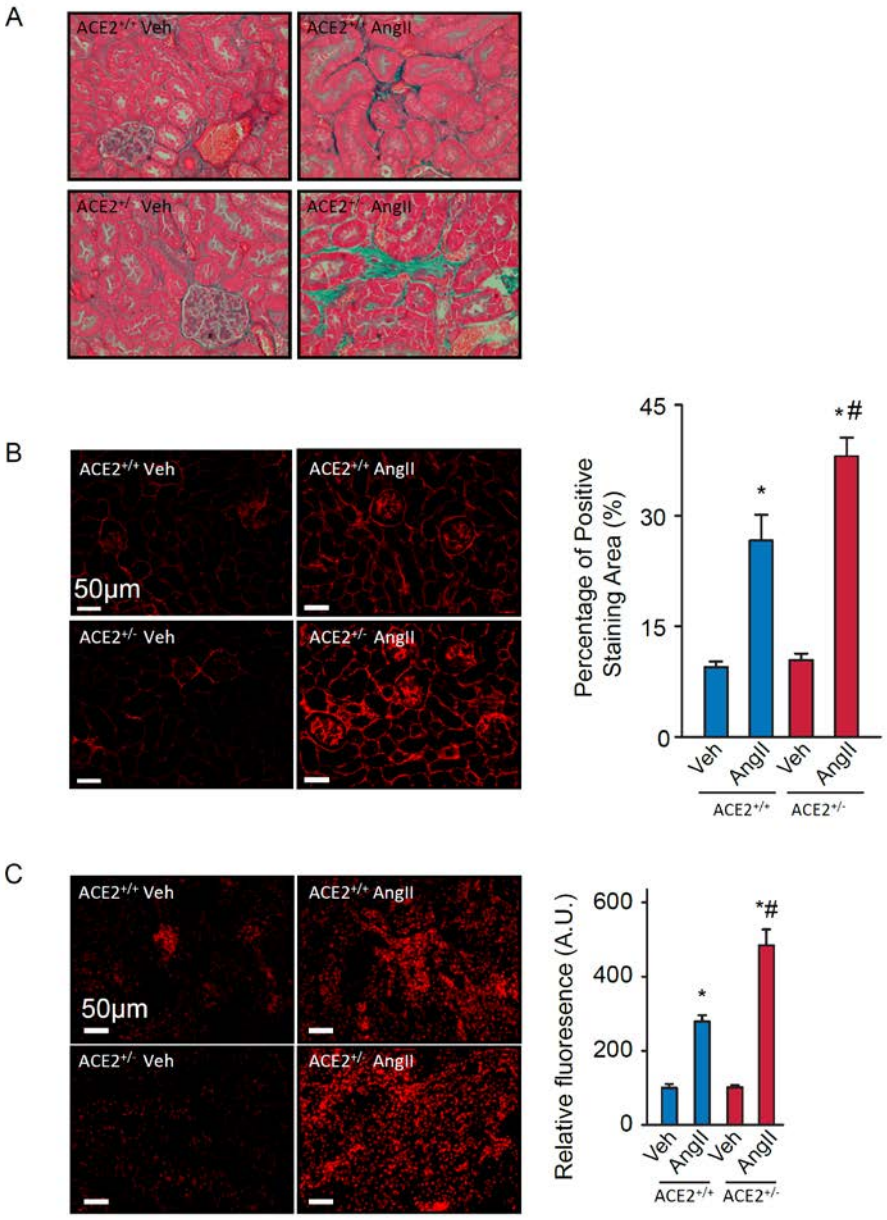

Figure 3.8 The fibrosis and DHE in kidney is response to Ang II. The renal effects of Ang II were also exacerbated as illustrated by the increased renal fibrosis shown using trichrome (A) and picrosirius staining (B) in association with increased superoxide generation based on dihydroethidium fluorescence (C) in the ACE2$^{+/-}$ mice. n=5 per group; *p<0.05 compared to corresponding vehicle group; #p<0.05 compared to all other groups.

3.5 Discussion

Genetic and functional loss of ACE2 is associated with an age-dependent cardiomyopathy [81, 85], adverse myocardial remodeling in response to myocardial infarction[152, 160] and pressure-overload [78, 142] and worsens Ang II-induced cardiac dysfunction.[68] The increased susceptibility to heart disease in relation to a loss of ACE2 correlates with elevated Ang II and lowered Ang 1-7 levels in the heart.[68, 142, 152] and recombinant human ACE2 attenuates Ang II-induced diastolic dysfunction.[68] Collectively, these studies provide definitive evidence that ACE2 plays a key role in heart disease. We have previously showed that in pre-clinical models of heart disease, myocardial ACE2 is partially decreased.[68, 152] Our study confirms these findings in patients with idiopathic and advanced dilated cardiomyopathy, whereby an activated RAS and elevated Ang II levels can decrease myocardial ACE2 levels due to proteolytic processing and shedding.[57] In contrast, ACE2 mRNA is upregulated in diseased hearts[57, 161] which may represent a negative feedback mechanism due to the loss of ACE2 action. Genetic variation in ACE2 is also associated with hypertension and reduced systolic function in men, and hypertension and increased LV mass in women.[162] However, whether this partial loss of ACE2 can play a direct role in enhancing heart disease remains elusive. ACE2 is an X-linked gene[85] and as such to address this question, we investigated heterozygote female ACE2 mutant ($ACE2^{+/-}$) and

their wildtype ($ACE2^{+/+}$) controls. Our results provide key evidence that in female preclinical models, ACE2 is protective against heart disease. With the use of the $ACE2^{+/-}$ mice, we showed that ACE2 plays a dominant pathogenic role in heart disease induced by pressure-overload and chronic exposure to Ang II.

Our results highlight a critical and dominant role of ACE2 in heart disease by demonstrating that a 50% loss of ACE2 is sufficient to enhance the susceptibility to heart disease. We provided definitive evidence that heterozygote loss of ACE2 leads to activation of the NADPH oxidase system and exacerbated oxidative stress leading to pressure-overload induced heart failure. In pressure-overloaded ACE2 deficient myocardium, relative loss of Ang 1-7 facilitated this adverse remodeling given the ability of Ang 1-7 to mediate direct cardioprotective effects.[145, 163] The translational importance of our findings is strengthened by the partial downregulation of myocardial ACE2 in failing human hearts, and in murine hearts following pressure-overload[68] and myocardial infarction.[152]. In a setting of elevated Ang II levels, partial deficiency of ACE2 exacerbates pathological ventricular hypertrophy and fibrosis resulting in worsening diastolic dysfunction. Mechanistically, we linked these changes to a greater elevation in myocardial Ang II levels leading to enhanced NADPH oxidase activation and superoxide generation, important mediators of pathological hypertrophy and fibrosis.[164] The development of myocardial fibrosis and pathological hypertrophy results in diastolic dysfunction and heart failure due to increased myocardial

stiffness.[68, 165] In response to Ang II, ACE2$^{+/-}$ vessels showed increased arterial stiffness which will likely impair ventriculoarterial coupling, a key driver of heart failure.[166] Ang II activates a plethora of signaling cascades, including those of MAPK and JAK2-STAT3 signaling pathways, resulting in myocardial hypertrophy and increased fibrosis.[68, 139, 141, 167] Ang II-AT1-mediated activation of ERK1/2 plays a key role in the downregulation of ACE2 expression thereby amplifying Ang II mediated effects.[70] These results are compatible with the exacerbation of Ang II-induced myocardial remodeling in male ACE2 knockout mice where there is complete loss of ACE2.[68] Importantly, we showed a heterozygote loss of ACE2 in isolated cardiomyocytes and cardiofibroblasts increased the sensitivity to Ang II showing a clear cellular basis for the phenotypic alterations in ACE2$^{+/-}$ hearts independent of systemic effects.

The present study demonstrates that heterozygote loss of ACE2 leads to enhanced susceptibility to pressure-overload and Ang II-induced heart disease. These murine models represent pre-clinical models of heart failure characterized by systolic dysfunction and diastolic dysfunction, respectively. The exacerbation of heart disease was linked to increased myocardial hypertrophy and fibrosis, increased oxidative stress and pathological signaling, key pathogenic players associated with an activated renin-angiotensin system. Since heart failure in male and female pre-clinical models of HF is associated with a partial downregulation of ACE2, our results clearly supports a key pathophysiological role of ACE2 in

heart disease independent of gender. Importantly, heterozygote loss of ACE2 also enhances vascular and renal disease in response to Ang II. Collectively, these results illustrate a dominant protective role of ACE2 and strongly support therapeutic strategies aimed at enhancing ACE2 action in the cardiovascular system.

CHAPTER FOUR

Angiotensin converting enzyme 2 metabolizes and partially inactivates pyr-apelin-13 and apelin-17: physiological effects in the cardiovascular system

Wang Wang[1,2], Shaun M. K. McKinnie[3], Maikel Farhan[4], Manish Paul[5], Tyler McDonald[3], Brent McLean[1,2], Saugata Hazra[6], Allan G. Murray[4], John C. Vederas[3] and Gavin Y. Oudit[1,2]

[1]Division of Cardiology, Department of Medicine, [2]Mazankowski Alberta Heart Institute, [3]Department of Chemistry, Faculty of Science, [4]Division of Nephrology, Department of Medicine, University of Alberta, Edmonton, Canada,[5]RBC College, West Bengal State University, India, [6]Department of Biotechnology, Indian Institute of Technology, Roorkee, India

Author contributions. Wang Wang and Gavin Oudit designed the experiments, and prepared the manuscript and figures with contributions from all other authors; Shaun McKinnie and John Vederas synthesized apelin analogues; Shaun McKinnie, Tyler McDonald and John Vederas performed all enzymatic kinetic study; Maikel Farhan and Allan Murray cultured HUVECs and performed eNOS Western blot assay; Brent Mclean guided the Western blot assay on Langendorff perfused hearts and edited the manuscript; Manish Paul and Saugata Hazra modeled the apelin-ACE2 binding *in silico*; Wang Wang performed blood pressure measurement *in vivo*, heart perfusion *ex vivo*; collected samples; performed ACE2 activity assay, CK and NO level assay.

A modified version of this chapter has been submitted for reviewing to *Hypertension.*

4.1 Abstract

Background: Apelin peptides mediate beneficial effects on the cardiovascular system and are being targeted as potential new drugs. However, apelin peptides have extremely short biological half-lives, making them impractical in their native form for use as a therapy. A better understanding of apelin peptide metabolism may lead to the discovery of a biologically stable analogue with significant therapeutic potential. **Methods and Results:** We examined the ability of angiotensin converting enzyme 2 (ACE2) to cleave and inactivate pyr-apelin 13 and apelin 17, the dominant apelin peptides. Computer-assisted modeling shows a conserved binding of pyr-apelin 13 and apelin 17 to the ACE2 catalytic site. In ACE2 knockout mice, hypotensive action of pyr-apelin 13 and apelin 17 were potentiated, with a corresponding greater elevation in plasma apelin levels. Similarly, pharmacological inhibition of ACE2 potentiated the vasodepressor action of apelin peptides. Biochemical analysis confirmed that recombinant human ACE2 can cleave pyr-apelin 13 and apelin 17 efficiently, and apelin peptides are degraded slower in ACE2 deficient plasma. The biological relevance of ACE2-mediated proteolytic processing of apelin peptides was further supported by the reduced potency of pyr-apelin 12 and apelin 16 on the activation of signaling pathways and nitric oxide production from endothelial cells. Importantly, while pyr-apelin 13 and apelin 17 rescued contractile function in a myocardial ischemia-reperfusion model, ACE2 cleavage products pyr-apelin 12

and 16 were devoid of these cardioprotective effects. We designed and synthesized active apelin analogues that were resistant to ACE2-mediated degradation, thereby confirming that stable apelin analogues can be designed as potential drugs. **Conclusion:** We conclude that ACE2 represents a major negative regulator of apelin action in the vasculature and heart.

4.2 Introduction

The apelin and angiotensin family of peptides have a wide range of related physiological and pathophysiological effects on the heart and vasculature.[40, 66, 68, 75, 85] Apelin is synthesized as a precursor 77 amino acid pre-pro-peptide and is subsequently processed into a family of apelin peptides, with pyr-apelin 13 and apelin 17 being the dominant apelin peptides found *in vivo*.[40, 133, 168] Apelin acts on the apelin receptor and regulates vascular homeostasis, angiogenesis, myocardial adaptation to stress and body fluid regulation, thereby playing a key role in vascular diseases such as systemic and pulmonary arterial hypertension, myocardial infarction and heart failure.[40, 49, 101, 169, 170]

The C-terminal region of the apelin peptide is central for its overall biological activity. N-terminal deletions of apelin-17 reveal that the 12 C-terminal amino acids are core requirements for the internalization and biological potency of apelin action on the apelin receptor.[62] Indeed, apelin-17 induced internalization of the apelin receptor decreases with every N-terminal deletion to apelin-12.

Similarly, the N-terminal residues 2-5 of apelin 13 are critical for functional potency [171] and the C-terminal sequence consisting of residues 8-11 is important for binding activity and receptor internalization.[62, 172]

The C-terminal residue of apelin, phenylalanine, is critical for binding of the apelin peptide to the apelin receptor.[173] However, the functional relevance of C-terminal phenylalanine residue and the enzymatic processes involved its removal from the native apelin peptide remains poorly defined. Using loss-of-function and gain-of-function strategies, we here define a critical role of angiotensin converting enzyme 2 (ACE2) in the proteolytic cleavage of the C-terminal phenylalanine residue in pyr-apelin 13 and apelin 17.

4.3 Materials and Methods

4.3.1 ***In Silico Modeling of Apelin Peptide Binding to ACE2.*** We selected the structure of human apo-ACE2 (PDB ID: 1R42) mainly because of its high resolution, appropriate R-factor and errorless electron density map.[174] This structure was equilibrated in constant pressure-temperature condition (NVT, NPT) in GROMACS.[175] We performed knowledge based docking using our understanding from ACE-substrate bound complex structure. For this purpose we have used the Ang II bound ACE complex (PDB ID: 4APH)[176] and MLN-4760

inhibitor bound ACE2 complex (PDB ID: 1R4L).[52, 174, 176, 177] We modeled the ACE2-Ang II, ACE2-pyr-apelin 13 and ACE2-apelin 17 complexes using these two above mentioned reference structures as a template. We built the structure of peptide substrates, pyr-apelin 13 and apelin 17, using the modeling server Peptide Builder.

To model the ACE2-substrate complexes, we have used the knowledge-based Autodock Vina docking method.[178] The grid for docking was developed using structurally aligned ACE/ACE2 structures. Using the in-built Grid map option, we prepared the axes dimensions and center points for performing the docking of Ang II, pyr-apelin 13 and apelin 17 with ACE2. In each docking experiment, we used 10 conformations of the ligand. The best conformation was selected based on scoring and posing function. After selecting the conformations of ligand that best fit with the ACE2, we have refined the complex based on the active site residues using COOT.[179] We optimized the substrate residues by using rotamer selection and regularize zone tools, and then conducted minimization of the model using the steepest descent algorithm in GROMACS within AMBER99SB-ILDN force field [180] at a time scale of 100ps with 50000 cycles. For visualization, analysis of the structural features, and detecting substrate interactions, we have used PyMol and Chimera.[181, 182]

4.3.2 Experimental Animals. Male ACE2 deficient ($ACE2^{-/y}$) and littermate wildtype ($ACE2^{+/y}$) mice were generated and bred in a C57Bl/6 background and used at 12 weeks of age as previously described.[68, 153] All animal experiments were carried out in accordance with the Canadian Council on Animal Care Guidelines, and animal protocols were reviewed and approved by the Animal Care and Use Committee at the University of Alberta.

4.3.3 Apelin Intravenous Injection, Blood Pressure measurement and Plasma Collection. Mice were anesthetized using 1.5% isoflurane/oxygen, and body temperature was monitored and maintained at 36 °C. The aorta was cannulated via the right carotid artery using a PV loop catheter (Model 1.2F from Scisense, Transonic) in order to continuously record arterial blood pressure and heart rate (LabScribe 2.0, Scisense). Pyr-apelin 13 (1.4 μM/kg body weight, Tocris Bioscience, Bristol, UK) or apelin 17 (1.4 μM/kg body weight, Tocris Bioscience, Bristol, UK) or same volume of saline were injected via the right jugular vein and blood was collected at 1 or 5 min post-apelin injection from the right carotid artery, and blood was centrifuged at 5000 G to isolate plasma. Samples were collected in the presence of a protease inhibitor cocktail (Catalog Number: S8830, Sigma-Aldrich®, St. Louis, USA) to stabilize the apelin peptides in plasma during sample collection, which was stored at -80°C until analysis.

4.3.4 LC-MS/MS based Quantification of Circulating Apelin Peptide Levels. Circulating levels of pyr-apelin 12, pyr-apelin 13, apelin 16 and apelin 17 were determined by mass spectrometry. Plasma samples were collected as described above. Samples were thawed and spiked with stable isotope-labeled internal standards at a concentration of 1 ng/ml. Following acidification and C18-based solid-phase-extraction, samples were subjected to LC-MS/MS analysis using a reversed-phase analytical column (Acquity UPLC® C18, Waters) operating in line with a XEVO TQ-S triple quadrupole mass spectrometer (Waters) in MRM mode. Apelin concentrations were calculated by relating endogenous peptide signals to internal individual standard apelin signals.

4.3.5 *In vitro* ACE2 hydrolysis of pyr-1-apelin-13 and apelin-17. Pyr-apelin 13 and apelin 17 (Tocris Bioscience, Bristol, UK) were diluted in Milli-Q water. Recombinant human ACE2 (rhACE2) was dissolved in MES buffer (50 mM MES, 300 mM NaCl, 10 μM $ZnCl_2$, 0.01% Brij L23, pH 6.5) at a concentration of 40 nM. 5 μL of apelin peptide (400 μM) was added to 45 μL of MES buffer, and had 50 μL of rhACE2 added and incubated at 37 °C for a defined period of time (final [apelin] = 20 μM, [rhACE2] 20 nM). Experiments (n = 3) were quenched by the addition of 100 μL EDTA (0.1 M); 5 μL of 1 mM Fmoc-Asp-OH was added as an internal standard, and analyzed by C18 RP-HPLC.

4.3.6 HPLC analyses of *in vitro* ACE2 degradation products. Apelin peptide products were resolved using a Vydac C18 RPLC Protein-Peptide Column (300Å, 5 μm, 4.6 mm x 250 mm). Peptides were separated using the following method: 0 – 3 min 10% B, 3 – 23 min 10 – 45% B, 23 – 25 min 45 – 100% B, 25 – 26 min 100% B, 26 – 27.25 min 100 – 10% B, 27.25 – 30 min 10% B (A = 0.1% aqueous trifluoroacetic acid (TFA); B, 0.1% TFA in acetonitrile. The extent of apelin peptide degradation was done by comparing the areas of substrate and product peaks (area of product peak/(area of product peak + area of substrate peak).

4.3.7 Kinetic determination of ACE2 hydrolysis of apelin peptides. *In vitro* ACE2 assays were set up as previously described with 5, 20, 50 and 100 μM apelin concentrations (n = 2 at each concentration for kinetic determinations). Assays were quenched after 30, 60 and 120 s, and analyzed by C18 RP-HPLC. The percent of apelin degradation products were converted to micromoles of products formed and used to calculate the initial velocities of apelin substrate degradation. These initial velocities were graphed against substrate concentration and analyzed using GraphPad PRISM version 4.0 software to determine kinetic parameters. A calculated ACE2 molecular mass of 85 KDa was used to determine the turnover numbers (kcat) analogous to that previously reported.[58]

4.3.8 Determination of hydrolysis of apelin peptides in plasma. Plasma (20 μL) was portioned into microfuge tubes and pre-warmed to 37 °C. 5 μL of apelin peptide (400 μM) was added and incubated at 37 °C for varying lengths of time (n=3 for each time point). Experiments were quenched by the addition of 20 μL of 10% aqueous TFA and 5 μL of internal standard (1 mM Fmoc-Asp-OH, mouse plasma; 1 mM dansyl-Tyr-Val-Gly-OH (Sigma-Aldrich), human plasma) were added. The experiments were diluted up to 100 μL with 0.1% aqueous TFA and loaded onto a pre-equilibrated Harvard Apparatus C18 spin column and centrifuged at 300G for 2 min. The resultant filtrate was reloaded to the top of the column and centrifuged at 300 x g for 2 min two additional times. Samples were washed with 2 x 300 μL of 0.1% aqueous TFA and centrifuged at 300 x g for 2 min, discarding the filtrate after each wash. Desired peptides were eluted with 300 μL of 75% acetonitrile (mouse plasma) or 40% acetonitrile (human plasma) in 0.1% aqueous TFA, centrifuged at 300 x g for 2 minutes, and analyzed by C18 RP-HPLC. The remaining apelin peptides in plasma were quantified by comparing the apelin:internal standard ratio of samples at 0 min to the ratio at other time points.

4.3.9 Langendorff isolated heart perfusion and ischemia-reperfusion Injury. Langendorff isolated heart perfusion was used as a model of global ischemia-reperfusion (IR) injury as described before.[169] Wildtype male murine (C57Bl6)

hearts were mounted on a Langendorff system and perfused at a constant pressure of 60 mmHg with modified Krebs-Henseleit solution (116 mmol/L NaCl, 3.2 mmol/L KCl, 2.0 mmol/L $CaCl_2$, 1.2 mmol/L $MgSO_4$, 25 mmol/L $NaHCO_3$, 1.2 mmol/L KH_2PO_4, 11 mmol/L glucose, 0.5 mmol/L EDTA and 2 mmol/L pyruvate), kept at 37°C and continuously oxygenated with 95% O_2 and 5% CO_2 to maintain a pH at 7.4. Left ventricular pressure was recorded continuously (PowerLab system, ADInstruments, Australia); after a 10 min baseline recording, global ischemia was induced for 30 min followed by 40 min of reperfusion. A post-conditioning protocol was used with pyr-apelin 13, pyr-apelin 12, apelin 17 or apelin 16 (1 μmol/L) given at the start of reperfusion. Hearts and coronary effluents were collected and flash frozen in liquid nitrogen.

4.3.10 ACE2 and creatine kinase activity assays. ACE2 enzymatic activity in plasma and tissue extract was assayed using a flurescence-based assay using 7-methoxycoumarin-Tyr-Val-Ala-Asp-Ala-Pro-Lys-(2,4-dinitrophenyl)-OH (R&D Systems) and a fluorescence plate reader (Spectramax M5® from Molecular Devices, LLC) as previously described.[153, 183] MLN-4760 (1 μM), a specific ACE2 inhibitor, was used to eliminate non-specific ACE2 activity. Creatine kinase activity was performed in coronary effluent from the Langendorff preparations at the indicted time points using a commercial kit (ECPK-100, BroAssay Systems, Hayward, CA).[169]

4.3.11 Western blot assay using Langendorff perfused hearts. Total protein extraction and immunoblotting (IB) were performed as previously described.[169] Left ventricle (LV) tissue was homogenized using a TissueLyserII (Qiagen) with PhosSTOP and cOmplete protease inhibitors (Roche) in CellLytic M Cell Lysis Reagent (Sigma),separated on 8% SDS-PAGE, transferred to a PVDF membrane, and subjected to IB of phospho-(Ser473)/total Akt, phospho-(Thr308)/total Akt and phospho/total Erk1/2 (Cell Signaling Technology, Beverly, MA). Blots were visualized and quantified with ImageQuant LAS 4000 (GE Healthcare, QC, Canada).

4.3.12 Human umbilical vein endothelial cells culture, Western blot analysis and nitric oxide assay. Human umbilical vein endothelial cells (HUVECs) were isolated and cultured as described previously.[184] HUVECs were serum starved in M199 + 1% FBS (Invitrogen, Burlington, ON), then stimulated with 100 ng/ml human derived stromal factor 1 (SDF1) or apelin peptides. HUVECs were washed once with ice cold PBS, and lysed immediately on ice with RIPA buffer. Cell lysates were boiled at 95°C for 5 min, resolved by SDS-PAGE, then electroblotted on nitrocellulose membranes (Bio-Rad). The membranes were immunoblotted using anti-phospho-eNOS^{S1177}, anti-phospho-Akt^{S473} (Cell Signaling Technology, Danvers, MA), anti-actin (Cytoskeleton, Denver, CO) and anti-Akt (Protein Tech, Chicago, IL) and proteins were detected using Luminata

forte (EMD Millipore, Billerica, MA) and a Fluorochem FC2 CCD camera (Alpha Innotech). For the NO assay, HUVECs were serum starved in M199 culture medium containing 5 μM DAF-FM (D-23841, Molecular Probes, Inc.) and cultured at 37°C for 60 min. The cells were then harvested and loaded to microplate and measured under fluorescence plate reader at excitation and emission of 495/515 nm. L-NMMA (10 μM) was used as a specific NOS inhibitor to determine the actual NO production.

4.4 Results

4.4.1 Modeling of the ACE2-Apelin complex. We performed *in silico* modeling of ACE2 bound with Ang II, pyr-apelin 13 and apelin 17, and analyzed the molecular interactions between ACE2 and substrate, formation of the zinc mediated tetrahedral intermediate and the substrate cleavage site.

I. ACE2 and pyr-Apelin 13. We initially modelled the ACE2-Angiotensin II (Ang II) interaction and showed that the substrate binding pocket of the electrostatic surface of the complex model is constructed by positively charged basic and non-polar residues (**Figure 4.1A**), with well delineated hydrogen bonds with Pro (P1) and Phe (P1') residues of Ang II and with the zinc-bound tetrahedral intermediate (**Figure 4.1B-D**).

Analysis of the ACE2-pyr-apelin13 model showed a similar electrostatic surface of the binding cleft in ACE2 with the substrate binding site S1 and S1' pockets binding with P1 (Pro) and P1' (Phe) residues of pyr-apelin 13 (**Figure 4.2A-B**). The oxygen atom of the aromatic side chain of Tyr385 and the nitrogen atom of His401 in the S1 pocket of ACE2 interact with the carbonyl oxygen of proline (P1) of pyr-apelin 13 (**Figure 4.2C**). Importantly, His345 and Pro346 of the S1' pocket of ACE2 interact with the amino terminal nitrogen atom of phenylalanine (P1') of pyr-apelin 13; pyr-apelin 13 is cleaved at its C-N peptide bond between the P1-P1' residues resulting in a loss of the C-terminal phenylalanine residue (**Figure 4.2D**).

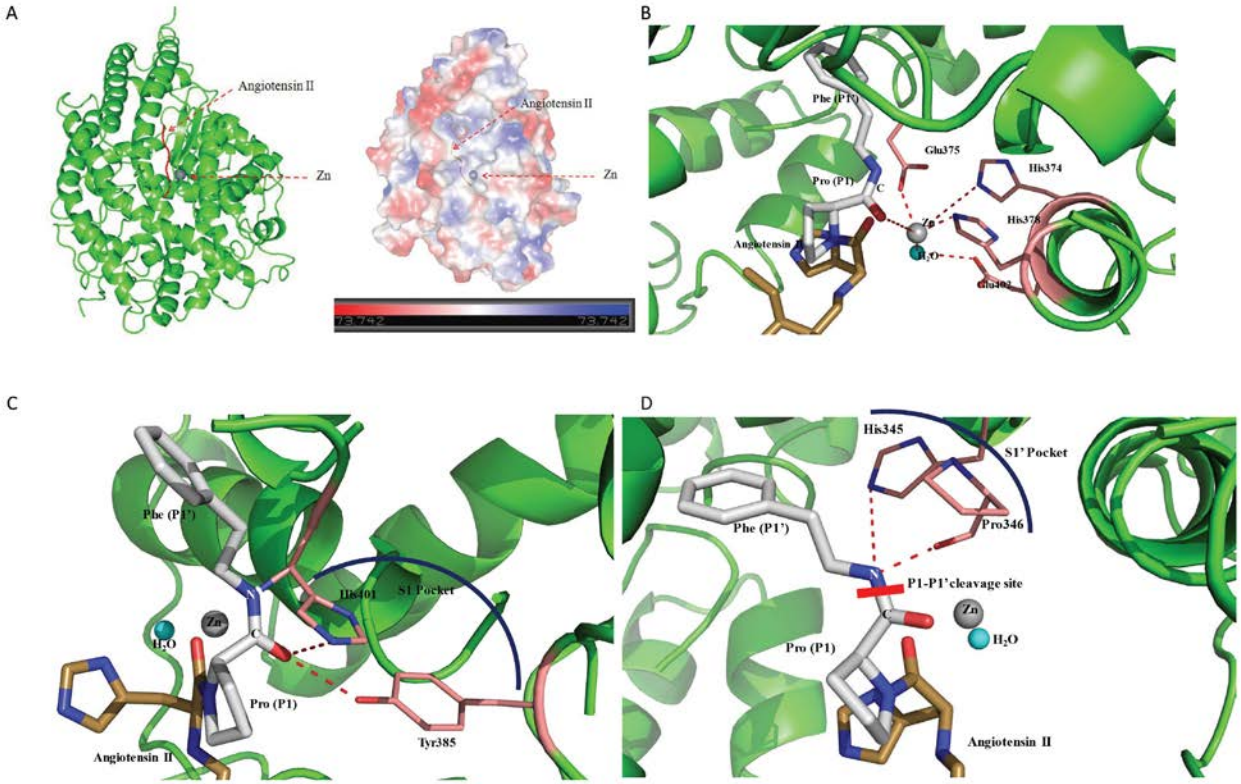

Figure 4.1 Modeling of the interactions between angiotensin converting enzyme 2 (ACE2) and angiotensin II. A computer-simulated model of angiotensin II and zinc-bound ACE2 (left) and the electrostatic surface of angiotensin II and zinc-bound ACE2 (right) (**A**). Catalytic site of the ACE2-angiotensin II interaction (**B**), interaction between the P1 site of angiotensin II and S1 pocket of ACE2 (**C**) and the interaction between the P1' site of angiotensin II and S1' pocket of ACE2 (**D**).

II. ACE2 and Apelin 17. The minimized model and electrostatic surface analysis of apelin-17 bound ACE2 showed that the peptide substrate fits within a positively charged cleft inside the ACE2 protein (**Figure 4.2E**). The P1 (proline) and P1' (phenylalanine) residues in peptide substrate are intruded into a

hydrophobic cleft (**Figure 4.2F**). Zinc forms a tetrahedral intermediate by making interactions with His374, His378 and Glu402 of ACE2, Pro (P1) of substrate and a water molecule. Glu375 of ACE2 deprotonates the zinc bound water molecule (**Figure 4.2G**). His401 and Tyr385 are two residues forming the S1 pocket in ACE2. These two residues interact with carboxyl oxygen atom of Pro (P1) of the substrate apelin 17 (**Figure 4.2H**). His345 and Pro346 form the S1' pocket in ACE2, which interact with the nitrogen atom of the Phe (P1') of substrate. The P1-P1'cleavage site of the substrate is identified at the C-N bond between Pro (P1) and Phe (P1') which results in the formation of apelin 16 which lacks the C-terminal phenylalanine residue (**Figure 4.2I**). Our *in silico* modeling data demonstrates that ACE2 interacts with pyr-apelin 13 and apelin 17 in a manner compatible with proteolytic cleavage of the substrate.

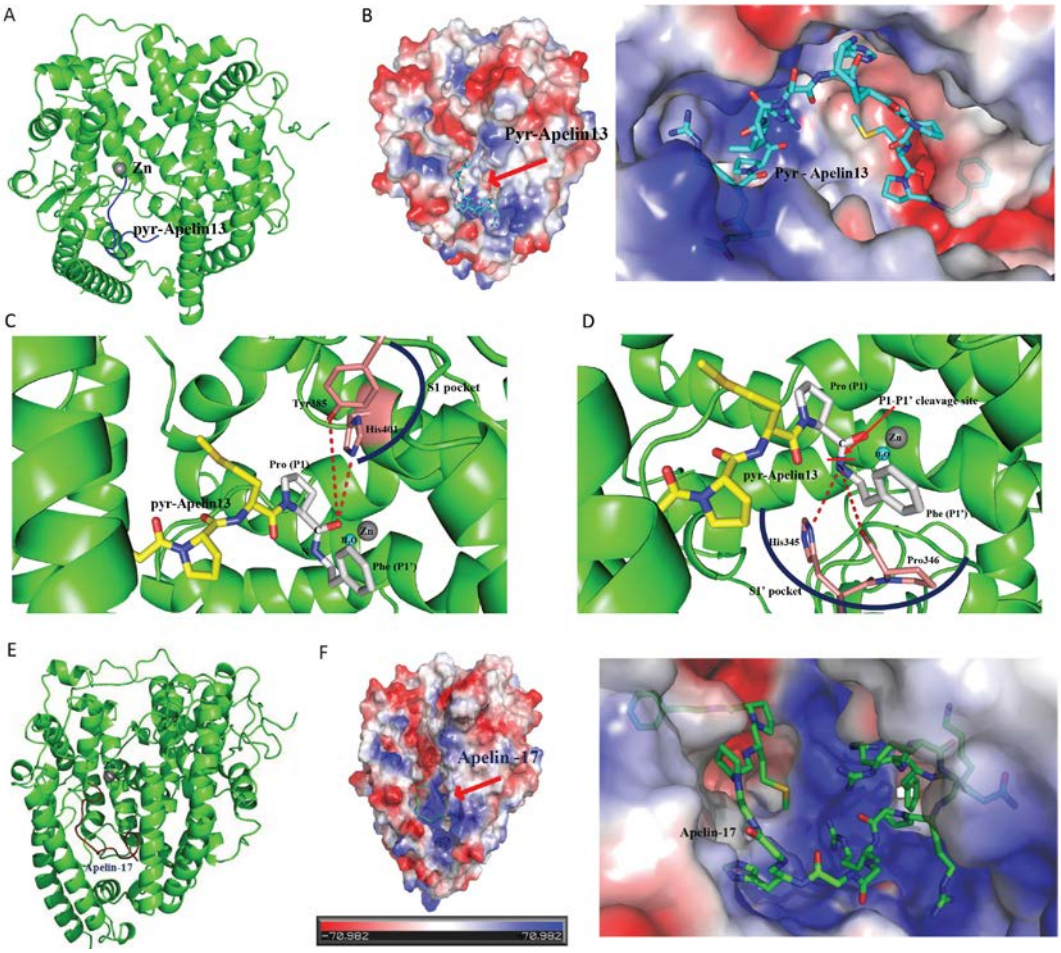
A
Zn
pyr-Apelin13
B
Pyr-Apelin13
Pyr - Apelin13
C
S1 pocket
Tyr385
His401
Pro (P1)
pyr-Apelin13
Zn
H2O
Phe (P1')
D
Pro (P1)
P1-P1' cleavage site
Zn
H2O
pyr-Apelin13
Phe (P1')
His345
Pro346
S1' pocket
E
Apelin-17
F
Apelin-17
-70.982
70.982
Apelin-17

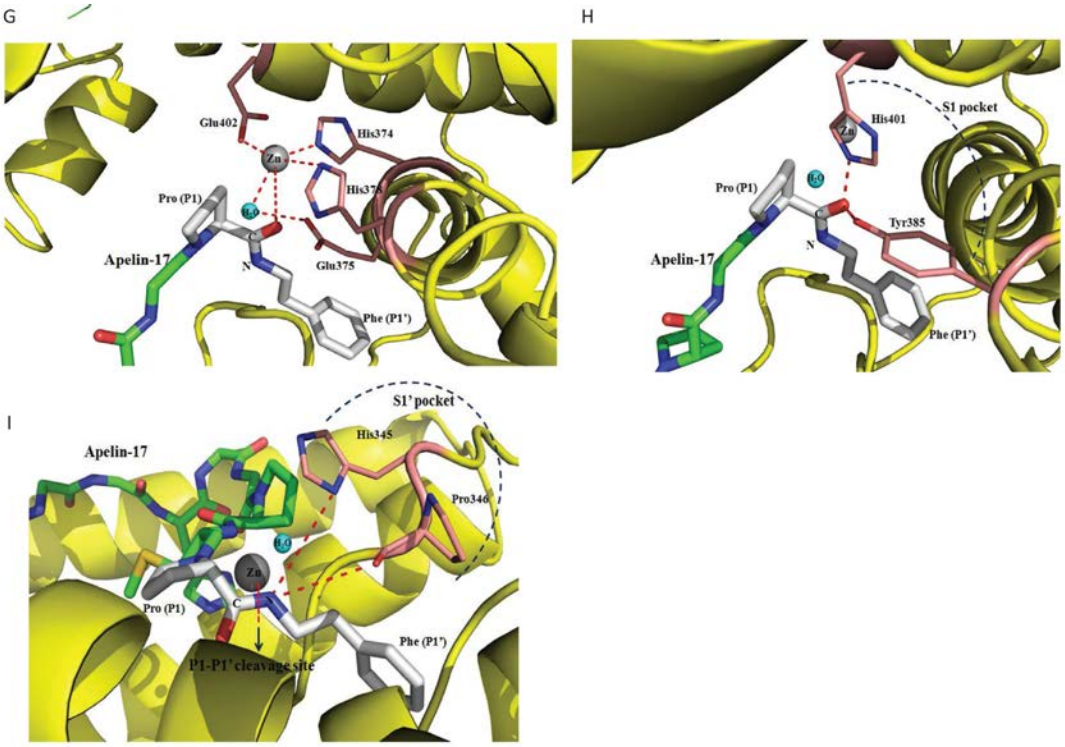

Figure 4.2 Modeling of the interactions between angiotensin converting enzyme 2 (ACE2) and pyr-apelin 13 and apelin 17. Pyr-apelin 13 and zinc bound with ACE2 (**A**) with the electrostatic surface of pyr-apelin 13 bound to ACE2 at a lower (left) and higher (right) magnification (**B**). Interaction between P1 site of pyr-apelin 13 and S1 pocket of ACE2 (**C**) and interaction between P1' site of pyr-apelin 13 and S1' pocket of ACE2 (**D**). The minimized model (**E**) and the electrostatic surface analysis of apelin 17 bound to ACE2 at a lower (left) and higher (right) magnification (**F**). The interaction in the zinc-mediated tetrahedral intermediate (**G**), interaction between P1 site of apelin 17 and S1 pocket of ACE2 (**H**) and interaction between P1' site of apelin 17 and S1' pocket of ACE2 (**I**).

4.4.2 Inhibition of ACE2 potentiates the hypotensive effect of apelin peptides in association with increased apelin peptide levels. We next tested a critical *in vivo* role of ACE2 in modulating the depressor response mediated by apelin peptides (**Figure 4.3A**). In male wildtype mice, intravenous (i.v.) administration of pyr-apelin 13 and apelin 17 resulted in a predictable hypotensive response

(**Figure 4.3B-G**). Interestingly, ACE2 knockout (KO) mice showed a marked increase in the hypotensive response which persisted over the 1 hr measurement period (**Figure 4.3B-G**). Indeed, the reduction in arterial blood pressure approached 50% of baseline values in the ACE2KO mice demonstrating a potent vasodepressor action of apelin peptides in

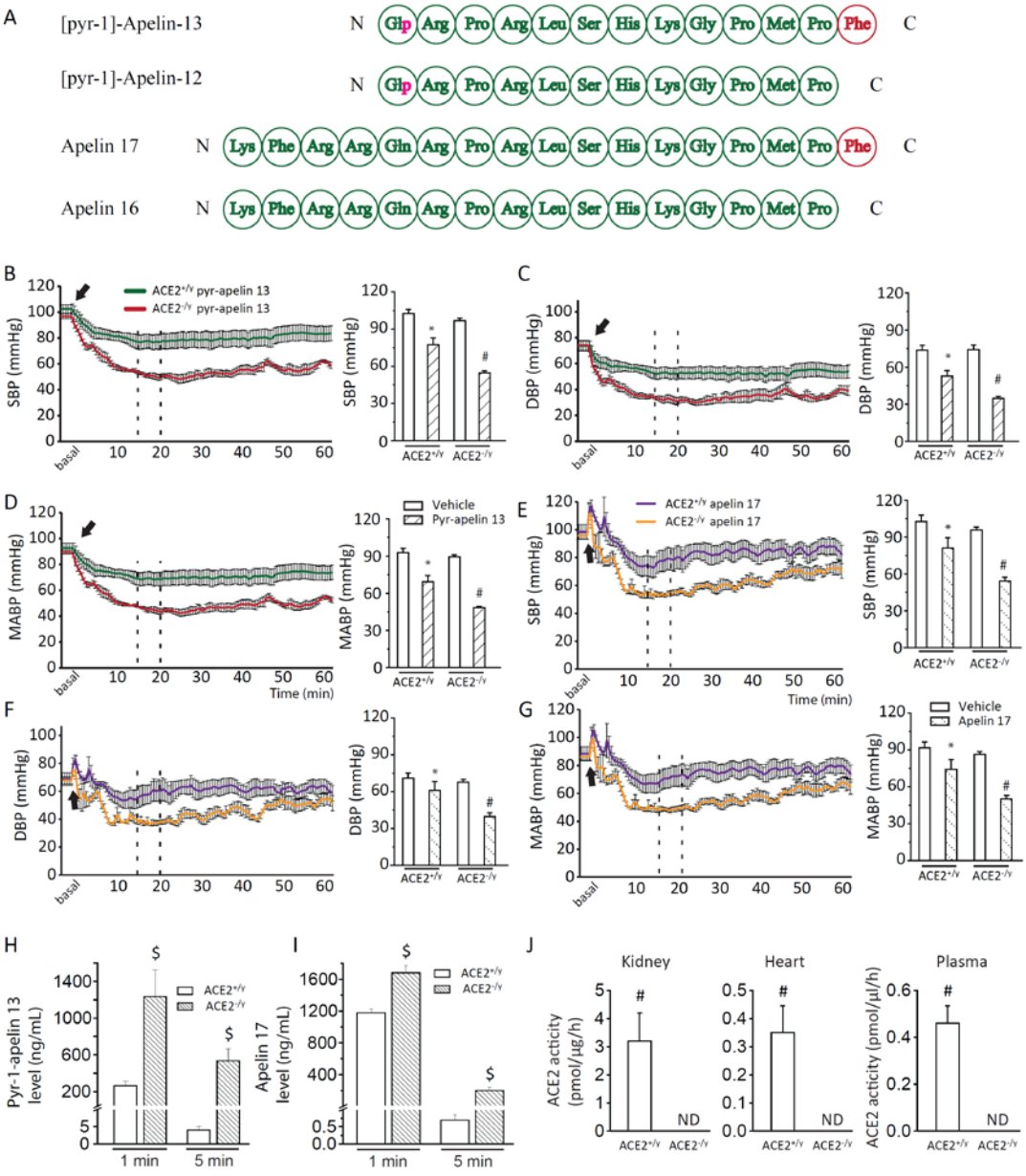
A
[pyr-1]-Apelin-13
[pyr-1]-Apelin-12
Apelin 17
Apelin 16
B
C
D
E
F
G
H
I
J
SBP (mmHg)
DBP (mmHg)
MABP (mmHg)
Time (min)
basal
ACE2+/y pyr-apelin 13
ACE2-/y pyr-apelin 13
Vehicle
Pyr-apelin 13
ACE2+/y apelin 17
ACE2-/y apelin 17
Vehicle
Apelin 17
Pyr-1-apelin 13 level (ng/mL)
Apelin 17 level (ng/mL)
1 min
5 min
Kidney
Heart
Plasma
ACE2 acticity (pmol/μg/h)
ACE2 acticity (pmol/μl/h)
ND

Figure 4.3 Genetic loss of angiotensin converting enzyme 2 (ACE2) potentiates the hypotensive response to apelin peptides in association with elevated plasma apelin levels. Schematic of the parent apelin peptides, pyr-apelin 13 and apelin 17 and their C-terminal truncated peptides, pyr-apelin 12 and apelin 16 (**A**). Blood pressure in anaesthetized mice showing systolic blood pressure (SBP) (**B**), diastolic blood pressure (DBP) (**C**), and mean arterial blood pressure (MABP) (**D**) in response to pyr-apelin 13 (1.4 μM/kg body weight i.v.). The SBP (**E**), DBP (**F**), and MABP (**G**) in response to apelin 17 (1.4 μM/kg body weight i.v.) in anaesthetized mice. Plasma levels of pyr-apelin 13 (**H**) and apelin 17 (**I**) in wildtype ($ACE2^{+/y}$) and ACE2KO ($ACE2^{-/y}$) mice at 1 min and 5 min following intravenous administration. Plasma and tissue ACE2 activity in wildtype ($ACE2^{+/y}$) and ACE2KO ($ACE2^{-/y}$) mice (**J**). Values are mean±SEM; n=8 for the vehicle group and n=10 for the apelin peptide group (A-F); n=12 for the $ACE2^{+/y}$ and $ACE2^{-/y}$ groups (G-I). *$p<0.05$ compared with the vehicle-injected group; $^{\#}p<0.05$ compared with the $ACE2^{+/y}$ group; $^{\$}p<0.05$ compared with the $ACE2^{+/y}$ group.

an ACE2 deficient state. The observed disparity in the hypotensive effects was concomitant with differences in steady-state plasma levels of apelin peptides in WT and ACE2KO mice. In wildtype mice, plasma levels of pyr-apelin13 levels (**Figure 4.3H**) and apelin 17 (**Figure 4.3I**) were markedly increased at 1 min and drastically lowered at 5 min following i.v. delivery. In contrast, plasma pyr-apelin 13 and apelin 17 levels were increased to a greater extent at 1 and 5 min following i.v. delivery in ACE2KO mice (**Figure 4.3H-I**). We confirmed that plasma and tissue ACE2 activity was markedly lowered in the ACE2KO mice (**Figure 4.3J**).

We also used a specific pharmacological inhibitor of ACE2, MLN-4760[174, 177], to provide further evidence for a role of ACE2 in metabolizing apelin peptides. Pharmacological inhibition of ACE2 using *in vivo* administration of MLN (10 mg/kg) increased plasma levels of pyr-apelin 13 (**Figure 4.4A**) and apelin 17 (**Figure 4.4B**) in association with marked suppression of plasma ACE2

activity (**Figure 4.4C**). We next performed *in vitro* assays to directly assess the ability of ACE2 to metabolize apelin peptides. Using HPLC analysis, incubation of plasma from wildtype and ACE2KO mice resulted in a greater loss of pyr-apelin 13 and apelin 17 illustrated by the HPLC tracing (**Figure 4.4D**) and quantitative analysis (**Figure 4.4E**). Recombinant human ACE2 was used to generate enzyme kinetics of the degradation of pyr-apelin 13 and apelin 17. The Hill plot and Michaelis-Menten analysis showed a classic concentration-dependent proteolytic degradation of pyr-apelin 13 and apelin 17 (**Figure 4.4F-H**). The catalytic efficiency determined by the ratio of kcat/Km was 4-times higher for pyr-apelin 13 compared to apelin 17 (**Figure 4.4F-I**). These data clearly demonstrate that genetic and pharmacological inhibition of ACE2 potentiates the hypotensive action of apelin peptides and ACE2 is a key enzyme which degrades apelin peptides.

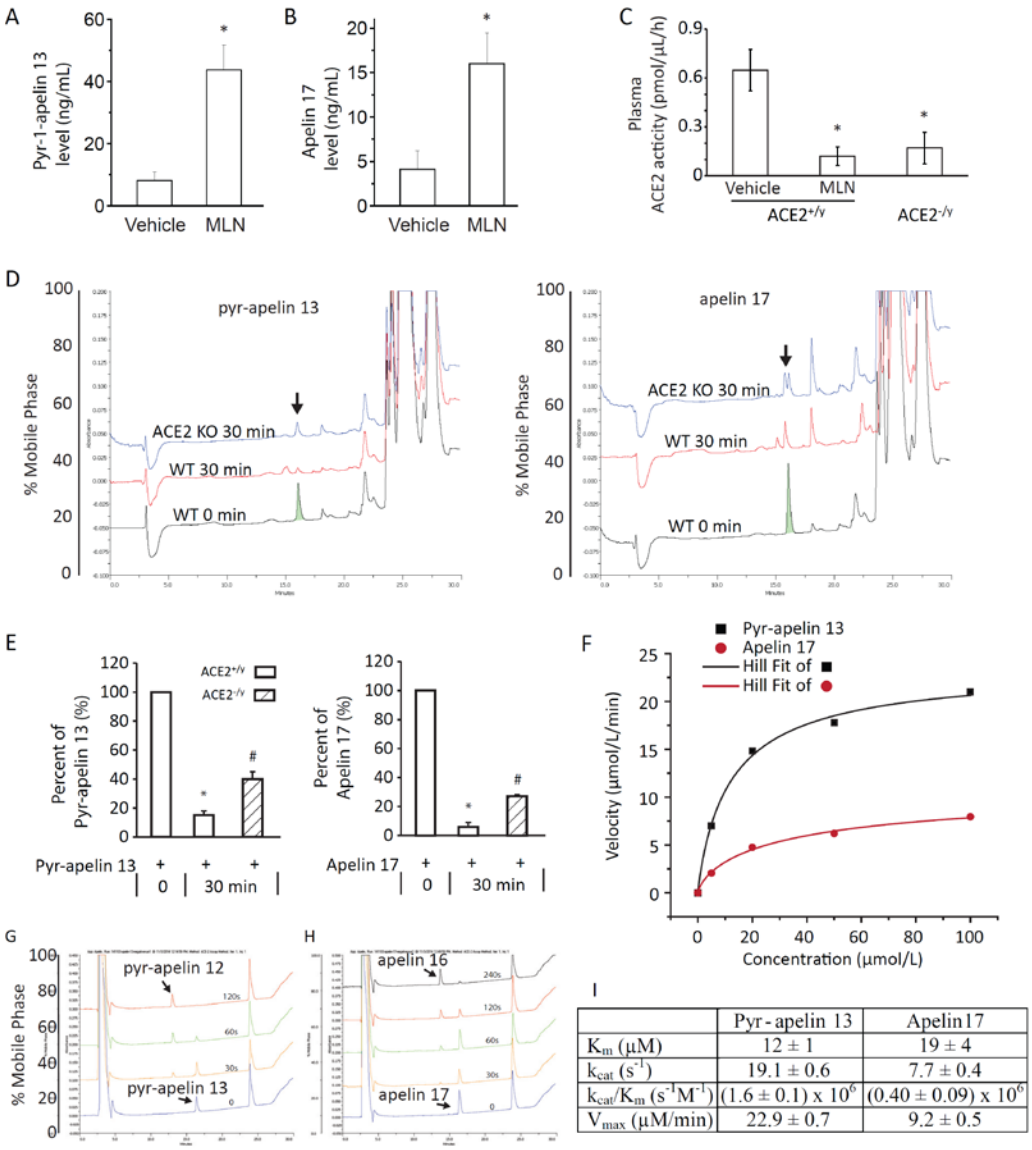

	Pyr-apelin 13	Apelin17
K_m (µM)	12 ± 1	19 ± 4
k_{cat} (s^{-1})	19.1 ± 0.6	7.7 ± 0.4
k_{cat}/K_m ($s^{-1}M^{-1}$)	(1.6 ± 0.1) x 10^6	(0.40 ± 0.09) x 10^6
V_{max} (µM/min)	22.9 ± 0.7	9.2 ± 0.5

Figure 4.4 Pharmacological inhibition of angiotensin converting enzyme 2 (ACE2) potentiates apelin peptides and biochemical analysis shows a key role of ACE2 in the proteolytic degradation of apelin peptides. Plasma levels of pyr-apelin 13 (**A**) and apelin 17 (**B**) in anaesthetized mice in response to pyr-apelin 13 and apelin 17 (1.4 µM/kg body weight i.v.) in wildtype ($ACE2^{+/y}$) mice pretreated with either placebo or MLN-4760 (10 mg/kg i.p.) for 1 hr. Plasma ACE2 activity in response to treatment with MLN-4760 (10 mg/kg i.p.) for 1 hr (**C**). Analysis of the degradation of pyr-apelin 13 (left) and apelin 17 (right) as illustrated by representative HPLC traces (**D**) and quantification (**E**) following incubation with plasma from wildtype ($ACE2^{+/y}$) and ACE2KO ($ACE2^{-/y}$) mice (**E**). Hill plot (**F**) showing

enzymatic degradation of apelin peptides when incubated with recombinant human ACE2 (rhACE2) and representative HPLC traces of the degradation of pyr-apelin 13 (**G**) and apelin 17 (**H**) in response to rhACE2 showing a complete loss of the native peptide within 120 and 240 seconds, respectively. Catalytic properties of the rhACE2-mediated proteolytic processing of pyr-apelin 13 and apelin 17 peptide substrates (**I**). Values are mean±SEM; n=8 for the vehicle group and n=10 for the MLN-4760 group (A-B); *$p<0.05$ compared with the vehicle-injected group; $^{\#}p<0.05$ compared with the $ACE2^{+/y}$ group.

4.4.3 Loss of C-terminal phenylalanine attenuates apelin peptide physiological effects. In order to elucidate the physiological relevance of C-terminal phenylalanine, we examined the effects of native and C-terminal truncated apelin peptides on blood pressure and endothelial cells, and in post-conditioning myocardial ischemia-reperfusion injury. The hypotensive effect of pyr-apelin 12 was clearly lowered compared to the hypotensive action of pyr-apelin 13 in wildtype mice (**Figure 4.5A-C**). Importantly, while pyr-apelin 12-mediated hypotension started to wane after 20 mins, pyr-apelin 13-induced hypotension persisted for a longer period (**Figure 4.5A-C**). Nitric oxide (NO) is a main final effector of the vasodilating effect of apelin in an endothelium-dependent manner.[50, 106] The ability of apelin to activate eNOS leading to NO production in human umbilical vein endothelial cells was used as a bioassay to assess the potency of the apelin peptides. Pyr-apelin 13 and apelin 17 stimulated a robust increase in NO production (**Figure 4.5D**) which was concordant with the alterations in signaling pathways characterized by a marked increase in phosphorylation of Akt at the serine-473 residue (**Figure 4.5E**) and eNOS at the serine-1177 residue (**Figure 4.5F**) in a time-dependent manner. Equimolar doses

of pyr-apelin 12 and apelin 16 resulted in lowered NO production (**Figure 4.5D**), and lowered phosphorylation of Akt and eNOS (**Figure 4.5E-F**).

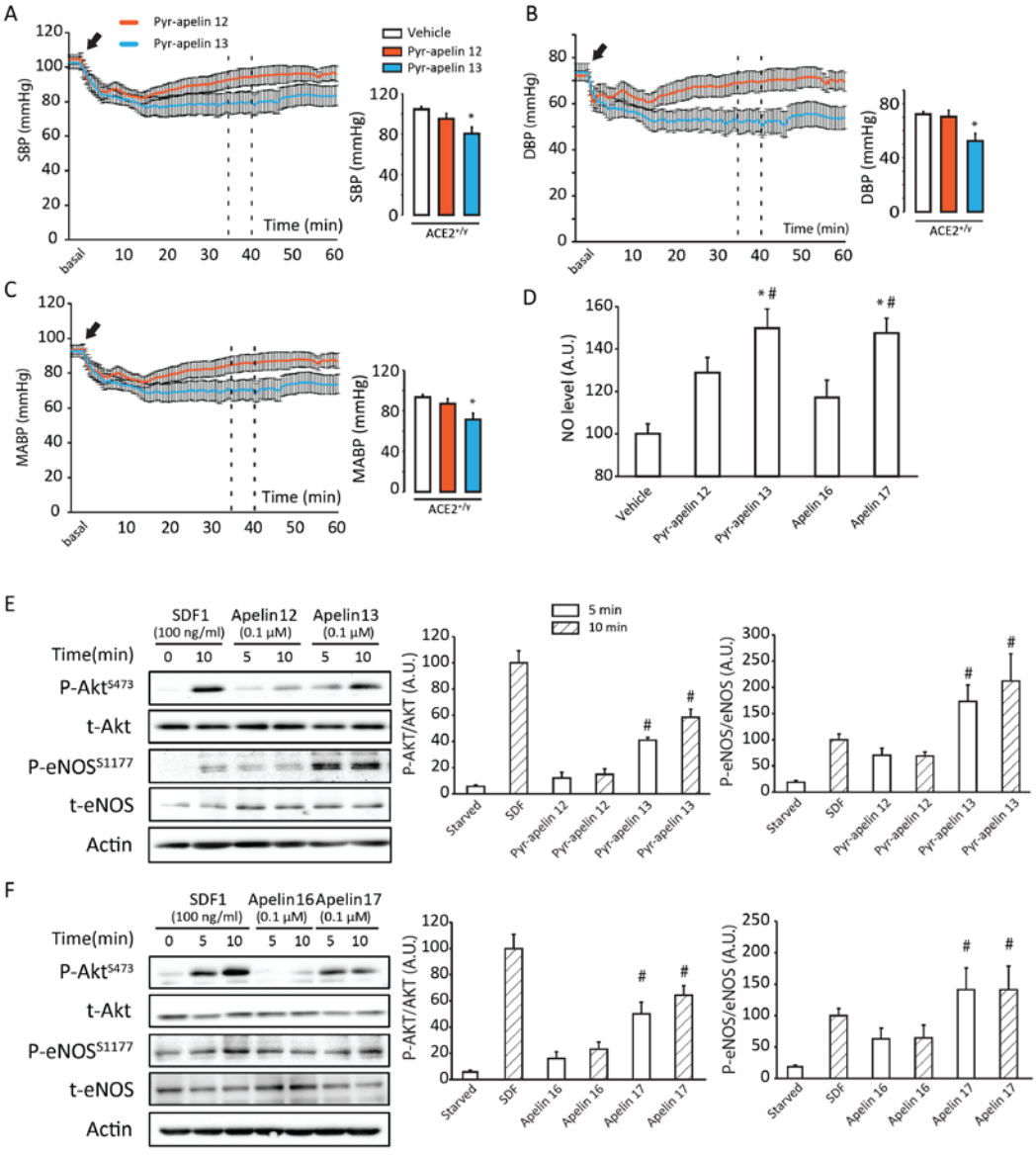

Figure 4.5 Vascular effects of pyr-apelin 12 and apelin 16 peptides display reduced potency compared to their native peptides, pyr-apelin 13 and apelin 17. Blood pressure response based on systolic blood pressure (SBP) (**A**), diastolic blood pressure (DBP) (**B**) and mean arterial blood pressure (MABP) (**C**) in anaesthetized wildtype ($ACE2^{+/y}$) mice in response to pyr-apelin 12 and pyr-apelin 13 (1.4 μM/kg body weight i.v.). Nitric oxide (NO) production by human umbilical vein endothelial cells (HUVEC) showing reduced NO production by pyr-apelin 12 and apelin 16 (**D**). Western blot analysis and quantification illustrating marked time and concentration-dependent increase in phosphorylation of Akt (serine-473 residue) and eNOS (serine-1177 residue) in HUVEC in response to pyr-apelin 13 (**E**) and apelin 17 (**F**) with a lowered phosphorylation seen in response to pyr-apelin 12 and apelin 16. A.U.=Arbitrary Unit, SDF1=stromal cell-derived factor 1. Values are mean±SEM; n=8 for the vehicle group and n=10 for the apelin peptide group (A-C); n=8 for the NO level (D) and n=3 for Western blot analysis (E-F). *$p<0.05$ compared with the vehicle-injected group; $^{\#}p<0.05$ compared with the corresponding pyr-apein 12 or apelin 16 group.

We also used the *ex vivo* Langendorff heart ischemia-reperfusion (I/R) preparation as a disease model to further determine the importance of the C-terminal phenylalanine residue. Using a post-conditioning protocol, we showed that 1 μM of pyr-apelin 13 and apelin 17 result in a predictable cardioprotection in response to global myocardial I/R injury (**Figure 4.6A-B**) In contrast, pyr-apelin 12 and apelin 16 failed to mediate any significant functional improvement following myocardial I/R injury.

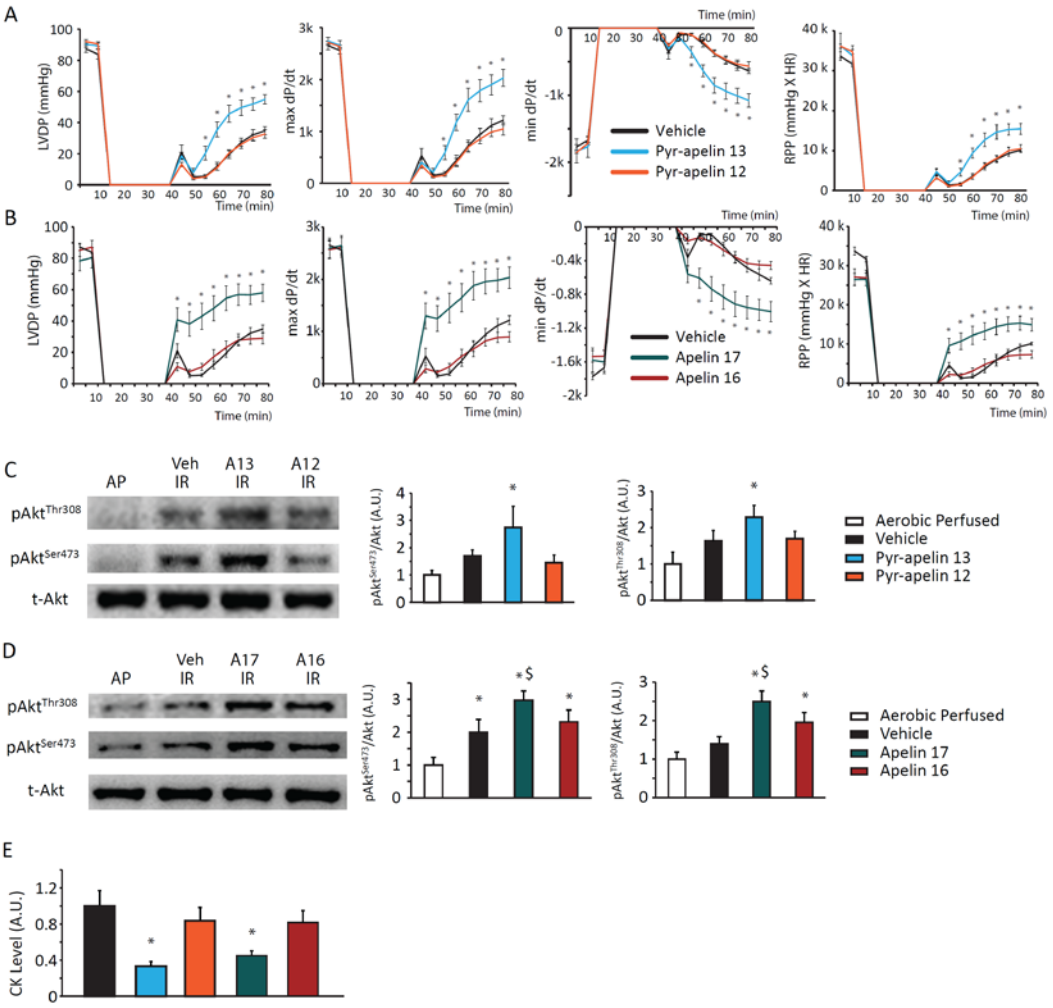

Figure 4.6 Pyr-apelin 12 and apelin 16 peptides failed to exert myocardial protective effects compared to their parent peptides, pyr-apelin 13 and apelin 17. Functional assessment based on the LV developed pressure (LVDP), maximum and minimum rate of change in LV pressure (±dP/dt) and rate-pressure product (RPP) showing marked improvement of post-ischemic functional recovery in response to native apelin peptides, pyr-apelin 13 (1 µM) (**A**) and apelin 17 (1 µM) **(B)** which was completely lost by the use of pyr-apelin 12 (1 µM) and apelin 16 (1 µM) in wildtype ($ACE2^{+/y}$) hearts. Western blot analysis showing increased phosphorylation of serine-473 Akt and threonine-308 Akt in response to myocardial ischemia-reperfusion (IR) injury which was further stimulated by pyr-apelin 13 (**C**) and apelin 17 **(D)** but not in response to pyr-apelin 12 and apelin 16. Creatine kinase activity in the coronary perfusate showing a marked increase in response to myocardial I/R injury and was reduced by pyr-apelin 13 and apelin 17 **(E)** which was completely lost with the use of pyr-apelin 12 and apelin 16. Values are mean±SEM; n=8 for the vehicle group and n=10 for the apelin peptide group (A-B);

n=3 for Western blot analysis (C-D) and n=8 for the CK activity (E). *$p<0.05$ compared with the vehicle-treated group; $^{S}p<0.05$ compared with the apelin 16 group.

Activation of the reperfusion-injury salvage kinase signaling pathway is responsible for mediating beneficial effect in response to I/R injury. Consistent with the differential response in functional recovery, Western blot analysis showed greater elevation in $pAkt^{Thr308}$ and $pAkt^{Ser473}$ (**Figure 4.6C-D**) resulting in lowered creatine kinase (CK) level in the coronary effluent in response to pyr-apelin 13 and apelin 17 (**Figure 4.6E**). In comparison, pyr-apelin 12 and apelin 16 resulted in lowered phosphorylation of the Akt pathway and failed to suppress CK release in the coronary effluent (**Figure 4.6C-E**). These results illustrate a critical role of the C-terminal residue in mediating vascular, endothelial and myocardial effects of the native pyr-apelin 13 and apelin 17 peptides.

4.4.4 Design and Synthesis of Apelin Analogues Resistant to ACE2 degradative Action. The identification of a key degradative site in native apelin peptides allowed us to design synthetic apelin analogues which are potentially resistant to ACE2 action. We modified, synthesized and purified two novel apelin analogues, NleAibBrF-pyr-apelin 13 and NleAibBrF-apelin 17, using a previous described method.[169, 185] Using structure-activity relationships conducted on pyr-apelin 13[169, 185], we made multiple novel single amino acid substitutions combined

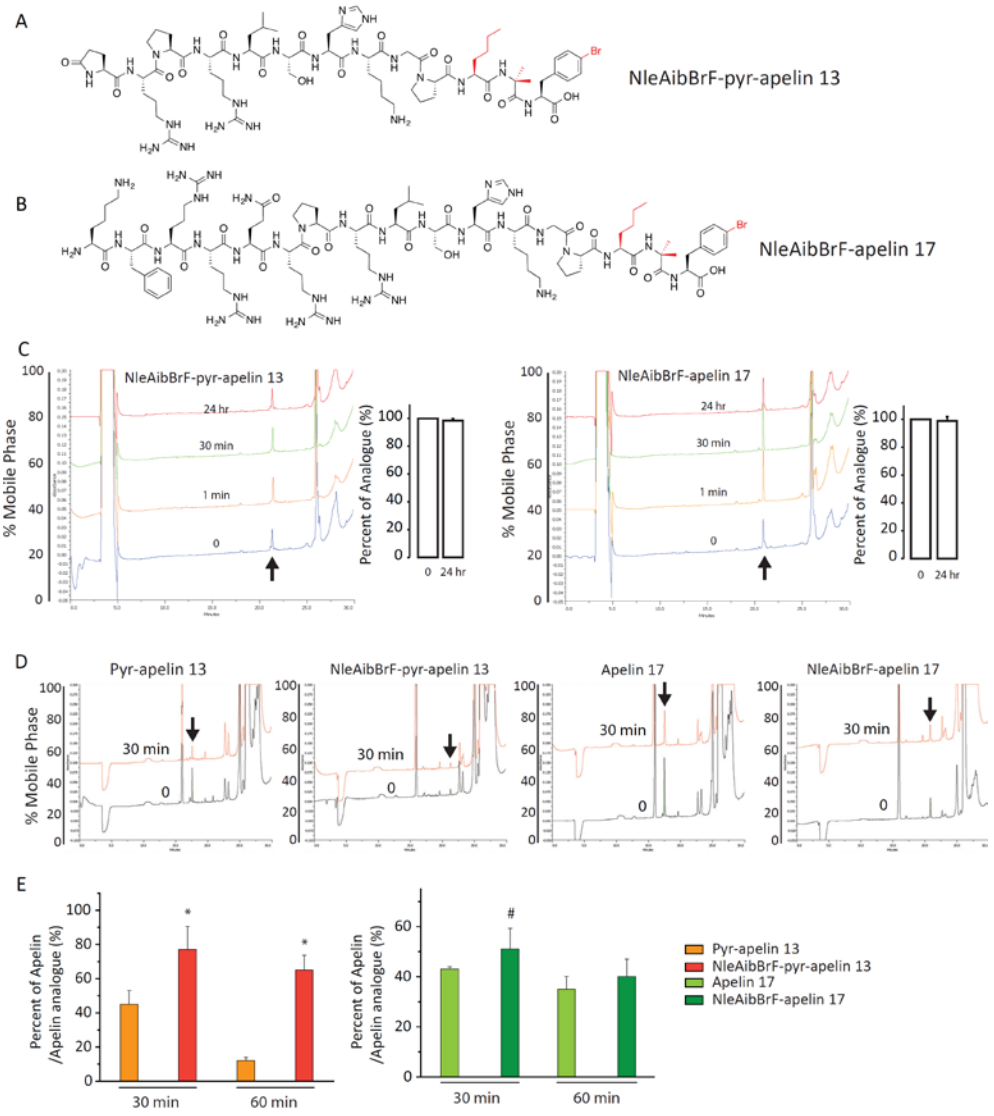

Figure 4.7 Apelin analogues with a chemically modified C-terminal phenylalanine residue are resistant to ACE2-mediated degradation. Schematic of the synthesized apelin analogues, NleAibBrF-pyr-apelin 13 (**A**) and NleAibBrF-apelin 17 (**B**) with new regions highlighted in red. Incubation of the apelin analogues with rhACE2 showed a marked resistance to proteolytic degradation with a minimal loss of the apelin analogue over a 24-hr time period (**C**). Incubation of the apelin analogues with human plasma compared to native apelin peptides further confirming that these apelin analogues are resistant to enzymatic degradation as illustrated by representative HPLC traces (**D**) and relative quantification at 30 and 60 min following the incubation (**E**). Values are mean±SEM; n=3. *$p<0.05$ compared with pyr-apelin 13; $^{\#}p=0.14$ compared with apelin 17.

into the same peptide with the aim of "masking" the susceptible C-terminal amide bond from proteolytic cleavage. These analogues were purified using high-performance liquid chromatography, and high-resolution mass spectrometry and nuclear magnetic resonance were used to confirm the sequence of the synthesized analogues (**Figure 4.7A-B**). In contrast to native apelin peptides which were completely degraded within 4 min (**Figure 4.4G-H**), incubation of the apelin analogues with rhACE2 showed a marked resistance to proteolytic degradation with a minimal loss of apelin analogue over a 24-hr time period (**Figure 4.7C**). Similarly, incubation of the apelin analogues with human plasma further confirmed that these apelin analogues are partially resistant to enzymatic degradation with a greater resistance seen with NleAibBrF-pyr-apelin 13 compared to the NleAibBrF-apelin 17 analogue (**Figure 4.7D-E**). These results highlight that apelin peptides can be manipulated to create apelin analogues resistant to ACE2 degradative action, supporting a potential therapeutic application of apelin analogues.

4.5 Disccusion

Apelin peptides are known to mediate a range of beneficial effects in the cardiovascular system and on fluid homeostasis.[40, 66, 170] Endogenous apelin maintains endothelium structure and function, promotes angiogenesis, counteracts the renin-angiotensin system, and regulates metabolism, myocardial hypertrophy

and fibrosis, and inflammation.[40, 66, 170] The 13 amino acid apelin peptide with a post-translational pyroglutamate substitution at the N terminus (pyr1-apelin-13) has the most affinity for the apelin receptor and appears to be the predominant isopeptide in the human myocardium and plasma.[40, 168] Importantly, pyr-apelin 13 is beneficial in patients with heart failure.[49] However, apelin peptides have extremely short half-lives *in vivo*, suggesting the presence of a high efficiency degradative system. Based on *in vitro* kinetic assays, ACE2 is also known to cleave several peptides essentially functioning as a monocarboxypeptidase.[58] Angiotensin converting enzyme 2 has emerged as a dominant modulator of angiotensin metabolism and is one of the key enzymes that converts Ang II into Ang 1-7.[68, 85] We identified ACE2 as a major enzyme that determines the magnitude and duration of native apelin peptide action in the cardiovascular system. Collectively, these results support a propensity of ACE2 to cleave the peptide amide bond characterized by proline-phenylalanine as the penultimate and C-terminal residues, respectively.

Importantly, in our current studies, we proved that the endogenous levels of ACE2 dramatically affect the action of exogenous apelin on the cardiovascular system. ACE2 is widely expressed, including expression in the heart, kidneys, vasculature, gut and central nervous system, and is proteolytically shed by ADAM-17/TACE into the plasma.[56, 57] Therefore, ACE2 can be categorized into tissue ACE2 or soluble ACE2 existing in plasma. We showed that soluble ACE2

is able to cleave apelin, as demonstrated *in vitro* plasma incubation. However, the kinetics of the degradation of native apelin peptides was markedly slower compared to the *in vivo* responses, suggesting that tissue ACE2 is the dominant form of ACE2 which modulates native apelin peptide degradation *in vivo*. The use of rhACE2 in healthy human volunteers lowered plasm Ang II levels and increased plasma Ang 1-7 levels without altering systolic or diastolic blood pressure.[186] The ability of rhACE2 to degrade pyr-apelin 13 and apelin 17 into product peptides with lowered vasodepressor action may explain the lack of rhACE2 depressor action *in vivo*. Based on blood pressure responses, loss of function experiments involving ACE2, and degradation assays, ACE2 has a greater efficacy for metabolizing pyr-apelin 13 compared to apelin 17.

Our results are consistent with several elegant biochemical studies showing that apelin-induced activation of intracellular signaling involves both Gαi- and β-arrestin dependent pathways and that the β-arrestin-dependent effects require the presence of the C-terminal phenylalanine residue.[173, 187] The loss of phenylalanine in pyr-apelin 13 and apelin 17 clearly lowered its ability to produce a hypotensive effect through systemic vasodilation. These results are consistent with previous studies using the apelin 17 peptide where the deletion of the phenylalanine reduced its hypotensive effect by 80%.[62] We linked these differences in physiological response to the differential ability of the apelin peptides to activate and increase NO production. Given the beneficial effect of apelin peptides

coupled with its short half-life *in vivo*, modification of apelin by protecting the C-terminal phenylalanine residue is a critical step in the generation of stable apelin analogues with therapeutic potential.

CHAPTER FIVE

Loss of Apelin exacerbates myocardial infarction adverse remodeling and ischemia-reperfusion injury: therapeutic potential of synthetic Apelin analogues

Wang Wang[1,2] , Shaun M.K. McKinnie[3], Vaibhav B. Patel[2,4], George Haddad[5], Zuocheng Wang[2,4], Pavel Zhabyeyev[2,4], Subhash K. Das[2,4], Ratnadeep Basu[1,2], Brent McLean[1,2],Vijay Kandalam[1,2], Josef M. Penninger[6], John C. Vederas[4], Zamaneh Kassiri[1,2], Allan G. Murray[5] and Gavin Y. Oudit[1,2,4]

[1]Department of Physiology,[2]Mazankowski Alberta Heart Institute, [3]Department of Chemistry, [4]Division of Cardiology, Department of Medicine, [5]Division of Nephrology, Department of Medicine, University of Alberta, Edmonton, Canada, [6]Institute of Molecular Biotechnology of the Austrian Academy of Sciences, Vienna, Austria

Author Contribution: Wang Wang and Gavin Oudit designed and wrote the manuscript and figures; Wang Wang created the animal models, functional recordings and analysis, collected the samples and coordinated the study with contributing authors; Shaun McKinnie and John Vederas synthesized the apelin analgues and kinetic assay; Vaibhav Patel performed immunostaining and imaging analysis; George Haddad and Allan Murray performed and quantified the siRNA against Apelin; Zuocheng Wang and Brent Mclean performed the western blot assay; Pavel Zhabyyeyev performed the cardiomyocye culture and characterization; Subhash Das performed the inflammation staining and analysis; Ratnadeep Basu and Zam Kassiri performed the ultrasound analysis; Vijay Kandalam performed the in vitro angiogenesis assay; Josef Penninger reviewed and edited the manuscript.

A modified version of this chapter has been published in *J Am Heart Assoc.* 2013 Jul 1;2(4):e000249. doi: 10.1161/JAHA.113.000249.

5.1 Abstract

Coronary artery disease leading to myocardial ischemia is the most common cause of heart failure. Apelin (APLN), the endogenous peptide ligand of the APJ receptor, has emerged as a novel regulator of the cardiovascular system. Here we show a critical role of APLN in myocardial infarction (MI) and ischemia-reperfusion (IR) injury in patients and animal models. Myocardial APLN levels were reduced in patients with ischemic heart failure. Loss of APLN increased MI-related mortality, infarct size, and inflammation with drastic reductions in pro-survival pathways resulting in greater systolic dysfunction and heart failure. APLN deficiency decreased vascular sprouting, impaired sprouting of human endothelial progenitor cells and compromised *in vivo* myocardial angiogenesis. Lack of APLN enhanced susceptibility to ischemic injury and compromised functional recovery following *ex vivo* and *in vivo* IR injury. We designed and synthesized two novel APLN analogues resistant to angiotensin converting enzyme 2 cleavage and identified one analogue that mimicked the function of APLN to be markedly protective against *ex vivo* and *in vivo* myocardial IR injury linked to greater activation of survival pathways and promotion of angiogenesis. We conclude that APLN is a critical regulator of the myocardial response to infarction and ischemia and pharmacologically targeting this pathway is feasible and represents a new class of potential therapeutic agents.

Keywords: Myocardial infarction, Angiogenesis, Cardiomyopathy, Heart failure, Ischemia-reperfusion injury

5.2 Introduction

Apelin is the endogenous ligand for APJ receptor and is synthesized as a 77-amino acid prepropeptide which is processed into C-terminal fragments denoted by their lengths as Apelin-36, Apelin-19, Apelin-17 and Apelin-13.[39, 40] Apelin is predominantly expressed in the endocardial and vascular endothelial cells while the APJ receptor is localized to endothelial and smooth muscle cells as well as cardiomyocytes, allowing for autocrine and paracrine effects of apelin in the heart.[40-42] Apelin mediates positive inotropic effect on isolated cardiomyocytes[43], isolated perfused rat heart[44] and *in vivo*[45] and mediates endothelium-dependent vasodilation.[46] Genetic variation in the APJ receptor modifies the progression of heart failure in patients with dilated cardiomyopathy[47] and the apelin/APJ system is compromised in human heart failure.[41, 48] In patients with chronic heart failure, apelin administration increased cardiac index and lowered peripheral vascular resistance in the absence of hypotension providing a promising new drug target for heart failure.[49]

Coronary artery disease is now the most common cause of heart failure.[188] Apelin promotes the phosphorylation of Akt and increases the proliferation of endothelial cells *in vitro* suggesting an important pro-angiogenic role.[50, 51, 189] Given the plethora of biochemical and cellular effects of apelin, we hypothesized that loss of apelin may enhance the susceptibility to myocardial ischemic injury. We used apelin knockout ($APLN^{-/y}$) and wildtype ($APLN^{+/y}$) mice and showed that loss of apelin impaired the functional recovery, post MI remodeling and angiogenesis and exacerbate myocardial ischemia-reperfusion (IR) injury. We used novel synthetic APLN analogues which were markedly resistant to proteolytic cleavage by angiotensin converting enzyme 2 (ACE2) in contrast to the native pyr1-apelin-13, and identified one analogue that mimicked the function of APLN and resulted in marked protection against *ex vivo* and *in vivo* myocardial IR injury linked to greater activation of survival pathways and promotion of angiogenesis. We conclude that APLN critical regulates the myocardial response to ischemia and pharmacologically targeting this pathway is feasible and represents a new class of potential therapeutic agents.

5.3 Methods

Experimental Animals. Apelin deficient ($APLN^{-/y}$) and littermate wildtype ($APLN^{+/y}$) mice were generated and breed in a C57BL/6 background as

previously described.[130] All animal experiments were carried out in accordance with the Canadian Council on Animal Care Guidelines, and animal protocols were reviewed and approved by the Animal Care and Use Committee at the University of Alberta.

Human Explanted Hearts. Cardiac tissues from patients with subacute MI or idiopathic dilated cardiomyopathy and with advanced heart failure were collected from the explanted hearts at the time of cardiac transplantation as part of the Human Explanted Heart Program (HELP) at the Mazankowski Alberta Heart Institute. Non-failing control hearts were obtained by the Human Organ Procurement and Exchange (HOPE) program. All experiments were performed in accordance with the institutional guidelines and were approved by Institutional Ethics Committee.

Myocardial Infarction. Ten-week-old male mice of both genotypes were subjected to MI by permanent ligation of the proximal left anterior descending (LAD) coronary artery in a manner blinded to the genotype as previously described.[152, 190] Anaesthetized mice underwent left thoracotomy in the fourth intercostal space. The pericardium was opened to expose the left ventricle (LV) and the LAD was encircled and ligated with a 6-0 silk suture; the muscle and skin were closed in layers. In sham-operated mice, LAD was encircled but not ligated. Animals were inspected at least 2 times daily. Following 1 day and 7days after LAD ligation or sham-operation, mice were anaesthetized and sacrificed. Hearts

were quickly excised, dissected into infarct, peri-infarct, and non-infarct regions, and then flash-frozen separately for further protein and RNA analyses. For immunohistochemical analysis, whole hearts were arrested in diastole with 1 M KCl and then fixed in 10% formalin or embedded in OCT and flash frozen.

Infarct Size Measurement and Neutrophil and Macrophage Staining. For infarct size measurement, hearts were quickly excised and sectioned in 0.5-mm slices from apex to the point of ligation, then incubating with 1% Triphenyl Tetrazolium Chloride (Sigma, Canada) at 37 °C for 10 min. The brick red represents viable tissue, while pale indicates necrosis. Image Proplus software was used for image analysis. Infarct size was reported as a percentage of the total LV size. Neutrophils and macrophages were stained in sham, 1-day and 3-days post-MI LVs using rat anti-mouse neutrophil (AbD Serotec, NC, USA) and rat anti-mouse Mac-3 (BD Biosciences) primary antibodies and Cy3 conjugated goat anti-rat and Alexa Fluor 488 conjugated goat anti-rabbit secondary antibodies (Invitrogen, CA, USA), respectively. The sections were visualized and imaged under fluorescence microscope (Olympus IX81) and images were analyzed using Metamorph software (Version 7.7.0.0).

Apelin and CD31 Immunofluorescence. Apelin and CD31 double immunofluorescence staining was carried out in human heart and coronary arteries as well as in murine heart tissues. Briefly, 5 μm thick OCT embedded

cryosections were fixed with 4% paraformaldyhyde followed by rehydration, permeabilization and blocking with PBS, 0.1% triton X-100 and 4% BSA, respectively. The sections were then incubated with primary antibodies, goat anti-apelin (Santa Cruz Biotechnology Inc., CA, USA) and mouse anti-human CD31 (BD Biosciences, Mississauga, Canada) for human LV and goat anti-apelin (Santa Cruz Biotechnology Inc., CA, USA) and rat anti-mouse CD31 (BD Biosciences, Mississauga, Canada), at 4°C for overnight. The sections were then washed with PBS and incubated with secondary antibodies, Alexa Fluor 488 conjugated donkey anti-goat and Alexa Fluor 594 conjugated donkey anti-mouse for human LV and Alexa Fluor 488 conjugated donkey anti-goat and Alexa Fluor 594 conjugated donkey anti-rat (Invitrogen, Burlington, Canada) for mouse LV, at 37°C for 1 hour. The sections were washed with PBS, mounted with Prolong Gold antifade mounting medium with DAPI (Invitrogen, Burlington, Canada) and visualized and imaged under the fluorescence microscope (Olympus IX81).

Echocardiography Measurements and Invasive Pressure-Volume Analysis. Transthoracic echocardiography was performed noninvasively as described previously using a Vevo 770 high-resolution imaging system equipped with a 30-MHz transducer (RMV-707B; VisualSonics, Toronto, ON, Canada). The temporal resolution for M-mode imaging in this system is a pulse repetition frequency of 8 kHz with an axial resolution of 55μm, lateral resolution of 115 μm, focal length of 12.7 mm, and depth of field of 2.2 mm. Mice were anesthetized with 0.8%

isoflurane for the duration of the recordings. LV ejection fraction (EF) was calculated as a measure of systolic function using the following equation: EF (%) = [(LV end-diastolic volume-LV end-systolic volume)/LV end-diastolic volume]/100. The maximal anteroposterior LA diameter was measured by M-mode in the parasternal long-axis view and used as LA size. Qualitative and quantitative measurements were made offline using analytic software (VisualSonics, Toronto, Canada). Electrocardiogram kilohertz-based visualization (EKV™) software analysis produced offline reconstruction for simulated 250 to 1,000 Hz static and cine loop images. Modified parasternal long axis EKV loops were also used to measure ejection fraction (EF) via Simpson's method. M-mode images were used to measure left ventricular (LV) chamber sizes and wall thicknesses. The wall motion score index (WMSI) was calculated based on the *American Society of Echocardiography* recommended assessment of wall motion function of the 17-segment LV model.[191-193] In the murine model, use of WMSI and analysis of segmental wall motion abnormalities in the post-MI hearts has been validated.[191, 192]

To measure left ventricular pressure-volume relationship, 1.2F admittance catheter (Scisense Inc., London, Canada) was used as previously described[194, 195]. Briefly, mice were anaesthetized with isoflurane; an incision was made in the right carotid artery and catheter was inserted into the incision. The catheter was advanced to left ventricle via ascending aorta and aortic valve. The position of the

catheter was monitored by pressure along with the magnitude and phase using ADvantage pressure-volume system (Scisense Inc., London, Canada) and iworx (iWorx Systems Inc., Dover, USA) data acquisition system connected to the catheter. Initially, the catheter position was set in the LV to obtain the magnitude difference of more than 200 μS along with a physiological pressure-volume loop shape. After the magnitude was accomplished in the desired range, the phase was adjusted to 4-8 with slightly adjusting the position of the catheter in the LV where phase represents the conductivity imparted by the LV tissue. Once, the desired range for magnitude and phase was achieved, baseline scan was performed to derive volume using Baan's equation and pressure-volume loop was obtained using the LabScribe2 software (version 2.347000). After instrument (ADvantage, Scisense Inc., London, Canada) was adjusted and PV measurements were obtained, the inferior vena cava was briefly occluded to obtain alterations in venous returns to derive end-systolic and end-diastolic PV relations. Online as well as offline calculations were performed using LabScribe2 software (version 2.347000).

Synthesis and Characterization of Novel Apelin Analogues

a. Reagents and solvents: All commercially available reagents and protected amino acids were purchased and used without further purification. Dichloromethane (DCM) used for anhydrous reaction was distilled over calcium

hydride prior to use. HPLC grade dimethylformamide (DMF) and methanol were used without further purification.

b. Loading of C-terminal 4-bromophenylalanine onto Wang resin: A flame dried 3-necked round bottom flask equipped with a stirring bar was flushed with Ar gas. Fmoc-4-bromophenylalanine (0.933 g, 2.0 mmol) was dissolved in dried DCM and cooled to 0 °C. Diisopropylcarbodiimide (0.155 mL, 1.0 mmol) was added to the mixture and stirred at 0 °C for 20 minutes. The reaction mixture was concentrated *in vacuo* and redissolved in a DMF:DCM solution (3:1). Wang resin (2.00 g) was added to a solid phase peptide synthesis vessel and washed with dry DCM (2 x 10 mL) and DMF (2 x 10 mL). The resin was pre-swollen by bubbling with Ar gas in DMF (10 mL) for 1 h and filtered. The activated Fmoc-4-bromophenylalanine anhydride was added to the resin followed by catalytic 4-dimethylaminopyridine (DMAP) and bubbled under Ar gas for 1.5 h. The solution was drained, and the resin was washed with DMF (3 x 10 mL). To cap additional reactive sites on the resin, 20 % acetic anhydride in DMF (15 mL, 15 min.) was used and followed by washing with DMF (3 x 10 mL) and DCM (3 x 10 mL), yielding Fmoc-4-bromophenylalanine on Wang resin in 0.5 mmol/g loading.

c. General procedure for elongation using manual Fmoc Solid Phase Peptide Synthesis (SPPS): NMM (6 equiv) was added to a solution of Fmoc protected amino acid (5.0 equiv to resin loading), HOBt (5.0 equiv) and PyBOP (4.9 equiv)

in DMF (10 mL). The solution was allowed to pre-activate for 5 min. The solution was transferred to the reaction vessel containing pre-swelled resin and was bubbled with argon for 2 h. A small sample of the peptide was cleaved from the resin (by treatment with 95% TFA/2.5% TIPS/2.5% H_2O for 2 h) and the completion of the reaction was determined by MALDI-TOF analysis using 4-hydroxy-α-cyanocinnamic acid (HCCA) as a matrix. Resin was washed with DMF (3 × 10 mL), then 20% Ac_2O in DMF (10 mL) was added to the resin for 10 min to effect end capping. Resin was again washed with DMF (3 × 10 mL). Then 20% piperidine in DMF (3 × 10 mL) was added to remove the N-terminal Fmoc protecting group, this reaction was monitored by UV-Vis spectroscopy, observing the dibenzofulvene-piperidine adduct at λ = 301 nm.

d. General procedure for peptide synthesis using automated Fmoc Solid Phase Peptide Synthesis (SPPS). All peptides were synthesized on a CEM Liberty 1 Microwave Peptide Synthesizer. Solid phase synthesis was carried out on a 0.1 mmol scale using Fmoc chemistry on Wang resin (0.65 mmol/g loading). Commercially available protected amino acids and were loaded on the peptide synthesizer as 0.2 M solutions in DMF. All amino acid subunits were coupled using O-benzotriazole-N,N,N',N'-tetramethyl-uronium-hexafluoro-phosphate (HBTU) as the activating agent and heated at 70 ^{o}C for a 5 min coupling time. Fmoc residues were deprotected using a 20% solution of piperidine in DMF using

UV-Vis spectroscopy to observe the dibenzofulvene-piperidine adduct absorption monitored at $\lambda = 301$ nm.

e. Syntheses of NleInpBrF pyr-1-apelin-13 and NleAibBrF pyr-1-apelin-13 analogues. For both analogues, 4-bromophenylalanine-loaded Wang resin was subjected to Fmoc deprotection as described above, and either Fmoc-Inp-OH or Fmoc-Aib-OH were coupled onto the free amine to initiate the synthesis of NleInpBrF or NleAibBrF pyr-1-apelin-13 respectively. The following amino acids were coupled as previously described in the following order: Fmoc-Nle-OH, Fmoc-Pro-OH, Fmoc-Gly-OH, Fmoc-Lys(Boc)-OH, Fmoc-His(Trt)-OH, Fmoc-Ser(O^{t}Bu)-OH, Fmoc-Leu-OH, Fmoc-Arg(Pmc)-OH, Fmoc-Pro-OH, Fmoc-Arg(Pmc)-OH, and pyroglutamic acid.

f. General procedure for cleavage and purification of pyr-1-apelin-13 analogues. To simultaneously cleave the peptide from Wang resin and remove side chain protecting groups, a solution of 95:2.5:2.5 TFA: anisole: H_2O was added to the resin-bound peptide for 2 hours. The resin beads were removed via filtration through glass wool and the filtrate was concentrated *in vacuo*. The crude peptide was obtained by precipitation with cold Et_2O. The crude peptide was redissolved in a 9:1 water: methanol (0.1% TFA) solution and purified by high performance liquid chromatography (HPLC). High performance liquid chromatography (HPLC) was performed on a Varian Prostar chromatograph equipped with a model 325 variable wavelength UV detector and a Rheodyne 7725i injector fitted

with a 1000 μL sample loop. The column used for semi-preparative purification was a Phenomenex Luna C18(2) column (5 μm, 10.00 x 250 mm), and for analytical purification was a C18 reverse-phase peptide/protein HPLC column (Vydac, 4.6 x 250 mm, 5 μm) using water (0.1% TFA) and acetonitrile (0.1% TFA) as eluents. All HPLC solvents were filtered with a Millipore filtration system under vacuum before use.

The HPLC method followed was: gradient beginning at 2% acetonitrile, climb to 50% acetonitrile over 10 min, then climb to 100% acetonitrile over 4 min, remain at 100% for 4 min, return to 2% over 4 min, hold at 2% over 3 min (flow rate 1 mL/min (analytical) or 2.5 mL/min (semi-preparative) with UV detection at 220 nm). The peptide was collected as a sharp peak at 13.5 min and solvent was removed *in vacuo*. The residue was then resuspended in 0.1% TFA in water and lyophilized to give the final product. NleInpBrF pyr-1-apelin-13 (apelin analogue I) was isolated as a white solid powder after lyophilization in 25.6% yield (10.5 mg purified). NleAibBrF pyr-1-apelin-13 (apelin analogue II) was isolated as a white solid powder after lyophilization in 36.4% yield (17.9 mg purified).

Angiotensin-converting enzyme 2 proteolysis assay of pyr-1-apelin-13 and apelin analogues. Recombinant human angiotensin converting enzyme 2 (rhACE2) was suspended in Tris buffer (25 mM Tris, 200 mM NaCl, 5 μM

$ZnCl_2$, pH 8.0) to a final concentration of 1 μM.[68] 1 mM solutions of apelin peptides (pyr-1-apelin-12 (65-76) (New England Peptide Inc, Gardner, MA) and pyr-1-apelin-13 (65-77) (Tocris Bioscience, Ellisville, MO)) and apelin analogues were prepared in Milli-Q water. A modified procedure was adapted to determine the extent of apelin peptides and apelin analogues susceptibility to ACE2 proteolysis.[58] 5 μL of 1 μM ACE2 was added to 90 μL of buffer (25 mM Tris, 200 mM NaCl, 5 μM $ZnCl_2$, pH 8.0) and 5 μL of aqueous 1 mM apelin peptide or apelin analogue were added to the reaction mixture for varying quantities of time at room temperature or 37°C to achieve final concentrations of 5 nM rhACE2 and 5 μM apelin peptide/analogue, respectively. Reactions were quenched upon addition of 100 μL of 100 mM EDTA (ethylenediaminetetraacetic acid) pH 7.0, and products were monitored by both HPLC and MALDI-TOF analyses. Analytical HPLC separation of peptides was accomplished using a C18 reverse-phase peptide/protein HPLC column (Vydac, 4.6 x 250 mm, 5 μm) using a gradient of 10 – 45% B (A: water (0.1% TFA); B: acetonitrile (0.1% TFA)). A flow rate of 1 mL/min was used and peptides were detected by absorbance at 220 nm. The amount of hydrolyzed product was determined by comparing the areas under the substrate and product peaks after integration as previously reported.[58] Hydrolysis products and initial substrates were analyzed on a Perspective Biosystems Voyager™ Elite MALDI-TOF MS using 4-hydroxy-α-cyanocinnamic acid (HCCA) as a matrix to confirm masses.

Isolated Langendorff Heart Perfusion and Ischemia-Reperfusion Protocol. Langendorff heart perfusion was used to study the contractile function. Mice were heparinized and anaesthetized with 1.5-2% isoflurane inhalation. Heart was excised and mounted on Langendorff system and perfused at a consistent pressure of 80 mmHg with modified Krebs-Henseleit solution (116 mM NaCl, 3.2 mM KCl, 2.0 mM $CaCl_2$, 1.2 mM $MgSO_4$, 25 mM $NaHCO_3$, 1.2 mM KH_2PO_4, 11 mM glucose, 0.5 mM EDTA and 2 mM pyruvate), which was kept at 37 °C and continuously oxygenated with 95% O_2 and 5% CO_2 to maintain a pH at 7.4. By inserting a water-filled balloon into the LV chamber, which on the other side connected to a pressure transducer, the pressure changes were recorded by PowerLab system (ADInstruments, Australia). After stabilization and 10 mins baseline recording, global ischemia was induced for 30 min followed by 40 mins of reperfusion and hearts were flash frozen in liquid nitrogen. The coronary effluents were collected at baseline, start of reperfusion and following 10 min of reperfusion, for the determination of CK activity. A post-conditioning protocol with wildtype ($APLN^{+/y}$) hearts was used with apelin analogue I and II (1.5 µg/ml for 20 mins) given at the start of reperfusion.

Myocardial Ischemia-Reperfusion Injury In-Vivo. Ten-week-old male mice of both genotypes were subjected to ischemia by LAD ligation followed by reperfusion. Reliability of ischemia-reperfusion (IR) was confirmed by Evan's blue staining. Anaesthetized mice underwent left thoracotomy in the fourth

intercostal space. The pericardium was opened to expose the left ventricle (LV) and the left anterior descending (LAD) coronary artery was encircled and ligated with a 6-0 silk suture for 30 min; the reperfusion was established by releasing the ligation. In sham-operated mice, LAD was encircled but not ligated. Following 3 hours of reperfusion or sham-operation, mice were re-anaesthetized and sacrificed. The non-IR parts of hearts were distinguished with Evan's Blue by injection into the coronary circulation after the LAD was ligated again at the same location. Hearts were quickly excised and sectioned in 1-mm slices from apex to the point of ligation, then incubating with 1% Triphenyl Tetrazolium Chloride (TTC) (Sigma, Canada) at 37 °C for 10 min. The blue stained area represents the non-IR myocardium while the rest was termed area at risk (AAR) in which the brick red represents viable tissue, while the while/yellowish region indicates non-viable tissue. In a separate group of wildtype mice, apelin analogue II (60 μg/kg/min for 10 mins) was administered via the right internal jugular vein at the moment of reperfusion.

CK activity Assay. Perfusates from the Langendorff preparations and plasma from 1 day post MI mice were collected and preserved at -80 °C for creatine kinase (CK) activity assay using a commercial kit (BioAssay).

Aortic Ring Angiogenesis Assay. The *ex vivo* mouse ring angiogenesis assay was carried as previously described.[196] Thoracic aorta excised from 10-week old

$APLN^{+/y}$ and $APLN^{-/y}$ mice under sterile conditions were cut into 1 mm-thick rings under a stereomicroscope. The aortic rings were placed between two layers of Matrigel matrix (BD Biosciences; 354234) in a 48-well culture plate. EBM-2 media (Lonza; CC-3156) with 2% FBS was added containing PBS, rhVEGF (20 ng/mL; Lonza; CC-4114A), apelin analogue I and II (100ng/ml). Rings were cultured at 37°C and 5% CO_2 for 12 days. Phase-contrast images were taken using an Olympus IX81 microscope.

Fibrin Gel Bead Angiogenesis Assay. Human endothelial progenitor cells (hEPCs) were isolated from peripheral blood as previously described.[197] Briefly, mononuclear blood cells were isolated from leukopheresis products under a protocol approved by the Health Ethics Review Board of the University of Alberta. After density separation over a ficol gradient, $CD34^+$ cells were isolated using antibody-coated magnetic beads (StemCell Technologies, Vancouver, BC). The late outgrowth ECFC clones were expanded in EBM-2 medium with 10% FBS, and routinely monitored for expression of endothelial marker gene products using quantitative RT- PCR, flow cytometry, or Western blot. Where indicated, hEPCs were transfected with 50 nM non-silencing or siRNA directed to Apelin (Qiagen, Mississauga, ON) and *in vitro* angiogenesis of hEPCs was evaluated as described previously.[184, 198] EPCs transfected with siNS or siApelin were loaded onto Cytodex (Sigma) beads (~400 cells/bead) and cultured for 2 hours, then the beads were suspended in fibrinogen/ fibronectin solution (2 mg/ml) containing

aprotinin (0.15 U/ml) and 0.625 U/ml thrombin was added. Images of the beads after 16 h culture were captured using a 20X objective and a CCD camera-equipped inverted microscope (Leica, Concord, ON). The number and length of sprouts were analyzed using image analysis software (OpenLab, Lexington, MA) of 30 beads/ experiment. Sprout length was grouped into tertiles established from mock-transfected hEPC (<75, 76-125, >126 μm).

Isolated cardiomyocyte contractility. Adult murine left ventricular (LV) cardiomyocytes were isolated and cultured as previously described except that the 2,3-butanedione monoxime was omitted to preserve contractile function.[154, 199, 200] Briefly, mice were injected with 0.05 mL of 1000 USP/mL heparin for 15 min and then anesthetised using 2% isoflurane (1 L/min oxygen flow rate) provided through a nose cone. After opening the chest cavity, the heart was quickly excised and perfused using a Langendorff system within 45s. Following 3-min perfusion, the heart was then digested with 2.4 mg/mL collagenase type 2 (Worthington) for 7-8 min. After sufficient digestion, the ventricles were removed, dissociated using forceps and transfer pipettes, and resuspended in stopping buffer (10% FBS perfusion buffer). The isolated cardiomyocytes were then exposed to increasing Ca^{2+} concentrations (100 μmol/L, 400 μmol/L, and 900 μmol/L) for 15 min each and were kept in perfusion buffer solution (pH 7.4). An aliquot of isolated cardiac myocytes were transferred in a glass-bottomed recording chamber on top of inverted microscope (Olympus IX71) and allowed to settle for 5-6 min. Cells

were superfused at a rate of 1.5-2 mL/min with modified Tyrode's solution (containing in mmol/L: 135 NaCl, 5.4 KCl, 1.2 $CaCl_2$, 1 $MgCl_2$, 1 NaH_2PO_4, 10 Taurine, 10 HEPES, 10 glucose; pH 7.4 with NaOH). The perfusion solutions were heated to in-bath temperature of 35-36°C using in-line heater (SH-27B, Harvard Apparatus) controlled by automatic temperature controller (TC-324B, Harvard Apparatus). Quiescent rod-shaped myocytes with clear striations were selected for study. Platinum-wire electrodes were placed near the cell just outside of the microscope view at 400X magnification. Myocytes were paced at 1 Hz with voltage of 3-4 V (50% above threshold) and pulse duration of 2.5 ms using S48 stimulator (Grass Technology). Sarcomere length was estimated in real time from images captured at a rate 200 frame/sec via 40X objective (UAPO 40X3/340, Olympus) using high-speed camera (IMPERX IPX-VGA-210, Aurora Scientific). Sarcomere length was calculated by HVSL software v. 1.75 (Aurora Scientific) using auto-correlation function (ACF/Sine-fit) algorithm. Myocytes were paced for at least 2 min. Only recordings of myocytes that produced stable contractions of similar amplitude and kinetics at a steady-state (past 2 min) were selected for analysis. At about 2 min of stimulation time, 10 consecutive contractions were selected and averaged to reduce noise and make calculations of derivatives more precise. Averaged contraction was used to calculate fractional shortening (FS), relaxation times (t50 and t90), and ±dL/dt. Calculations were performed in Origin 8.5 (OriginLab) using custom-made script of built-in LabTalk language.

TUNEL, CD31, Lectin and HIF-1α Immunofluorescence. In situ DNA fragmentation was detected by TUNEL assay kit (Invitrogen) according to manufacturer's instructions. Briefly, 5 μm thick LV cryosections were fixed with 4% paraformaldehyde and washed in Dulbecco's PBS. The sections were then permeabilized with 0.1% Triton X-100 in 0.1% sodium citrate and washed with wash buffer. After one hour incubation with DNA labeling solution (terminal deoxynucleotidyl transferase and BrdUTP in reaction buffer) the sections were treated with Alexa Fluor 488 conjugated mouse anti-BrdU and counterstained with propidium iodide. The sections were mounted using Prolong Gold antifade mounting medium and visualized under fluorescence microscope (Olympus IX 81). TUNEL positive cells were counted using 20X magnification images with MetaMorph (Basic version 7.7.0.0) software and magnitude of apoptosis was expressed as % apoptotic cells.

Vascular endothelial cells were stained in sham and 7 day post-MI LVs by immunohistochemistry using rat anti-CD31 (BD Pharmingen, USA) primary antibody and Cy3 conjugated goat anti-rat (Invitrogen, USA) secondary antibody. Briefly, five-micrometer thick OCT embedded cryosections were fixed with 4% paraformaldehyde, permeabilized with 0.2% Triton X100 and blocked with 4% bovine serum albumin. The sections were then incubated with primary antibody (1:10, clone MEC 13.3, BD Pharmingen, USA) overnight at 4°C in a humidified chamber. After several washings the sections were incubated with Cy3 conjugated

goat anti-rat (Invitrogen) secondary antibody for 1 hour at 37°C. The sections were visualized and imaged under fluorescence microscope (Olympus IX81) after mounting with Prolong Gold antifade mounting medium (Invitrogen). The images were analyzed using Metamorph software (Version 7.7.0.0) and the magnitude of vascularization was represented as CD31[+] area/mm^2 of the myocardium.

Lectin immunofluoresence assay using fluorescein conjugated *Ricinus communis* agglutinin I (RCA; lectin; Vectorlabs) perfusion method was used to assess blood flow and new vessel formation in peri-infarct area after 7 days of MI or sham surgery in $APLN^{+/y}$ and $APLN^{-/y}$ mice. Briefly, heparinized mice were anesthetized with ketamine (100mg/kg) and xylazine (10 mg/kg) and right jugular vein was cannulated using PE10 tubing. 0.2 mg of lectin in 100 µl saline was injected into the jugular vein; 50 µl of saline was injected immediately to expel lectin from cannula. After 18 minutes of lectin circulation, 0.2 mg of papaverine HCl (Sigma Aldrich) in 50 µl saline was injected through the same cannula to promote maximal dilation of blood vessels and circulated for 2 minute. After 20 minutes of lectin administration, hearts were collected in OCT in cold conditions. 5 µm thick cryosections were cut, fixed with 4% paraformaldehyde for 20 minutes followed by rehydration using PBS for 30 minutes. The sections were mounted in Prolong Gold antifade mounting medium with DAPI (Invitrogen), visualized and imaged under fluorescence microscope (Olympus IX81). Images were analyzed using Metamorph (Version 7.7.0.0) software and magnitude of

vascularization in peri-infarct area was represented as lectin perfused area/mm^2 of the myocardium.

To assess the nuclear translocation of hypoxia inducible factor-1α (HIF-1α), a key mediator of cellular adaptation to hypoxia, immunofluorescence was performed on 5 μm thick formalin fixed-paraffin embedded sections. Briefly, after deparaffinization sections were heated to 95-100°C in citrate buffer pH 6.0 for the antigen retrieval. The sections were than immune-stained with anti-Hif-1α primary antibody (Novus Biologicals) and TRITC conjugated anti-rabbit secondary antibody (Invitrogen) and counterstained DAPI. The sections were mounted and visualized under fluorescence microscope (Olympus IX81) and nuclear HIF-1α expression in the peri-infarct region was morphometrically measured using Metamorph (Version 7.7.0.0) software.

TaqMan Real-time PCR. RNA expression levels of various genes were determined by TaqMan real-time PCR as previously described (see Supplemental Table 1 for list of primers and probes).[152, 201] Total RNA was extracted from flash-frozen tissues using TRIzol, and cDNA was synthesized from 1 μg RNA by using a random hexamer. For each gene, a standard curve was generated using known concentrations of cDNA (0.625, 1.25, 2.5, 5, 10 and 20 μg) as a function of cycle threshold (CT). Expression analysis of the reported genes was performed by TaqMan real-time-PCR using ABI 7900 Sequence Detection System. The SDS2.2 software (integral to ABI7900 real-time machine) fits the CT values for the

experimental samples and generates values for cDNA levels. All samples were run in triplicates in 384 well plates. 18S rRNA was used as an endogenous control.

Western Blot Analysis and Nuclear Fractionation. Total protein extraction and immunoblotting (IB) were performed as previously.[199] Typically, 150 μg of total protein isolated from left ventricle (LV) was separated on 8% or 14% SDS-PAGE and subject to IB of phospho-(Ser473)/total Akt and phospho/total Erk1/2 (Cell Signaling Technology); and of anti-apelin (ab59469) and anti-APJ receptor (ab84296) from Abcam Inc. (Cambridge, MA, USA). The anti-apelin antibody (ab59469) was raised against the conserved C-terminus of apelin. VEGF (147) and α-Tubulin (DM1A) antibodies were purchased from Santa Cruz Biotechnology Inc. (Santa Cruz, CA, USA). Blots were visualized and quantified with ImageQuant LAS 4000 (GE Healthcare, Baie d'Urfe, QC, Canada). Western blot for phospho-(serine-473)/total Akt was also performed on human EPCs. hEPCs were serum-starved overnight in incomplete EBM2 supplemented with 2% FBS. The next day EPCs were stimulated with placebo (PBS), apelin analogue I and II at 30 and 100 ng/ml for 10 mins and cells were collected for analysis of phospho-Akt (Ser473)/total Akt levels.

Nuclear fractionation was performed as previously described[202] with modifications. Briefly, LV tissues were homogenized in hypotonic lysis buffer

(10 mM K-HEPES (pH 7.9), 1.5 mM $MgCl_2$, 10 mM KCl, 1 mM DTT, 0.2 mM Na_3VO_4, 1 x protease inhibitor cocktail (Calbiochem), 1 x phosphatase inhibitors (Sigma and Calbiochem). The total homogenate was centrifuged at 100 g for 5 minutes to collect unbroken tissues. The supernatant was then centrifuged at 2,000 g for 10 minutes to precipitate crude nuclei from cell membrane and cytosolic proteins (second supernatant). The second supernatant was further centrifuged at 100,000 g for 90 minutes to separate soluble cytosolic proteins (third supernatant) from membrane pellet. The crude nuclear fraction was resuspended in hypotonic lysis buffer supplemented with 2.4 M sucrose, and then layered on top of a 2.4 M sucrose cushion and purified by centrifugation at 100,000 g for 90 minutes. Following ultracentrifugation, the purified nuclear pellet was resuspended in storage buffer (20 mM Na-HEPES (pH 7.9), 0.42 M NaCl, 1.5 mM $MgCl_2$, 0.2 mM EDTA, 0.2 mM EGTA, 0.5 mM PMSF, 0.5 mM DTT, 25% Glycerol, 1 x protease and phosphatase inhibitors). 30 μg of nuclear protein from LV was subject to HIF1α blotting (Novus, Oakville, ON, Canada). The purity of nuclear and cytosolic fractions was verified by using Histone H-3 (Cell Signaling; nuclear marker) and Caspase-3 (Cell Signaling; cytosolic marker).

Statistical Analysis. Student t-test or one-way ANOVA, followed by multiple-comparison Student Neuman-Keuls testing was performed to compare the data between two or more experimental groups, respectively. Survival data was

analyzed using the Kaplan-Meier method and the log-rank test was used to test for statistical significance. Statistical analyses were performed using the SPSS Statistics 19 software. Statistical significance is recognized at $p<0.05$.

5.4 Results

Downregulation of apelin in diseased murine and human hearts.

Acute myocardial infarction (MI), by ligation of the left anterior descending (LAD) artery, resulted in a drastic reduction in APLN levels in the infarct and peri-infarct regions at 1 day post-MI which persisted at 7 days post-MI; in contrast, APJ levels showed a bimodal change in the post-MI setting with an early increase followed by downregulation at 7 days post-MI **(Figure 5.1A)**. In failing human hearts explanted following subacute MI,

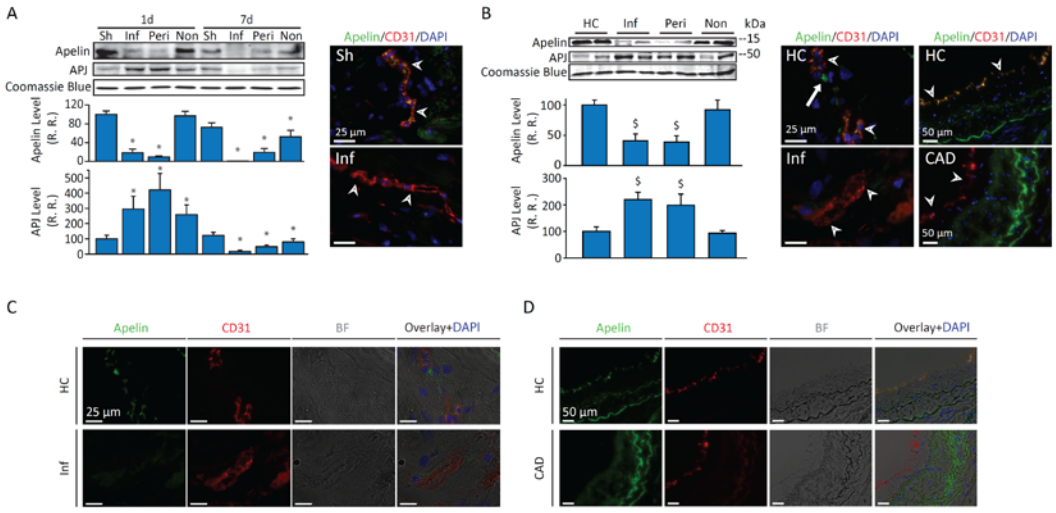

Figure 5.1. Myocardial apelin is downregulated in diseased murine and human hearts. Western blot analysis and immunofluorescence staining for apelin (green) and CD31 (red) illustrating marked loss of myocardial apelin in infarcted murine (**A**) and human hearts (**B**) with coronary artery disease (CAD) associated with a drastic loss of apelin in human epicardial coronary arteries (**B**). Immunofluorescence staining for apelin (green) and CD31 (red) with the individual brightfield images shown on the right illustrating a marked loss of apelin in infarcted human myocardium (**C**) and in the left anterior descending coronary arteries from patients with CAD compared to healthy controls (HC) (**D**). The arrow indicates the human myocardial interstitium while the arrowheads illustrate the diseased human coronary endothelium. Sh=Sham-Operated, MI=Myocardial Infarction, Inf=Infarct Region; Peri=Peri-Infarct Region and Non=Non-Infarct Region. CAD=Coronary Artery Disease and LAD=Left Anterior Descending artery. R.R.=relative ratio; n=3; *$p<0.05$ compared to the corresponding sham group; $^{\$}p<0.05$ compared with healthy controls (HC) and non-infarcted LV.

APLN levels showed a marked decrease with a corresponding increase in APJ levels **(Figure 5.1B)**. Immunofluorescence staining confirmed a down-regulation of APLN in the endothelial compartment of the infarcted murine and human hearts and in the myocardial interstitium with a concordant loss of APLN in epicardial coronary arteries in patients with coronary artery disease **(Figure 5.1C-D; Figure 5.2)**.

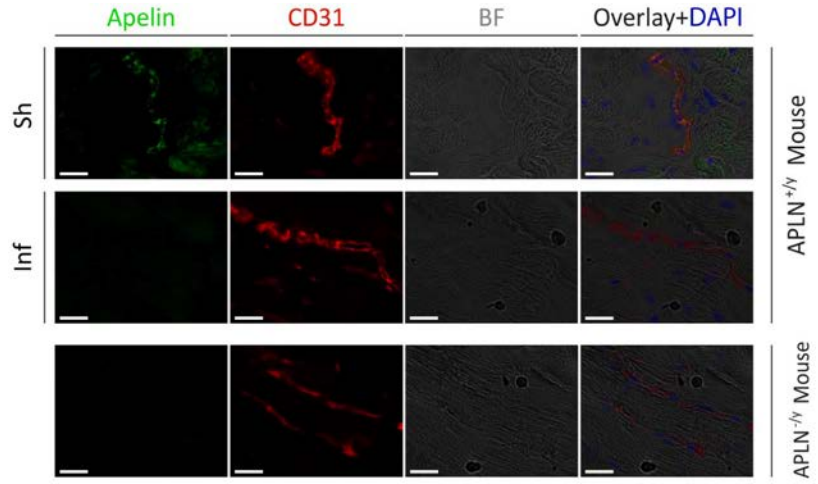

Figure 5.2 Immunofluorescence staining for apelin (green) and CD31 (red) with the individual bright field images shown on the right illustrating a marked loss of apelin in infarcted (Inf) murine hearts compared to non-failing healthy control (HC). The specificity of the apelin antibody was confirmed in the $APLN^{-/y}$ hearts which did not show any evidence of non-specific staining.

Loss of apelin enhances the susceptibility to myocardial infarction.

To ascertain whether APLN is a critical determinant of the cardiac response to ischemic injury, we subjected APLN knockout ($APLN^{-/y}$) and littermate wild-type ($APLN^{+/y}$) mice to MI. Western blot analysis confirmed loss of apelin in the absence of an upregulation of APJ levels in $APLN^{-/y}$ hearts **(Figure 5.3A)**. Acute MI resulted in increased mortality in $APLN^{-/y}$ compared to $APLN^{+/y}$ mice based on Kaplan-Meier survival analysis **(Figure 5.3B)**. The greater mortality in $APLN^{-/y}$ mice correlated with larger infarct size as demonstrated by TTC staining and greater elevation in plasma creatine kinase activity at 1 day post-MI **(Figure 5.3C)** leading to greater ventricular dilation and fibrosis **(Figure 5.3D)**.

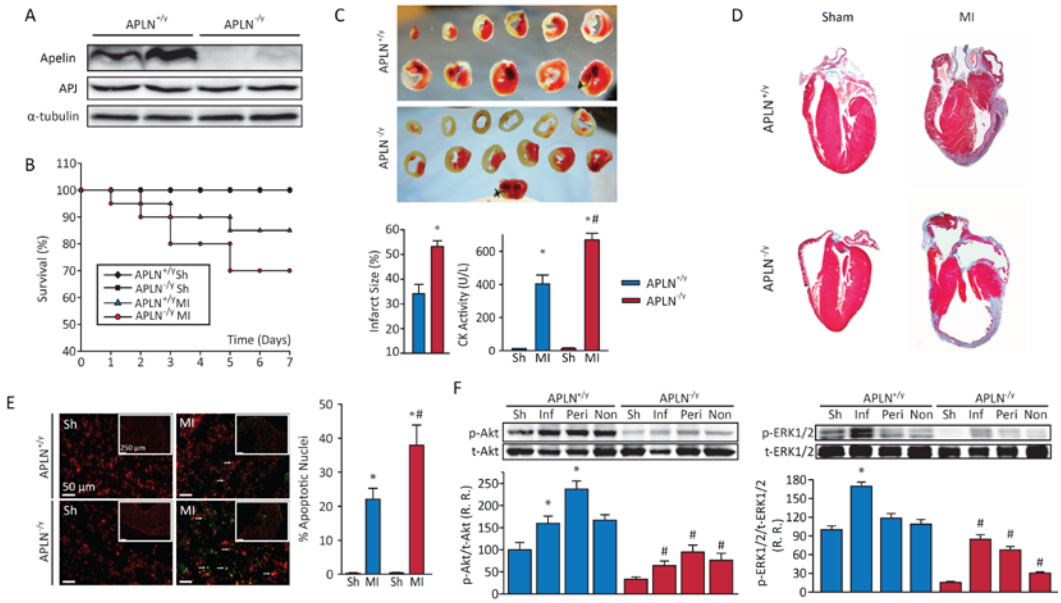

Figure 5.3 Loss of apelin enhances susceptibility to myocardial infarction. Western blot analysis of APLN and APJ levels showing a compete loss of APLN in APLN knockout ($APLN^{-/y}$) hearts without compensatory changes in APJ level (**A**). LAD-ligation resulting in increased mortality in $APLN^{-/y}$ mice based on Kaplan-Meier survival analysis (**B**), larger infarct size shown as representative images of triphenyl tetrazolium chloride (TTC)-stained heart sections and plasma creatine kinase (CK) activity at 1 day post-MI (**C**) and greater ventricular dilation and fibrosis at 7 day post-MI (**D**). TUNEL staining and quantification of apoptotic nuclei (**E**) revealed a greater increase in apoptosis in APLN deficient hearts with Western blot analysis of serine-473 Akt and Erk1/2 phosphorylation showing increased levels at 1 day post-MI in $APLN^{+/y}$ hearts but with a dramatic loss of Akt and Erk1/2 phosphorylation in $APLN^{-/y}$ hearts (**F**). Sh=Sham-Operated, MI=Myocardial Infarction, Inf=Infarct Region; Peri=Peri-Infarct Region and Non=Non-Infarct Region. p=phospho, t=total, R.R.=relative ratio. Values are mean±SEM; n=5 for each group except for **B** where n=50 ($p<0.01$ based on Kaplan-Meier survival analysis) and **C** where n=8. *$p<0.05$ compared to the corresponding sham group; $^{\#}p<0.05$ compared to the $APLN^{+/y}$ group.

Modulation of pro-survival pathways and angiogenesis are critical determinants of post-MI adverse myocardial remodeling.[203] Apelin is an agonist of the G-protein coupled receptor, APJ, and can activate the well-known pro-survival kinase, PI3K/Akt. The TUNEL assay revealed a greater degree of

apoptosis in the infarct-related region **(Figure 5.3E)** in 1-day post-MI APLN$^{-/y}$ hearts. Western blot analysis showed a consistent increase in phospho-Akt and Erk1/2 in the infarct, peri-infarct and non-infarct regions in APLN$^{+/y}$ hearts **(Figure 5.3F)**. In contrast, loss of APLN resulted in a drastic lowering of phospho-Akt and Erk1/2 levels in the infarct and peri-infarct regions in APLN$^{-/y}$ hearts **(Figure 5.3F)**.

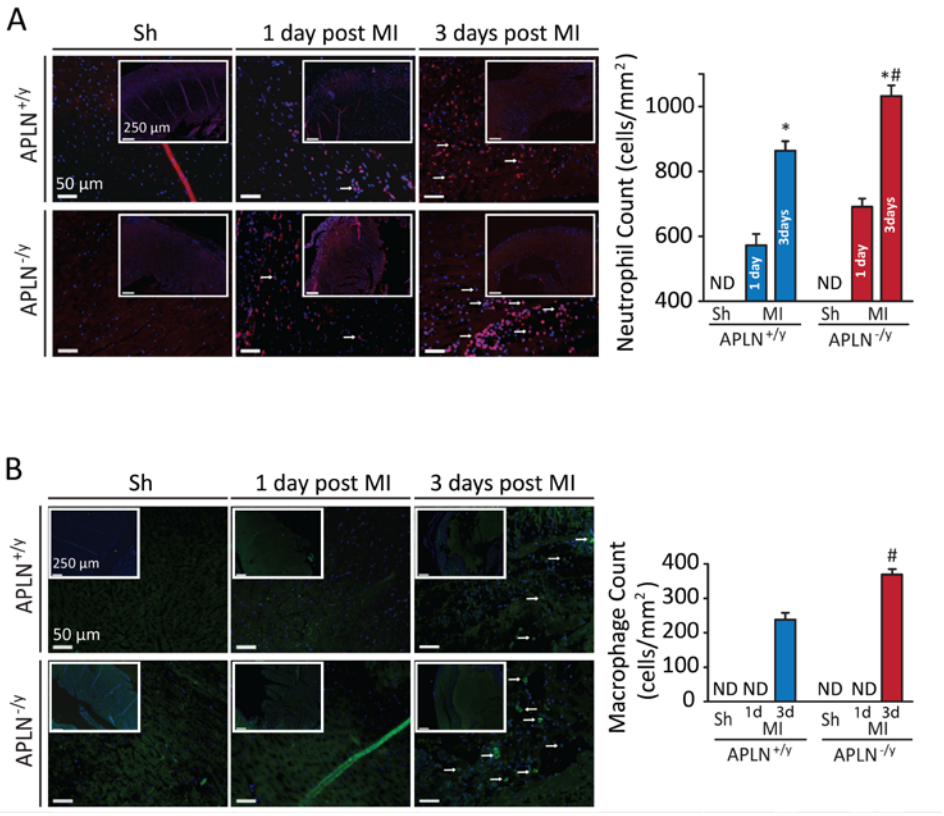

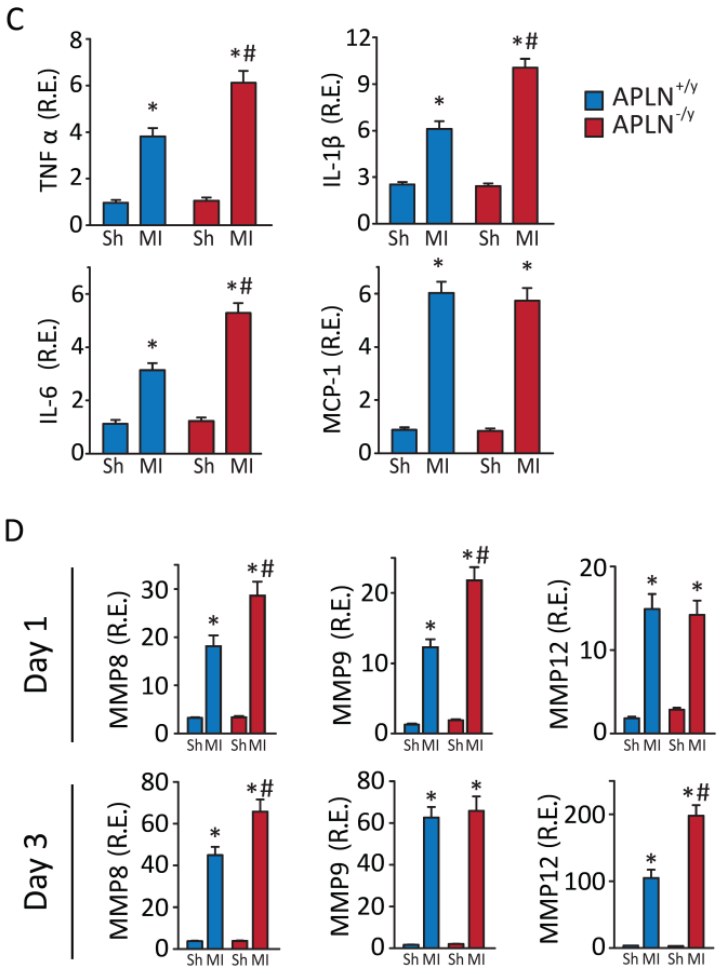

Figure 5.4 Increased myocardial inflammation following myocardial infarction in apelin deficient hearts. Neutrophil-specific and macrophage-specific staining and quantification showing a greater increase in neutrophil (**A**) and macrophage infiltration (**B**) in infarcted $APLN^{-/y}$ compared to $APLN^{+/y}$ hearts. ND=not detected. (**C**) Expression analysis of inflammatory cytokines and MMPs showing greater expression of TNFα, interleukin 1beta (IL-1β), interleukin-6 (IL-6) and monocyte chemoattractant protein-1 (MCP-1) at 1 day post-MI in the infarct area of APLN knockout hearts. (**D**) Expression analysis of the inflammatory MMPs (matrix metalloproteinases) showing the neutrophil-specific MMPs, MMP8 and MMP9, were increased at 1 day post-MI while at day 3 post-MI, the macrophage-specific MMP, MMP12 level was increased in APLN deficient hearts. Values are mean±SEM; n=6 for each sham group and n=8 for each MI group. *$p<0.05$ compared with corresponding 1 day group; $^{\#}p<0.05$ compared with the corresponding $APLN^{+/y}$ group.

Increased cell death in APLN$^{-/y}$ hearts was also associated with greater neutrophil and macrophage infiltration **(Figure 5.4A and B)** associated with increased expression of pro-inflammatory cytokines **(Figure 5.4C)**, and matrix metalloproteinases (MMPs), MMP8, MMP9 and MMP12 **(Figure 5.4D)** which will likely lead to degradation of the myocardial extracellular matrix.

The greater infarct size and increased myocardial inflammation coupled with compromised pros-survival signaling pathways likely contributes to worsened systolic dysfunction in APLN knockout mice. While baseline systolic function was not significantly different between APLN$^{+/y}$ and APLN$^{-/y}$ mice (**Figure 5.5**), which was confirmed at the single cardiomyocyte level (**Figure 5.6**), echocardiographic M-mode, parasternal long axis and left atrial (Figure 5.5A) views showed worsening of systolic dysfunction, greater LV and left atrial dilation at 1week post MI in APLN$^{-/y}$ hearts. Quantitative assessment of systolic function showed increased LVESV **(Figure 5.5B)** and left atrial size **(Figure 5.5C)** with greater reduction in ejection fraction **(Figure 5.5D)** and worsening wall motion score index **(Figure 5.5E)** in APLN deficient hearts. Invasive LV pressure-volume loop analysis confirmed equivalent basal systolic function and that APLN$^{-/y}$ mice showed a marked exacerbation of systolic dysfunction in response to MI independent of alterations in preload and afterload **(Figure 5.5F-L)**.

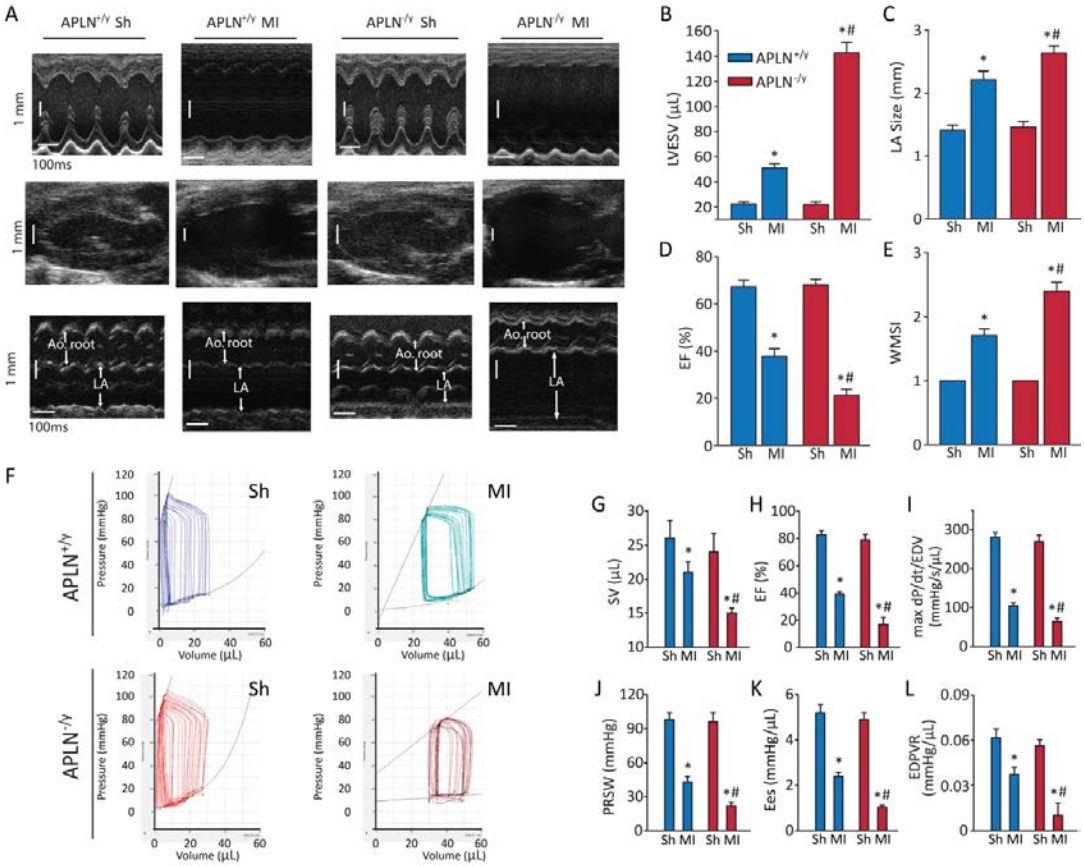

Figure 5.5 Echocardiographic and invasive pressure-volume assessment of heart function revealed increased left ventricular dilation and dysfunction post-MI in apelin deficient hearts. Representative M-mode images, parasternal long axis views and left atrial size (**A**) from APLN$^{+/y}$ and APLN$^{-/y}$ hearts after sham or 1wk post-MI with greater increase in left ventricular end-systolic volume (LVESV) (**B**) and left atrial (LA) size (**C**) with lowering of the ejection fraction (EF) (**D**) and worsening wall motion score index (WMSI) (**E**) in APLN$^{-/y}$ hearts compared with APLN$^{+/y}$ hearts at 1wk post-MI. Invasive pressure-volume hemodynamic analysis showing marked deterioration in the post-MI ventricular function in apelin deficient hearts (**F**) with quantitative assessment of LV function showing reduced stroke volume (SV) (**G**), ejection fraction (EF) (**H**), max dP/dt/EDV (**I**), pre-load recruitable stroke work (PRSW) (**J**) and end-systolic elastance (Ees) (**K**) with elevated slope of the end-diastolic pressure volume relationship (EDPVR) (**L**). Sh=Sham-Operated; MI=Myocardial Infarction; EDV=End Diastolic Volume. Values are mean±SEM; n=8 for each sham group and n=10 for each MI group. *p<0.05 compared to the corresponding sham group; $^{\#}$p<0.05 compared to the APLN$^{+/y}$ group.

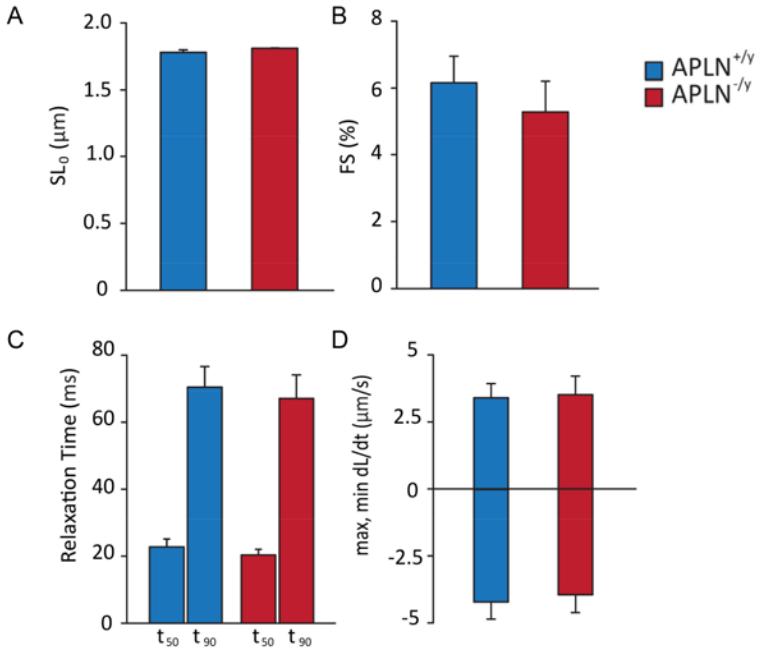

Figure 5.6 Basal cardiomyocyte length, contractility and relaxation in APLN$^{+/y}$ and APLN$^{-/y}$. Preserved basal cardiomyocyte length (A), contractility (B) and relaxation (C-D) in isolated APLN$^{-/y}$ cardiomyocytes compared to APLN$^{+/y}$ cardiomyocytes (n=8 cardiomyocytes in each group).

Beneficial effects of apelin analogue in myocardial ischemic injury. Exacerbation of post-MI dysfunction in APLN deficient hearts suggests that enhancing APLN action can have salutary beneficial effects in ischemic heart disease. Given the short half-life of native APLN peptides[49, 58, 99], we modified, synthesized and purified two novel APLN analogues with the aim to enhance their therapeutic effects: NleInpBrF pyr-1-apelin-13 (apelin analogue I) and NleAibBrF pyr-1-apelin-13 (apelin analogue II) (**Table 5.1 and Table 5.2; Figure 5.7**).

Table 5.1 Taqman Primers and Probes.

Ang-1	Assay ID: Mm01223051_m1
Ang-2	Assay ID: Mm00456499_m1
TNFα	Forward: 5'-ACAAGGCTGCCCCGACTAC-3', Reverse: 5'-TTTCTCCTGGTATGAGATAGCAAATC-3', Probe: 5'-FAM-TGCTCCTCACCCAC ACCGTCAGC-TAMRA-3'
IL-1β	Forward: 5'-AACCTGCTGGTGTGTGACGTTC-3' Reverse: 5'-CAGCACGAGGCTTTTTTGTTGT-3' Probe: 5'- FAM-TTAGACAGCTGCACTACAGGCTCCGAGATG-TAMRA-3'
IL-6	Forward: 5'-ACAACCACGGCCTTCCCTACTT-3' Reverse: 5'-CACGATTTCCCAGAGAACATGTG-3' Probe: 5'-FAM-TTCACAGAGGATACCACTCCCAACAGACCT-TAMRA-3'
MCP-1	Forward: 5'- GTTGGCTCAGCCAGATGCA-3' Reverse: 5'-AGCCTACTCATTGGGATCATCTTG-3' Probe: 5'-FAM-TTAACGCCCCACTCACCTGCTGCTACT-TAMRA3'
MMP8	Forward: 5'- GATTCAGAAGAAACGTGGACTCAA -3' Reverse: 5'- CATCAAGGCACCAGGATCAGT -3' Probe: 5'-FAM-ATGAATTTGGACATTCTTTGGGACTCTCTCACTAMRA-3'
MMP9	Forward: 5'-CGAACTTCGACACTGACAAGAAGT -3' Reverse: 5'- GCACGCTGGAATGATCTAAGC-3' Probe: 5'-FAM-TCTGTCCAGACCAAGGGTACAGCCTGTTCTAMRA-3'
MMP12	Forward: 5'- GAAACCCCCATCCTTGACAA -3' Reverse: 5'- TTCCACCAGAAGAACCAGTCTTTAA -3' Probe: 5'-FAM-AGTCCACCATCAACTTTCTGTCACCAAAGC-TAMRA -3'
HPRT	Forward: 5'-AGCTTGCTGGTGAAAAGGAC-3' Reverse: 5'-CAACTTGCGCTCATCTTAGG-3' Probe: 5'-FAM-CAACAAAGTCTGGCCTGTATCCAAC-TAMRA-3'

Ang-1 = angiopoietin-1; Ang-2 = angiopoietin-2, TNF α = tumor necrosis factor alpha, IL-1 β = Interleukin-1-beta; IL-6 = interleuking-6; MMP = matrix refers to the commercial assay available from Applied Biosystems.

Table 5.2 NMR proton chemical shifts of Apelin Analogue I (NleInpBrF pyr-1-apelin-13).

	HN	Hα	Hβ	others
pyrE-1	7.88	4.35	2.52, 2.40	γCH_2 2.02
Arg 2	8.38	4.61	1.84, 1.72	γCH_2 1.65 δCH_2 3.20 δNH 7.20
Pro 3	-	4.39	2.28, 2.00	γCH_2 1.84 δCH_2 3.80, 3.61
Arg 4	8.46	4.28	1.81, 1.74	γCH_2 1.64 δCH_2 3.18 δNH 7.14
Leu 5	8.26	4.39	1.59, 1,55	γCH 1.52 δCH_3 0.89, 0.83
Ser 6	8.29	4.40	3.80	
His 7	8.48	4.68	3.25, 3.15	
Lys 8	8.40	4.37	1.82	γCH_2 1.40 δCH_2 1.69 εCH_2 2.97 εNH 7.50
Gly 9	8.26	4.11		
Pro 10	-	4.43	2.26, 1.99	γCH_2 1.90 δCH_2 3.79, 3.61
Nle 11	8.27 8.22	4.69 4.69	1.64 1.63	γCH_2 1.27 δCH_2 1.27 εCH_3 0.83 γCH_2 1.29 δCH_2 1.23 εCH_2 0.83
Inp 12	-	4.27, 4.16 3.90, 3.14	2.51, 1.75, 1.59, 1.38	γCH 2.73
***p*-BrF 13**	7.89	4.55	3.21, 2.87	Ar-H 7.42, 7.10

*2 sets of signals were observed for Nle11 due to rotamers

Using structure-activity relationships conducted on pyr-1-apelin[185], we made multiple novel successful single amino acid substitutions combined into the same peptide with the aim of "masking" the susceptible C-terminal amide bond from proteolytic cleavage (apelin analogue I) or combined two potent APJ binding substitutions into the same peptide analogue while maintaining comparable stability to the native peptide (apelin analogue II). These analogues were purified using high performance liquid chromatography (HPLC) (**Figures 5.8 and 5.9**), and high-resolution mass spectrometry and NMR were used to confirm the sequence of the synthesized analogues (**Figures 5.10 and 5.11**).

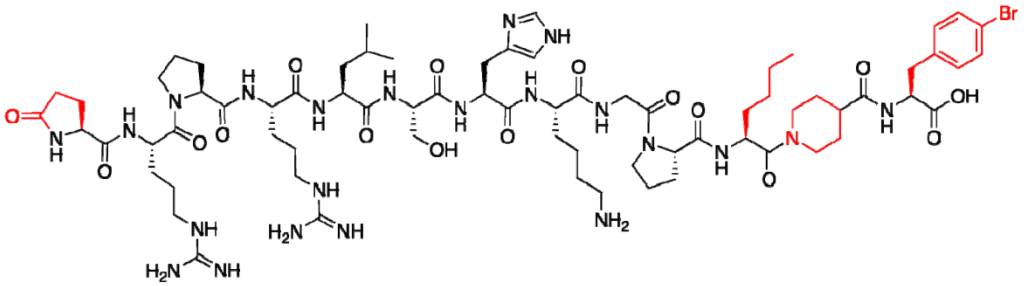

Analogue I
(NleInpBrF pyr-1-apelin-13)

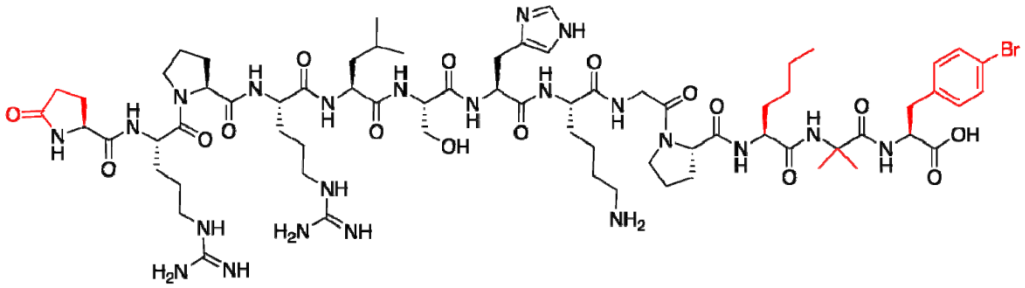

Analogue II
(NleAibBrF pyr-1-apelin-13)

Figure 5.7 Schematic representation of apelin analogue I and II. Schematic representation of the synthesized NleInpBrF pyr-1-apelin-13 (apelin analogue I) and NleAibBrF pyr-1-apelin-13 (apelin analogue II) analogues. Regions indicated in red represent synthetic alterations from the native apelin-13.

Semi-preparative purification

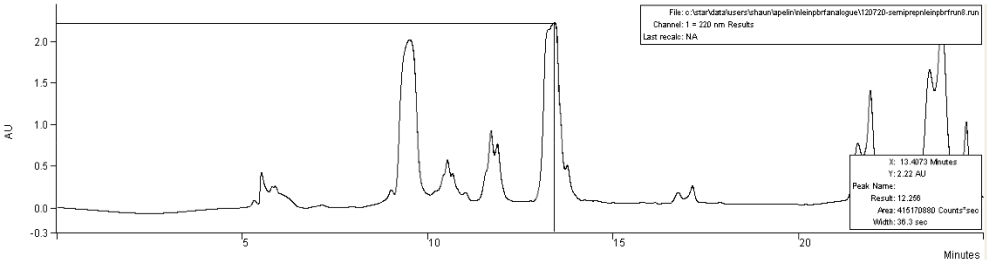

Analytical reinjection

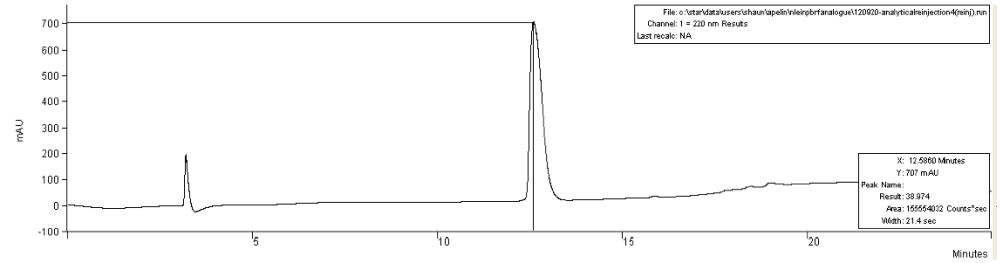

Figure 5.8. High performance liquid chromatography (HPLC) trace of NleInpBrF pyr-1-apelin-13 analogue (analogue I) showing semi-preparative purification and analytical reinjection of isolated peptide peak.

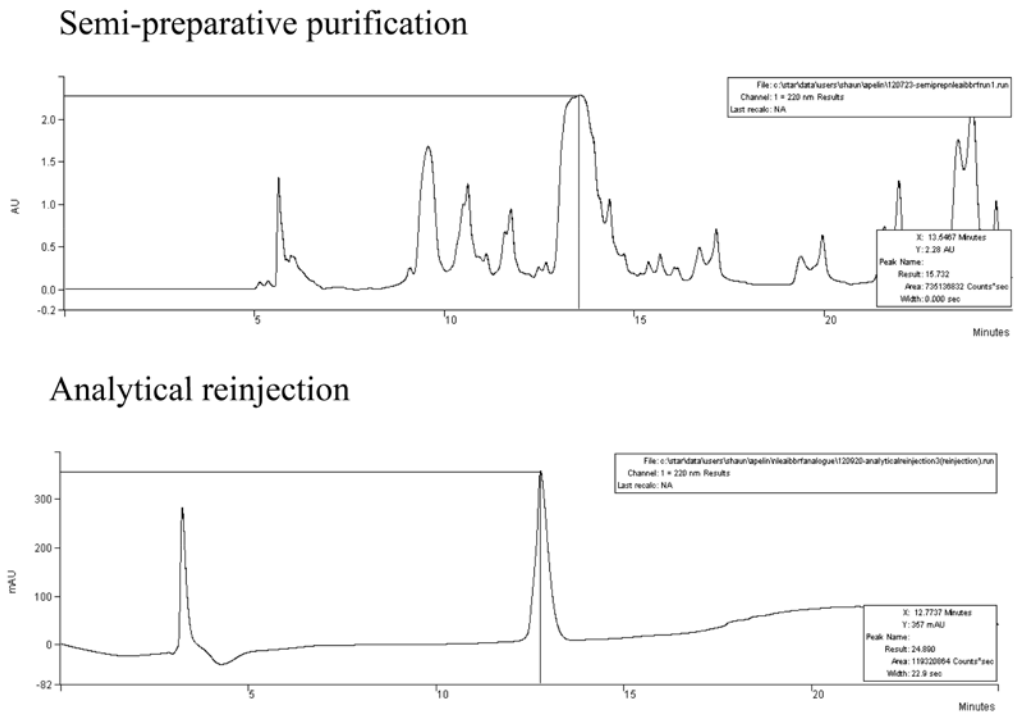

Figure 5.9. High performance liquid chromatography (HPLC) trace of NleAibBrF pyr-1-apelin-13 analogue (analogue II) showing semi-preparative purification and analytical reinjection of isolated peptide peak.

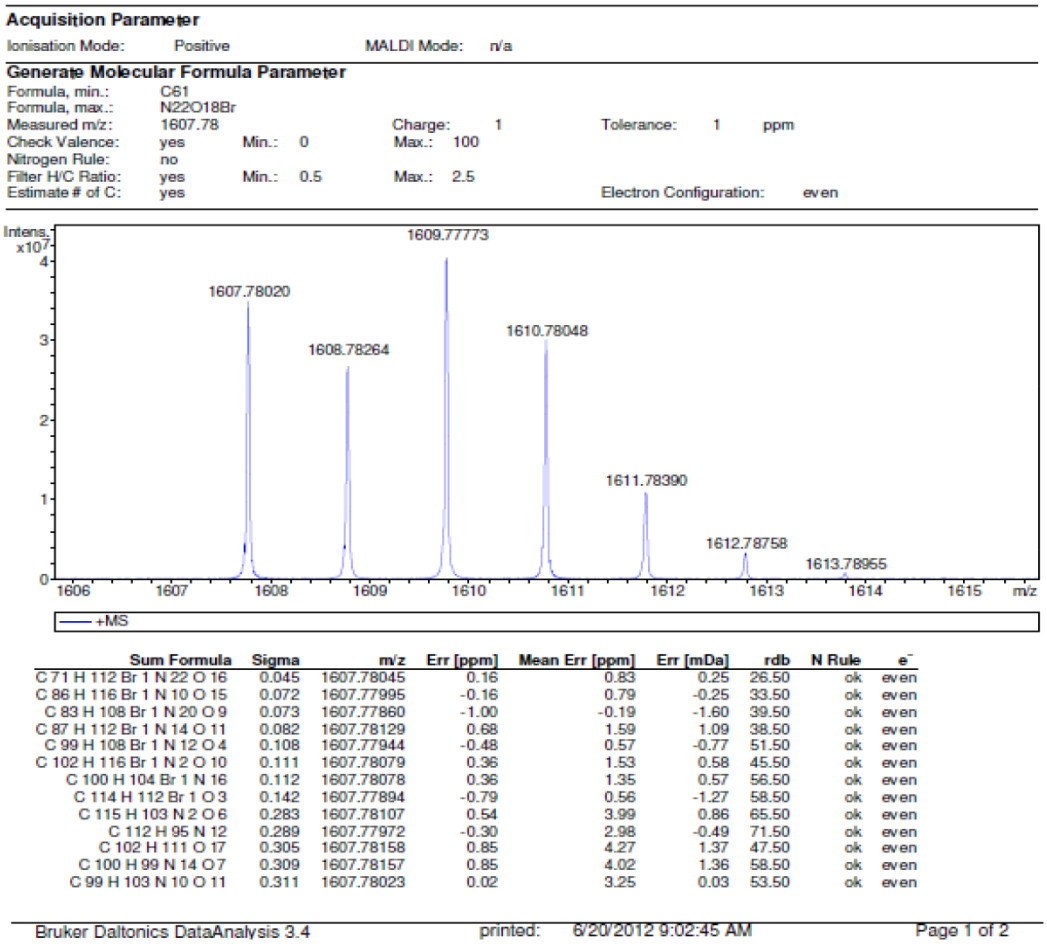

Sum Formula	Sigma	m/z	Err [ppm]	Mean Err [ppm]	Err [mDa]	rdb	N Rule	e⁻
C 71 H 112 Br 1 N 22 O 16	0.045	1607.78045	0.16	0.83	0.25	26.50	ok	even
C 86 H 116 Br 1 N 10 O 15	0.072	1607.77995	-0.16	0.79	-0.25	33.50	ok	even
C 83 H 108 Br 1 N 20 O 9	0.073	1607.77860	-1.00	-0.19	-1.60	39.50	ok	even
C 87 H 112 Br 1 N 14 O 11	0.082	1607.78129	0.68	1.59	1.09	38.50	ok	even
C 99 H 108 Br 1 N 12 O 4	0.108	1607.77944	-0.48	0.57	-0.77	51.50	ok	even
C 102 H 116 Br 1 N 2 O 10	0.111	1607.78079	0.36	1.53	0.58	45.50	ok	even
C 100 H 104 Br 1 N 16	0.112	1607.78078	0.36	1.35	0.57	56.50	ok	even
C 114 H 112 Br 1 O 3	0.142	1607.77894	-0.79	0.56	-1.27	58.50	ok	even
C 115 H 103 N 2 O 6	0.283	1607.78107	0.54	3.99	0.86	65.50	ok	even
C 112 H 95 N 12	0.289	1607.77972	-0.30	2.98	-0.49	71.50	ok	even
C 102 H 111 O 17	0.305	1607.78158	0.85	4.27	1.37	47.50	ok	even
C 100 H 99 N 14 O 7	0.309	1607.78157	0.85	4.02	1.36	58.50	ok	even
C 99 H 103 N 10 O 11	0.311	1607.78023	0.02	3.25	0.03	53.50	ok	even

Figure 5.10 High Resolution Mass Spectrometry of NleInpBrF pyr-1-apelin-13 analogue (analogue I). Mass spectra (MS) were recorded on a Kratos AEIMS-50 Bruker 9.4T Apex-Qe FTICR (high resolution, HRMS) using either 4-hydroxy-α-cyanocinnamic acid (HCCA) or 3, 5-dimethoxy-4-hydroxycinnamic acid (sinapinic acid) as matrices. MS/MS was performed on aBruker Ultraflextreme MALDI/TOF/TOF to successfully confirm the peptides' sequences.

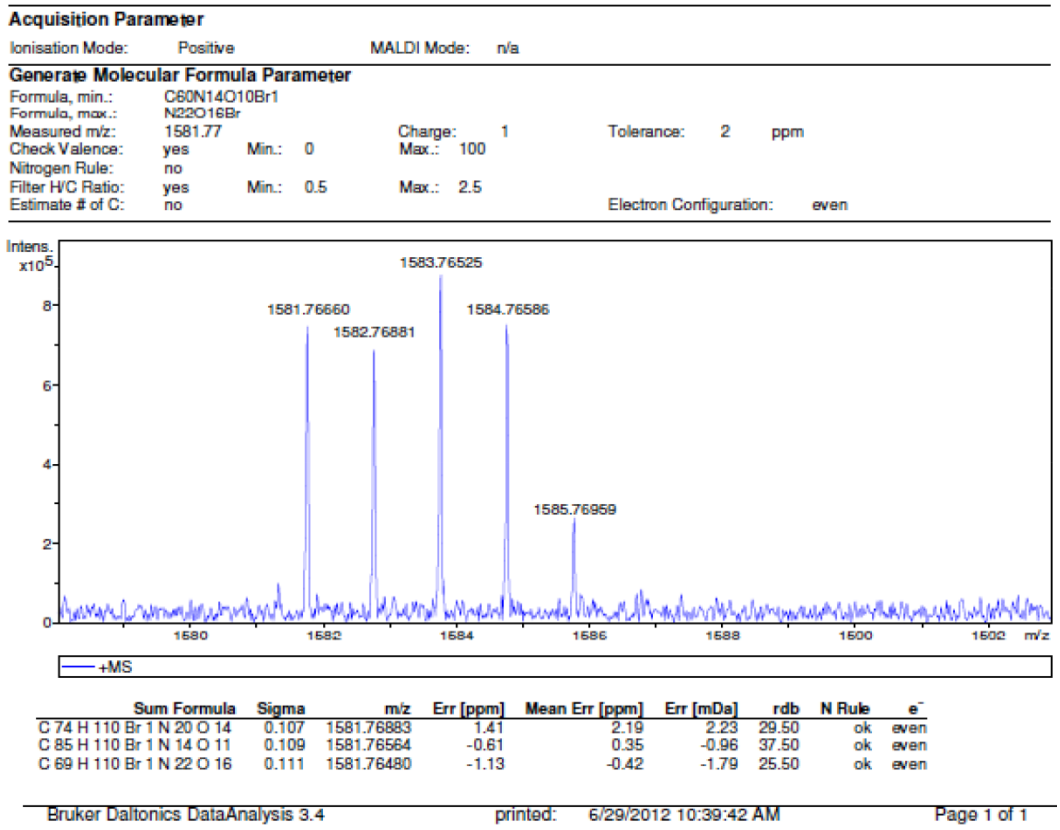

Figure 5.11 High Resolution Mass Spectrometry of NleAibBrF pyr-1-apelin-13 analogue (analogue II). Mass spectra (MS) were recorded on a Kratos AEIMS-50, Bruker 9.4T Apex-Qe FTICR (high resolution, HRMS) using either 4-hydroxy-α-cyanocinnamic acid (HCCA) or 3,5-dimethoxy-4-hydroxycinnamic acid (sinapinic acid) as matrices. MS/MS was performed on a Bruker Ultraflextreme MALDI/TOF/TOF to successfully confirm the peptides'sequences.

Proteolysis analysis using HPLC coupled with MALDI-TOF mass spectrometry confirmed efficient ACE2-mediated cleavage of pyr-1-apelin-13 (but not pyr-1-apelin-12) with 79.5±2.2, 54.6±4.2 and 18.3±3.8 % (n=3) of pyr-1-apelin-13 remaining at 30 sec, 1 min and 2 min following incubation with ACE2 (**Figure 5.12**) while apelin analogue I and analogue II were markedly resistant to ACE2-mediated proteolysis (**Figure 5.13**). We confirmed that apelin analogue I and II were not inhibitors of ACE2 activity (**Figure 5.14**) and as such the lack of degradation products is due to the intrinsic resistance of the apelin analogues to ACE2 action.

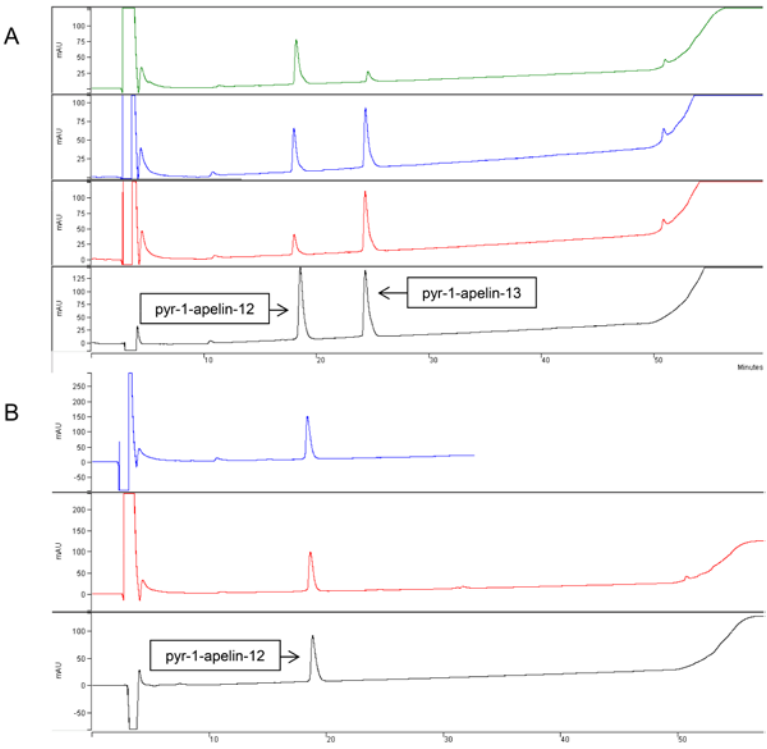

Figure 5.12 Analytical high performance liquid chromatography (HPLC) analysis of apelin. Analytical high performance liquid chromatography (HPLC) analysis showing efficient degradation of pyr-1-apelin-13 (A), but not pyr-1-apelin-12 (B), by ACE2. A. Pyr-1-apelin-13 incubation with ACE2; black: pyr-1-apelin-12 and pyr-1-apelin-13 co-injection; red: 30 s pyr-1-apelin-13 incubation; blue: 1 min pyr-1-apelin-13 incubation; green: 2 min pyr-1-apelin-13 incubation. B. Pyr-1-apelin-12 incubation with ACE2; black: pyr-1-apelin-12 standard; red: 1 h pyr-1-apelin-12 incubation; blue: 48 h pyr-1-apelin-12 incubation.

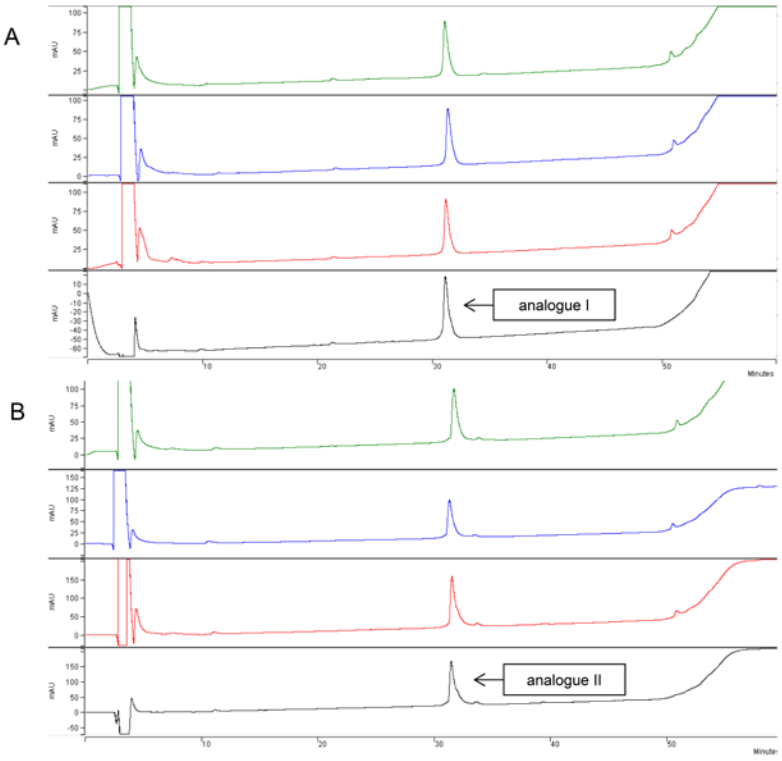

Figure 5.13 Analytical high performance liquid chromatography (HPLC) analysis of apelin analogue I and II. Analytical high performance liquid chromatography (HPLC) analysis showing a complete lack of degradation of apelin analogue I (A) and apelin analogue II (B) ACE2. A. Apelin analogue I incubation with ACE2; black: analogue I standard; red – 1 h incubation; blue – 24 h incubation; green – 48 h incubation (at 37 ^{o}C). B. Apelin Analogue II incubation with ACE2; black- analogue II standard; red – 1 h analogue II incubation; blue- 48 h analogue II incubation; green- 48 h analogue II incubation (at 37 ^{o}C).

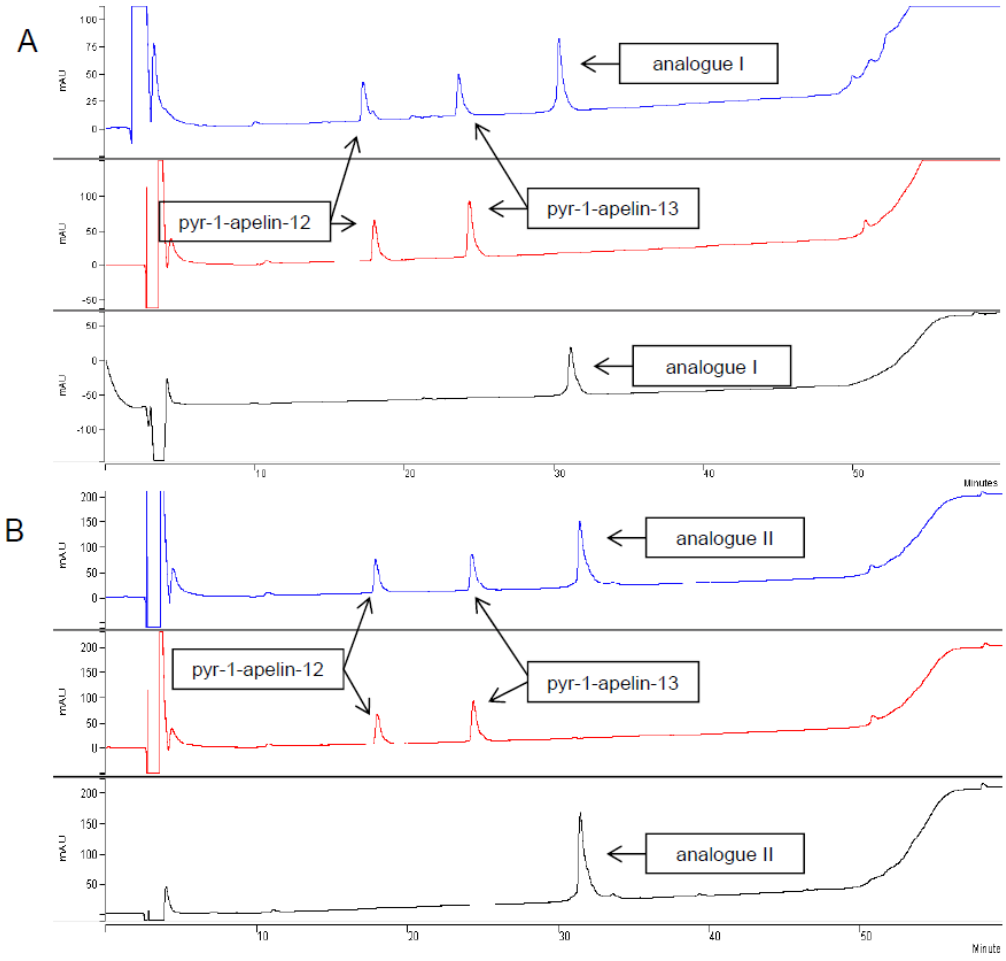

Figure 5.14 Analytical high performance liquid chromatography (HPLC) analysis of apelin analogue I and II. Analytical high performance liquid chromatography (HPLC) analysis showing inability of apelin analogue I (A) and apelin analogue II (B) to inhibit the ability of ACE2 to cleave pyr-1-apelin-13. **Apelin Analogue I (A);** black – analogue I standard; red – 1 min of pyr-1-apelin-13 incubation with ACE2; blue – 1 min of pyr-1-apelin-13 incubation with 1:1 (pyr-1-apelin-13:analogue I with analogue I) preincubated with ACE2 for 1 h. **Apelin Analogue II (B);** black – analogue II standard; red – 1 min of pyr-1-apelin-13 incubation with ACE2; blue – 1 min of pyr-1-apelin-13 incubation with 1:1 (pyr-1-apelin-13:analogue II) with analogue II preincubated with ACE2 for 1 h.

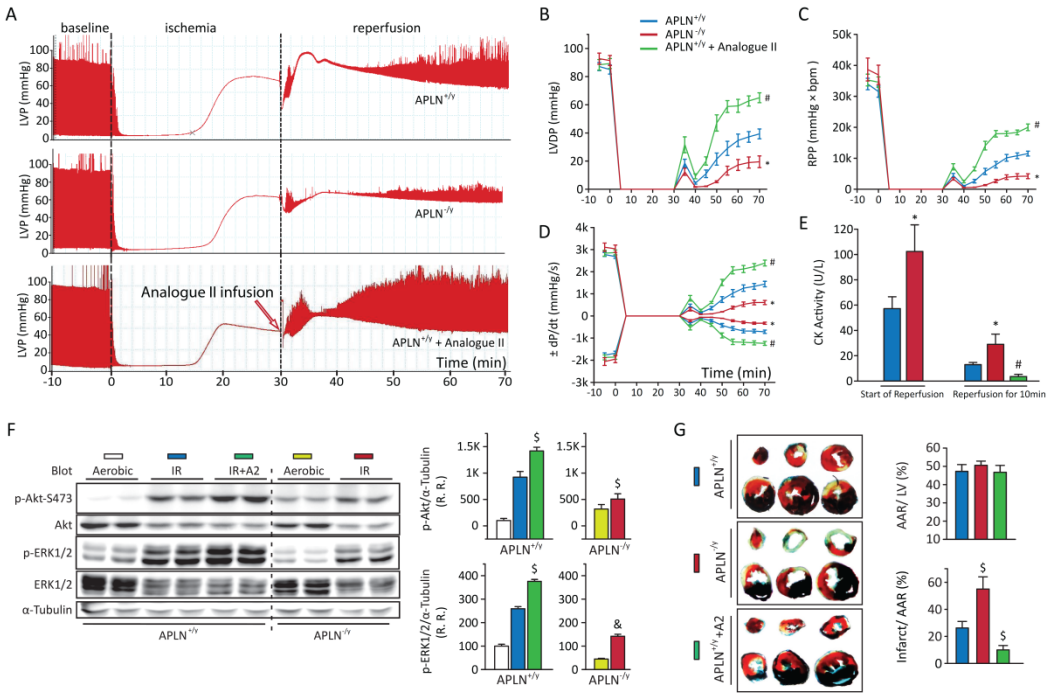

Figure 5.15 Myocardial ischemia-reperfusion injury using the *ex vivo* Langendorff system is exacerbated by the absence of apelin and is rescued by apelin analogue. (**A**) Representative hemodynamic tracings of APLN$^{+/y}$ and APLN$^{-/y}$ hearts showing a marked reduction in post-ischemic functional recovery of APLN$^{-/y}$ hearts with a dramatic protection in response to apelin analogue II (1.5 µg/ml for 20 min) at the start of reperfusion. Functional assessment of the LV developed pressure (LVDP) (**B**), rate-pressure product (RPP) (**C**), maximum and minimum rate of change in LV pressure (±dP/dt) (**D**) showing marked suppression of post-ischemic functional recovery in apelin deficient hearts and a dramatic protection in response to apelin analogue II. (**E**) Creatine kinase activity in the coronary perfusate showing a marked increase in APLN$^{-/y}$ compared to APLN$^{+/y}$ hearts at the start and after 10 min of reperfusion with reduced damage in response to apelin analogue II. (**F**) Western blot analysis of serine-473 Akt and Erk1/2 phosphorylation showing increased phosphorylation in response to ischemia-reperfusion (IR) injury in APLN$^{+/y}$ hearts which was markedly suppressed by loss of APLN and further stimulated by apelin analogue II. (**G**) *In vivo* IR due to 30 min ischemia in the LAD territory followed by 3 hr reperfusion with Evan's blue and TTC staining showing greater infarct size in APLN$^{-/y}$ hearts and a marked reduction in infarct size in response to apelin analogue II (2 µg/min for 10 min i.v.) at the start of reperfusion. p=phospho, t=total, R.R.=relative ratio. AAR=Area at Risk. Values are mean ±SEM; n=8 per groups except for **F** where n=5. *p<0.05 compared to the APLN$^{+/y}$ group; $^{\#}$p<0.05 compared to all other groups; $^{\$}$p<0.05 compared with the APLN$^{+/y}$ IR group and $^{\&}$p<0.05 compared with corresponding aerobic group.

We used the *ex vivo* Langendorff heart preparation to further determine the role of APLN in myocardial ischemic injury and to evaluate the therapeutic effects of the synthetic apelin analogues. Notably, in response to myocardial IR injury, $APLN^{-/y}$ hearts exhibited suppressed functional recovery compared to $APLN^{+/y}$ hearts as illustrated by representative hemodynamic responses (**Figure 5.15A**), LV developed pressure (**Figure 5.15B**), rate-pressure product (**Figure 5.15C**) and measures of myocardial contractility, dP/dt_{max} and dP/dt_{min} (**Figure 5.15D**).

A post-conditioning protocol was used in which APLN analogues were applied following the ischemic period in $APLN^{+/y}$ (wildtype) hearts in order to simulate a potential clinical application. While apelin analogue I (1 μM) failed to prevent the IR injury, apelin analogue II (1 μM) resulted in a greater recovery of function as illustrated by representative hemodynamic responses (**Figure 5.15A**) and the quantitative measure of myocardial performance (**Figure 5.15B-D**). Analysis of creatine kinase activity in the coronary perfusate corroborated the greater myocardial damage in the reperfused $APLN^{-/y}$ hearts with a marked protection seen in response to apelin analogue II (**Figure 5.15E**). The increased phosphorylation of Akt and Erk1/2, two critical pathways in mediating cardioprotection against myocardial IR injury[204], were reduced in the absence of APLN at 10 min (**Figure 5.15F**) and at 40 min post-reperfusion (**Figure 16**) with apelin analogue II leading to greater activation of these protective signaling pathways (**Figure 5.15F**). Next, we extrapolated our findings to an *in vivo* model

of IR injury in which the proximal LAD coronary artery was occluded for 30 min followed by 3 hr of reperfusion. While loss of APLN resulted in a greater infarct size, apelin analogue II administered at the time of perfusion significantly reduced the *in vivo* IR injury in APLN$^{+/y}$ hearts (**Figure 5.15G**).

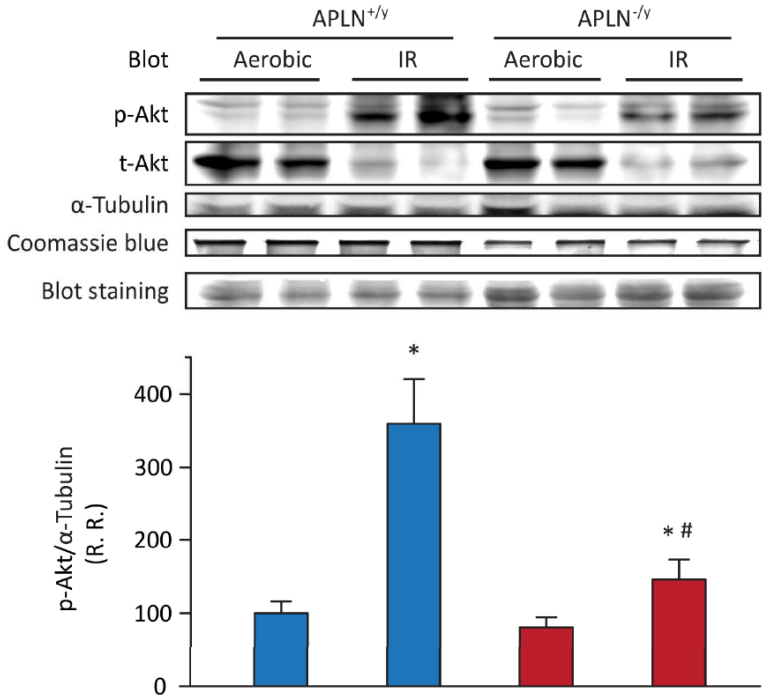

Figure 5.16 Western blot analysis of phosho Akt (serine-473) signaling pathway in the *ex vivo* hearts. Western blot analysis of phosho Akt (serine-473) signaling pathway in the *ex vivo* hearts following ischemia-reperfusion injury at 40 mins ischemia of reperfusion. *p<0.05 compared with corresponding aerobic group; #p<0.05 compared with the APLN+/y group.

Critical role of apelin in myocardial angiogenesis: stimulation by apelin analogue.

Apelin stimulates the angiogenic response, a key adaptive mechanism in ischemic heart disease and a determinant of infarct expansion.[203, 205, 206] We next examined the role of APLN in the adaptive angiogenesis response. We next examined the role of APLN in the adaptive angiogenesis response. Nuclear translocation of the key transcription factor, hypoxia inducible factor-1 alpha (HIF-1α), was reduced in the infarct region as delineated by immunofluorescence staining **(Figure 5.17A)** and Western blot analysis **(Figure 5.17B)** resulting in a lack of upregulation of vascular endothelial growth factor (VEGF) in the infarcted APLN deficient myocardium **(Figure 5.17C)**. While the regional expression of angiopoeitin-1 (Ang-1) was not differentially affected, angiopoetin-2 (Ang-2) levels were decreased in infarcted $APLN^{-/y}$ hearts at 3 days post-MI **(Figure 5.17D)**. Collectively, these data show a clear and important role of angiogenesis and as such we examined the *in situ* angiogenic response in the post-MI heart using CD31 immunofluorescence **(Figure 5.17E)** and lectin staining **(Figure 5.17F)** of the coronary endothelial cells and microvasculature, respectively. Our results show a marked reduction in capillary density and vessel integrity in the post-MI $APLN^{-/y}$ hearts compared to $APLN^{+/y}$ hearts **(Figure 5.17E-F)**.

We used the aortic ring culture method and showed that vessel sprouting was impaired in APLN deficient vessels, which was rescued by supplementation with

apelin analogue II and recombinant human VEGF (**Figure 5.18A**). To further substantiate the role of APLN in angiogenesis, we isolated and purified human endothelial progenitor cells (hEPCs) and confirmed the endothelial lineage by flow-cytometry for the endothelial-specific marker, VE-cadherin and expression of Von Willebrand factor and eNOS (**Figure 5.18B**). siRNA knockdown of APLN in hEPCs reduced apelin expression by ~80% (**Figure 5.18C**) and using an *in vitro* angiogenesis culture, expression of characteristic tip cell genes revealed markedly decreased expression of DLL4 (**Figure 5.18D**), a gene implicated in directing the tip versus stalk cell phenotype[207-209] without affecting Flt1 and KDR expression (**Figure 5.19**).

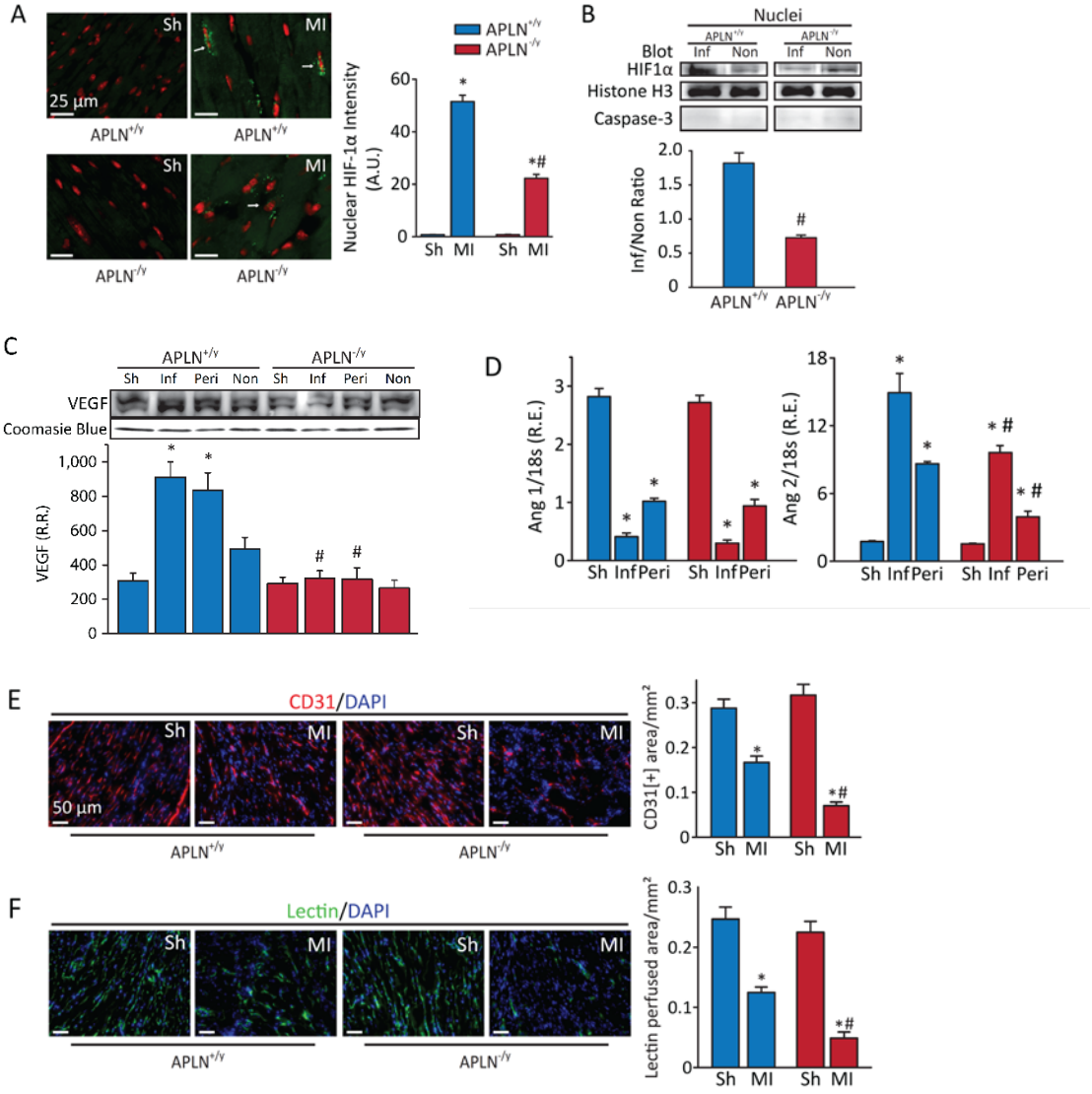

Figure 5.17 Disruption of apelin impairs the *in vivo* angiogenic response. Immunofluorescence staining for HIF-1α showing lowered levels of HIF-1α with decrease in nuclear translocation (**A**) which was confirmed by Western blot analysis of nuclear HIF-1α (relative to cytosolic) (**B**) in response to myocardial infarction in APLN$^{-/y}$ hearts. (**C**) Western blot analysis of VEGF levels in 1-day post-infarcted hearts showing a significant increase in APLN$^{+/y}$ hearts which was absent in APLN$^{-/y}$ hearts. (**D**) Regional expression analysis of angiopoeitin-1 (Ang-1) and angiopoetin-2 (Ang-2) levels in APLN$^{+/y}$ and APLN$^{-/y}$ post-infarcted hearts showing reduced Ang-2 levels in apelin-deficient hearts. *In situ* assessment and quantification of angiogenesis in 7-day post-MI hearts by using CD31 staining of the coronary endothelial cells (**E**) and lectin immunofluorescence of the coronary vasculature (**F**) showing a greater loss of endothelial cells and vascular integrity in apelin deficient hearts. Sh=Sham-Operated;

MI=Myocardial Infarction; Inf=Infarct Region; Peri=Peri-Infarct Region and Non=Non-Infarct Region. p=phospho, t=total, R.R.=relative ratio. n=5 except for D where n=8; *p<0.05 compared to the corresponding sham group; #p<0.05 compared to the APLN$^{+/y}$ group.

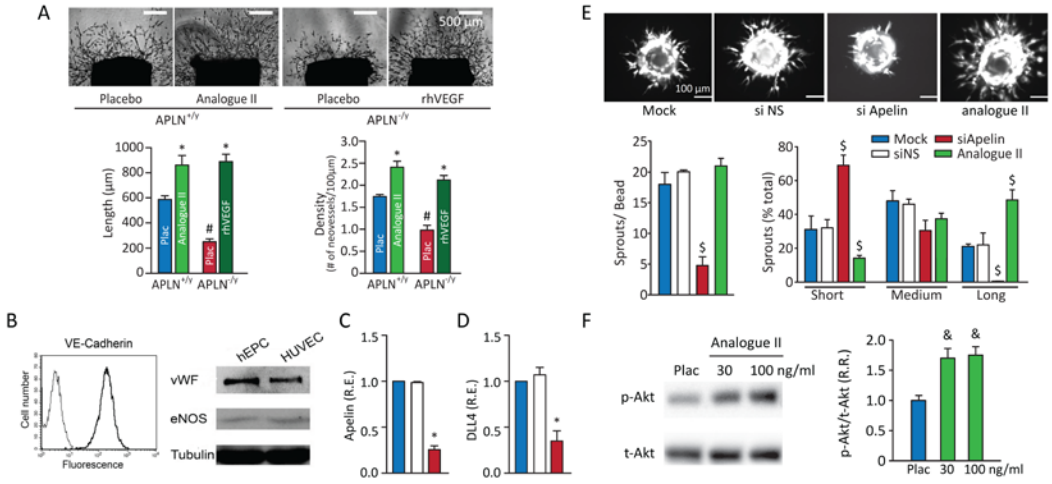

Figure 5.18 Loss of apelin impairs the *in vitro* angiogenic response in murine aorta and human endothelial progenitor cells while apelin analogue stimulates angiogenesis. (**A**) Representative aortic ring cultures from APLN$^{+/y}$ and APLN$^{-/y}$ mice showing a marked decrease in sprout length and density which was rescued by supplementation with apelin analogue II (100 ng/ml) and rhVEGF (20 ng/mL). (**B**) Characterization of the isolated human endothelial progenitor cells (hEPCs) using flow cytometry of the endothelial-specific marker, VE-cadherin while Western blot analysis of Von Willebrand factor and eNOS showed comparable expression with a positive control, human umbilical vein endothelial cells (HUVEC). Transfection of human endothelial progenitor cells (hEPCs) with a non-silencing control siRNA (siNS) or siRNA against apelin (siApelin) resulting in 80% decrease in apelin (**C**) and DLL4 (**D**) expression. (**E**) Representative beads and quantification of sprout length based on tertiles established from mock-transfected hEPC (Mock) and sprout density showing a drastic reduction in endothelial sprout density and sprout lengthening with knockdown of apelin. Apelin analogue II (100 ng/mL) stimulates endothelial lengthening (**E**) and increased phospho-Akt (serine-473) in hEPCs (**F**). rhVEGF=recombinant human vascular endothelial growth factor. NS=Non-sense. Values are mean±SEM; n=5 for each group. *p<0.05 compared to the corresponding sham/placebo group; #p<0.05 compared to the APLN$^{+/y}$ group; $p<0.05 compared to all other groups and &p<0.05 compared with placebo.

Silencing of APLN function disrupted endothelial sprouting with increased short/long vessel ratio and reduced endothelial sprout density correlating with a marked suppression of DLL4 (**Figure 5.18E**). Importantly, apelin analogue II stimulated the endothelial sprouting resulting in longer capillary tube formation (**Figure 5.18E**) in association with increased phospho-Akt in hEPCs (**Figure 5.18F**). In contrast, apelin analogue I failed to alter the angiogenic response and Akt phosphorylation of hEPCs. These findings confirmed that APLN deficiency inhibit the angiogenic response in the post-MI heart and in hEPCs.

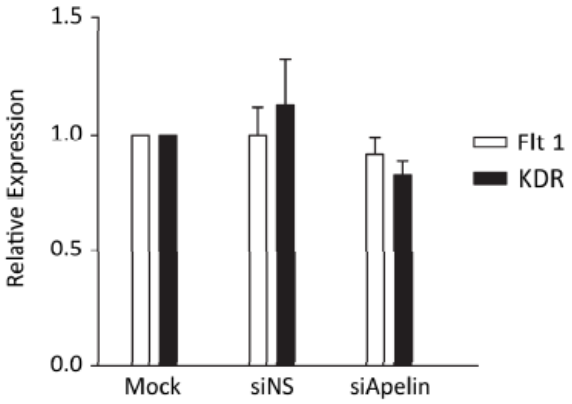

Figure 5.19 Flt1 and KDR expression using qRT-PCR. Apelin knockdown using siRNA did not affect Flt1 and KDR expression using qRT-PCR and mRNA isolated from angiogenic sprout cultures of hEPCs.

5.5 Discussion

Coronary artery disease characterized by adverse post-MI remodeling and IR injury is now the most common cause of heart failure.[188204] We showed the APLN/APJ pathway is drastically altered in post-MI myocardial tissue characterized by a marked reduction in APLN levels in murine hearts. Importantly, in explanted human hearts with primary ischemic injury, there was a marked loss of APLN in various compartments confirming a critical role of APLN in human heart failure secondary to ischemic heart disease. Using a genetic model we showed that loss of APLN impaired post-MI remodeling, angiogenesis and functional recovery, and exacerbated myocardial ischemia-reperfusion (IR) injury *ex vivo* and *in vivo* demonstrating a critical causal role of APLN in myocardial ischemic injury. The loss of APLN clearly compromises the activation of the protective Akt/PI3K[210] and Erk1/2 signaling pathways[167], both *in vivo* and *ex vivo*, resulting in increased myocardial damage and worsening heart function. Our synthetic apelin analogue provided salutary beneficial effects against *ex vivo* and *in vivo* myocardial injury. The C-terminal phenylalanine residue of the apelin-13 is essential and truncation of the C-terminal leads to a 10-fold decrease in binding and functional efficacy.[171, 185] We showed that in contrast to pyr-1-apelin-13, apelin analogue I and II were extremely resistant to the proteolytic cleavage of the C-terminal phenylalanine by ACE2. The ability of apelin analogue II to improve both systolic and diastolic function is particularly useful in the setting of

myocardial ischemia. In addition to the pro-survival effects of apelin and apelin analogues, the ability of these agonists to activate Akt and eNOS[211] can directly improve the contractility and relaxation of the cardiomyocytes.[212, 213]

Genetic variation in the APJ receptor modifies the progression of heart failure in patients with dilated cardiomyopathy.[47] In Dahl salt-sensitive hypertensive (DS) rats, cardiac apelin/APJ pathway is markedly downregulated with the onset of HF.[214] Apelin mediates positive inotropic effect *in vitro*[43,44] and *in vivo*[45] and minimizes increases in systemic arterial and venous tone[40-42] with corresponding reductions in left ventricular afterload and preload. The integrative physiological role of the APLN system strongly suggest that enhancing APLN action may serve to minimize myocardial ischemic damage and the progression to advanced HF.[45, 49] The APLN/APJ signaling pathway is downstream of Cripto, a member of the EGF-CFC family of signaling molecules, promotes cardiomyocyte differentiation[215] and enhanced cardiac differentiation of embryonic stem cells[216], processes which may be recruited in the post-MI setting. Using *in vitro* and *in vivo* assessment of angiogenesis, we showed that APLN is required for normal angiogenesis, a key adaptive mechanism in ischemic and pressure-overload induced heart failure.[205, 206, 217] We observed a marked deficiency in angiogenic sprout formation in a robust assay of 3-dimensional angiogenesis using primary human endothelial progenitor cells when APLN was silenced. Apelin induces phosphorylation of eNOS and NO release from endothelial cells thereby

stimulating angiogenesis[51] while loss of APLN may sensitize endothelial cells to apoptosis.[51, 101] As such, the APLN/APJ system has emerged as a critical mediator of the spatial and temporal control of angiogenesis in heart disease. Our study has several limitations. We used a germ-line knockout of apelin and therefore we cannot distinguish cell-specific effects of apelin action versus the systemic changes associated with a whole-body knockout of apelin. In addition, a detailed molecular pharmacological characterization of the apelin analogues including *in vivo* pharmacokinetics and their binding properties to their cognate receptors is needed.

Collectively, our results and previous studies have delineated a critical role of the APLN/APJ axis in the regulation of cardiovascular functions and fluid homeostasis. Apelin increases cardiac contractility *in vitro*[43, 44] and *in vivo*[45] and minimizes increases in systemic arterial and venous tone[40-42] with corresponding reductions in left ventricular afterload and preload. In addition, apelin receptor agonism mediates central effect and suppresses arginine vasopressin[218] thereby promoting renal fluid loss which may be particularly attractive in patients with HF. Since the APLN/APJ system is compromised in human heart failure[41, 48], the integrative physiological role of the APLN/APJ system strongly suggest that enhancing apelin action may serve to minimize myocardial ischemic damage and the progression to advanced HF. Enhancing apelin action represents a new potential drug target for the treatment of ischemic heart failure. The short half-life

of native APLN peptides[49, 58, 99] implies a need to generate APLN analogues which are more potent and less susceptible to degradation. Our ability to design and synthesize novel APLN analogues illustrate that APLN can be targeted pharmacologically to enhance the therapeutic effects and to provide potential drugs.

CHAPTER SIX

Loss of Apelin leads to Down-regulation of ACE2 and Adverse Aortic Remodeling in response to Ang II Stimulation: The interaction of Apelin, ACE2 and Ang II in Vasculature

Wang Wang[1,2], Mengcheng Shen[3], Vaibhav B. Patel[1,2], Ratnadeep Basu[1,2],

Zamaneh Kassiri[2,3] and Gavin Y. Oudit[1,2,3]

[1]Division of Cardiology, Department of Medicine, [2]Mazankowski Alberta Heart Institute, University of Alberta, Edmonton, Canada, and [3]Department of Physiology, University of Alberta, Edmonton, Canada

Author Contributions: Wang Wang and Gavin Oudit designed the experiment, wrote and manuscript and figures; Wang Wang performed the histological studies, collected the samples, performed myography study, part of the flow cytometry and immunostaining; Mengcheng Shen cultured the aortic SMCs and flow cytometry assay; Vaibhav Patel performed the immunostaining or SMCs and part of aortic tissue staining, imaging and analysis; Ratnadeep Basu performed the ultrasound analysis; Zam Kassiri gave insight into the experimental design, reviewed and edited the manuscript.

6.1 Abstract

Apelin has been shown cardiovascular protective effects. It maintains the endothelial function and structure and counteracts activity of rein angiotensin system. In the current study we explored the role of apelin in aortic remodeling. $APLN^{-/y}$ and littermate wildtype ($APLN^{+/y}$) mice were used in current study. Mice were infused with exogenous Ang II. We found pathological remodeling and the formation of aortic abdominal aneurysm in $APLN^{-/y}$ mice in response to Ang II. This pathological remodeling is companied by increased apoptosis, which is further confirmed in cultured primary mice or human aortic SMCs. In the isolated mesenteric artery, we found loss of apelin leads to increased sensitivity to Ang II. Finally, in protein expressional study we found apelin is a positive regulator of ACE2 in the aortic SMCs. Ang II leads to ACE2 up-regulation which is partly apelin mediated. The current study clearly showed the importance of apelin in maintain aortic homeostasis in Ang II stimulation; Apelin showed the ability to attenuate Ang II induced aortic SMCs apoptosis, vascular tone and aneurysm. The mechanism study shows the ability of apelin to up-regulate ACE2 and mediate Ang II induced up-regulation of ACE2. Our current results showed that apelin can be a promising target for counteracting Ang II and treating cardiovascular disease.

Key Words: Apelin, Angiotensin II, AAA, Remodeling, Aortic SMCs, Apoptosis

6.2 Introduction

Renin Angiotensin System (RAS) has been intensively studied and demonstrated to play a central role in cardiovascular system homeostasis and pathologies including hypertension[219], atherosclerosis[220] and abdominal aortic aneurysm (AAA)[221], while Angiotensin II (Ang II) has been identified as one of the core effector in these diseases. Ang II can contribute to a number of events such stimulating protein synthesis and hypertrophy in vascular smooth muscle cells (SMCs) via AT1 receptor[222], mediating several key events of the inflammatory processes,[223, 224] stimulating the production of molecular oxygen species that trigger mitochondrial dysfunction and cellular injury,[225, 226] thereby contributing significantly to various age-associated organ failures.[226, 227] Based on this understanding, ACE inhibitors and Ang II receptor blockers are currently widely used in the treatment of Ang II related cardiovascular end-organ damage.[228] Since being identified in 2000[54], Angiotensin Converting Enzyme 2 (ACE2) has emerged as a new efficient regulator of Ang II *in vitro* and *in vivo*,[68, 152] and has extended the RAS signaling pathway to the ACE2-Angiotensin 1-7 axis, which

has shown multiple cardio-protective effects by down-regulating Ang II as well as up regulating Ang 1-7 which exerts beneficial effects.[229] A study from our group showed that loss of ACE2 contributed to loss of aortic smooth muscle and adverse vascular remodeling upon whole-body Ang II treatment,[72] while Ang 1-7 supplementation prevented the increase in Ang II-induced reactive oxygen species and apoptotic cell death.[72]

Moreover, another cardiovascular active peptide, apelin has been proved to be cleaved at C-terminal by ACE2 at a comparable rate to Ang II cleavage by ACE2.[58] Importantly, we have found that apelins (pyr-Apelin 13 and Apelin 17) also function as efficient physiological substrates of ACE2 in mice as demonstrated in regulating vascular tone *in vivo* and in nitride oxide (NO) generation *in vitro* as well as in protecting against ischemia-reperfusion injury in ACE2-knockout or pharmacologically knocked down models. There have been several reports about the involvement of apelin in vascular disease[135, 169, 230, 231], however it is not clear how this proposed ACE2-apelin axis functions in vascular diseases, In this Chapter, we explored how apelin interacts with Ang II, ACE2 and their impact on vascular tone and Ang II induced aortic remodeling.

6.3 Materials and Methods

Experimental Animals and Protocols. Apelin deficient ($APLN^{-/y}$) and littermate wildtype ($APLN^{+/y}$) mice were generated and bred in C57BL/6 background. All animal experiments were carried out in accordance with the Canadian Council on Animal Care Guidelines, and animal protocols were reviewed and approved by the Animal Care and Use Committee at the University of Alberta.

Ang II and PE Infusion. Osmotic micro-pump (model 1002; Alza, Palo Alto, Calif., USA) was implanted subcutaneously at the dorsum of the neck to infuse a pressor dose of Ang II (1.5 $mg/kg^{-1}d^{-1}$) or phenylephrine (PE) (40 $mg/ kg^{-1}d^{-1}$) or saline (Vehicle) for 14 days or 28 days in $APLN^{+/y}$ and $APLN^{-/y}$ mice.[68, 134]

Ultrasonic Imaging of Aorta. Ultrasonic images of the aorta were obtained in mice anesthetized with 1.5% isoflurane using a Vevo 2100 high resolution-imaging system equipped with a real time microvisualization scan head (RMV 704, Visual Sonics, Toronto, Canada). The aortic diameters were measured by M-mode at thoracic aorta and abdominal aorta The maximum aortic lumen diameter (aortic systolic diameter corresponding to cardiac systole) and the minimum aortic lumen diameter (aortic diastolic diameter corresponding to cardiac diastole) monitored by simultaneous ECG recordings were measured and used to calculate the aortic expansion index [(Systolic aortic diameter-Diastolic aortic diameter)/Systolic diameter x 100].[232]

Primary Aortic Smooth Muscle Cells (SMCs) Culture. Primary mouse aortic SMCs were isolated using enzymatic digestion method from 5-6 weeks old male mice of both genotypes as reported before.[233] Briefly, after removal of the surrounding adipose tissue, the whole aorta was incubated in HBSS (Giboco) containing 0.744 U/mL elastase (Worthington), 1 mg/mL collagenase type II (Worthington), and 1 mg/mL trypsin inhibitor (Worthington) for 10 min at 37 °C to facilitate the complete removal of the adventitial layer. The intimal layer was scraped off gently with curved fine-tip forceps after the aorta was cut longitudinally. Then the aorta was minced into small pieces (1 mm× 1 mm) and further digested for 2 hours at 37°C. The digestion process was terminated by adding equal volume of 20% FBS and DMEM/F12 culture medium. The isolated cell pellet was collected by centrifugation at 300 *g* for 5 min, and was suspended in 1 mL of 20% FBS+ DMEM/F12 culture medium. The cells were left undisturbed for 48 hours to allow attachment and spreading. Primary mouse aortic SMCs were weaned into 10% FBS+DMEM/F12 culture medium after passage 3. Cells at passage 4-7 were used for experiments. Human VSMCs were isolated using tissue explant method.[234] Tissue specimens from the aortic root of healthy donors were washed twice with sterile cold PBS containing 0.5 μg/ml fungizone (Giboco) and 50 μg/ml gentamycin (Giboco). The endothelial cells were scrapped off from the intimal layer by a sterile scalpel blade. The adventitial layer was removed by curved forceps. The remaining medial layer of the aortic tissue was

then gently agitated in HBSS (Giboco) for three times. Next, the transverse muscle strips (approximately 2 mm in width) was peeled off from the media by layers using fine-tip forceps. All the collected muscle strips were cut into smaller cubes (2 mm× 2 mm) using sterile blade. The chopped muscle cubes were then washed twice with HBSS, and evenly distributed into 25-cm^2 culture flasks with a minimum 25 cubes/flask. A total volume of 2 mL 20% FBS+ DMEM/F12 medium was added to the flask to keep the muscle cubes moist. Then the flasks were left in the incubator undisturbed for 24 hours before additional 2 mL of full-growth medium was carefully added. The culture medium was changed every 3 days. After 2-3 weeks, the cells migrated from aortic tissue explants were subcultured in 10% FBS+DMEM/F12 culture medium. Cells at passages 3-8 were used for experiment. For both primary mouse and human VSMCs, the medium was supplemented with 100 U/mL penicillin, and 100 μg/mL streptomycin at a final concentration.

APLN siRNA treatment. VSMCs were seeded into 6-well plate at a density of 2×105 cells/well. The cells were infected with APLN siRNA (10 μM) or scrambled negative control siRNA (10 μM) for 48 hours in 10% FBS+DMEM/F12 culture medium as per the manufacture's instruction (Ambion). The efficiency of APLN knockdown in APLN siRNA treated cells (~97.3%) was confirmed by Taqman[235].

Continuous Blood Pressure Recording in Conscious Mice. The $APLN^{+/y}$ and $APLN^{-/y}$ mice were individually housed at constant temperature (21 ±1°C) and relative humidity (50% ± 2%) to give them sufficient cage space and avoid signal interference. DSI PhysioTel PA-C10 Pressure Transmitter (Data Sciences International) was implanted subcutaneously on the right side of abdomen with the catheter reaching the aorta via right carotid artery.[236] Mice were allowed to recover from surgery for one week, after which baseline blood pressure was recorded for 3 days. The recording hours for blood pressure on each day were 12am to 2am at night and 12 pm to 2pm as day. Subsequently, Ang II-containing micro-osmotic pumps were implanted subcutaneously at abdomen.

Annexin V/Propidium iodide (PI) staining and flow cytometry assay. When reached 90% confluency, $APLN^{+/y}$, $APLN^{-/y}$ and APLN siRNA treated VSMCs were serum-starved for 24 hours in 0.5% FBS DMEM/F12 culture medium. Cells were then treated with 1 μM Ang II or vehicle for 24 hours. VSMCs treated with 1 μM staurosporine (Santa Cruz Biotechnology, Inc.) for 6 hours were used as positive control. Ang II induced apoptosis in VSMCs were assessed using an Annexin V-FITC/Propidium iodide (PI) kit for flow cytometry (Invitrogen) as per manufacturer's instruction. In brief, VSMCs were rinsed with ice-cold PBS and incubagted with accutase (BD Biosciences) at room temperature for 5 min. The detached cells were collected by centrifugation (300 *g*, 5 min). Cell pellets were further washed twice with ice-cold PBS and resuspended in 100μl 1×binding

buffer. Five microliter of Annexin-V-FITC and 1µl of PI (100 µg/mL) were added to the cells and incubated at room temperature for 15 minutes. After incubation, 400µl binding buffer was added to each sample. Cell apopotosis/death was evaluated using a BD LSR Fortessa and FACSDiva software (BD Biosciences). The acquired data were analyzed with FlowJo software (Treestar, Inc., San Carlos, CA).[237]

Histological Analyses, Terminal Deoxynucleotidyl Transferase dUTP nick end labeling (TUNEL) and immunofluorescence staining. After 2 weeks or 4 weeks of Ang II or saline infusion, mice underwent whole body perfuse-fixation via the heart, with paraformaldehyde at 80mmHg for 25min, to allow the blood vessels to be fixed at its native state.[238, 239] Then, mesenteric vessels were dissected out carefully without being stretched which could alter the structure of the vessels, and further fixed in 10% buffered formalin for 48 hours and embedded in paraffin. Aortas were dissected, imaged and then fixed in the same way as for the mesenteric vessels. In a separate set of experiments, aortas were collected fresh (without perfuse-fixation) and preserved in OCT at -80°C for cryosections. Five micro-meter thickness of formalin fixed paraffin embedded (FFPE) sections were used for the histological staining including Movat's pentachrome and Gomori Trichrome.[232, 240] Collagen positive area in the aorta or mesenteric artery was quantified by the morphometric analysis using the

Metamorph Basic (version 7.7.0.0) software. *In situ* DNA fragmentation was detected in 5μm thick FFPE sections of aorta using the commercially available terminal deoxynucleotidyltransferase-mediated dUTP nick-end labeling (TUNEL) assay kit according to manufacturer's instructions (Invitrogen) as previously described.[153, 155] Five micrometer thick FFPE sections were used for the immunofluorescence staining for ACE2, calponin and nitrotyrosine immunofluorescence.[155, 229, 241] Thickness of the medial layer of the aorta was measured in calibrated images as the mean distance between the external elastin lamella and the internal elastin lamella from 8 different regions in the cross-section of an aorta using the Metamorph Basic software (version 7.7.0.0).[242-244] Calponin positive cells in the aorta were counted to determine the VSMC density. Paraformaldehyde-fixed VSMCs were double stained for calponin and vimentin to assess the purity of the VSMC culture. Briefly, the VSMCs were stained with rabbit anti-calponin (Abcam) and rabbit anti-vimentin (Abcam) primary antibodies and Alexa Fluor 488 conjugated anti-rabbit and Alexa Fluor 594 conjugated anti-mouse secondary antibodies. The cells were imaged using the fluorescence microscope (Olympus IX81), analyzed and reported as the cells sizes. Briefly, 10 images were taken randomly from the stained cells at 100X magnification. Calponin positive cells were outlined manually to determine the size of the SMCs.

Ex vivo **Mesenteric Artery Pressure Myography.** Mesenteric artery pressure myography was performed using DMT Pressure myography system (Danish Myo Technology; Model, P110) according to the protocol provided by DMT with modification. Briefly, $APLN^{+/y}$ of $APLN^{-/y}$ mice are anesthetized with 2% isoflurane in oxygen; an intact small segment (around 4 mm long) of third order mesenteric artery was isolated and mounted on the pressure myography system. Consequently, mounted vessels are pressurized in steps of 10 mmHg for 5 min per step from 10 mmHg to 60 mmHg; a "wake-up" procedure was performed for all vessels before treatments were introduced. The "wake up" includes: 1. Once the vessel is equilibrated at 60 mmHg, remove the PSS and add 60mM KPSS (HK) to cause a contraction. 2. Allow the vessel to contract for 3 min. 3. Wash the KPSS with PSS until baseline diameter is reached. 4. Repeat the KPSS contraction and PSS washes. 5. Noradrenaline (10^{-6} M) to be added in PSS to cause a contraction. 6. Once the vessel is contracted reaching a plateau, Acetyl-Choline (10^{-5} M final in the PSS bath) can be added to assess endothelium dependent vasodilation. 7. Wash the vessel 5 times over 30 minutes. 8. Vessel is then ready for experiments. The volume of the bath was maintained at 10 mL for all treatments. In Ang II dose-response experiments, different concentrations of Ang II were added cumulatively and mixed well to reach each desired final concentration in the bath after the vessel constriction reaches a plateau with the previous dose. In a different set of experiments, to study the vasoconstriction and relaxation of Ang II

over time, 0.1 μM of Ang II was used to induce vasoconstriction over time for 5 min, then washed with PSS buffer 4 times in 5 min; then vessels were allowed to recover for 30 min. Then for the second treatment of 0.1 μM of Ang II was used to induce vasoconstriction for another 5 min.

Statistical Analysis. All data are shown as mean±SEM. All statistical analyses were performed using SPSS software (Chicago, Illinois; Version 10.1). The effects of genotype were evaluated using ANOVA followed by the Student Neuman-Keuls test for multiple comparison testing and comparison between two groups were made using the Student's t test.

6.4 Results

Ang II caused Abdominal Aortic Aneurysm (AAA) in APLN$^{-/y}$ Mice but not in APLN$^{+/y}$ mice

Ang II is a well-known stimulant for cardiovascular remodeling, and has been used widely in creating cardiovascular disease models.[140, 228, 245, 246] In our current study, Ang II infusion (1.5 mg·kg^{-1}·day^{-1}) lead to hypertrophy or hyperplasia of aorta in APLN$^{+/y}$ and APLN$^{-/y}$ mice. However, only in APLN$^{-/y}$ mice it showed greater diffusely dilated aortic diameter as well as dramatic abdominal aortic aneurysm, which was absent in APLN$^{+/y}$ mice. Representative gross histological

imaging of aorta after 4 weeks of Ang II infusion are shown in Figure 1A, with red arrow indicating AAA in $APLN^{-/y}$ Ang II group (Figure 6.1A). No mortality in $APLN^{+/y}$ Ang II group during the experiment, but 3 samples out of a total of 12 Ang II-treated $APLN^{-/y}$ mice developed aortic rupture-related mortality between 11 to 14 days post-Ang II infusion. Green arrow points to the rupture site with a visible blood clot at this site (**Figure 6.1A**). Movat pentachrome staining was performed at the of the aneurysmal dilation in comparison with counterparts of non-aneurysm. The intact continuous elastic sheet in both $APLN^{+/y}$ and $APLN^{-/y}$ Sham groups (**Figure 6.1B**). However, Ang II infusion in $APLN^{-/y}$ mice lead to dramatic aortic wall structure disruptions, consistent of broken down elastic sheet (stained as black), aortic dissection (black arrow), intramural bleeding, with significantly increased diameter. (**Figure 6.1B**).

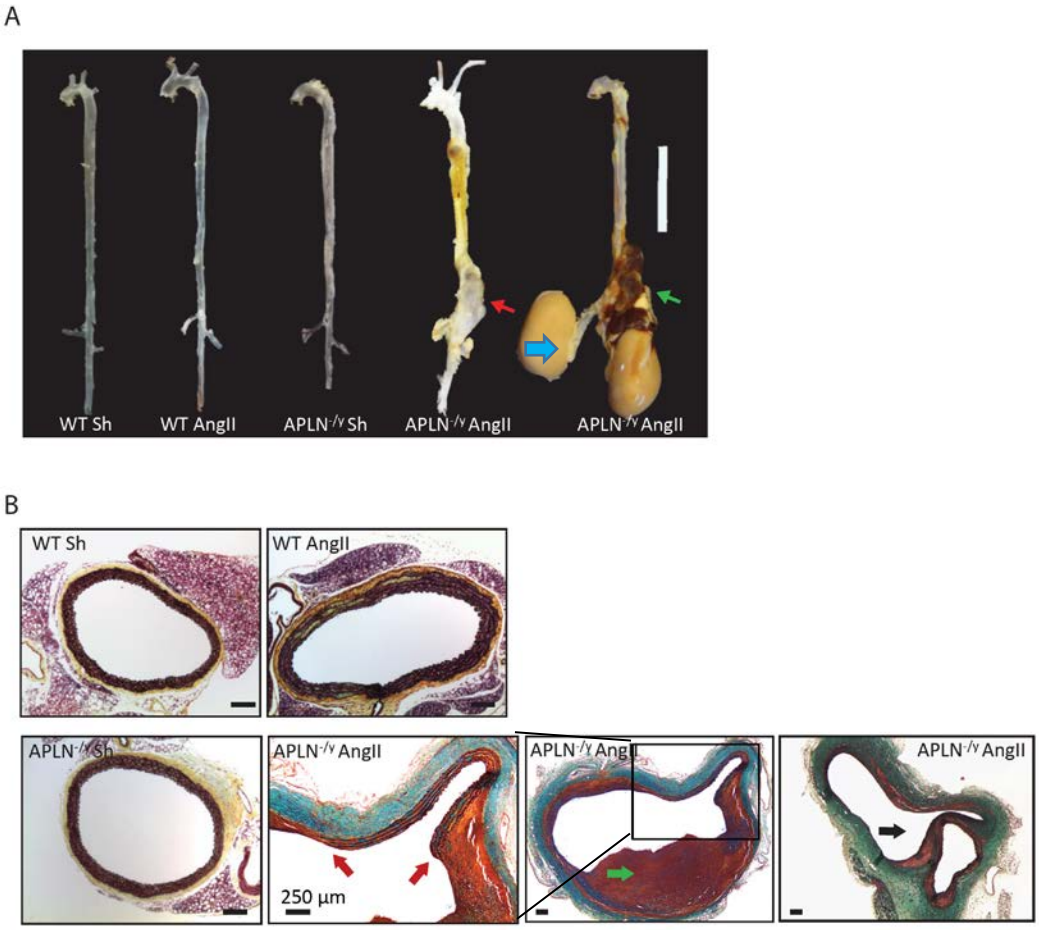

Figure 6.1 Ang II infusion leads to aortic lectin disruption, rupture or aneurysm in APLN$^{-/y}$ mice. Representative images of aorta showing the gross morphology after perfusion fix and dissected to display the overall morphology. (Figure 6.1A) While scale bar is 1 cm. Red arrow and green arrow point out abdominal aorta developing aneurysm and hemorrhage respectively. Movat pentachrome staining, cross section view of abdominal aorta showing aortic wall thickness and structure of lectin (Figure 6.1B); Ang II treatment in APLN$^{-/y}$ mice leads to dramatically aortic wall structure disruptions, including broken down lectin layers (stained as black), aortic dissection (black arrow), intramural bleeding, with largely dilated diameter, red arrows indicate the two ends of discontinued elastin layers, green arrow indicates neointima (Figure 6.1B). Blue arrow indicates kidney.

Ang II causes greater aortic dilation and rigidity in APLN$^{-/y}$ mice

Functional diameter and vascular flexibility *in vivo* was monitored by ultrasonic imaging after 2 weeks and 4 weeks of Ang II infusion. Three main sections of the aorta (aortic arch, thoracic aorta and abdominal aorta) were imaged for measurement of the systolic and diastolic diameters; aortic expansion index was derived based on these parameters.[232, 247] The results show no difference in baseline diameter and aortic expansion index between APLN$^{+/y}$ and APLN$^{-/y}$ Sham (Figure 6.2A-F). At the thoracic arch, aortic diameter increased over time after Ang II infusion, but the increase in diameter did not reach statistical significance between APLN$^{+/y}$ and APLN$^{-/y}$ Ang II treatment groups. A similar trend was observed in the proximal segment of the abdominal **Figure 6.2A, B** aorta where indicated by yellow lines (**Figure 6.2C, D**). In the distal segment of the abdominal aorta, however, the diastolic and systolic aortic diameter increased significantly in both APLN$^{+/y}$ and APLN$^{-/y}$ groups, accompanied with significantly decreased aortic expansion index (**Figure 6.2 E, F**). Importantly, in line with the histological observation performed at the same anatomical location, we saw the increase in aortic diameter and the decrease in aortic expansion index were significantly greater in Ang II treated APLN$^{-/y}$ group. These observations show that Ang II infusion leads to aortic dilation and decreased aortic compliance in both genotypes, but aortic abdominal aneurysm only in apelin-deficient mice.

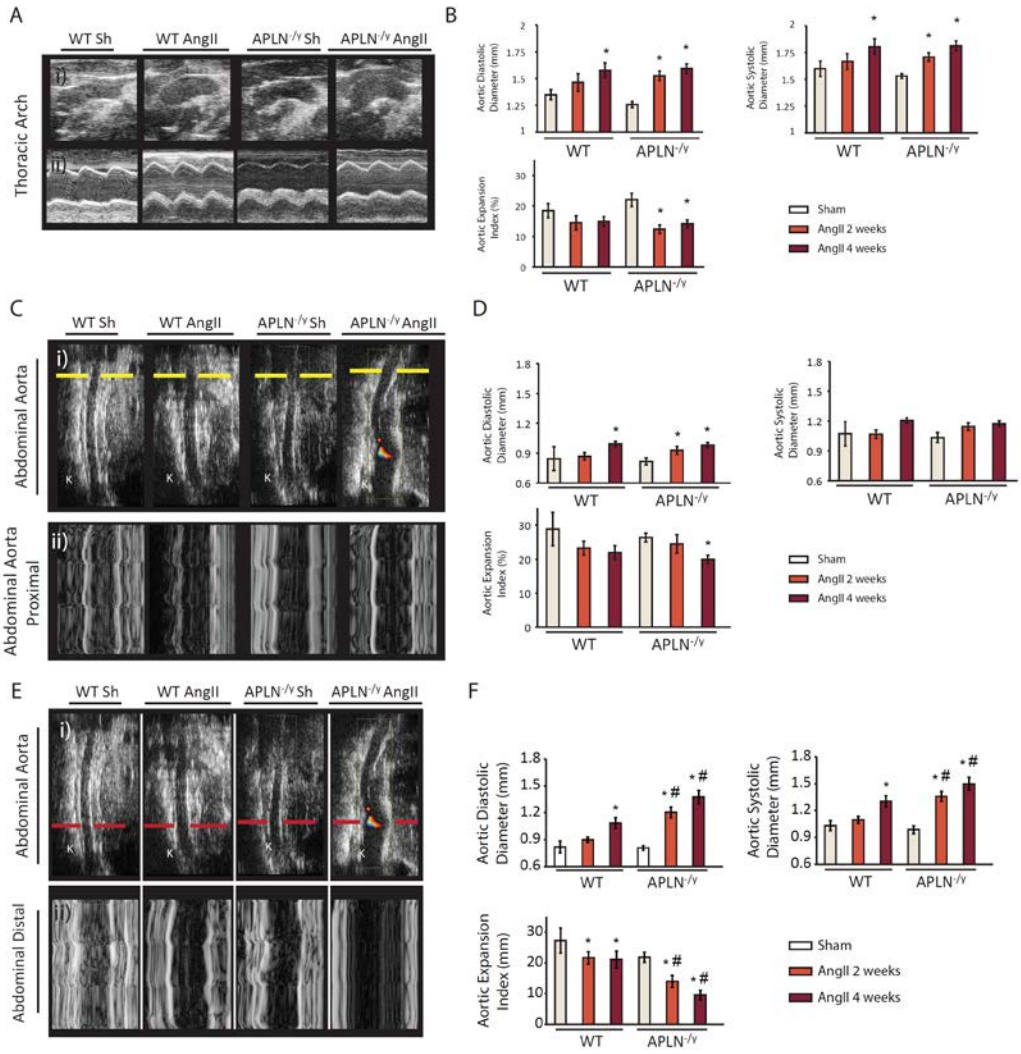

Figure 6.2 Ultrasonography of aorta showing APLN$^{-/y}$ mice developed AAA after 4 weeks of Ang II infusion. Ultrasonographic B-mode (panel i) and M-mode (panel ii) images of the aorta in saline- and Ang II-infused APLN$^{+/y}$ and APLN$^{-/y}$ mice. (Figure 6.2A, C, E) The red lines show where measurements of distal abdominal aortic diameter were obtained (Figure 6.2 E) and the yellow lines indicate proximal abdominal aortic diameter (Figure 6.2 C). "K" indicates the top of the left kidney as reference. Bar graph plot of averaged parameter aortic systolic and diastolic diameters and aortic systolic expansion index of thoracic aorta (Figure 6.2B), proximal abdominal aorta (Figure 6.2D) and distal abdominal aorta (Figure 6.2F) in saline- or Ang II-infused APLN$^{+/y}$ and APLN$^{-/y}$ mice. n = 12/group/genotype. *,$p < 0.05$ compared to sham control within genotype; #, $p < 0.05$ comparing with APLN$^{+/y}$. Averaged data represent mean ± S.E (error bars).

Ang II leads to vascular remodeling and AAA independent of vascular tone.

Because of the common coexistence of aortic aneurysm and systemic hypertension, which is in association with the fact that Apelin is a potent vasodilator, so it is possible the AAA in $APLN^{-/y}$ group may largely be due to the greater increase in vascular tone in the absence of apelin. To determine the involvement of blood pressure in the formation of AAA in Ang II treated $APLN^{-/y}$ mice, we treated $APLN^{-/y}$ mice with phenylephrine (PE) to achieve a comparable hypertensive effect as Ang II. PE is a vasopressor, but aortic aneurysm counts only 0.3466% of reported side effect of PE, according to Food and Drug Administration (FDA). Our results show that PE increases blood pressure to a similar level of AngII induced in $APLN^{-/y}$ mice (**Figure 6.3A**).

After 4 weeks of PE infusion, it did not cause any change in aortic diameter or in the expansion index as assessed by ultrasonic imaging of aorta (**Figure 6.3B, C**). Therefore, the similar hypertensive effects and time course led by Ang II perhaps did not contribute to the overall aortic wall destruction as observed in $APLN^{-/y}$-Ang II mice. These results point out that the Ang II-induced AAA in $APLN^{-/y}$ mice is likely independent of vascular tone.

Ang II leads to diffuse aortic hypertrophy and loss of VSMCs with increased apoptosis in APLN$^{-/y}$ mice.

We further examined the non-aneurysm regions of the aorta from APLN-KO mice to study the response to Ang II. Gomori trichrome staining on non-aneurysm thoracic aorta after 2 weeks or 4 weeks Ang II infusion showed hypertrophic and fibrotic remodeling in APLN$^{+/y}$ aorta featuring increased aortic media thickness as well as increased perivascular fibrosis (**Figure 6.4A**). In up in the adventitial layer (**Figure 6.4B**). Quantification of these images is shown in (**Figure** comparison, the APLN$^{-/y}$ mice showed a similar hypertrophic response at 2 weeks post-Ang II, but after 4 weeks, the APLN$^{-/y}$ aorta showed thinner aortic media with more fibrotic tissue build **6.4C**). This indicates a different patter of remodeling in APLN$^{-/y}$ aorta. Movat Pentachrome staining on 4 weeks Ang II infused aortas confirmed the aortic hypertrophy in APLN$^{+/y}$, but thinning of aortic media in APLN$^{-/y}$ group with turquoise stained ground substance or mucin[248, 249] (**Figure 6.4D**).

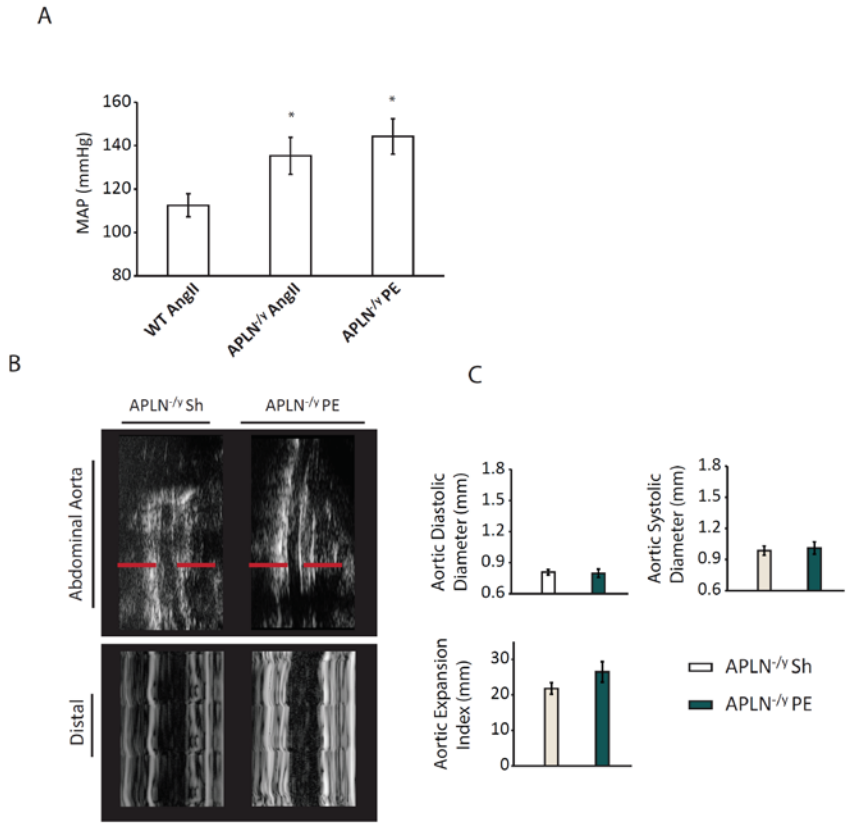

Figure 6.3 PE infusion leads hypertensive effect but no significant aortic dilation. PE infusion increases blood pressure to a comparable level around MAP 140 mmHg as Ang II infusion in APLN$^{-/y}$ mice. (Figure 6.3A) Ultrasonographic B-mode (panel i) and M-mode (panel ii) images of the distal abdominal aorta in saline- and Ang II-infused APLN$^{-/y}$ mice. The red lines show where measurements of distal abdominal aortic diameter were obtained. (Figure 6.3B) Bar graph plot of averaged parameter aortic systolic and diastolic diameters and aortic systolic expansion index demonstrate on different between PE and saline treated group. (Figure 6.3C)

The thinning of aortic media in APLN$^{-/y}$ aorta could suggest loss of VSMCs[250], therefore performed calponin staining, a specific marker of VSMCs, which showed decreased number of calponin positive cells in APLN$^{-/y}$ aorta relating to the decreased media thickness (**Figure 6.4E, F**). Ang II increased the number of calponin-positive cells (SMCs) in APLN$^{+/y}$ mice (**Figure 6.4E, F**). These results

suggest that Ang II promotes VSMCs proliferation and/or hypertrophy in $APLN^{+/y}$ but triggers VSMC loss in $APLN^{-/y}$. Apoptosis represents a dominant mode of VSMC loss contributing to adverse vascular remodeling.[251-253] Terminal deoxynucleotidyl transferase dUTP nick end labeling (TUNEL) staining was performed in the aorta and significant apoptosis was detected in $APLN^{-/y}$ aorta in response to Ang II (**Figure 6.4G, H**) consistent with the reduced VSMCs density in these mice.

Knock down of *Apln* leads to increased apoptosis in cultured aortic SMCs

To rule out the interference of systematic effects of Ang II, we isolated and cultured aortic VSMCs from $APLN^{+/y}$ and $APLN^{-/y}$ mice. APLN downregulation was achieved by siRNA technique (**Figure 6.5A**), and cells were subject to Ang II treatment. Flow cytometry analysis was employed to assess apoptosis using annexin V/ propidium iodide (PI) double staining. The results show increased apoptotic cell population after 24 hours of Ang II treatment in *Alpn* knockdown aortic SMCs but not in $APLN^{+/y}$ aortic SMCs (**Figure 6.5B, C**).

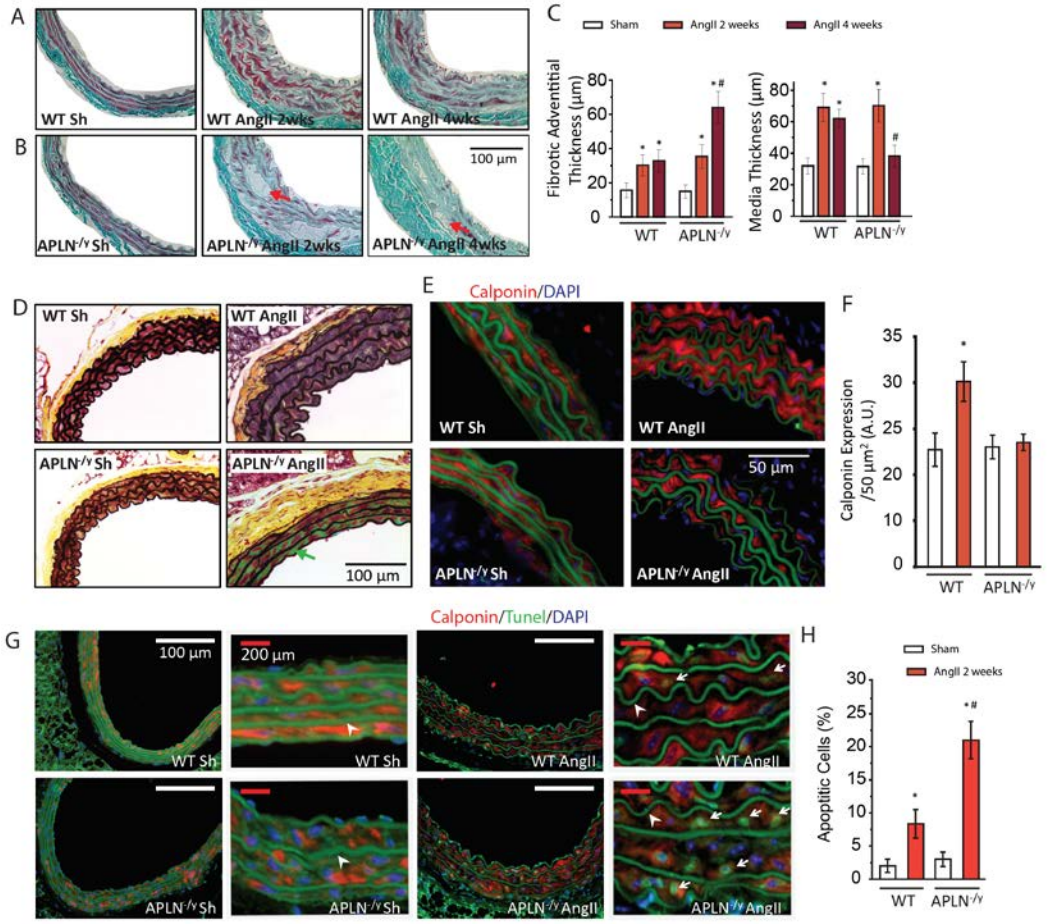

Figure 6.4 Histological studies show hypertrophy, loss of SMCs with increased apoptosis in APLN$^{-/y}$ mice with Ang II infusion. Gomori trichrome staining of aorta shows thickened media and fibrotic adventitia at 2 weeks and 4 weeks post AngII infusion (Figure 6.4A); in APLN$^{-/y}$ mice, it shows thinner media with even more blue stained fibrotic tissue at adventitia (Figure 6.4B). The image analysis of media and adventitia thickness are averaged (Figure 6.4C). Movate pentachrome staining shows much decreased media thickness and blue-green stained ground substance in APLN$^{-/y}$ mice 4 weeks of Ang II infusion (Figure 6.4D). Calponin immuostaining shows increased calponin staining in APLN$^{+/y}$ aorta on 2 weeks Ang II staining but no significant increase in APLN$^{-/y}$ aorta (Figure 6.4E), average expression quantification shows significant increase in APLN$^{+/y}$ aorta but not in APLN$^{-/y}$ (Figure 6.4F). TUNEL staining shows dramatic increase apoptotic staining in APLN$^{-/y}$ aorta but much less in APLN$^{+/y}$ on 2 weeks of Ang II infusion (Figure 6.4G), with averaged apoptotic cells counting (Figure 6.4H). Red arrows in B and green arrow in D indicate the non-cellular substance between layers of lectin. White arrow heads indicate auto-fluorescent lectin. White arrows indicate apoptotic cells. *, P< 0.05 comparing to sham control group; #, P< 0.01, comparing to Ang II treated group in APLN$^{+/y}$.

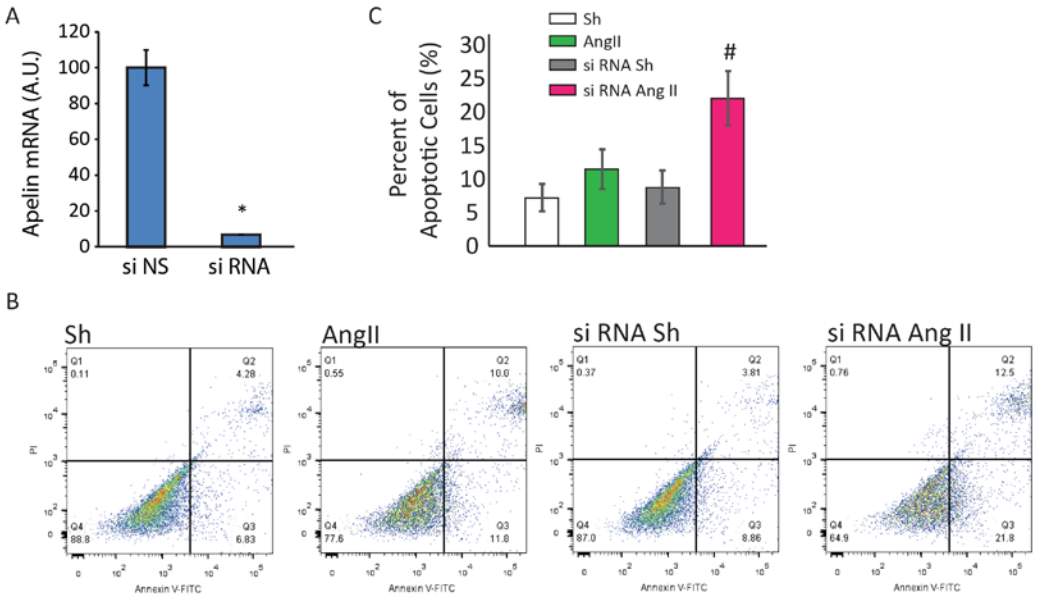

Figure 6.5 Down regulated Apelin expression potentiates apoptosis of aortic SMCs in response to Ang II. Taqman assay shows Apelin mRNA expression is knock down by 97% (A); Flow cytometry analysis of annexin V/propidium iodide-stained aortic SMCs (B) and quantification of % apoptotic cells (C) showing increased apoptosis in the Apelin siRNA group in response to Ang II. *P<0.01 compared with sham treated group; #P<0.01 compared with $APLN^{+/y}$-Ang II group.

Loss of apelin potentiates vasoconstriction in response to Ang II stimulation

To study the role of apelin in Ang II induced vasoconstriction in acute phase, we isolated third order mesenteric arteries from $APLN^{+/y}$ and $APLN^{-/y}$ mice and performed pressure myography *in vitro*. The outer diameter was monitored as the size of the vessel on test (**Figure 6.6A**). At base line, $APLN^{+/y}$ and $APLN^{-/y}$ mesenteric arteries showed the same elastic property in stepwise increase of

lumen pressure (**Figure 6.6C**). High-potassium perfusion buffer was used to induce maximum vasoconstriction (**Figure 6.6B**), the results show that $APLN^{+/y}$ and $APLN^{-/y}$ mesenteric arteries have comparable capabilities to reach a maximum constriction and percentage of constriction (**Figure 6.6D**) when corrected by vessel diameter. Subsequently, the dose-response study in response to Ang II or PE were performed. The constrictive response to Ang II showed a "bell-shaped" curve and $APLN^{-/y}$ mesenteric arteries exhibited a greater constriction and greater percentage of constriction than $APLN^{+/y}$ (**Figure 6.6E, F**). In contrast, PE showed a stronger vaso-constrictive effect in $APLN^{+/y}$ mesenteric arteries (**Figure 6.6G**). In addition to the difference in the degree of Ang II-induced constriction, this response to Ang II was prolonged in $APLN^{-/y}$ mesenteric arteries (**Figure 6.6H, I**), and they were more response to repeated Ang II stimulations (**Figure 6.6H, I**).

We then examined if the *in vivo* blood pressure in response to Ang II was also altered in $APLN^{-/y}$ mice. Ang II was infused for 14 days and the blood pressure was recorded in conscious $APLN^{+/y}$ and $APLN^{-/y}$ mice by implanted telemetry pressure transmitter. In line with the acute vascular responses, $APLN^{-/y}$ mice showed greater hypertension than $APLN^{+/y}$ mice following Ang II infusion, at both day time (**Figure 6.6J**) and night time (**Figure 6.6K**), while there was no difference at basal blood pressure.

Ang II-mediated upregulation of ACE2 expression is mediated by Apelin

Apelin has been reported to be a positive ACE2 regulator in the heart.[75] To study how apelin regulates expression of ACE2 in the aorta, we performed immunofluorescence staining to detect ACE2 in aorta sections. The results show that ACE2 expression is down-regulated in $APLN^{-/y}$ aorta (**Figure 6.7A, B**). In $APLN^{+/y}$ mice, Ang II infusion lead to up-regulation of ACE2 (**Figure 6.7 A, B**); however, in the $APLN^{-/y}$ mice, the ACE2 up-regulation was much less than that in the $APLN^{+/y}$ (**Figure 6.7A, B**). The increase of ACE2 expression following Ang II stimulation was companied by a dramatic upregulation of apelin in $APLN^{+/y}$ aortas (**Figure 6.7 C, D**), suggesting an apelin-dependent pathway of ACE2 compensational up-regulation responding to systematically increased Ang II.

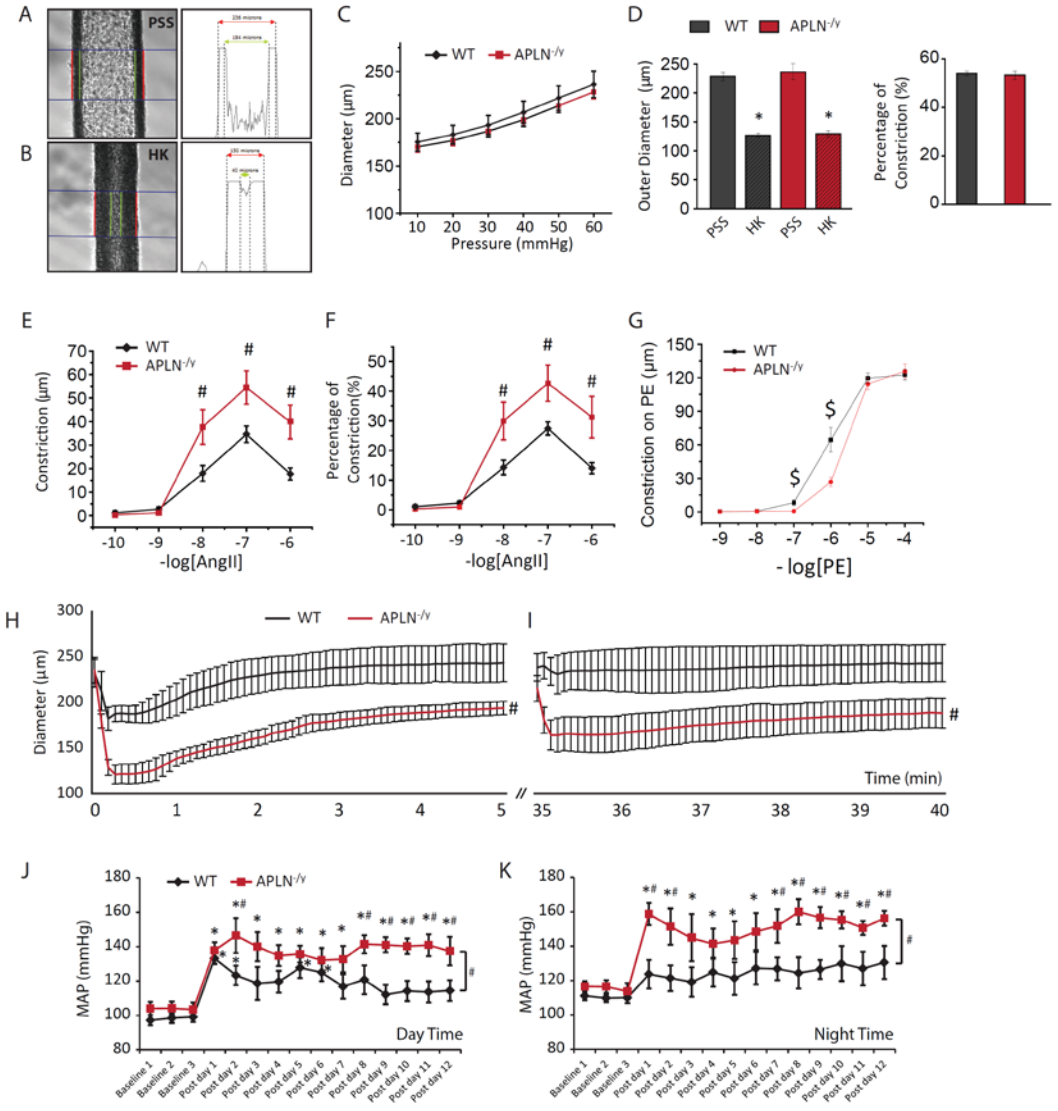

Figure 6.6 Loss of Apelin potentiates vaso-constrictive effect of Ang II. Representative images of mesenteric artery with red lines defining the outer diameter of the vessel (A); vessel constricts drastically upon HK treatment (B), where the outer diameter is automatically traced as indicted by red lines; Vessels are intro-lumen pressurized step wise (C), $APLN^{+/y}$ and $APLN^{-/y}$ mesenteric artery show no difference in passive elasticity and no difference in the max capacity of constriction (D); Dose-response curve shows Ang II leads to increased mount of constriction in $APLN^{-/y}$ mesenteric artery as well as percentage of constriction to vessel size (F); however, $APLN^{+/y}$ vessels show more sensitivity in response to PE (G); Single dose of Ang II (0.1 μM) treatment leads to increased mount of constriction in $APLN^{-/y}$ mesenteric artery (H) and preserved responsiveness in $APLN^{-/y}$ (I); in vivo infusion of Ang II leads to increased systematic blood pressure at day time (J) and night time (K).

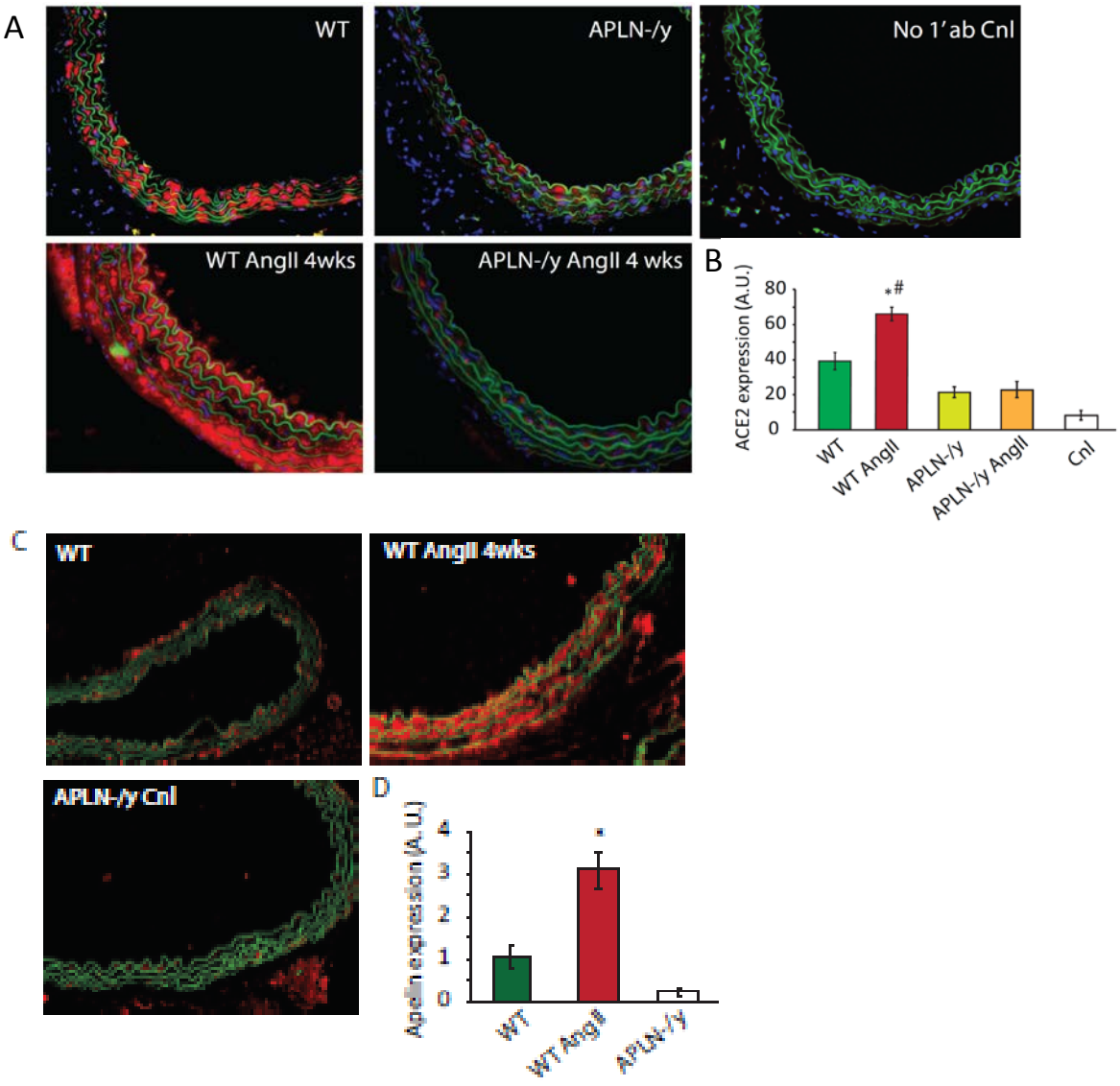

Figure 6.7 Ang II up-regulates of Apelin and ACE2 expression in aorta. Immunofluorescent staining of ACE2 in cross section of abdominal aorta, in which ACE2 is stained red and auto fluorescence of lectin is green. (A) ACE2 expression quantification shows higher expression and dramatic increase in APLN$^{+/y}$ in response to Ang II (B); there is a limited up-regulation of ACE2 in APLN$^{-/y}$ in response to Ang II (B); Apelin staining shows up-regulation of Apelin (C, D) in APLN$^{+/y}$ in response to Ang II concomitant to ACE2 up-regulation. *P<0.01 compared with sham treated group; #P<0.01 compared with APLN$^{+/y}$-Ang II group.

6.5 Discussion

In the current study, we treated $APLN^{-/y}$ mice with Ang II to explore the roles of apelin in Ang II induced adverse remodeling in aorta *in vivo* and vascular SMCs *in vitro.* We also studied the effect of Apelin on Ang II induced vasoconstriction. Ang II is a well-known cardiovascular bioactive peptide involved in a number of cardiovascular system diseases. A previous study from our group showed that Ang II caused a diffuse dilation in aorta diameter in $APLN^{+/y}$ and $ACE2^{-/y}$ mice[72]. In the current study, for the first time we observed that Ang II caused AAA formation in $APLN^{-/y}$ mice and mortality due to cases of rupture at abdominal aorta and greater increase in systemic blood pressure in these mice compared to the $APLN^{+/y}$ group. It has been reported that Apelin is an endothelium-NO dependent vasodilator[106], counteracting vascular inflammation and aortic arteriosclerosis[135]. Our study is the first to demonstrate AAA in apelin-deficient mice in response to Ang II stimulation.

At the same time, we suspected the potential involvement of greater elevation in vascular tone in the contribution of AAA formation. Then we used PE infusion to cause a similar degree of hypertension as Ang II in $APLN^{-/y}$ mice. The dose of PE was tested in pre-experiments to achieve the hypertensive effect we needed. PE did no cause AAA nor an obvious aortic dilation compared to sham treated $APLN^{-/y}$ mice. So the increased vascular tone in response to Ang II

is not a major contributor to the formation of AAA in $APLN^{-/y}$ mice, it is rather secondary to direct cellular effects of Ang II in the absence of apelin.

Being well known for causing hypertrophy and fibrosis, as we also observed such changes in $APLN^{+/y}$ Ang II treated mice, however in $APLN^{-/y}$ mice we saw the increase of aortic mural thickness at 2 weeks of Ang II infusion but decrease at 4 weeks as demonstrated in Gomori trichrome as well as Movat pentachrome staining. These wall thickness changes in aorta are in line with the calponin immunostaining results, indicating the hypertrophic or hypotrophic aortic SMCs. The decreased calponin staining together with decreased media thickness indicating there is a loss of aortic SMCs in $APLN^{-/y}$ mice, which is further supported by the increase of apoptosis by TUNEL staining. To rule out the systematic and hemodynamic effects of Ang II, we employed cultured primary aortic SMCs of mice or human origin. In the isolated aortic SMCs, we used siRNA technique and successfully knocked down apelin mRNA expression by 97%. Ang II leads to doubled apoptotic population in siApln cells.

There was also 25% mortality of aortic rupture in $APLN^{-/y}$ mice on Ang II treatment, but no mortality in $APLN^{+/y}$. All the rupture happened during 12 to 14 days post the start of Ang II infusion. Considering apelin has been reported counteracting cardiovascular inflammatory response, the rupture may due to drastic inflammation in the absence of apelin and disruption of the balance

between MMPs and TIMPs which leading to elastic structure degradation[254, 255]. But our Taqman assay in aorta tissue of inflammatory markers, MMPs and TIMPs showed equally elevated value in $APLN^{+/y}$ and $APLN^{-/y}$ mice upon Ang II stimulation. These factors may contribute to the dilation of aorta or initial hypertrophic changes, but not the determinants to AAA formation in $APLN^{-/y}$ mice. However, the dramatic loss of aortic SMCs and increased apoptosis in $APLN^{-/y}$ mice or cells could be likely the driver leading to AAA formation[256, 257].

In addition to the chronic systematic effects, loss of apelin also potentiates the acute vascular constrictive effect of Ang II. The third to fourth order of mesenteric arteries with average diameter around 200 micro meter represents a resistance small artery, which also explains the greater blood pressure increase in $APLN^{-/y}$ mice on Ang II infusion *in vivo*, implying involvement of apelin in chronic hypertension. In another study from our group we used apelin treatment in endothelial cells, which activated eNOS and increased the NO generation (data not shown). This could explain the high responsiveness to Ang II in apelin knockout vessel. Another explanation for this high responsiveness could be the downregulation of ACE2 in $APLN^{-/y}$ mice leads to weaker counteraction to Ang II; it is also worth to explore how the loss of apelin affect the AT1 receptor expression and configuration in vivo in association with the Apelin receptor.

From discovering the roles of Apelin in apoptosis and enhanced vascular responsiveness, and most importantly, from mRNA and protein expressional studies about apelin, ACE2 with either cultured primary VSMCs or aorta from systematical Ang II treatment *in vivo*, our current study revealed an inter-regulation between Ang II, Apelin and ACE2. It is the first time apelin is found mediating Ang II induced ACE2 upregulation. Together with our another study in which we showed how ACE2 down regulated Apelin in vitro and in vivo as well as its physiological and pathophysiological impact; the current study on the other hand established a way of how Apelin regulate ACE2 expression or mediate Ang II induced ACE2 upregulation, which could further upregulate Ang 1-7 by converting Ang II. By these experimental observations, we extended traditional RAS to ACE2-Aplein axis based on solid expressional and functional studies *in vivo* beyond previously reported biochemistry feasibility.

Considering the cardiovascular beneficial effects by apelin itself and the ability to up-regulate ACE2 expression with or without excessive Ang II, modified apelin can be a promising path for treatment cardiovascular diseases in the light that ACE2 efficiently down-regulate Apelin *in vitro* and *in vivo*.

CHAPTER SEVEN

Discussion and Future Direction

7.1 Discussion

Cardiovascular disease is one of the leading causes of death in Canada. More than 1.4 million Canadians have heart disease, claiming more than 33,600 lives per year. The overall goals of current studies performed in this thesis are to explore the roles and mechanisms about two peptides, ACE2 and apelin, in cardiovascular homeostasis and in disease conditions and to try to explore new ways of treating cardiovascular diseases by targeting ACE2 and apelin. The most closely relevant backgrounds of the current studies include biomedical research progresses about 1), understanding that RAS system, especially Ang II as a central effector in many cardiovascular diseases; 2), accumulating evidence of cardiovascular protective peptide ACE2 and its mechanism; and 3) Apelin emerges as a family of cardiovascular protective peptides tested in several disease models by counteracting RAS system.

The Renin angiotensin system (RAS) plays a central role in regulating the cardiovascular function. Wherein Angiotensin II (Ang II) is found to be the critical effector in pathological conditions leading to many heart and vascular diseases[258]. Treating cardiovascular disease by targeting Ang II by AT1R

blocker[259] or ACEi[260, 261] leads to positive outcomes. ACE2 emerges as an new and efficient peptidase converting Ang II to generate Ang 1-7, a cardioprotective peptide. We started studying how partial loss of ACE2 would affect cardiac structure and function in disease models of (Transverse aortic constriction) TAC and systematic Ang II infusion. The results show that partial heterozygote loss of ACE2 is sufficient to increase the susceptibility to heart disease secondary to pressure-overload and Ang II infusion. But Ang II is not the only substrate of ACE2. Apelin is another efficient substrate *in vitro*. While both ACE2 and apelin were suggested as potential new targets for treating cardiovascular disease, it is necessary to know how ACE2 would metabolize apelin *in vivo* and the functional impacts. Then, we employed ACE2 gene knockout and ACE2 pharmacological knockdown mice to extinguish the roles of ACE2 in metabolizing apelin *in vivo*, which is supported by intensive peptide/fragments characterization *in vitro*. We also directlly compared native apelin and ACE2 metabolized apelin in a range of experimental systems. And finally, we designed and synthesized apelin analogues which are resistant to ACE2 cleavage. These results showed the direction of how to modify apelin for better clinical application.

We also studied the roles of apelin in several different ischemic heart disease animal models. More importantly in animal models we found a handful of synthesized apelin analogues with comparable bioactivities and resistance to ACE2. These results expanded our understanding of the roles of apelin the

ischemic heart diseases and cardiac angiogenesis; it also brings apelin analogues closer to clinical application.

Apelin also plays critical roles in vasculature and ACE2's hydrolysis degrading of apelin is not just an one-way regulatory relationship. At last, we studied the role of apelin in Ang II induced vascular disease. We found that loss of apelin potentiates effect of Ang II with systemic vascular tone, aortic adverse remodeling and increased apoptosis in VSMCs. These observation are further supported by gain or loss of function of apelin, wherein apelin is showed to be a positive regulator of ACE2 in vasculature and mediator of Ang II induced ACE2 up-regulation.

To understand the function of our target genes or proteins, the very basic approach in the current studies is based on gene manipulated animals, as a popular trend in the past decades it leads to huge increased knowledge about function of individual genes or proteins. We used ACE2 gene knockout or knock down mice, APLN gene knockout mice, to study function of these individual gene or protein in the scenarios of normal conditions or in various cardiovascular diseases. These cardiovascular diseases were introduced by surgeries or pathogens, mostly Ang II.

Although our studies were based on this genetic manipulation technique in mice, we also aimed for translational applications. For example, we started our experimental design and hypothesis based on clinical investigation and data

obtained with human samples. Started from a clinical scenario, and more importantly our studies ended with solutions. Specifically based on our finding and understanding of how apelin is protective peptides and highly subjected to several peptidases degradation, we designed and synthesized apelin analogues, which are still under strict test and have already been showing promising results.

Our effort to find new solutions for treating heart failure started with ACE2. ACE2 is the first known homolog of ACE[54]. It is a pleiotropic monocarboxypeptidase that metabolizes of various of peptides including Ang II or apelin with high catalytic efficiency[54]. Before the current study described in Chapter 3, our group intensively studied the roles of ACE2 in the setting of elevated Ang II and in the pressure-overload model of heart failure[262]. Loss of ACE2 potentiated Ang II or pressure-overload–induced oxidative stress, myocardial hypertrophy with increased fibrosis. With respect to cardiac function, loss of ACE2 worsen the diastolic dysfunction in myocardial hypertrophy. We had found that in pre-clinical models of heart disease, myocardial ACE2 is partially decreased in human.[68, 152] So in Chapter 3 we employed genetic modified female mouse with half decreased ACE2 expression in our study and confirmed these findings in patients with idiopathic and advanced dilated cardiomyopathy. These results also highlight a critical and role of ACE2 in heart disease by demonstrating that a 50% loss of ACE2 in patients with heart failure is sufficient

to enhance the susceptibility to heart disease, which in another way is supporting the potential application of rhACE2.

Apelin is another potential substrate of ACE2 as a pleiotropic monocarboxypeptidase. Apelin is synthesized as a precursor 77 amino acid pre-pro-peptide and is subsequently processed into "fragments" of various size of C-terminal[40, 133, 168]. It has been reported that the C-terminal region of the apelin peptide is central for its overall biological activity.[62, 171, 172] So in Chapter 4 we studied how ACE2 would act on the C-terminal Phe of apelins and effect function *in vivo*. Apelin has been reported to mediate a range of beneficial effects in the cardiovascular system and on fluid homeostasis including[40, 66, 170] maintaining endothelium structure and function, promoting angiogenesis, counteracting the renin-angiotensin system, and regulating myocardial metabolism, hypertrophy, fibrosis, and inflammation.[40, 66, 170] But apelin have extremely short plasma half-lives in vivo.[49] Endogenous apelin has a very low tissue expression or plasma concentration, but our data shows endogenous levels of ACE2 have the great potential to dramatically affect the action of exogenous apelin as measured in plasma or tissue concentration as well as hypotensive effect. In another set of experiments, by directly comparing the chunked apelin and native apelin, we concluded that ACE2 is a degrading enzyme for apelin. Although ACE2 is unlikely the only peptidase cleaving apelin (data not shown), it is a quite efficient one and leading to significant functional changes.

When we consider the cardiovascular beneficial effects and potential clinical application of ACE2 in treating cardiovascular disease, the degrading effect of ACE2 on apelin is unfavourable for apelin's potential clinical application. We then went on and performed the studies covered in Chapter 5. We explored the function of apelin in ischemic heart disease and heart failure. In particular, we studied angiogenesis as an important mechanism that might counteract the pathological remodeling observed in chronic heart disease and fibrosis. To address this question in Chapter 4 we developed apelin analogues which were functioning and resistant to ACE2 cleavage.

The downregulating of apelin by ACE2 is not a one-way effect. It has been reported that apelin is a positive regulator of ACE2 in the heart. In Chapter 6, we found that apelin is a positive regulator of ACE2 in VSMCs. It also mediates Ang II induced ACE2 expression. It data shows apelin is in a central role exerting cardioprotective benefit. The inter-regulatory relationship is summarized in **(Figure 7.1)**.

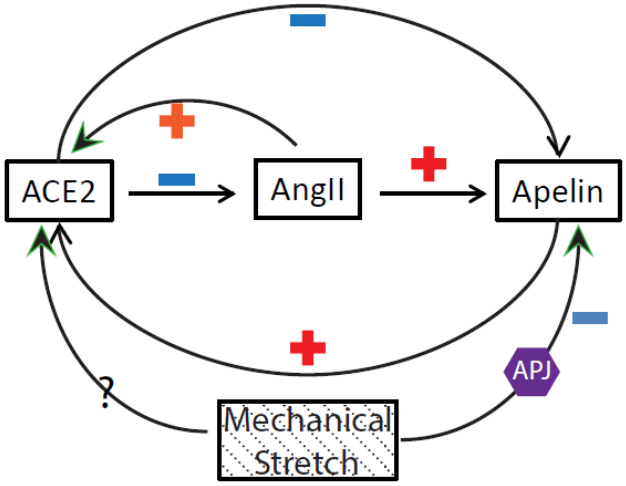

Figure 7.1 Schematic regulatory relationship between Ang II, Apelin and ACE2. ACE2 hydrolyzes and degrades apelin *in vitro* and *in vivo*; in turn, apelin up-regulates ACE2 expression; Ang II induces ACE2 and apelin up-regulation, and the ACE2 up-regulation induced by Ang II is mediated by apelin. Mechanical stretch down-regulates apelin via APJ, apelin receptor[44]. There is not clear answer about how mechanical stretch regulates ACE2 expression.

7.2 Future Direction

We have found that Ang II leads to greater increase of apoptosis in the partial loss of Apelin *in vitro* and development of aortic aneurysm *in vivo* as demonstrated in Ang II systematic infusion model in mice. As reactive oxygen species (ROS) mediated cellular damages of Ang II, we could perform ROS assays to evaluated how ROS contribute to SMCs apoptosis and aorta adverse remodeling in the WT and Apelin knockout mice, to determine how Apelin may counteract the Ang II's effect in terms of attenuating ROS generation in the SMCs. The development of aneurysm also implies a direction to look into extra cellular matrix (ECM). We could perform more specific ECM structural studies. With tissue inhibitors of metalloproteinases (TIMPs) are closed involved in the regulation and maintenance of ECM, we could study how apelin may interact with TIMPs and the impact on ECM remodeling.

For the apelin analogue, we showed the hydrolytic site which ACE2 works on. With revealing the new cleaving sites, we generated new apelin analogues. Accordingly, the new apelin analogues need to be tested in organ or physiological functional level *in vivo* as well as characterization of their property in receptor interaction and cellular signal transduction.

Reference

1. Goss RJ. Hypertrophy versus hyperplasia. *Science*. 1966;153:1615-20.

2. Eaton LW, Weiss JL, Bulkley BH, Garrison JB and Weisfeldt ML. Regional cardiac dilatation after acute myocardial infarction: recognition by two-dimensional echocardiography. *The New England journal of medicine*. 1979;300:57-62.

3. McKay RG, Pfeffer MA, Pasternak RC, Markis JE, Come PC, Nakao S, Alderman JD, Ferguson JJ, Safian RD and Grossman W. Left ventricular remodeling after myocardial infarction: a corollary to infarct expansion. *Circulation*. 1986;74:693-702.

4. Hughes SE. The pathology of hypertrophic cardiomyopathy. *Histopathology*. 2004;44:412-27.

5. Levy D, Garrison RJ, Savage DD, Kannel WB and Castelli WP. Prognostic implications of echocardiographically determined left ventricular mass in the Framingham Heart Study. *The New England journal of medicine*. 1990;322:1561-6.

6. Kupari M, Turto H and Lommi J. Left ventricular hypertrophy in aortic valve stenosis: preventive or promotive of systolic dysfunction and heart failure? *European heart journal*. 2005;26:1790-6.

7. Moser M. Hypertensive Heart Disease, Hypertrophic Cardiomyopathy and Heart Failure in the Elderly. *The American journal of geriatric cardiology*. 1996;5:60-64.

8. Northridge DB, McMurray JM, Colledge NR and Fraser DM. Hypertensive hypertrophic cardiomyopathy of the elderly. *British journal of hospital medicine*. 1987;38:567.

9. Topol EJ, Traill TA and Fortuin NJ. Hypertensive hypertrophic cardiomyopathy of the elderly. *The New England journal of medicine*. 1985;312:277-83.

10. Ogino K, Ogura K, Kinugawa T, Osaki S, Kato M, Furuse Y, Kinugasa Y, Tomikura Y, Igawa O, Hisatome I and Shigemasa C. Neurohumoral profiles in patients with hypertrophic cardiomyopathy: differences to hypertensive left ventricular hypertrophy. *Circulation journal : official journal of the Japanese Circulation Society*. 2004;68:444-50.

11. Geisterfer-Lowrance AA, Kass S, Tanigawa G, Vosberg HP, McKenna W, Seidman CE and Seidman JG. A molecular basis for familial hypertrophic cardiomyopathy: a beta cardiac myosin heavy chain gene missense mutation. *Cell*. 1990;62:999-1006.

12. Thierfelder L, Watkins H, MacRae C, Lamas R, McKenna W, Vosberg HP, Seidman JG and Seidman CE. Alpha-tropomyosin and cardiac troponin T mutations cause familial hypertrophic cardiomyopathy: a disease of the sarcomere. *Cell*. 1994;77:701-12.

13. Kimura A, Harada H, Park JE, Nishi H, Satoh M, Takahashi M, Hiroi S, Sasaoka T, Ohbuchi N, Nakamura T, Koyanagi T, Hwang TH, Choo JA, Chung KS, Hasegawa A, Nagai R, Okazaki O, Nakamura H, Matsuzaki M, Sakamoto T, Toshima H, Koga Y, Imaizumi T and Sasazuki T. Mutations in the cardiac troponin I gene associated with hypertrophic cardiomyopathy. *Nature genetics*. 1997;16:379-82.

14. Benjamin EJ and Levy D. Why is left ventricular hypertrophy so predictive of morbidity and mortality? *The American journal of the medical sciences*. 1999;317:168-75.

15. Pluim BM, Zwinderman AH, van der Laarse A and van der Wall EE. The athlete's heart. A meta-analysis of cardiac structure and function. *Circulation*. 2000;101:336-44.

16. Prior DL and La Gerche A. The athlete's heart. *Heart*. 2012;98:947-55.

17. Thompson D, Karpe F, Lafontan M and Frayn K. Physical activity and exercise in the regulation of human adipose tissue physiology. *Physiological reviews*. 2012;92:157-91.

18. Hambrecht R, Wolf A, Gielen S, Linke A, Hofer J, Erbs S, Schoene N and Schuler G. Effect of exercise on coronary endothelial function in patients with coronary artery disease. *The New England journal of medicine*. 2000;342:454-60.

19. Nualnim N, Parkhurst K, Dhindsa M, Tarumi T, Vavrek J and Tanaka H. Effects of swimming training on blood pressure and vascular function in adults >50 years of age. *The American journal of cardiology*. 2012;109:1005-10.

20. Wisloff U, Loennechen JP, Falck G, Beisvag V, Currie S, Smith G and Ellingsen O. Increased contractility and calcium sensitivity in cardiac myocytes isolated from endurance trained rats. *Cardiovascular research*. 2001;50:495-508.

21. Wisloff U, Loennechen JP, Currie S, Smith GL and Ellingsen O. Aerobic exercise reduces cardiomyocyte hypertrophy and increases contractility, Ca2+ sensitivity and SERCA-2 in rat after myocardial infarction. *Cardiovascular research*. 2002;54:162-74.

22. Kemi OJ, Hoydal MA, Macquaide N, Haram PM, Koch LG, Britton SL, Ellingsen O, Smith GL and Wisloff U. The effect of exercise training on transverse tubules in normal, remodeled, and reverse remodeled hearts. *Journal of cellular physiology*. 2011;226:2235-43.

23. Duncker DJ and Bache RJ. Regulation of coronary blood flow during exercise. *Physiological reviews*. 2008;88:1009-86.

24. Riquelme CA, Magida JA, Harrison BC, Wall CE, Marr TG, Secor SM and Leinwand LA. Fatty acids identified in the Burmese python promote beneficial cardiac growth. *Science*. 2011;334:528-31.

25. Arany Z, He H, Lin J, Hoyer K, Handschin C, Toka O, Ahmad F, Matsui T, Chin S, Wu PH, Rybkin, II, Shelton JM, Manieri M, Cinti S, Schoen FJ, Bassel-Duby R, Rosenzweig A, Ingwall JS and Spiegelman BM. Transcriptional coactivator PGC-1 alpha controls the energy state and contractile function of cardiac muscle. *Cell metabolism*. 2005;1:259-71.

26. Bostrom P, Mann N, Wu J, Quintero PA, Plovie ER, Panakova D, Gupta RK, Xiao C, MacRae CA, Rosenzweig A and Spiegelman BM. C/EBPbeta controls exercise-induced cardiac growth and protects against pathological cardiac remodeling. *Cell*. 2010;143:1072-83.

27. Mende U, Kagen A, Cohen A, Aramburu J, Schoen FJ and Neer EJ. Transient cardiac expression of constitutively active Galphaq leads to hypertrophy and dilated cardiomyopathy by calcineurin-dependent and independent pathways. *Proceedings of the National Academy of Sciences of the United States of America*. 1998;95:13893-8.

28. Akhter SA, Luttrell LM, Rockman HA, Iaccarino G, Lefkowitz RJ and Koch WJ. Targeting the receptor-Gq interface to inhibit in vivo pressure overload myocardial hypertrophy. *Science*. 1998;280:574-7.

29. Wettschureck N, Rutten H, Zywietz A, Gehring D, Wilkie TM, Chen J, Chien KR and Offermanns S. Absence of pressure overload induced myocardial hypertrophy after conditional inactivation of Galphaq/Galpha11 in cardiomyocytes. *Nature medicine*. 2001;7:1236-40.

30. Calvert JW, Condit ME, Aragon JP, Nicholson CK, Moody BF, Hood RL, Sindler AL, Gundewar S, Seals DR, Barouch LA and Lefer DJ. Exercise protects against myocardial ischemia-reperfusion injury via stimulation of beta(3)-adrenergic receptors and increased nitric oxide signaling: role of nitrite and nitrosothiols. *Circulation research*. 2011;108:1448-58.

31. Mann N and Rosenzweig A. Can exercise teach us how to treat heart disease? *Circulation*. 2012;126:2625-35.

32. Shiojima I, Sato K, Izumiya Y, Schiekofer S, Ito M, Liao R, Colucci WS and Walsh K. Disruption of coordinated cardiac hypertrophy and angiogenesis contributes to the transition to heart failure. *The Journal of clinical investigation*. 2005;115:2108-18.

33. Shiojima I and Walsh K. Regulation of cardiac growth and coronary angiogenesis by the Akt/PKB signaling pathway. *Genes & development*. 2006;20:3347-65.

34. Chavakis E, Carmona G, Urbich C, Gottig S, Henschler R, Penninger JM, Zeiher AM, Chavakis T and Dimmeler S. Phosphatidylinositol-3-kinase-gamma is integral to homing functions of progenitor cells. *Circulation research*. 2008;102:942-9.

35. Oudit GY, Kassiri Z, Zhou J, Liu QC, Liu PP, Backx PH, Dawood F, Crackower MA, Scholey JW and Penninger JM. Loss of PTEN attenuates the development of pathological

hypertrophy and heart failure in response to biomechanical stress. *Cardiovascular research*. 2008;78:505-14.

36. Tempel D, de Boer M, van Deel ED, Haasdijk RA, Duncker DJ, Cheng C, Schulte-Merker S and Duckers HJ. Apelin enhances cardiac neovascularization after myocardial infarction by recruiting aplnr+ circulating cells. *Circulation research*. 2012;111:585-98.

37. Arany Z, Foo SY, Ma Y, Ruas JL, Bommi-Reddy A, Girnun G, Cooper M, Laznik D, Chinsomboon J, Rangwala SM, Baek KH, Rosenzweig A and Spiegelman BM. HIF-independent regulation of VEGF and angiogenesis by the transcriptional coactivator PGC-1alpha. *Nature*. 2008;451:1008-12.

38. O'Dowd BF, Heiber M, Chan A, Heng HH, Tsui LC, Kennedy JL, Shi X, Petronis A, George SR and Nguyen T. A human gene that shows identity with the gene encoding the angiotensin receptor is located on chromosome 11. *Gene*. 1993;136:355-60.

39. Tatemoto K, Hosoya M, Habata Y, Fujii R, Kakegawa T, Zou MX, Kawamata Y, Fukusumi S, Hinuma S, Kitada C, Kurokawa T, Onda H and Fujino M. Isolation and characterization of a novel endogenous peptide ligand for the human APJ receptor. *Biochemical and biophysical research communications*. 1998;251:471-6.

40. Pitkin SL, Maguire JJ, Bonner TI and Davenport AP. International Union of Basic and Clinical Pharmacology. LXXIV. Apelin receptor nomenclature, distribution, pharmacology, and function. *Pharmacol Rev*. 2010;62:331-42.

41. Chen MM, Ashley EA, Deng DX, Tsalenko A, Deng A, Tabibiazar R, Ben-Dor A, Fenster B, Yang E, King JY, Fowler M, Robbins R, Johnson FL, Bruhn L, McDonagh T,

Dargie H, Yakhini Z, Tsao PS and Quertermous T. Novel role for the potent endogenous inotrope apelin in human cardiac dysfunction. *Circulation*. 2003;108:1432-9.

42. Kleinz MJ, Skepper JN and Davenport AP. Immunocytochemical localisation of the apelin receptor, APJ, to human cardiomyocytes, vascular smooth muscle and endothelial cells. *Regul Pept*. 2005;126:233-40.

43. Wang C, Du JF, Wu F and Wang HC. Apelin decreases the SR Ca2+ content but enhances the amplitude of [Ca2+]i transient and contractions during twitches in isolated rat cardiac myocytes. *American journal of physiology Heart and circulatory physiology*. 2008;294:H2540-6.

44. Szokodi I, Tavi P, Foldes G, Voutilainen-Myllyla S, Ilves M, Tokola H, Pikkarainen S, Piuhola J, Rysa J, Toth M and Ruskoaho H. Apelin, the novel endogenous ligand of the orphan receptor APJ, regulates cardiac contractility. *Circulation research*. 2002;91:434-40.

45. Berry MF, Pirolli TJ, Jayasankar V, Burdick J, Morine KJ, Gardner TJ and Woo YJ. Apelin has in vivo inotropic effects on normal and failing hearts. *Circulation*. 2004;110:II187-93.

46. Pitkin SL, Maguire JJ, Kuc RE and Davenport AP. Modulation of the apelin/APJ system in heart failure and atherosclerosis in man. *British journal of pharmacology*. 2010;160:1785-95.

47. Sarzani R, Forleo C, Pietrucci F, Capestro A, Soura E, Guida P, Sorrentino S, Iacoviello M, Romito R, Dessi-Fulgheri P, Pitzalis M and Rappelli A. The 212A variant of

the APJ receptor gene for the endogenous inotrope apelin is associated with slower heart failure progression in idiopathic dilated cardiomyopathy. *J Card Fail*. 2007;13:521-9.

48. Chong KS, Gardner RS, Morton JJ, Ashley EA and McDonagh TA. Plasma concentrations of the novel peptide apelin are decreased in patients with chronic heart failure. *European journal of heart failure*. 2006;8:355-60.

49. Japp AG, Cruden NL, Barnes G, van Gemeren N, Mathews J, Adamson J, Johnston NR, Denvir MA, Megson IL, Flapan AD and Newby DE. Acute cardiovascular effects of apelin in humans: potential role in patients with chronic heart failure. *Circulation*. 2010;121:1818-27.

50. Kidoya H, Naito H and Takakura N. Apelin induces enlarged and nonleaky blood vessels for functional recovery from ischemia. *Blood*. 2010;115:3166-74.

51. Kidoya H, Ueno M, Yamada Y, Mochizuki N, Nakata M, Yano T, Fujii R and Takakura N. Spatial and temporal role of the apelin/APJ system in the caliber size regulation of blood vessels during angiogenesis. *The EMBO journal*. 2008;27:522-34.

52. Guy JL, Jackson RM, Acharya KR, Sturrock ED, Hooper NM and Turner AJ. Angiotensin-converting enzyme-2 (ACE2): comparative modeling of the active site, specificity requirements, and chloride dependence. *Biochemistry*. 2003;42:13185-92.

53. Tipnis SR, Hooper NM, Hyde R, Karran E, Christie G and Turner AJ. A human homolog of angiotensin-converting enzyme. Cloning and functional expression as a

captopril-insensitive carboxypeptidase. *The Journal of biological chemistry*. 2000;275:33238-43.

54. Donoghue M, Hsieh F, Baronas E, Godbout K, Gosselin M, Stagliano N, Donovan M, Woolf B, Robison K, Jeyaseelan R, Breitbart RE and Acton S. A novel angiotensin-converting enzyme-related carboxypeptidase (ACE2) converts angiotensin I to angiotensin 1-9. *Circulation research*. 2000;87:E1-9.

55. Epelman S, Shrestha K, Troughton RW, Francis GS, Sen S, Klein AL and Tang WH. Soluble angiotensin-converting enzyme 2 in human heart failure: relation with myocardial function and clinical outcomes. *J Card Fail*. 2009;15:565-71.

56. Lambert DW, Yarski M, Warner FJ, Thornhill P, Parkin ET, Smith AI, Hooper NM and Turner AJ. Tumor necrosis factor-alpha convertase (ADAM17) mediates regulated ectodomain shedding of the severe-acute respiratory syndrome-coronavirus (SARS-CoV) receptor, angiotensin-converting enzyme-2 (ACE2). *The Journal of biological chemistry*. 2005;280:30113-9.

57. Patel VB, Clarke N, Wang Z, Fan D, Parajuli N, Basu R, Putko B, Kassiri Z, Turner AJ and Oudit GY. Angiotensin II induced proteolytic cleavage of myocardial ACE2 is mediated by TACE/ADAM-17: a positive feedback mechanism in the RAS. *J Mol Cell Cardiol*. 2014;66:167-76.

58. Vickers C, Hales P, Kaushik V, Dick L, Gavin J, Tang J, Godbout K, Parsons T, Baronas E, Hsieh F, Acton S, Patane M, Nichols A and Tummino P. Hydrolysis of

biological peptides by human angiotensin-converting enzyme-related carboxypeptidase. *The Journal of biological chemistry*. 2002;277:14838-43.

59. Wang G, Qi X, Wei W, Englander EW and Greeley GH, Jr. Characterization of the 5'-regulatory regions of the rat and human apelin genes and regulation of breast apelin by USF. *FASEB journal : official publication of the Federation of American Societies for Experimental Biology*. 2006;20:2639-41.

60. Habata Y, Fujii R, Hosoya M, Fukusumi S, Kawamata Y, Hinuma S, Kitada C, Nishizawa N, Murosaki S, Kurokawa T, Onda H, Tatemoto K and Fujino M. Apelin, the natural ligand of the orphan receptor APJ, is abundantly secreted in the colostrum. *Biochim Biophys Acta*. 1999;1452:25-35.

61. Lee DK, Saldivia VR, Nguyen T, Cheng R, George SR and O'Dowd BF. Modification of the terminal residue of apelin-13 antagonizes its hypotensive action. *Endocrinology*. 2005;146:231-6.

62. El Messari S, Iturrioz X, Fassot C, De Mota N, Roesch D and Llorens-Cortes C. Functional dissociation of apelin receptor signaling and endocytosis: implications for the effects of apelin on arterial blood pressure. *Journal of neurochemistry*. 2004;90:1290-301.

63. Iturrioz X, El Messari S, De Mota N, Fassot C, Alvear-Perez R, Maigret B and Llorens-Cortes C. [Functional dissociation between apelin receptor signaling and endocytosis: implications for the effects of apelin on arterial blood pressure]. *Archives des maladies du coeur et des vaisseaux*. 2007;100:704-8.

64. Masri B, Morin N, Pedebernade L, Knibiehler B and Audigier Y. The apelin receptor is coupled to Gi1 or Gi2 protein and is differentially desensitized by apelin fragments. *The Journal of biological chemistry*. 2006;281:18317-26.

65. Zhou N, Fan X, Mukhtar M, Fang J, Patel CA, DuBois GC and Pomerantz RJ. Cell-cell fusion and internalization of the CNS-based, HIV-1 co-receptor, APJ. *Virology*. 2003;307:22-36.

66. Scimia MC, Hurtado C, Ray S, Metzler S, Wei K, Wang J, Woods CE, Purcell NH, Catalucci D, Akasaka T, Bueno OF, Vlasuk GP, Kaliman P, Bodmer R, Smith LH, Ashley E, Mercola M, Brown JH and Ruiz-Lozano P. APJ acts as a dual receptor in cardiac hypertrophy. *Nature*. 2012;488:394-8.

67. Kleinz MJ and Davenport AP. Immunocytochemical localization of the endogenous vasoactive peptide apelin to human vascular and endocardial endothelial cells. *Regul Pept*. 2004;118:119-25.

68. Zhong J, Basu R, Guo D, Chow FL, Byrns S, Schuster M, Loibner H, Wang XH, Penninger JM, Kassiri Z and Oudit GY. Angiotensin-converting enzyme 2 suppresses pathological hypertrophy, myocardial fibrosis, and cardiac dysfunction. *Circulation*. 2010;122:717-28, 18 p following 728.

69. Gallagher PE, Chappell MC, Ferrario CM and Tallant EA. Distinct roles for ANG II and ANG-(1-7) in the regulation of angiotensin-converting enzyme 2 in rat astrocytes. *American journal of physiology Cell physiology*. 2006;290:C420-6.

70. Koka V, Huang XR, Chung AC, Wang W, Truong LD and Lan HY. Angiotensin II up-regulates angiotensin I-converting enzyme (ACE), but down-regulates ACE2 via the AT1-ERK/p38 MAP kinase pathway. *The American journal of pathology*. 2008;172:1174-83.

71. Jin HY, Song B, Oudit GY, Davidge ST, Yu HM, Jiang YY, Gao PJ, Zhu DL, Ning G, Kassiri Z, Penninger JM and Zhong JC. ACE2 deficiency enhances angiotensin II-mediated aortic profilin-1 expression, inflammation and peroxynitrite production. *PloS one*. 2012;7:e38502.

72. Patel VB, Zhong JC, Fan D, Basu R, Morton JS, Parajuli N, McMurtry MS, Davidge ST, Kassiri Z and Oudit GY. Angiotensin-converting enzyme 2 is a critical determinant of angiotensin II-induced loss of vascular smooth muscle cells and adverse vascular remodeling. *Hypertension*. 2014;64:157-64.

73. Yamamuro M, Yoshimura M, Nakayama M, Abe K, Sumida H, Sugiyama S, Saito Y, Nakao K, Yasue H and Ogawa H. Aldosterone, but not angiotensin II, reduces angiotensin converting enzyme 2 gene expression levels in cultured neonatal rat cardiomyocytes. *Circulation journal : official journal of the Japanese Circulation Society*. 2008;72:1346-50.

74. Lin CS, Pan CH, Wen CH, Yang TH and Kuan TC. Regulation of angiotensin converting enzyme II by angiotensin peptides in human cardiofibroblasts. *Peptides*. 2010;31:1334-40.

75. Sato T, Suzuki T, Watanabe H, Kadowaki A, Fukamizu A, Liu PP, Kimura A, Ito H, Penninger JM, Imai Y and Kuba K. Apelin is a positive regulator of ACE2 in failing hearts. *The Journal of clinical investigation*. 2013;123:5203-11.

76. Ferrario CM, Jessup J, Chappell MC, Averill DB, Brosnihan KB, Tallant EA, Diz DI and Gallagher PE. Effect of angiotensin-converting enzyme inhibition and angiotensin II receptor blockers on cardiac angiotensin-converting enzyme 2. *Circulation*. 2005;111:2605-10.

77. Gurley SB, Allred A, Le TH, Griffiths R, Mao L, Philip N, Haystead TA, Donoghue M, Breitbart RE, Acton SL, Rockman HA and Coffman TM. Altered blood pressure responses and normal cardiac phenotype in ACE2-null mice. *The Journal of clinical investigation*. 2006;116:2218-25.

78. Yamamoto K, Ohishi M, Katsuya T, Ito N, Ikushima M, Kaibe M, Tatara Y, Shiota A, Sugano S, Takeda S, Rakugi H and Ogihara T. Deletion of angiotensin-converting enzyme 2 accelerates pressure overload-induced cardiac dysfunction by increasing local angiotensin II. *Hypertension*. 2006;47:718-26.

79. Gallagher PE, Ferrario CM and Tallant EA. Regulation of ACE2 in cardiac myocytes and fibroblasts. *American journal of physiology Heart and circulatory physiology*. 2008;295:H2373-9.

80. Wang W, Bodiga S, Das SK, Lo J, Patel V and Oudit GY. Role of ACE2 in diastolic and systolic heart failure. *Heart Fail Rev*. 2012;17:683-91.

81. Oudit GY, Kassiri Z, Patel MP, Chappell M, Butany J, Backx PH, Tsushima RG, Scholey JW, Khokha R and Penninger JM. Angiotensin II-mediated oxidative stress and inflammation mediate the age-dependent cardiomyopathy in ACE2 null mice. *Cardiovascular research*. 2007;75:29-39.

82. Goulter AB, Goddard MJ, Allen JC and Clark KL. ACE2 gene expression is up-regulated in the human failing heart. *BMC medicine*. 2004;2:19.

83. Carretero OA and Oparil S. Essential hypertension. Part I: definition and etiology. *Circulation*. 2000;101:329-35.

84. Stoll M and Jacob HJ. Genetic rat models of hypertension: relationship to human hypertension. *Current hypertension reports*. 2001;3:157-64.

85. Crackower MA, Sarao R, Oudit GY, Yagil C, Kozieradzki I, Scanga SE, Oliveira-dos-Santos AJ, da Costa J, Zhang L, Pei Y, Scholey J, Ferrario CM, Manoukian AS, Chappell MC, Backx PH, Yagil Y and Penninger JM. Angiotensin-converting enzyme 2 is an essential regulator of heart function. *Nature*. 2002;417:822-8.

86. Wysocki J, Ye M, Rodriguez E, Gonzalez-Pacheco FR, Barrios C, Evora K, Schuster M, Loibner H, Brosnihan KB, Ferrario CM, Penninger JM and Batlle D. Targeting the degradation of angiotensin II with recombinant angiotensin-converting enzyme 2: prevention of angiotensin II-dependent hypertension. *Hypertension*. 2010;55:90-8.

87. Yamazato M, Yamazato Y, Sun C, Diez-Freire C and Raizada MK. Overexpression of angiotensin-converting enzyme 2 in the rostral ventrolateral medulla causes long-term decrease in blood pressure in the spontaneously hypertensive rats. *Hypertension*. 2007;49:926-31.

88. Feng Y, Xia H, Cai Y, Halabi CM, Becker LK, Santos RA, Speth RC, Sigmund CD and Lazartigues E. Brain-selective overexpression of human Angiotensin-converting enzyme type 2 attenuates neurogenic hypertension. *Circulation research*. 2010;106:373-82.

89. Rentzsch B, Todiras M, Iliescu R, Popova E, Campos LA, Oliveira ML, Baltatu OC, Santos RA and Bader M. Transgenic angiotensin-converting enzyme 2 overexpression in vessels of SHRSP rats reduces blood pressure and improves endothelial function. *Hypertension*. 2008;52:967-73.

90. Lovren F, Pan Y, Quan A, Teoh H, Wang G, Shukla PC, Levitt KS, Oudit GY, Al-Omran M, Stewart DJ, Slutsky AS, Peterson MD, Backx PH, Penninger JM and Verma S. Angiotensin converting enzyme-2 confers endothelial protection and attenuates atherosclerosis. *American journal of physiology Heart and circulatory physiology*. 2008;295:H1377-84.

91. Thomas MC, Pickering RJ, Tsorotes D, Koitka A, Sheehy K, Bernardi S, Toffoli B, Nguyen-Huu TP, Head GA, Fu Y, Chin-Dusting J, Cooper ME and Tikellis C. Genetic Ace2 deficiency accentuates vascular inflammation and atherosclerosis in the ApoE knockout mouse. *Circulation research*. 2010;107:888-97.

92. Zhang C, Zhao YX, Zhang YH, Zhu L, Deng BP, Zhou ZL, Li SY, Lu XT, Song LL, Lei XM, Tang WB, Wang N, Pan CM, Song HD, Liu CX, Dong B, Zhang Y and Cao Y. Angiotensin-converting enzyme 2 attenuates atherosclerotic lesions by targeting vascular cells. *Proceedings of the National Academy of Sciences of the United States of America*. 2010;107:15886-91.

93. Chandrasekaran B, Dar O and McDonagh T. The role of apelin in cardiovascular function and heart failure. *European journal of heart failure*. 2008;10:725-32.

94. Przewlocka-Kosmala M, Kotwica T, Mysiak A and Kosmala W. Reduced circulating apelin in essential hypertension and its association with cardiac dysfunction. *Journal of hypertension*. 2011;29:971-9.

95. Sonmez A, Celebi G, Erdem G, Tapan S, Genc H, Tasci I, Ercin CN, Dogru T, Kilic S, Uckaya G, Yilmaz MI, Erbil MK and Kutlu M. Plasma apelin and ADMA Levels in patients with essential hypertension. *Clin Exp Hypertens*. 2010;32:179-83.

96. Li WW, Niu WQ, Zhang Y, Wu S, Gao PJ and Zhu DL. Family-based analysis of apelin and AGTRL1 gene polymorphisms with hypertension in Han Chinese. *Journal of hypertension*. 2009;27:1194-201.

97. Tatemoto K, Takayama K, Zou MX, Kumaki I, Zhang W, Kumano K and Fujimiya M. The novel peptide apelin lowers blood pressure via a nitric oxide-dependent mechanism. *Regul Pept*. 2001;99:87-92.

98. Cheng X, Cheng XS and Pang CC. Venous dilator effect of apelin, an endogenous peptide ligand for the orphan APJ receptor, in conscious rats. *Eur J Pharmacol*. 2003;470:171-5.

99. Japp AG, Cruden NL, Amer DA, Li VK, Goudie EB, Johnston NR, Sharma S, Neilson I, Webb DJ, Megson IL, Flapan AD and Newby DE. Vascular effects of apelin in vivo in man. *Journal of the American College of Cardiology*. 2008;52:908-13.

100. Chandra SM, Razavi H, Kim J, Agrawal R, Kundu RK, de Jesus Perez V, Zamanian RT, Quertermous T and Chun HJ. Disruption of the apelin-APJ system worsens hypoxia-

induced pulmonary hypertension. *Arteriosclerosis, thrombosis, and vascular biology*. 2011;31:814-20.

101. Alastalo TP, Li M, Perez Vde J, Pham D, Sawada H, Wang JK, Koskenvuo M, Wang L, Freeman BA, Chang HY and Rabinovitch M. Disruption of PPARgamma/beta-catenin-mediated regulation of apelin impairs BMP-induced mouse and human pulmonary arterial EC survival. *The Journal of clinical investigation*. 2011;121:3735-46.

102. Falcao-Pires I, Goncalves N, Henriques-Coelho T, Moreira-Goncalves D, Roncon-Albuquerque R, Jr. and Leite-Moreira AF. Apelin decreases myocardial injury and improves right ventricular function in monocrotaline-induced pulmonary hypertension. *American journal of physiology Heart and circulatory physiology*. 2009;296:H2007-14.

103. Castan-Laurell I, Dray C, Attane C, Duparc T, Knauf C and Valet P. Apelin, diabetes, and obesity. *Endocrine*. 2011;40:1-9.

104. Erdem G, Dogru T, Tasci I, Sonmez A and Tapan S. Low plasma apelin levels in newly diagnosed type 2 diabetes mellitus. *Experimental and clinical endocrinology & diabetes : official journal, German Society of Endocrinology [and] German Diabetes Association*. 2008;116:289-92.

105. Soriguer F, Garrido-Sanchez L, Garcia-Serrano S, Garcia-Almeida JM, Garcia-Arnes J, Tinahones FJ and Garcia-Fuentes E. Apelin levels are increased in morbidly obese subjects with type 2 diabetes mellitus. *Obesity surgery*. 2009;19:1574-80.

106. Zhong JC, Yu XY, Huang Y, Yung LM, Lau CW and Lin SG. Apelin modulates aortic vascular tone via endothelial nitric oxide synthase phosphorylation pathway in diabetic mice. *Cardiovascular research*. 2007;74:388-95.

107. Rittig K, Hildebrandt U, Thamer C, Staiger H, Peter A, Stefan N, Fritsche A, Haring HU, Balletshofer BM and Siegel-Axel D. Apelin serum levels are not associated with early atherosclerosis or fat distribution in young subjects with increased risk for type 2 diabetes. *Experimental and clinical endocrinology & diabetes : official journal, German Society of Endocrinology [and] German Diabetes Association*. 2011;119:358-61.

108. Duparc T, Colom A, Cani PD, Massaly N, Rastrelli S, Drougard A, Le Gonidec S, Mouledous L, Frances B, Leclercq I, Llorens-Cortes C, Pospisilik JA, Delzenne NM, Valet P, Castan-Laurell I and Knauf C. Central apelin controls glucose homeostasis via a nitric oxide-dependent pathway in mice. *Antioxidants & redox signaling*. 2011;15:1477-96.

109. Chen H, Zheng C, Zhang X, Li J, Zheng L and Huang K. Apelin alleviates diabetes-associated endoplasmic reticulum stress in the pancreas of Akita mice. *Peptides*. 2011;32:1634-9.

110. Dray C, Knauf C, Daviaud D, Waget A, Boucher J, Buleon M, Cani PD, Attane C, Guigne C, Carpene C, Burcelin R, Castan-Laurell I and Valet P. Apelin stimulates glucose utilization in normal and obese insulin-resistant mice. *Cell metabolism*. 2008;8:437-45.

111. El-Shehaby AM, El-Khatib MM, Battah AA and Roshdy AR. Apelin: a potential link between inflammation and cardiovascular disease in end stage renal disease patients. *Scandinavian journal of clinical and laboratory investigation*. 2010;70:421-7.

112. Leeper NJ, Tedesco MM, Kojima Y, Schultz GM, Kundu RK, Ashley EA, Tsao PS, Dalman RL and Quertermous T. Apelin prevents aortic aneurysm formation by inhibiting macrophage inflammation. *American journal of physiology Heart and circulatory physiology*. 2009;296:H1329-35.

113. Sawane M, Kidoya H, Muramatsu F, Takakura N and Kajiya K. Apelin Attenuates UVB-Induced Edema and Inflammation by Promoting Vessel Function. *The American journal of pathology*. 2011.

114. Tiani C, Garcia-Pras E, Mejias M, de Gottardi A, Berzigotti A, Bosch J and Fernandez M. Apelin signaling modulates splanchnic angiogenesis and portosystemic collateral vessel formation in rats with portal hypertension. *Journal of hepatology*. 2009;50:296-305.

115. Kunduzova O, Alet N, Delesque-Touchard N, Millet L, Castan-Laurell I, Muller C, Dray C, Schaeffer P, Herault JP, Savi P, Bono F and Valet P. Apelin/APJ signaling system: a potential link between adipose tissue and endothelial angiogenic processes. *FASEB journal : official publication of the Federation of American Societies for Experimental Biology*. 2008;22:4146-53.

116. Kasai A, Ishimaru Y, Kinjo T, Satooka T, Matsumoto N, Yoshioka Y, Yamamuro A, Gomi F, Shintani N, Baba A and Maeda S. Apelin is a crucial factor for hypoxia-induced retinal angiogenesis. *Arteriosclerosis, thrombosis, and vascular biology*. 2010;30:2182-7.

117. Kuklinska AM, Sobkowicz B, Sawicki R, Musial WJ, Waszkiewicz E, Bolinska S and Malyszko J. Apelin: a novel marker for the patients with first ST-elevation myocardial infarction. *Heart and vessels*. 2010;25:363-7.

118. Tycinska AM, Sobkowicz B, Mroczko B, Sawicki R, Musial WJ, Dobrzycki S, Waszkiewicz E, Knapp MA and Szmitkowski M. The value of apelin-36 and brain natriuretic peptide measurements in patients with first ST-elevation myocardial infarction. *Clinica chimica acta; international journal of clinical chemistry*. 2010;411:2014-8.

119. Weir RA, Chong KS, Dalzell JR, Petrie CJ, Murphy CA, Steedman T, Mark PB, McDonagh TA, Dargie HJ and McMurray JJ. Plasma apelin concentration is depressed following acute myocardial infarction in man. *European journal of heart failure*. 2009;11:551-8.

120. Kadoglou NP, Lampropoulos S, Kapelouzou A, Gkontopoulos A, Theofilogiannakos EK, Fotiadis G and Kottas G. Serum levels of apelin and ghrelin in patients with acute coronary syndromes and established coronary artery disease--KOZANI STUDY. *Translational research : the journal of laboratory and clinical medicine*. 2010;155:238-46.

121. Smith CC, Mocanu MM, Bowen J, Wynne AM, Simpkin JC, Dixon RA, Cooper MB and Yellon DM. Temporal changes in myocardial salvage kinases during reperfusion following ischemia: studies involving the cardioprotective adipocytokine apelin.

Cardiovascular drugs and therapy / sponsored by the International Society of Cardiovascular Pharmacotherapy. 2007;21:409-14.

122. Zeng XJ, Zhang LK, Wang HX, Lu LQ, Ma LQ and Tang CS. Apelin protects heart against ischemia/reperfusion injury in rat. *Peptides*. 2009;30:1144-52.

123. Ellinor PT, Low AF and Macrae CA. Reduced apelin levels in lone atrial fibrillation. *European heart journal*. 2006;27:222-6.

124. Kallergis EM, Manios EG, Kanoupakis EM, Mavrakis HE, Goudis CA, Maliaraki NE, Saloustros IG, Milathianaki ME, Chlouverakis GI and Vardas PE. Effect of sinus rhythm restoration after electrical cardioversion on apelin and brain natriuretic Peptide prohormone levels in patients with persistent atrial fibrillation. *The American journal of cardiology*. 2010;105:90-4.

125. Falcone C, Buzzi MP, D'Angelo A, Schirinzi S, Falcone R, Rordorf R, Capettini AC, Landolina M, Storti C and Pelissero G. Apelin plasma levels predict arrhythmia recurrence in patients with persistent atrial fibrillation. *International journal of immunopathology and pharmacology*. 2010;23:917-25.

126. Farkasfalvi K, Stagg MA, Coppen SR, Siedlecka U, Lee J, Soppa GK, Marczin N, Szokodi I, Yacoub MH and Terracciano CM. Direct effects of apelin on cardiomyocyte contractility and electrophysiology. *Biochemical and biophysical research communications*. 2007;357:889-95.

127. Gao LR, Xu RY, Zhang NK, Chen Y, Wang ZG, Zhu ZM, Fei YX, Cao Y, Xu HT and Yang Y. Increased apelin following bone marrow mononuclear cell transplantation

contributes to the improvement of cardiac function in patients with severe heart failure. *Cell transplantation*. 2009;18:1311-8.

128. Gao LR, Zhang NK, Bai J, Ding QA, Wang ZG, Zhu ZM, Fei YX, Yang Y, Xu RY and Chen Y. The apelin-APJ pathway exists in cardiomyogenic cells derived from mesenchymal stem cells in vitro and in vivo. *Cell transplantation*. 2010;19:949-58.

129. Ashley EA, Powers J, Chen M, Kundu R, Finsterbach T, Caffarelli A, Deng A, Eichhorn J, Mahajan R, Agrawal R, Greve J, Robbins R, Patterson AJ, Bernstein D and Quertermous T. The endogenous peptide apelin potently improves cardiac contractility and reduces cardiac loading in vivo. *Cardiovascular research*. 2005;65:73-82.

130. Kuba K, Zhang L, Imai Y, Arab S, Chen M, Maekawa Y, Leschnik M, Leibbrandt A, Markovic M, Schwaighofer J, Beetz N, Musialek R, Neely GG, Komnenovic V, Kolm U, Metzler B, Ricci R, Hara H, Meixner A, Nghiem M, Chen X, Dawood F, Wong KM, Sarao R, Cukerman E, Kimura A, Hein L, Thalhammer J, Liu PP and Penninger JM. Impaired heart contractility in Apelin gene-deficient mice associated with aging and pressure overload. *Circulation research*. 2007;101:e32-42.

131. Atluri P, Morine KJ, Liao GP, Panlilio CM, Berry MF, Hsu VM, Hiesinger W, Cohen JE and Joseph Woo Y. Ischemic heart failure enhances endogenous myocardial apelin and APJ receptor expression. *Cell Mol Biol Lett*. 2007;12:127-38.

132. Dai T, Ramirez-Correa G and Gao WD. Apelin increases contractility in failing cardiac muscle. *Eur J Pharmacol*. 2006;553:222-8.

133. Hosoya M, Kawamata Y, Fukusumi S, Fujii R, Habata Y, Hinuma S, Kitada C, Honda S, Kurokawa T, Onda H, Nishimura O and Fujino M. Molecular and functional characteristics of APJ. Tissue distribution of mRNA and interaction with the endogenous ligand apelin. *The Journal of biological chemistry*. 2000;275:21061-7.

134. Zhong J, Guo D, Chen CB, Wang W, Schuster M, Loibner H, Penninger JM, Scholey JW, Kassiri Z and Oudit GY. Prevention of Angiotensin II-Mediated Renal Oxidative Stress, Inflammation, and Fibrosis by Angiotensin-Converting Enzyme 2. *Hypertension*. 2011;57:314-22.

135. Chun HJ, Ali ZA, Kojima Y, Kundu RK, Sheikh AY, Agrawal R, Zheng L, Leeper NJ, Pearl NE, Patterson AJ, Anderson JP, Tsao PS, Lenardo MJ, Ashley EA and Quertermous T. Apelin signaling antagonizes Ang II effects in mouse models of atherosclerosis. *The Journal of clinical investigation*. 2008;118:3343-54.

136. Siddiquee K, Hampton J, Khan S, Zadory D, Gleaves L, Vaughan DE and Smith LH. Apelin protects against angiotensin II-induced cardiovascular fibrosis and decreases plasminogen activator inhibitor type-1 production. *Journal of hypertension*. 2011;29:724-31.

137. Gurzu B, Petrescu BC, Costuleanu M and Petrescu G. Interactions between apelin and angiotensin II on rat portal vein. *Journal of the renin-angiotensin-aldosterone system : JRAAS*. 2006;7:212-6.

138. Kazemi-Bajestani SM, Patel VB, Wang W and Oudit GY. Targeting the ACE2 and Apelin Pathways Are Novel Therapies for Heart Failure: Opportunities and Challenges. *Cardiol Res Pract*. 2012;2012:823193.

139. Weber KT and Brilla CG. Pathological hypertrophy and cardiac interstitium. Fibrosis and renin-angiotensin-aldosterone system. *Circulation*. 1991;83:1849-65.

140. Kim S and Iwao H. Molecular and cellular mechanisms of angiotensin II-mediated cardiovascular and renal diseases. *Pharmacol Rev*. 2000;52:11-34.

141. Mehta PK and Griendling KK. Angiotensin II cell signaling: physiological and pathological effects in the cardiovascular system. *American journal of physiology Cell physiology*. 2007;292:C82-97.

142. Bodiga S, Zhong JC, Wang W, Basu R, Lo J, Liu GC, Guo D, Holland SM, Scholey JW, Penninger JM, Kassiri Z and Oudit GY. Enhanced susceptibility to biomechanical stress in ACE2 null mice is prevented by loss of the p47phox NADPH oxidase subunit. *Cardiovascular research*. 2011;91:151-61.

143. Ishiyama Y, Gallagher PE, Averill DB, Tallant EA, Brosnihan KB and Ferrario CM. Upregulation of angiotensin-converting enzyme 2 after myocardial infarction by blockade of angiotensin II receptors. *Hypertension*. 2004;43:970-6.

144. Benter IF, Yousif MH, Anim JT, Cojocel C and Diz DI. Angiotensin-(1-7) prevents development of severe hypertension and end-organ damage in spontaneously hypertensive rats treated with L-NAME. *American journal of physiology Heart and circulatory physiology*. 2006;290:H684-91.

145. Mercure C, Yogi A, Callera GE, Aranha AB, Bader M, Ferreira AJ, Santos RA, Walther T, Touyz RM and Reudelhuber TL. Angiotensin(1-7) blunts hypertensive cardiac remodeling by a direct effect on the heart. *Circulation research*. 2008;103:1319-26.

146. Kostenis E, Milligan G, Christopoulos A, Sanchez-Ferrer CF, Heringer-Walther S, Sexton PM, Gembardt F, Kellett E, Martini L, Vanderheyden P, Schultheiss HP and Walther T. G-protein-coupled receptor Mas is a physiological antagonist of the angiotensin II type 1 receptor. *Circulation*. 2005;111:1806-13.

147. Castro CH, Santos RA, Ferreira AJ, Bader M, Alenina N and Almeida AP. Evidence for a functional interaction of the angiotensin-(1-7) receptor Mas with AT1 and AT2 receptors in the mouse heart. *Hypertension*. 2005;46:937-42.

148. Grobe JL, Mecca AP, Lingis M, Shenoy V, Bolton TA, Machado JM, Speth RC, Raizada MK and Katovich MJ. Prevention of angiotensin II-induced cardiac remodeling by angiotensin-(1-7). *American journal of physiology Heart and circulatory physiology*. 2007;292:H736-42.

149. Mori J, Patel VB, Abo Alrob O, Basu R, Altamimi T, Desaulniers J, Wagg CS, Kassiri Z, Lopaschuk GD and Oudit GY. Angiotensin 1-7 Ameliorates Diabetic Cardiomyopathy and Diastolic Dysfunction in db/db Mice by Reducing Lipotoxicity and Inflammation. *Circulation Heart failure*. 2014.

150. Bendall JK, Cave AC, Heymes C, Gall N and Shah AM. Pivotal role of a gp91(phox)-containing NADPH oxidase in angiotensin II-induced cardiac hypertrophy in mice. *Circulation*. 2002;105:293-6.

151. Byrne JA, Grieve DJ, Bendall JK, Li JM, Gove C, Lambeth JD, Cave AC and Shah AM. Contrasting roles of NADPH oxidase isoforms in pressure-overload versus angiotensin II-induced cardiac hypertrophy. *Circulation research*. 2003;93:802-5.

152. Kassiri Z, Zhong J, Guo D, Basu R, Wang X, Liu PP, Scholey JW, Penninger JM and Oudit GY. Loss of angiotensin-converting enzyme 2 accelerates maladaptive left ventricular remodeling in response to myocardial infarction. *Circulation Heart failure*. 2009;2:446-55.

153. Patel VB, Bodiga S, Basu R, Das SK, Wang W, Wang Z, Lo J, Grant MB, Zhong J, Kassiri Z and Oudit GY. Loss of angiotensin-converting enzyme-2 exacerbates diabetic cardiovascular complications and leads to systolic and vascular dysfunction: a critical role of the angiotensin II/AT1 receptor axis. *Circulation research*. 2012;110:1322-35.

154. Guo D, Kassiri Z, Basu R, Chow FL, Kandalam V, Damilano F, Liang W, Izumo S, Hirsch E, Penninger JM, Backx PH and Oudit GY. Loss of PI3K{gamma} Enhances cAMP-Dependent MMP Remodeling of the Myocardial N-Cadherin Adhesion Complexes and Extracellular Matrix in Response to Early Biomechanical Stress. *Circulation research*. 2010;107:1275-89.

155. Patel VB, Wang Z, Fan D, Zhabyeyev P, Basu R, Das SK, Wang W, Desaulniers J, Holland SM, Kassiri Z and Oudit GY. Loss of p47phox subunit enhances susceptibility to biomechanical stress and heart failure because of dysregulation of cortactin and actin filaments. *Circulation research*. 2013;112:1542-56.

156. Swedberg K, Eneroth P, Kjekshus J and Wilhelmsen L. Hormones regulating cardiovascular function in patients with severe congestive heart failure and their relation to mortality. CONSENSUS Trial Study Group. *Circulation*. 1990;82:1730-6.

157. Serneri GG, Boddi M, Cecioni I, Vanni S, Coppo M, Papa ML, Bandinelli B, Bertolozzi I, Polidori G, Toscano T, Maccherini M and Modesti PA. Cardiac angiotensin II formation in the clinical course of heart failure and its relationship with left ventricular function. *Circulation research*. 2001;88:961-8.

158. Li JM and Shah AM. Mechanism of endothelial cell NADPH oxidase activation by angiotensin II. Role of the p47phox subunit. *The Journal of biological chemistry*. 2003;278:12094-100.

159. Li JM, Wheatcroft S, Fan LM, Kearney MT and Shah AM. Opposing roles of p47phox in basal versus angiotensin II-stimulated alterations in vascular O2- production, vascular tone, and mitogen-activated protein kinase activation. *Circulation*. 2004;109:1307-13.

160. Kim MA, Yang D, Kida K, Molotkova N, Yeo SJ, Varki N, Iwata M, Dalton ND, Peterson KL, Siems WE, Walther T, Cowling RT, Kjekshus J and Greenberg B. Effects of ACE2 inhibition in the post-myocardial infarction heart. *J Card Fail*. 2010;16:777-85.

161. Burrell LM, Risvanis J, Kubota E, Dean RG, MacDonald PS, Lu S, Tikellis C, Grant SL, Lew RA, Smith AI, Cooper ME and Johnston CI. Myocardial infarction increases ACE2 expression in rat and humans. *European heart journal*. 2005;26:369-75; discussion 322-4.

162. Patel SK, Wai B, Ord M, MacIsaac RJ, Grant S, Velkoska E, Panagiotopoulos S, Jerums G, Srivastava PM and Burrell LM. Association of ACE2 genetic variants with blood pressure, left ventricular mass, and cardiac function in Caucasians with type 2 diabetes. *American journal of hypertension*. 2012;25:216-22.

163. Tallant EA, Ferrario CM and Gallagher PE. Angiotensin-(1-7) inhibits growth of cardiac myocytes through activation of the mas receptor. *American journal of physiology Heart and circulatory physiology*. 2005;289:H1560-6.

164. Takimoto E and Kass DA. Role of oxidative stress in cardiac hypertrophy and remodeling. *Hypertension*. 2007;49:241-8.

165. Zile MR and Brutsaert DL. New concepts in diastolic dysfunction and diastolic heart failure: Part II: causal mechanisms and treatment. *Circulation*. 2002;105:1503-8.

166. Borlaug BA, Lam CS, Roger VL, Rodeheffer RJ and Redfield MM. Contractility and ventricular systolic stiffening in hypertensive heart disease insights into the pathogenesis of heart failure with preserved ejection fraction. *Journal of the American College of Cardiology*. 2009;54:410-8.

167. Heineke J and Molkentin JD. Regulation of cardiac hypertrophy by intracellular signalling pathways. *Nat Rev Mol Cell Biol*. 2006;7:589-600.

168. Maguire JJ, Kleinz MJ, Pitkin SL and Davenport AP. [Pyr1]apelin-13 identified as the predominant apelin isoform in the human heart: vasoactive mechanisms and inotropic action in disease. *Hypertension*. 2009;54:598-604.

169. Wang W, McKinnie SM, Patel VB, Haddad G, Wang Z, Zhabyeyev P, Das SK, Basu R, McLean B, Kandalam V, Penninger JM, Kassiri Z, Vederas JC, Murray AG and Oudit GY. Loss of Apelin exacerbates myocardial infarction adverse remodeling and ischemia-reperfusion injury: therapeutic potential of synthetic Apelin analogues. *Journal of the American Heart Association*. 2013;2:e000249.

170. De Mota N, Reaux-Le Goazigo A, El Messari S, Chartrel N, Roesch D, Dujardin C, Kordon C, Vaudry H, Moos F and Llorens-Cortes C. Apelin, a potent diuretic neuropeptide counteracting vasopressin actions through inhibition of vasopressin neuron activity and vasopressin release. *Proceedings of the National Academy of Sciences of the United States of America*. 2004;101:10464-9.

171. Medhurst AD, Jennings CA, Robbins MJ, Davis RP, Ellis C, Winborn KY, Lawrie KW, Hervieu G, Riley G, Bolaky JE, Herrity NC, Murdock P and Darker JG. Pharmacological and immunohistochemical characterization of the APJ receptor and its endogenous ligand apelin. *Journal of neurochemistry*. 2003;84:1162-72.

172. Fan X, Zhou N, Zhang X, Mukhtar M, Lu Z, Fang J, DuBois GC and Pomerantz RJ. Structural and functional study of the apelin-13 peptide, an endogenous ligand of the HIV-1 coreceptor, APJ. *Biochemistry*. 2003;42:10163-8.

173. Iturrioz X, Gerbier R, Leroux V, Alvear-Perez R, Maigret B and Llorens-Cortes C. By interacting with the C-terminal Phe of apelin, Phe255 and Trp259 in helix VI of the apelin receptor are critical for internalization. *The Journal of biological chemistry*. 2010;285:32627-37.

174. Towler P, Staker B, Prasad SG, Menon S, Tang J, Parsons T, Ryan D, Fisher M, Williams D, Dales NA, Patane MA and Pantoliano MW. ACE2 X-ray structures reveal a large hinge-bending motion important for inhibitor binding and catalysis. *The Journal of biological chemistry*. 2004;279:17996-8007.

175. Van Der Spoel D, Lindahl E, Hess B, Groenhof G, Mark AE and Berendsen HJ. GROMACS: fast, flexible, and free. *Journal of computational chemistry*. 2005;26:1701-18.

176. Guy JL, Jackson RM, Jensen HA, Hooper NM and Turner AJ. Identification of critical active-site residues in angiotensin-converting enzyme-2 (ACE2) by site-directed mutagenesis. *The FEBS journal*. 2005;272:3512-20.

177. Dales NA, Gould AE, Brown JA, Calderwood EF, Guan B, Minor CA, Gavin JM, Hales P, Kaushik VK, Stewart M, Tummino PJ, Vickers CS, Ocain TD and Patane MA. Substrate-based design of the first class of angiotensin-converting enzyme-related carboxypeptidase (ACE2) inhibitors. *Journal of the American Chemical Society*. 2002;124:11852-3.

178. Trott O and Olson AJ. AutoDock Vina: improving the speed and accuracy of docking with a new scoring function, efficient optimization, and multithreading. *Journal of computational chemistry*. 2010;31:455-61.

179. Emsley P and Cowtan K. Coot: model-building tools for molecular graphics. *Acta crystallographica Section D, Biological crystallography*. 2004;60:2126-32.

180. Hornak V, Abel R, Okur A, Strockbine B, Roitberg A and Simmerling C. Comparison of multiple Amber force fields and development of improved protein backbone parameters. *Proteins*. 2006;65:712-25.

181. Pettersen EF, Goddard TD, Huang CC, Couch GS, Greenblatt DM, Meng EC and Ferrin TE. UCSF Chimera--a visualization system for exploratory research and analysis. *Journal of computational chemistry*. 2004;25:1605-12.

182. The PyMOL MOlecular Graphics System Vrp, Schrodinger, LLC. 2010.

183. Wang W, Patel VB, Parajuli N, Fan D, Basu R, Wang Z, Ramprasath T, Kassiri Z, Penninger JM and Oudit GY. Heterozygote loss of ACE2 is sufficient to increase the susceptibility to heart disease. *Journal of molecular medicine*. 2014;92:847-58.

184. Zhang QX, Nakhaei-Nejad M, Haddad G, Wang X, Loutzenhiser R and Murray AG. Glomerular endothelial PI3 kinase-alpha couples to VEGFR2, but is not required for eNOS activation. *American journal of physiology Renal physiology*. 2011;301:F1242-50.

185. Murza A, Parent A, Besserer-Offroy E, Tremblay H, Karadereye F, Beaudet N, Leduc R, Sarret P and Marsault E. Elucidation of the structure-activity relationships of apelin: influence of unnatural amino acids on binding, signaling, and plasma stability. *ChemMedChem*. 2012;7:318-25.

186. Haschke M, Schuster M, Poglitsch M, Loibner H, Salzberg M, Bruggisser M, Penninger J and Krahenbuhl S. Pharmacokinetics and pharmacodynamics of recombinant human angiotensin-converting enzyme 2 in healthy human subjects. *Clinical pharmacokinetics*. 2013;52:783-92.

187. Ceraudo E, Galanth C, Carpentier E, Banegas-Font I, Schonegge AM, Alvear-Perez R, Iturrioz X, Bouvier M and Llorens-Cortes C. Biased signaling favoring gi over beta-arrestin promoted by an apelin fragment lacking the C-terminal phenylalanine. *The Journal of biological chemistry*. 2014;289:24599-610.

188. Hunt SA, Abraham WT, Chin MH, Feldman AM, Francis GS, Ganiats TG, Jessup M, Konstam MA, Mancini DM, Michl K, Oates JA, Rahko PS, Silver MA, Stevenson LW and Yancy CW. 2009 focused update incorporated into the ACC/AHA 2005 Guidelines for the Diagnosis and Management of Heart Failure in Adults: a report of the American College of Cardiology Foundation/American Heart Association Task Force on Practice Guidelines: developed in collaboration with the International Society for Heart and Lung Transplantation. *Circulation*. 2009;119:e391-479.

189. Tao J, Zhu W, Li Y, Xin P, Li J, Liu M, Redington AN and Wei M. Apelin-13 protects the heart against ischemia-reperfusion injury through inhibition of ER-dependent apoptotic pathways in a time-dependent fashion. *American journal of physiology Heart and circulatory physiology*. 2011;301:H1471-86.

190. Gao E, Lei YH, Shang X, Huang ZM, Zuo L, Boucher M, Fan Q, Chuprun JK, Ma XL and Koch WJ. A novel and efficient model of coronary artery ligation and myocardial infarction in the mouse. *Circulation research*. 2010;107:1445-53.

191. Kandalam V, Basu R, Abraham T, Wang X, Soloway PD, Jaworski DM, Oudit GY and Kassiri Z. TIMP2 deficiency accelerates adverse post-myocardial infarction

remodeling because of enhanced MT1-MMP activity despite lack of MMP2 activation. *Circulation research*. 2010;106:796-808.

192. Zhang Y, Takagawa J, Sievers RE, Khan MF, Viswanathan MN, Springer ML, Foster E and Yeghiazarians Y. Validation of the wall motion score and myocardial performance indexes as novel techniques to assess cardiac function in mice after myocardial infarction. *American journal of physiology Heart and circulatory physiology*. 2007;292:H1187-92.

193. Cerqueira MD, Weissman NJ, Dilsizian V, Jacobs AK, Kaul S, Laskey WK, Pennell DJ, Rumberger JA, Ryan T and Verani MS. Standardized myocardial segmentation and nomenclature for tomographic imaging of the heart: a statement for healthcare professionals from the Cardiac Imaging Committee of the Council on Clinical Cardiology of the American Heart Association. *Circulation*. 2002;105:539-42.

194. Clark JE, Kottam A, Motterlini R and Marber MS. Measuring left ventricular function in the normal, infarcted and CORM-3-preconditioned mouse heart using complex admittance-derived pressure volume loops. *Journal of Pharmacological and Toxicological Methods*. 2009;59:94-99.

195. Kottam AT, Porterfield J, Raghavan K, Fernandez D, Feldman MD, Valvano JW and Pearce JA. Real time pressure-volume loops in mice using complex admittance: measurement and implications. *Conference proceedings: Annual International Conference of the IEEE Engineering in Medicine and Biology Society IEEE Engineering in Medicine and Biology Society Conference*. 2006;1:4336-9.

196. Baker M, Robinson SD, Lechertier T, Barber PR, Tavora B, D'Amico G, Jones DT, Vojnovic B and Hodivala-Dilke K. Use of the mouse aortic ring assay to study angiogenesis. *Nature protocols*. 2012;7:89-104.

197. Ingram DA, Mead LE, Tanaka H, Meade V, Fenoglio A, Mortell K, Pollok K, Ferkowicz MJ, Gilley D and Yoder MC. Identification of a novel hierarchy of endothelial progenitor cells using human peripheral and umbilical cord blood. *Blood*. 2004;104:2752-60.

198. Nakatsu MN and Hughes CC. An optimized three-dimensional in vitro model for the analysis of angiogenesis. *Methods in enzymology*. 2008;443:65-82.

199. Zhong JC, Basu R, Guo D, Chow FL, Byrns S, Shuster M, Loibner H, Wang X, Penninger JM, Kassiri Z and Oudit GY. Angiotensin Converting Enzyme 2 Suppresses Pathological Hypertrophy, Myocardial Fibrosis and Cardiac Dysfunction. *Circulation*. 2010;122:717-728.

200. Patel VB, Bodiga S, Fan D, Das SK, Wang Z, Wang W, Basu R, Zhong J, Kassiri Z and Oudit GY. Cardioprotective Effects Mediated by Angiotensin II Type 1 Receptor Blockade and Enhancing Angiotensin 1-7 in Experimental Heart Failure in Angiotensin-Converting Enzyme 2-Null Mice. *Hypertension*. 2012.

201. Kassiri Z, Oudit GY, Sanchez O, Dawood F, Mohammed FF, Nuttall RK, Edwards DR, Liu PP, Backx PH and Khokha R. Combination of tumor necrosis factor-alpha ablation and matrix metalloproteinase inhibition prevents heart failure after pressure overload in

tissue inhibitor of metalloproteinase-3 knock-out mice. *Circulation research*. 2005;97:380-90.

202. Wright CD, Chen Q, Baye NL, Huang Y, Healy CL, Kasinathan S and O'Connell TD. Nuclear alpha1-adrenergic receptors signal activated ERK localization to caveolae in adult cardiac myocytes. *Circulation research*. 2008;103:992-1000.

203. Sutton MG and Sharpe N. Left ventricular remodeling after myocardial infarction: pathophysiology and therapy. *Circulation*. 2000;101:2981-8.

204. Yellon DM and Hausenloy DJ. Myocardial reperfusion injury. *The New England journal of medicine*. 2007;357:1121-35.

205. Ware JA and Simons M. Angiogenesis in ischemic heart disease. *Nature medicine*. 1997;3:158-64.

206. Carmeliet P. Angiogenesis in life, disease and medicine. *Nature*. 2005;438:932-6.

207. Liu S, Premont RT, Kontos CD, Huang J and Rockey DC. Endothelin-1 activates endothelial cell nitric-oxide synthase via heterotrimeric G-protein betagamma subunit signaling to protein jinase B/Akt. *The Journal of biological chemistry*. 2003;278:49929-35.

208. Ridgway J, Zhang G, Wu Y, Stawicki S, Liang WC, Chanthery Y, Kowalski J, Watts RJ, Callahan C, Kasman I, Singh M, Chien M, Tan C, Hongo JA, de Sauvage F, Plowman G and Yan M. Inhibition of Dll4 signalling inhibits tumour growth by deregulating angiogenesis. *Nature*. 2006;444:1083-7.

209. del Toro R, Prahst C, Mathivet T, Siegfried G, Kaminker JS, Larrivee B, Breant C, Duarte A, Takakura N, Fukamizu A, Penninger J and Eichmann A. Identification and functional analysis of endothelial tip cell-enriched genes. *Blood*. 2010;116:4025-33.

210. Oudit GY and Penninger JM. Cardiac regulation by phosphoinositide 3-kinases and PTEN. *Cardiovascular research*. 2009;82:250-60.

211. Khan BQ, Gandhi MS, Edmonds H, Ahmad K, Rasberry RD, Corbett C, Jukkola AF and Carbone LC. Lymphoma mimicking carcinoma erysipeloides. *International journal of dermatology*. 2008;47:269-71.

212. Condorelli G, Drusco A, Stassi G, Bellacosa A, Roncarati R, Iaccarino G, Russo MA, Gu Y, Dalton N, Chung C, Latronico MV, Napoli C, Sadoshima J, Croce CM and Ross J, Jr. Akt induces enhanced myocardial contractility and cell size in vivo in transgenic mice. *Proceedings of the National Academy of Sciences of the United States of America*. 2002;99:12333-8.

213. Merenstein DJ, Schneider MF, Cox C, Schwartz R, Weber K, Robison E, Gandhi M, Richardson J and Plankey MW. Association between living with children and adherence to highly active antiretroviral therapy in the Women's Interagency HIV Study. *Pediatrics*. 2008;121:e787-93.

214. Iwanaga Y, Kihara Y, Takenaka H and Kita T. Down-regulation of cardiac apelin system in hypertrophied and failing hearts: Possible role of angiotensin II-angiotensin type 1 receptor system. *J Mol Cell Cardiol*. 2006;41:798-806.

215. D'Aniello C, Lonardo E, Iaconis S, Guardiola O, Liguoro AM, Liguori GL, Autiero M, Carmeliet P and Minchiotti G. G protein-coupled receptor APJ and its ligand apelin act downstream of Cripto to specify embryonic stem cells toward the cardiac lineage through extracellular signal-regulated kinase/p70S6 kinase signaling pathway. *Circulation research*. 2009;105:231-8.

216. Wang IN, Wang X, Ge X, Anderson J, Ho M, Ashley E, Liu J, Butte MJ, Yazawa M, Dolmetsch RE, Quertermous T and Yang PC. Apelin enhances directed cardiac differentiation of mouse and human embryonic stem cells. *PloS one*. 2012;7:e38328.

217. Walsh K and Shiojima I. Cardiac growth and angiogenesis coordinated by intertissue interactions. *The Journal of clinical investigation*. 2007;117:3176-9.

218. Iturrioz X, Alvear-Perez R, De Mota N, Franchet C, Guillier F, Leroux V, Dabire H, Le Jouan M, Chabane H, Gerbier R, Bonnet D, Berdeaux A, Maigret B, Galzi JL, Hibert M and Llorens-Cortes C. Identification and pharmacological properties of E339-3D6, the first nonpeptidic apelin receptor agonist. *FASEB journal : official publication of the Federation of American Societies for Experimental Biology*. 2010;24:1506-17.

219. Ruiz-Ortega M, Lorenzo O, Ruperez M, Esteban V, Suzuki Y, Mezzano S, Plaza JJ and Egido J. Role of the renin-angiotensin system in vascular diseases: expanding the field. *Hypertension*. 2001;38:1382-7.

220. Daugherty A, Manning MW and Cassis LA. Angiotensin II promotes atherosclerotic lesions and aneurysms in apolipoprotein E-deficient mice. *The Journal of clinical investigation*. 2000;105:1605-12.

221. Cassis LA, Gupte M, Thayer S, Zhang X, Charnigo R, Howatt DA, Rateri DL and Daugherty A. ANG II infusion promotes abdominal aortic aneurysms independent of increased blood pressure in hypercholesterolemic mice. *American journal of physiology Heart and circulatory physiology*. 2009;296:H1660-5.

222. Geisterfer AA, Peach MJ and Owens GK. Angiotensin II induces hypertrophy, not hyperplasia, of cultured rat aortic smooth muscle cells. *Circulation research*. 1988;62:749-56.

223. Marchesi C, Paradis P and Schiffrin EL. Role of the renin-angiotensin system in vascular inflammation. *Trends in pharmacological sciences*. 2008;29:367-74.

224. Medzhitov R and Horng T. Transcriptional control of the inflammatory response. *Nature reviews Immunology*. 2009;9:692-703.

225. Wilson SK. Role of oxygen-derived free radicals in acute angiotensin II--induced hypertensive vascular disease in the rat. *Circulation research*. 1990;66:722-34.

226. de Cavanagh EM, Inserra F, Ferder M and Ferder L. From mitochondria to disease: role of the renin-angiotensin system. *American journal of nephrology*. 2007;27:545-53.

227. Min LJ, Mogi M, Iwai M and Horiuchi M. Signaling mechanisms of angiotensin II in regulating vascular senescence. *Ageing research reviews*. 2009;8:113-21.

228. de Gasparo M, Catt KJ, Inagami T, Wright JW and Unger T. International union of pharmacology. XXIII. The angiotensin II receptors. *Pharmacol Rev*. 2000;52:415-72.

229. Patel VB, Bodiga S, Fan D, Das SK, Wang Z, Wang W, Basu R, Zhong J, Kassiri Z and Oudit GY. Cardioprotective effects mediated by angiotensin II type 1 receptor blockade and enhancing angiotensin 1-7 in experimental heart failure in angiotensin-converting enzyme 2-null mice. *Hypertension*. 2012;59:1195-203.

230. McLean DL, Kim J, Kang Y, Shi H, Atkins GB, Jain MK and Chun HJ. Apelin/APJ signaling is a critical regulator of statin effects in vascular endothelial cells--brief report. *Arteriosclerosis, thrombosis, and vascular biology*. 2012;32:2640-3.

231. Kidoya H, Kunii N, Naito H, Muramatsu F, Okamoto Y, Nakayama T and Takakura N. The apelin/APJ system induces maturation of the tumor vasculature and improves the efficiency of immune therapy. *Oncogene*. 2012;31:3254-64.

232. Basu R, Lee J, Morton JS, Takawale A, Fan D, Kandalam V, Wang X, Davidge ST and Kassiri Z. TIMP3 is the primary TIMP to regulate agonist-induced vascular remodelling and hypertension. *Cardiovascular research*. 2013;98:360-71.

233. Metz RP, Patterson JL and Wilson E. Vascular smooth muscle cells: isolation, culture, and characterization. *Methods Mol Biol*. 2012;843:169-76.

234. Proudfoot D and Shanahan C. Human vascular smooth muscle cell culture. *Methods Mol Biol*. 2012;806:251-63.

235. Kasai A, Ishimaru Y, Higashino K, Kobayashi K, Yamamuro A, Yoshioka Y and Maeda S. Inhibition of apelin expression switches endothelial cells from proliferative to mature state in pathological retinal angiogenesis. *Angiogenesis*. 2013;16:723-34.

236. Cesarovic N, Jirkof P, Rettich A and Arras M. Implantation of radiotelemetry transmitters yielding data on ECG, heart rate, core body temperature and activity in free-moving laboratory mice. *Journal of visualized experiments : JoVE*. 2011.

237. Rieger AM, Nelson KL, Konowalchuk JD and Barreda DR. Modified annexin V/propidium iodide apoptosis assay for accurate assessment of cell death. *Journal of visualized experiments : JoVE*. 2011.

238. Basu R, Lee J, Morton JS, Takawale A, Fan D, Kandalam V, Wang XH, Davidge ST and Kassiri Z. TIMP3 is the primary TIMP to regulate agonist-induced vascular remodelling and hypertension. *Cardiovascular research*. 2013;98:360-371.

239. Gage GJ, Kipke DR and Shain W. Whole animal perfusion fixation for rodents. *Journal of visualized experiments : JoVE*. 2012.

240. Basu R, Fan D, Kandalam V, Lee J, Das SK, Wang XH, Baldwin TA, Oudit GY and Kassiri Z. Loss of Timp3 Gene Leads to Abdominal Aortic Aneurysm Formation in Response to Angiotensin II. *Journal of Biological Chemistry*. 2012;287:44083-44096.

241. Basu R, Lee J, Wang Z, Patel VB, Fan D, Das SK, Liu GC, John R, Scholey JW, Oudit GY and Kassiri Z. Loss of TIMP3 selectively exacerbates diabetic nephropathy. *American journal of physiology Renal physiology*. 2012;303:F1341-52.

242. Isoda K, Kitagaki M, Niida T, Kondo H, Matsubara O, Kikuchi M, Ohsuzu F and Adachi T. Deficiency of interleukin-1 receptor antagonist promotes spontaneous femoral artery aneurysm formation in mice. *The American journal of pathology*. 2012;180:1254-63.

243. Levi M, Moons L, Bouche A, Shapiro SD, Collen D and Carmeliet P. Deficiency of urokinase-type plasminogen activator-mediated plasmin generation impairs vascular remodeling during hypoxia-induced pulmonary hypertension in mice. *Circulation*. 2001;103:2014-20.

244. Marque V, Kieffer P, Gayraud B, Lartaud-Idjouadiene I, Ramirez F and Atkinson J. Aortic wall mechanics and composition in a transgenic mouse model of Marfan syndrome. *Arteriosclerosis, thrombosis, and vascular biology*. 2001;21:1184-9.

245. Irani K. Angiotensin II-stimulated vascular remodeling: the search for the culprit oxidase. *Circulation research*. 2001;88:858-60.

246. Cohn JN, Ferrari R and Sharpe N. Cardiac remodeling--concepts and clinical implications: a consensus paper from an international forum on cardiac remodeling. Behalf of an International Forum on Cardiac Remodeling. *Journal of the American College of Cardiology*. 2000;35:569-82.

247. Brady AR, Thompson SG, Fowkes FG, Greenhalgh RM and Powell JT. Abdominal aortic aneurysm expansion: risk factors and time intervals for surveillance. *Circulation*. 2004;110:16-21.

248. Movat HZ. Demonstration of all connective tissue elements in a single section; pentachrome stains. *AMA Arch Pathol*. 1955;60:289-95.

249. Russell HK, Jr. A modification of Movat's pentachrome stain. *Arch Pathol*. 1972;94:187-91.

250. Gomori G. A rapid one-step trichrome stain. *American journal of clinical pathology*. 1950;20:661-4.

251. Clarke MC, Figg N, Maguire JJ, Davenport AP, Goddard M, Littlewood TD and Bennett MR. Apoptosis of vascular smooth muscle cells induces features of plaque vulnerability in atherosclerosis. *Nature medicine*. 2006;12:1075-80.

252. McCarthy NJ and Bennett MR. The regulation of vascular smooth muscle cell apoptosis. *Cardiovascular research*. 2000;45:747-55.

253. Bai H, Pollman MJ, Inishi Y and Gibbons GH. Regulation of vascular smooth muscle cell apoptosis. Modulation of bad by a phosphatidylinositol 3-kinase-dependent pathway. *Circulation research*. 1999;85:229-37.

254. Page-McCaw A, Ewald AJ and Werb Z. Matrix metalloproteinases and the regulation of tissue remodelling. *Nat Rev Mol Cell Biol*. 2007;8:221-33.

255. Brew K and Nagase H. The tissue inhibitors of metalloproteinases (TIMPs): an ancient family with structural and functional diversity. *Biochim Biophys Acta*. 2010;1803:55-71.

256. Pentimalli L, Modesti A, Vignati A, Marchese E, Albanese A, Di Rocco F, Coletti A, Di Nardo P, Fantini C, Tirpakova B and Maira G. Role of apoptosis in intracranial aneurysm rupture. *J Neurosurg*. 2004;101:1018-25.

257. Yamanouchi D, Morgan S, Stair C, Seedial S, Lengfeld J, Kent KC and Liu B. Accelerated aneurysmal dilation associated with apoptosis and inflammation in a newly

developed calcium phosphate rodent abdominal aortic aneurysm model. *J Vasc Surg*. 2012;56:455-61.

258. Benigni A, Cassis P and Remuzzi G. Angiotensin II revisited: new roles in inflammation, immunology and aging. *EMBO Mol Med*. 2010;2:247-57.

259. Cheetham C, Collis J, O'Driscoll G, Stanton K, Taylor R and Green D. Losartan, an angiotensin type 1 receptor antagonist, improves endothelial function in non-insulin-dependent diabetes. *Journal of the American College of Cardiology*. 2000;36:1461-6.

260. Maione A, Navaneethan SD, Graziano G, Mitchell R, Johnson D, Mann JF, Gao P, Craig JC, Tognoni G, Perkovic V, Nicolucci A, De Cosmo S, Sasso A, Lamacchia O, Cignarelli M, Manfreda VM, Gentile G and Strippoli GF. Angiotensin-converting enzyme inhibitors, angiotensin receptor blockers and combined therapy in patients with micro- and macroalbuminuria and other cardiovascular risk factors: a systematic review of randomized controlled trials. *Nephrol Dial Transplant*. 2011;26:2827-47.

261. Doulton TW, He FJ and MacGregor GA. Systematic review of combined angiotensin-converting enzyme inhibition and angiotensin receptor blockade in hypertension. *Hypertension*. 2005;45:880-6.

262. Oudit GY, Liu GC, Zhong J, Basu R, Chow FL, Zhou J, Loibner H, Janzek E, Schuster M, Penninger JM, Herzenberg AM, Kassiri Z and Scholey JW. Human recombinant ACE2 reduces the progression of diabetic nephropathy. *Diabetes*. 2010;59:529-38.